2017-01-01

Method & Madness: Advanced Techniques for Characterizing Rat Hypothalamic Chemoarchitecture and for Modernizing Legacy Data

Claire Eugenia Wells
University of Texas at El Paso, claire.eugenia.wells@gmail.com

METHOD & MADNESS – ADVANCED TECHNIQUES FOR CHARACTERIZING RAT HYPOTHALAMIC CHEMOARCHITECTURE AND FOR MODERNIZING LEGACY DATA

CLAIRE EUGENIA WELLS

Doctoral Program in Biological Sciences – Pathobiology

APPROVED:

Arshad M. Khan, Ph.D., Chair

Edward Castañeda, Ph.D.

Germán Rosas-Acosta, Ph.D.

Manuel Miranda-Arango, Ph.D.

Kristin Gosselink, Ph. D., Advocate

Charles Ambler, Ph.D.
Dean of the Graduate School

Dedication

To entropy.

METHOD & MADNESS – ADVANCED TECHNIQUES FOR CHARACTERIZING RAT HYPOTHALAMIC CHEMOARCHITECTURE AND FOR MODERNIZING LEGACY DATA

by

CLAIRE EUGENIA WELLS, B.A.

DISSERTATION

Presented to the Faculty of the Graduate School of

The University of Texas at El Paso

in Partial Fulfillment

of the Requirements

for the Degree of

DOCTOR OF PHILOSOPHY

Biological Sciences

THE UNIVERSITY OF TEXAS AT EL PASO

December 2017

Acknowledgements

I could not have completed the work described in this document without the aid and support of many people. I would like to thank my father James Wells, for funding this naïve journey; my partner in life Steven Michelmann, for supporting me and for mapping by my side; and my mentor Dr. Arshad Khan, for believing in me when I did not, for consistently smoothing my path, and for making a publication of my work possible. And I have many more to thank: Dr. Ellen Walker, for training me in histology and microscopy, and for doing confocal imaging for me; Dr. Soyoung Jeon, for performing the statistical analyses presented here; Dr. Chris D'Arcy, for committing to mapping to ensure the project's future fruition; my mother Mary Wells, for her support; Kristen Pennington, for sharing the burden of imaging with me; Briana Pinales and Nicole Dominguez, for completing some of the histology on my behalf; Anais Martinez, for training me in the use of the microtome and for taking over PERSIST; Kenichiro Negishi, for comradery and for sharing with me his fortuitous discovery concerning hypothalamic MCH/nNOS cells; Alexa Escapita, for sticking with me; Dr. Rick Thompson, for his identification of stable fiducials; my students in PERSIST, for bearing with me; my students in Molecular Cell Biology Lab, for fun times; Elizabeth Anaya, for training me in cell culture and for being an ally; Kristina Barron, for comradery and for helping me find my feet as a teaching assistant; Jonathan Abou-Fadel, for comradery and for giving me the idea in the first place; and the SMARTS program at UTEP, for granting me funding. Last but not least, I thank the members of my committee, for their time, patience, advice, and support.

Abstract

The hypothalamus is a region of the brain with exceptionally high anatomical, chemical, and functional diversity. It regulates homeostatic functions and a number of motivated behaviors impacting homeostasis, such as ingestion and reproduction; it also serves as a point of connection between the forebrain and hindbrain. An improved understanding of the chemical anatomy of this area would benefit scientists working in many neuroscientific disciplines. The work described herein contributes to a chemoarchitectural atlas of the rat hypothalamus, which will include data on the distribution of various hypothalamic neurotransmitters, and on their co-localizations and synaptic interactions. Importantly, the methodology used to generate this contribution to the atlas has been rigorously documented and discussed. Additionally, new methodologies for easily transferring mapped data between atlases have been explored, in order that the new chemoarchitectural atlas may benefit from the decades of behavioral and functional work performed in the rat hypothalamus. Finally, the beginnings of a comprehensive analysis of the differences between major brain atlases based on stereotaxic coordinates has been created.

Table of Contents

Acknowledgements iv

Abstract v

Table of Contents vi

List of Tables ix

List of Figures x

Introduction 1

Anatomy of the Hypothalamus 1

Neuropeptides 6

Functions of the Hypothalamus 7

Interactions among Functionally-Defined Circuits in the Hypothalamus 10

The Need for an Improved Understanding of Hypothalamic Circuitry 12

α-Melanocyte-Stimulating Hormone (α-MSH) 13

Melanin-Concentrating Hormone (MCH) 14

Nitric Oxide (NO) 16

The Boxed-Data Dilemma 17

Specific Aim 1: Contribute To A Chemoarchitectural Atlas Of The Rat Hypothalamus 20

Objective 20

Materials and Methods 20

Animals 20

Tissue Processing 21

Immunofluorescence Histochemistry 21

Nissl 22

Imaging 22

Mapping 22

Results 42

α-MSH-ir Cell Bodies 42

α-MSH-ir Fibers 43

MCH-ir Cell Bodies 49

MCH-ir Fibers 51

nNOS-ir Cell Bodies 56
nNOS-ir fibers 62
MCH/nNOS-ir cell bodies 70
Potential Synaptic Interaction Zones (PSIZs) 71
Discussion 100
Regarding Results 100
Some Issues of Representation in Mapping 101
Limitations of the Technique 103
Future Directions 104
Probabilistic Maps 104
The Great Atlas 105
Specific Aim 2: Develop Techniques For Data Migration Among Atlases 110
Objective 110
Materials and Methods 110
Description of Unpublished Legacy Dataset 110
Atlas Plate Preparation 111
Nearest Neighbor Migration Method 112
Nearest Neighbor Warped Migration Method 113
Stable Fiducial Migration Method 113
Average Migration Method 114
Average Closest Migration Method 115
Average No Outlier Migration Method 115
Systematic Comparison of Three Reference Spaces 116
Statistical Analyses 118
Results 128
Data Migration 128
Systematic Comparison of Three Reference Spaces 128
Discussion 135
Data Migration 135
Systematic Comparison of Three Reference Spaces 136
Future Directions 138
The Great Atlas 138

Computer Algorithms in Atlas Comparison 139
Geometric Morphometrics 139
References 142
Appendix 160
Abbreviations 160
Structures 160
Molecular Species 162
Miscellaneous 163
Hypothalamic Maps Based on a Different Brain 164
Systematic Comparison of Three Reference Spaces 177
Vita 238

List of Tables

Table 2.1: Antibodies and Conjugates Used in Immunofluorescence Histochemistry. 31
Table 2.2: Legend for Maps. 77
Table 3.1: Distances between Fiducial Pairs in Swanson 2004 versus Paxinos & Watson 1998. 120
Table 3.2: Results of Statistical Tests for Differences in Selected Structures' Coordinates between Atlases. 131
Table 4.1: Stereotaxic Coordinates of Bounding Points of Corresponding Structures at Corresponding Levels in the Swanson 2004 atlas (S), Paxinos & Watson 1998 atlas (PW1), and Paxinos & Watson 2005 atlas (PW2). 177
Table 4.2: Correspondence of Structures at Corresponding Levels in the Swanson 2004 (S), Paxinos & Watson 1998 (PW1), and Paxinos & Watson 2005 (PW2) Atlases. 234

List of Figures

Figure 1.1: Schematic of hypothalamic anatomy, with a transverse view. Adapted from Swanson [4]. 5
Figure 2.1: Workflow for Specific Aim 1. 32
Figure 2.2: Overview of the Mapping Process. 33
Figure 2.3: Determination of Plane of Section. 34
Figure 2.4: Accounting for Plane of Section in Mapping. 35
Figure 2.5: Nissl Parcellation. 36
Figure 2.6: Vessel Alignments. 37
Figure 2.7: Increasing Background Visibility for Vessel Alignments. 38
Figure 2.8: Quality of Alignments. 38
Figure 2.9: Transferring Nissl Parcellation to Fluorescent Sections. 39
Figure 2.10: Identifying Colocalization. 40
Figure 2.11: Resolving Conflicts between Reference and Experimental Parcellations. 41
Figure 2.12: Level 15 Maps. 77
Figure 2.13: Level 16 Maps. 78
Figure 2.14: Level 17 Maps. 79
Figure 2.15: Level 18 Maps. 80
Figure 2.16: Level 19 Maps. 81
Figure 2.17: Level 20 Maps. 82
Figure 2.18: Level 21 Maps. 83
Figure 2.19: Level 22 Maps. 84
Figure 2.20: Level 23 Maps. 85
Figure 2.21: Level 24 Maps. 86
Figure 2.22: Level 25 Maps. 87
Figure 2.23: Level 26 Maps. 88
Figure 2.24: Level 27 Maps. 89
Figure 2.25: Level 28 Maps. 90
Figure 2.26: Level 29 Maps. 91
Figure 2.27: Level 30 Maps. 92
Figure 2.28: Level 31 Maps. 93
Figure 2.29: Level 32 Maps. 94
Figure 2.30: Level 33 Maps. 95
Figure 2.31: Level 34 Maps. 96
Figure 2.32: Level 35 Maps. 97
Figure 2.33: Level 36 Maps. 98
Figure 2.34: Graphical Summary of α-MSH, MCH, and nNOS Distributions and Interactions at Selected Levels for Selected Structures in the Rat Hypothalamus. 99
Figure 3.1: Dot Plots of Atlas Levels Calibrated to Bregma (β). Adapted from [121]. 121
Figure 3.2: Digitization of Maps of Injection Sites (A. M. Khan, unpublished data) and Preparation of Atlas Plates. 122
Figure 3.3: Nearest Neighbor Migration Method. 122
Figure 3.4: Nearest Neighbor Warped Migration Method. 123
Figure 3.5: Average Migration Method. 124
Figure 3.6: Histograms for the Average No Outlier Migration Method. 125

Figure 3.7: Points used for Atlas Comparison. 126
Figure 3.8: Juxtaposiing of Nissl Images for Comparison of Atlases. 127
Figure 3.9: Data Migration between Atlases using Different Methods. 132
Figure 3.10: Dot Plots of Atlas Levels Matched by Fiducial Analysis. Revised from 121. 134
Figure 4.1: Level 22 Maps. 164
Figure 4.2: Level 23 Maps. 165
Figure 4.3: Level 24 Maps. 166
Figure 4.4: Level 25 Maps. 167
Figure 4.5: Level 26 Maps. 168
Figure 4.6: Level 27 Maps. 169
Figure 4.7: Level 28 Maps. 170
Figure 4.8: Level 29 Maps. 171
Figure 4.9: Level 30 Maps. 172
Figure 4.10: Level 31 Maps. 173
Figure 4.11: Level 32 Maps. 174
Figure 4.12: Level 33 Maps. 175
Figure 4.13: Level 34 Maps. 176

Introduction

Anatomy of the Hypothalamus

It is difficult to positively identify the discoverer of the hypothalamus, as a number of individuals have produced descriptions of this area without necessarily recognizing it as a discrete entity. The first such was the physician Galen (131–201 C.E.). Leonardo da Vinci (1452–1519) and several others from around the same time period also fall into this category [1]. The famous anatomist Andreas Vesalius (1514–1564) is considered the first person to produce a detailed and accurate description, and so is oft cited as the discoverer of the hypothalamus, although Wilhelm His coined the term 'hypothalamus' in 1893 [1]. The symptoms resulting from lesions to the base of the brain (where the hypothalamus is located) were catalogued before formal investigations of the hypothalamus began, pioneered by Johann Paul Karplus and Alois Kreidl in 1909–1912 [1]. The boundaries of the hypothalamus have been variously arbitrarily defined throughout its history by different investigators. Descriptions of its internal structure were begun by G. T. Ziehen (1901) and Santiago Rámon y Cajal (1904) – although the preoptic area (the rostral-most portion of the hypothalamus) was described earlier by Charles Judson Herrick and Ludwig Edinger in the 1890s, it was not then considered part of the hypothalamus [1]. A standardized nomenclature was established in 1939 at a symposium on the hypothalamus organized by the Association for Research in Nervous and Mental Disease [1].

Currently the boundaries of the hypothalamus are considered to be: the thalamus, subthalamus, anterior commissure, and hypothalamic sulcus (a groove in the upper part of the wall of the third ventricle) dorsally; the optic chiasm, pituitary and infundibulum (the stalk of the pituitary), and base of the brain ventrally; the lamina terminalis (a membrane stretching from the rostral wall of the third ventricle to the intraventricular foramen, thereby connecting the third and lateral ventricles) rostrally; the end of the mammillary bodies caudally; the internal capsule/cerebral peduncle, optic tract, and basal ganglia laterally; and the third ventricle medially [2, 3]. It has been divided into four zones rostro-caudally – the preoptic, supraoptic (sometimes

the preoptic and supraoptic (or anterior) zones are combined under the term chiasmatic [2]), tuberal, and mammillary – by Le Gros Clark in 1938, and into three more zones mediolaterally – periventricular, medial, and lateral – by Crosby and Woodburne in 1940; these divisions have in large part withstood the test of time [3]. The major nuclei of the preoptic zone are the medial preoptic nucleus (MPN) and a number of smaller preoptic nuclei; those of the supraoptic zone are the anterior (ANH), suprachiasmatic (SCH), supraoptic (SO), and paraventricular (PVH); those of the tuberal zone the arcuate (ARH), dorsomedial (DMH), ventromedial (VMH), and tuberal nuclei (TU); and those of the mammillary zone the mammillary nuclei and posterior hypothalamic nucleus (PH). The periventricular nucleus (PV) of the periventricular zone runs throughout all the rostro-caudal divisions. The majority of the well-defined hypothalamic nuclei lie in the medial zone, while the lateral zone, though clearly heterogeneous, is less neatly differentiated, and contains the lateral hypothalamic area (LHA) and lateral preoptic area (LPO). The major white matter tracts are: the medial forebrain bundle (mfb), which is interspersed with the neurons of the LHA and carries information to and from the spinal cord, brainstem, amygdala, septum, and cortex; the fornix (fx) carrying axons mostly to and from the hippocampus; the stria terminalis (st), which contains axons travelling from the amygdala and which feeds into the medial forebrain bundle; and the mammillothalamic tract (mtt), traveling from the mammillary nuclei to the thalamus and cortex. There is also a wealth of fibers that do not run in a tract but are dispersed through the tissue [2-5]. **Figure 1.1** shows a schematized view of the overall organization.

The hypothalamus is intimately connected with the pituitary gland. Specific magnocellular neurons of the PVH and SO send axons directly into the posterior portion of the pituitary gland, and release the hormones vasopressin and oxytocin into the circulation. Relevant neurons of the PV, ARH, VMH, DMH, and PVH are connected to the anterior portion of the pituitary gland via the specialized hypophyseal portal system, as are neurons distributed in the LPO, and control the release of various pituitary hormones – these are called hypophysiotropic neurons [6, 7]. With reference to the organizational schematic presented in **Figure 1.1**, most

hypophysiotropic cell groups are found in the periventricular zone; except for those in the LPO which lies in the lateral zone [3]. Together with the magnocellular cell groups of the SO and PVH, these neurons can be classified as neuroendocrine motoneurons [7]. Hypophysiotropic neurons release hormones including gonadotropin-releasing hormone (GnRH), thyrotropin-releasing hormone (TRH), corticotropin-releasing hormone (CRH), growth hormone-releasing hormone (GHRH), and somatostatin into the hypophyseal portal system. The median eminence (ME) forms the gateway between hypothalamic axons and this system. The inner portion of the ME, forming the floor of the third ventricle, comprises both magnocellular axons from the SO and PVH destined for the posterior pituitary, and hypophysiotropic axons, which have their terminals in the external ME located immediately ventrally. Also found in the external ME is a plexus of fenestrated capillaries that drains into the pituitary's portal veins and supplies the anterior pituitary with blood – this is the hypophyseal portal system [6]. Interestingly, this system allows for a small amount of backflow from the anterior pituitary to the ME, that can form the basis of a local feedback loop between the hypothalamus and pituitary [8]. Ependymal cells called tanycytes found in the lining of the third ventricle have processes extending into the external ME, where they dynamically surround hypophysiotropic axon terminals and regulate their release of hormones into the capillary plexus. In the anterior pituitary these hormones stimulate the release of luteinizing hormone (LH) and follicle-stimulating hormone (FSH), thyroid-stimulating hormone (TSH), adrenocorticotropic hormone (ACTH), and growth hormone (GH) (respectively); or inhibit the release of GH and TSH in the case of somatostatin [6]. Another hormone of the anterior pituitary, prolactin, is constitutively released in a manner that is restrained as appropriate, chiefly by dopaminergic neurons in the ARH whose axons terminate in the external ME [9].

The hypothalamus receives extensive inputs from the cerebellum, brainstem, and spinal cord, including from the nucleus of the solitary tract, parabrachial nucleus, noradrenergic cell groups, locus coeruleus, VTA, raphe nuclei, reticular formation, and medial lemniscus. There are also inputs from the hippocampus, amygdala, septum, and regions of the cortex (some of these

may be via the thalamus). These connections relay sensory (particularly olfactory, visual, and somatic), emotional, and cognitive information to the hypothalamus. Hypothalamic outputs include but are not limited to the pituitary, amygdala, thalamus, hippocampus, cortex, septum, cerebellum, periaqueductal grey, reticular formation, parabrachial nucleus, nucleus of the solitary tract, dorsal motor nucleus of the vagus nerve, and spinal cord (including motor neurons and sympathetic/parasympathetic ganglia) [2, 10]. Almost all preganglionic nuclei of both branches of the autonomic nervous system, found in the brainstem and spinal cord, receive direct hypothalamic innervation; as well as an array of relay nuclei, some of which are listed above. This innervation derives from cell groups within the PVH, the retrochiasmatic area (RCH) with small contributions from the ARH and VMH, and the LHA and zona incerta (ZI; technically belonging to the subthalamus, this structure lies immediately dorsal to the LHA and shares with it some typically hypothalamic cell populations, e.g. those expressing hypocretin/orexin (H/O) and melanin-concentrating hormone (MCH)). The neurons involved can be classified as preautonomic neurons [7].

Thus, the hypothalamus is neuroanatomically poised to integrate sensory information, emotions, memory, cognitive faculties, and motor responses.

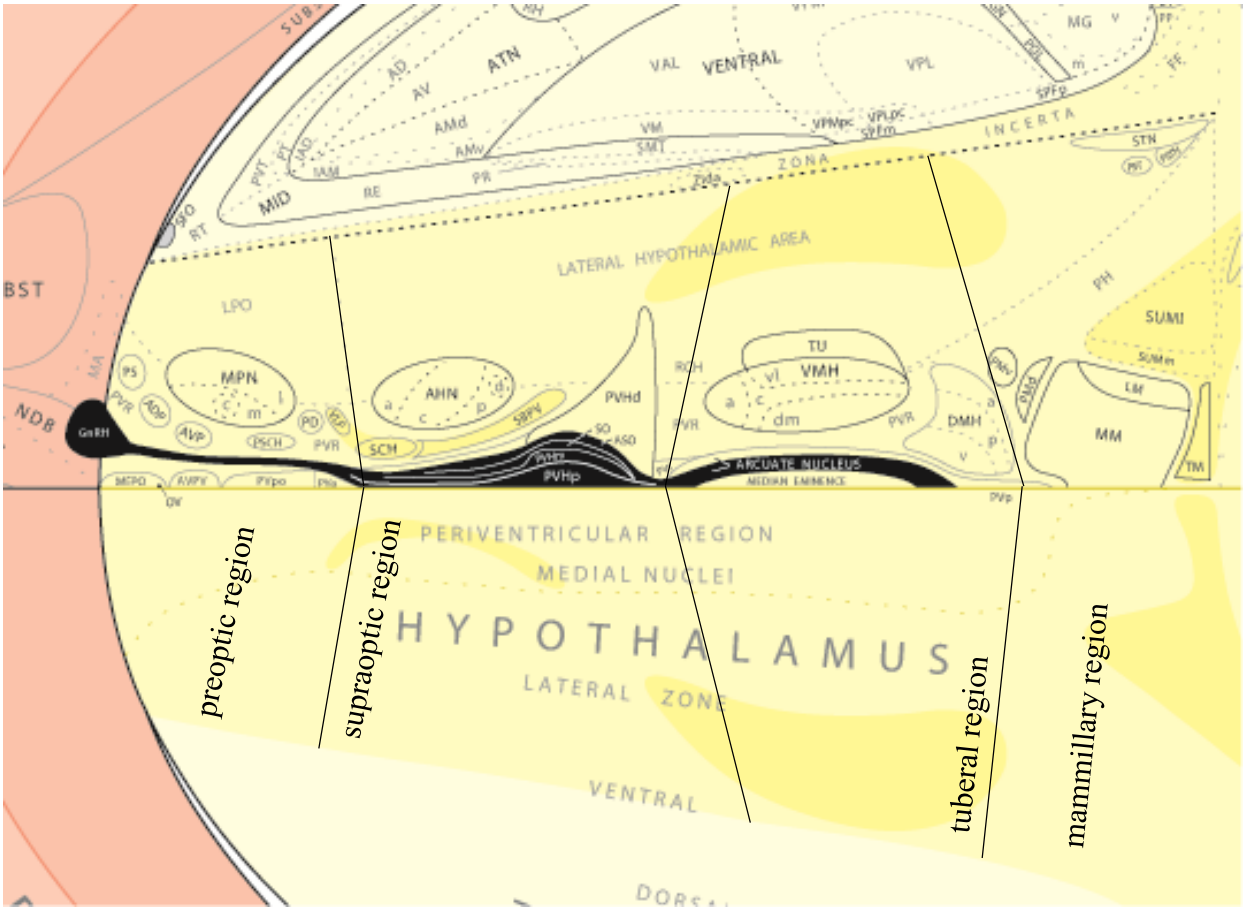

Figure 1.1: Schematic of hypothalamic anatomy, with a transverse view. Adapted from Swanson [4].

Neuropeptides

By the middle of the 20th century it had been known for some time that neurons of the pituitary secreted peptides into the periphery, and in 1953 F. Lembeck discovered that neurons of the spinal cord released substance P; however, that neurons secreted peptides centrally was not known until the 1960s, when David de Wied and colleagues noticed that ACTH, MSH, vasopressin, and other pituitary hormones, including fragments thereof, with no peripheral activity, exerted control over behavior [10, 11]. In 1968 Roger Guillemin and his group isolated the first hypothalamic neuropeptide, thyrotropin-releasing hormone (TRH) [12], and in 1971 de Wied's group coined the term 'neuropeptide' [11]. Presently, over 200 neuropeptides are recognized, and at least 50 of these are found in the hypothalamus [10].

Neuropeptides have several key differences from classical neurotransmitters. There is not a one-to-one relationship between neuropeptides and the genes encoding them; rather, several neuropeptides may be produced from a single gene that codes for a prohormone. Upon translation, this prohormone is targeted to secretory granules (also known as large dense core vesicles) by a signal sequence at its *N*-terminus, and within these granules it is cleaved by prohormone convertases into its products. The cleavage products may be matured by posttranslational modifications including amidation and acetylation [13].

Mature neuropeptides are stored in large dense core vesicles, rather than the small clear vesicles housing small-molecule neurotransmitters. Frequently two or more neuropeptides, derived from the same prohormone, may be contained in the same granule [14]. The fusion of dense core vesicles with the plasma membrane is triggered by a lower Ca^{2+} concentration than that required for small vesicles – and the Ca^{2+} source is not necessarily extracellular; release from intracellular stores such as the endoplasmic reticulum may suffice. Almost universally, neurons that express neuropeptides also express a small-molecule transmitter (the oxytocin/vasopressin magnocellular neurons of the PVH and SO are an exception) [13, 14]. Upon release, most small-molecule transmitters are subject to reuptake by the presynaptic neuron or an astrocyte; in this manner they are quickly cleared from the synaptic cleft and confined to a

small area in the extracellular space (for the most part). In contrast, neuropeptides are not subject to reuptake, instead being degraded by enzymes found in the extracellular matrix, and are free to diffuse through a relatively large volume of tissue – this is called volume transmission [13, 15]. The receptors for neuropeptides are generally G protein-coupled, and they tend to be activated at a much lower concentration of ligand than that required to activate receptors for classical neurotransmitters [13].

The profusion of neuropeptides expressed in the hypothalamus and the phenomenon of volume transmission greatly complicate hypothalamic circuitry.

Functions of the Hypothalamus

The hypothalamus plays a role in a vast array of functions, including motor, autonomic, and neuroendocrine control; reproductive and ingestive behavior; osmotic, metabolic, thermal, and cardiovascular homeostasis; respiration; aggression; sleep/wake cycles; and various motivated behaviors [1, 2]. It has been thought of as a point of connection between 'lower functions' (e.g., the amygdala, brainstem, and autonomic nervous system; emotion and reflexive/instinctual behaviors) and 'higher functions' (e.g., the cortex; cognition) [1]. It contains or is in intimate contact with several structures that have a compromised blood brain barrier: the subfornical organ, the organum vasculosum of the lamina terminalis (OV), the median eminence (ME), and the pituitary [2, 16]. By these routes, a variety of peripherally circulating substances gain access to the hypothalamus, where diverse populations of neurons sense them and thereby acquire information. Many neurons of the hypothalamus can respond to blood-borne factors and nutrients, such as glucose, free fatty acids, amino acids, CCK, ghrelin, leptin, insulin, pituitary hormones, sex steroids, angiotensin, etc. [17-21]. In addition, most hypothalamic structures have been found to possess neurons with axons terminating just subependymal to the third ventricle, where they may release a variety of neurotransmitters and/or neuropeptides, such as H/O, into the CSF. Volume transmission within the CSF is a mode by which several transmitter systems,

notably serotonin, have been proposed to exert a broadly distributed neuromodulatory effect, and the hypothalamus appears anatomically positioned to take full advantage of this mechanism [22].

The function of a number of hypothalamic structures is not known, but is herein briefly described for many nuclei. Running throughout the periventricular region of the preoptic, supraoptic, tuberal, and mammillary zones is the PV, which participates in neuroendocrine control by modulating the activity of hypophysiotropic neurons elsewhere in the hypothalamus. Most notably, the preoptic and supraoptic PV contains somatostatinergic neurons that project to the ME, and downregulate the release of GH and TRH [23, 24]. In the periventricular preoptic zone, the MEPO is involved in maintaining cardiovascular, osmotic, and thermal homeostasis; the AVPV regulates osmotic homeostasis, and GnRH release [3, 25]. In the medial preoptic zone, the sexually dimorphic MPN participates in the regulation and initiation of sexual (especially in males) and maternal behaviors [3, 26]. Also found in the medial preoptic is the AVP, which may function in thermoregulation; and the VLP, which functions in sleep initiation. The PS likely plays a role in osmotic homeostasis, and the PD may be involved in the regulation of sexual behavior, especially for males [3]. The MPO is involved in thermoregulation [25]. The lateral preoptic zone is occupied by the LPO. Investigations of the functionality of this area have been complicated by the presence of the mfb and its attendant multitudinous fibers-of-passage; however, it has been implicated in the promotion of sleep and reproductive physiology [3, 27, 28].

The periventricular supraoptic zone contains the SCH, which is one of the most important hypothalamic nuclei (and arguably one of the most important brain nuclei in general), as it contains the master pacemaker of the brain – most circadian rhythms in the brain (and body, if one includes the daily ebb and flow in quantities of circulating pituitary hormones) are entrained by input from the SCH, which itself is entrained by projections from intrinsically photosensitive retinal ganglion cells. Interestingly, the SCH receives few other inputs, while its strongest output is to the nearby SBPV. It also contains many cell bodies which output to the CSF via the third ventricle [3, 22, 29]. Also in the periventricular supraoptic zone is the PVH, which is one of the

best characterized hypothalamic nuclei. Populations within this nucleus project to the posterior pituitary to release oxytocin and vasopressin; project to the median eminence to release CRH, TRH, and somatostatin; and project to preganglionic autonomic nuclei in the brainstem and spinal cord; and as such the PVH is a center for neuroendocrine and autonomic motor control. It is a crucial regulator of metabolic and osmotic homeostasis, and of stress management [3, 7, 30]. The medial supraoptic zone includes the AHN, which may be involved in behavioral and autonomic components of the fight vs. flight response and in thermoregulation, especially fever generation [26, 31]. Appearing within the AHN is the NC, which likely participates in osmoregulation [32]. Bordering the AHN is the RCH, harboring a population of preautonomic neurons [7]. The lateral supraoptic zone is occupied by the LHA, which extends through the lateral tuberal and lateral mammillary zones as well. The connections of the LHA are highly complex, and as with the LPO, studies of its functionality have been complicated by axons of the mfb. Nonetheless it has emerged as an important region for the control of feeding behavior and sleep [33, 34].

The periventricular tuberal zone contains the ARH, a nucleus that plays an important role in maintaining metabolic homeostasis and also contains a number of hypophysiotropic neurons. There are two well-studied neuronal populations in the ARH: one is composed of neurons co-expressing AgRP and NPY, while the other contains neurons co-expressing POMC and CART; AgRP/NPY cells act to increase feeding while POMC/CART cells inhibit it. Hypophysiotropic neurons in the ARH release GHRH and dopamine [3, 7]. The medial tuberal zone contains the VMH, which is implicated in regulation of metabolic homeostasis, arousal, reproductive behavior, and the behavioral components of the fight vs. flight response [3, 35]. Close by are the TU nuclei, that are likely involved in regulating reproductive behaviors. Also located in the medial tuberal zone is the DMH, which is thought to have its fingers in the control of metabolic and thermal homeostasis, along with stress management and reproductive behaviors [3].

The periventricular mammillary zone is almost entirely occupied by the PVp, whose functions are unclear. The medial mammillary zone comprises the mammillary complex,

consisting of the mammillary bodies (MM and LM), supramammillary nuclei (SUMm and SUMl), premammillary nuclei (PMd and PMv), and PH [3]. The MM appears to respond to theta rhythms in the hippocampus – the rhythm most strongly associated with LTP – and may be involved in episodic memory; while various neurons in the LM code for different aspects of head positioning. Dorsal to the MM, the SUM is partially responsible for generating hippocampal theta rhythms and may also be involved in episodic memory [36-38]. The PMv is extensively connected with sexually dimorphic brain areas and is involved in regulating reproductive physiology and behaviors in response to odorants and metabolic signals, and possibly additionally regulates aggression [3, 39, 40]. The PMd figures prominently in the regulation of defensive behaviors, especially in response to odorants, and also participates in odor-related fear conditioning [41-43]. The PH may also play a role in the generation of hippocampal theta rhythms, similar to the SUM; and also appears to regulate cardiovascular homeostasis [38, 44]. The tuberomammillary nuclei (TMd and TMv) are also located in the medial mammillary zone, and are the sole neuronal source of histamine in the brain. Neuronal histamine is necessary for the maintenance of wakefulness and alertness, and thus the TMd, and especially the TMv, have been implicated in arousal [45-47].

Interactions among Functionally-Defined Circuits in the Hypothalamus

The entanglement of various functionally-defined circuits within the hypothalamus is complex. To illustrate this, an example will be discussed. It has long been noted that the mammalian reproductive cycle is influenced by nutritive status, such that individuals in a negative energy balance experience a suppression of their normal reproductive functions. The reproductive cycle is ultimately driven by the activity of GnRH neurons in the preoptic area of the hypothalamus, which excrete GnRH into the hypophyseal portal system in a pulsatile manner. In the anterior pituitary, GnRH acts to stimulate the release of LH and FSH, which then act upon the gonads to drive the menstrual cycle in females and testosterone production and spermatogenesis in males. This arrangement is known as the hypothalamic-pituitary-gonadal

(HPG) axis. Metabolic stress has been found to inhibit GnRH pulsatility, and thereby the activity of the HPG axis (although the HPG axis is also affected by metabolic stress directly at other levels, albeit with lesser intensity). The precise mechanisms by which signals related to metabolic stress are communicated to GnRH neurons, have been the subject of a large body of research, using techniques such as the analysis of epidemiological comorbidities, central injection studies, and variously precise gene manipulations. The major metabolic hormonal signals that centrally affect reproductive functions are leptin, insulin, and ghrelin; with lesser roles being played by GLP-1, PYY, adiponectin, and others. Generally, leptin (a satiety hormone released by adipose tissue) and insulin stimulate GnRH release, while ghrelin (an orexigenic hormone released by the gut, but also a neuropeptide released centrally) reduces it. GnRH neurons are themselves sensitive to a number of these hormones (insulin, ghrelin, PYY, adiponectin) and to glucose; however, genetic ablation of the underlying receptors is insufficient to cause infertility. Instead, the GnRH neuronal network (a network of neurons responsive to the mentioned hormones, converging on GnRH neurons) mediates the connection between metabolic signals and the HPG axis. In this way, different metabolic signals are integrated to determine if the suspension of reproductive activities is appropriate [20, 48].

A full description of the GnRH neuronal network has not yet been arrived at; but GABAergic neurons possessing leptin receptors (LepR) have already emerged as a key player – mice lacking LepR on GABAergic neurons are subfertile, with delayed puberty [49]. Glutamatergic neurons are also implicated, although less strongly – mice lacking either LepR or insulin receptors on their glutamatergic neurons have normal fertility [49, 50], but mice lacking LepR entirely that have LepR expression reinstated only in the PMv of the hypothalamus (which is almost wholly glutamatergic) show improvement in their fertility and puberty onset [51]. This suggests that at least one population of glutamatergic cells, in the PMv, participates in the GnRH neuronal network. However it should be noted that this network is highly redundant, and therefore difficult to interrogate using precise, simple knockout studies [48]. Therefore populations with an auxiliary role may not be revealed without more elaborate experimental

designs, and the possibility of more glutamatergic contributors should not be discounted. Despite this complication, several additional specific populations in the GnRH neuronal network have been identified (more or less tentatively). GABAergic AgRP/NPY cells in the ARH, whose dominant function is the promotion of feeding, are known to play an important role: these cells maintain an inhibitory tone on GnRH neurons and are themselves inhibited by insulin and leptin, but excited by ghrelin [48]. In infertile, diabetic leptin-deficient mice, ablating AgRP/NPY cells rescued fertility [52]. Also located in the ARH, POMC/CART neurons may function in the GnRH neuronal network in an opposite manner: their excitation in direct response to leptin and/or insulin acts as an excitatory input to the GnRH neuronal network [48]. POMC-specific ablation of LepR and insulin receptors together results in subfertility in mice [53]. Additionally, there is some evidence to suggest that GABAergic cells co-expressing kisspeptin or dopamine in the AVPV, SF1 in the VMH, and dopamine in the VTA are involved – the VTA lies immediately posterior to the LHA, from which it is poorly differentiated, in the midbrain; and participates in reward circuitry [48].

Altogether, this information presents an illustration of functional circuitry in the hypothalamus that possesses many small, redundant, and chemically diverse elements, coordinating to produce appropriate control of various behaviors and physiological events and parameters in many contexts.

The Need for an Improved Understanding of Hypothalamic Circuitry

Because the hypothalamus represents a crucial point of intersection for so many behaviors that are crucial to the quality and maintenance of life, for probably the majority of known hormones (including all those released from the pituitary and gut), and for ‘higher’ and ‘lower’ functionalities, it is one of the most complicated areas of the brain, and one of the most important to understand. Much work has been undertaken in this regard, but progress is hampered by the lack of knowledge concerning basic hypothalamic anatomy – in particular, of the precise distributions of and interactions among the many neurotransmitters that are expressed

in the hypothalamus or that innervate it. The Khan lab proposes to address this deficiency, by creating a high-resolution digital chemoarchitectural atlas of the hypothalamus, following the template provided by the 2004 Swanson atlas of the rat brain [4]. Building our atlas upon the foundation of an existing atlas, widely in use, will allow our data to be easily accessible to others and to be integrated with the large body of work, including a wealth of connectional information, that is already mapped to the Swanson atlas. The first transmitters that will populate this atlas are α-melanocyte stimulating hormone (α-MSH), melanin-concentrating hormone (MCH), and nitric oxide (NO). They have been mapped in Specific Aim 1 of this dissertation. The maximum number of compounds the Khan lab can stain for at once is three, and is limited by the spectra of the available fluorophores. It is of interest to study α-MSH simultaneously with MCH because these compounds have opposing effects on pigmentation peripherally, and on feeding centrally. Species constraints on antibody combinations provide the rationale for the inclusion of NO as the third transmitter.

α-Melanocyte-Stimulating Hormone (α-MSH)

α-MSH was first identified as a pigmentation modulator in fish and amphibians in the first part of the 20th century [54]. Its behavioral effects were noticed in the mid 20th century, and it was first identified in the mammalian brain in the 1970s [55]. In the 1980s it was demonstrated that α-MSH decreases food intake; its stimulatory effect on sexual behavior was already known by that time [56-58]. It has also been known to increase aggression, decrease hole-dipping (which has been used as a measure of exploratory behavior), and increase anxiety [57, 59] – and paradoxically, to increase grooming [60].

Cell bodies expressing this peptide are found exclusively in the ARH and nucleus of the solitary tract, while their fibers are dispersed throughout the hypothalamus, particularly in the PV, PVH, and DMH. They also extend outside the hypothalamus, to the cortex, thalamus, midbrain, and pons [61-66].

α-MSH may be colocalized with a variety of peptides with which it shares a transcript. As is typical for neuropeptides, α-MSH is a cleavage product, in this case of the POMC precursor peptide, which also generates γ-MSH, JP, ACTH, CLIP, β-LPH, γ-LPH, β-END in rats [67]. The distribution of ACTH is quite similar to that of α-MSH [68], and that of γ-MSH also closely matches with α-MSH except that γ-MSH fibers have a higher density in the LHA than do α-MSH fibers [69, 70]. The distribution of CLIP has been reported as very similar to that of ACTH [71]. Expression patterns of β-LPH are more divergent as it is not found in the PVH or DMH (areas of high α-MSH expression), is dense in the ZI (little if any α-MSH expression), and is found in cell bodies strung out along the lower border of the hypothalamus (whereas α-MSH cell bodies are limited to the ARH) [72]. β-END is also not found in the PVH or DMH [73]. In these studies no double labeling with antibodies against α-MSH or another POMC product was done. Studies using multi-antigen labeling have found overall similarity (with some differences) in hypothalamic distribution of ACTH, α-MSH, and β-END; α-MSH was found to have the most intense staining, although this can be no more than suggestive of differences in expression due to discrepancies in antibody affinities [62, 74, 75]. The situation is actually somewhat more complex than this, as some of these POMC products exist in multiple forms [70, 76].

Although the distribution of α-MSH in the brain has been studied a number of times, data have either not been mapped (and have been described textually instead), or have been mapped to atlases no longer in wide use (those of Konig and Klippel, and Palkovits and Jacobowitz) [61-66]. Additionally, no digital versions of these maps are available, and they are low-resolution.

Melanin-Concentrating Hormone (MCH)

In the 1950s MCH was identified as a hormone having an effect on pigmentation in fish antagonistic to that of α-MSH (where α-MSH darkens skin color, MCH lightens it) – however, MCH was not purified and characterized until 1983 [77, 78]. MCH's promotion of food intake was first noticed in 1996 [79] (and is opposite to the effect of α-MSH), and it also seems to have peripheral effects on leptin and insulin secretion, and thermogenesis [80]. However, some

investigators have obtained an inhibition of feeding in response to MCH, depending on the time of day of administration [81]. There is some evidence that MCH inputs to the ARH and PVH increase feeding, but not inputs to the LHA or VMH [82]. It also stimulates the hypothalamic-pituitary-adrenal (HPA) axis, while inhibiting the hypothalamic-pituitary-thyroid (HPT) axis [83, 84]. Additionally, MCH increases slow-wave sleep, and especially REM sleep [85] (interestingly, the dose-response relationship seems to be a bell-shaped curve [85-87]), and MCH may produce anxiety and depression-like behaviors [88] – although it has also been reported as an anxiolytic [89]. It enhances learning and memory [90], and increases sexual behavior [57]. MCH cell bodies are found mostly in the LHA and ZI. However they are also scattered in more medial regions of the hypothalamus, in the DMH and between nuclei. At least some fibers are located in virtually every region of the brain and spinal cord; hypothalamic regions with significant densities are the DMH, mammillary nuclei, AHN, preoptic area, and LHA. Outside the hypothalamus, high densities are found in portions of the cortex, thalamus, amygdala, hippocampus, septum, basal ganglia, ZI, colliculi, parabrachial nucleus, periaqueductal grey, VTA, raphe nuclei, interpeduncular nuclei, and reticular formation.

MCH is produced from prepro-MCH (ppMCH), along with NEI and NGE. MCH is extensively colocalized with NEI and the two peptides largely – but not entirely – share projection patterns [91-93]. Increased locomotion and grooming have been noted in response to NEI [60], and NEI has not been found to impact feeding behavior [94-96]. The distribution of NGE has been studied but not with simultaneous labeling of MCH or NEI in the same tissue set [97]. There is also an alternative splicing variant of MCH, called MCH gene overprinted polypeptide (MGOP), and a peptide whose gene sequence partially overlaps with the ppMCH gene (antisense RNA overlapping from MCH; AROM) – the functions of these species have not been determined [80].

Although the MCH distribution has been well documented with photomicrographs and summary tables, these studies do not report maps to a reference atlas [98, 99]. The distribution of

MCH cell bodies (not fibers) has been mapped in the hypothalamus and immediate surround to the Swanson atlas [100].

Nitric Oxide (NO)

In 1983, it was reported that there are several discretely located populations of cells within the brain that contain an NADPH-diaphorase enzyme, which can reduce a dye to a colored product and thus be used in staining procedures for these cells [101] – the use of endogenous dehydrogenases in staining had been known for at least two decades already. Around 1990, it was discovered that the endogenous NADPH-diaphorase was actually a neuronal nitric oxide synthase (nNOS) [102]. The presence of NO in the brain had been demonstrated a few years earlier but its function was not understood [103]. Peripherally, NO was well-known as a vasodilator, and soon it was learned that it promotes synaptic plasticity, thereby enhancing both learning and forgetting (LTP and LDP) [104]. It also suppresses drinking in dehydrated animals, and is a required messenger mediating the effects of a variety of neuropeptides and peripheral hormones on feeding, including ghrelin, leptin, CCK, H/O, and NPY. This means that it exerts either a positive or negative effect on feeding, depending on which of these systems is activated [105-108]. It is necessary for glucose-sensing by neurons of the VMH [109]. NO also underlies CRH release, needed for stimulation of the HPA axis, and GnRH release, needed for stimulation of the HPG axis [110]. It plays a complex role in nociception as well [111]. Mice lacking nNOS are aggressive and display increased sexual behavior [112]. NO has been noted to affect the release of acetylcholine, glutamate, GABA, dopamine, epinephrine, norepinephrine, histamine, serotonin, and adenosine [113].

There are three types of nitric oxide synthases: an endothelial form (eNOS), an inducible form (iNOS) that allows macrophages to generate NO as a means to kill bacteria, and the neuronal form (nNOS). Like other neurotransmitters, NO is released in response to increased intracellular Ca^{2+} levels, but unlike other transmitters, it passes easily through membranes and has no dedicated receptor(s). Instead, it targets a variety of intracellular enzymes; its activation of

guanylyl cyclase (which triggers production of the second messenger cGMP) is the best described [110]. It acts as a retrograde transmitter, one of the only such known, and can act in its neuron of origin as well [114, 115].

Because NO is a gas that can diffuse freely through tissue, because it has a very simple structure that is not easily recognized by antibodies, and because it has a half-life of less than 5 seconds, it is not stained for directly; rather, nNOS is stained, either with an antibody or by incubation with a substrate that nNOS can reduce to a colored product (NADPH-diaphorase method) [108]. Cell bodies expressing nNOS are dispersed throughout the brain, with particularly dense populations in the basal ganglia and tegmental nuclei, and less dense cell bodies/fibers in the periaqueductal grey, cerebellum, cortex, amygdala, thalamus, ZI, colliculi, VTA, interpeduncular nuclei, raphe nuclei, parabrachial nucleus, cerebellum, reticular formation, and several nuclei of the cranial nerves including the nucleus of the solitary tract. This is not an exhaustive list. The hippocampus has few nNOS neurons but a wealth of fibers. Within the hypothalamus, the preoptic and anterior hypothalamic areas, PV, PVH, LHA, SON, VMH, DMH, PH, TU, and mammillary nuclei contain cell bodies and fibers [102, 103, 116-120]. Although the distribution of nNOS has been studied by many investigators, it has only been mapped once, to the Paxinos & Watson atlas [119]. Another study has reported annotated photomicrographs [118]. No digital versions of nNOS maps are available.

The Boxed-Data Dilemma

The purpose of reporting data on the location of chemical labeling, central injections, or other physical or chemical manipulations of the brain, is to benefit the scientific community by providing additional context to experimental data such as behavioral measures, and by increasing the sum total of information available about how neuroanatomy is linked to neurophysiology. Verifying the anatomical location of injection sites, for instance, is also important within a lab, in order to confirm that targeted sites were actually injected, etc., but this use of the information is of less relevance to the scientific community as a whole as its relevance does not extend beyond

the particular study during which it was generated. However, the locations of injection sites are important to the scientific community insofar as they may help others interpret the associated data in their larger neuroanatomical context. It is logical to report such information in the form most useful to the community – which inevitably is a generalized and abstracted format (such as a map), rather than a literal presentation (such as a photomicrograph). Abstractions of research data in the form of maps and other models lose detail but gain salience.

However, not all model systems for representing brain anatomy are inter-compatible; in fact, as a rule they are worlds unto themselves, and the information contained within them has been siloed, whether by necessity or by practice. This curtails the represented information's utility. For instance, each atlas of the rat brain is a separate model of the rat brain. Data mapped to a particular atlas becomes represented in that rat brain model, and in no others. It is not simplistic to assess how the data might appear were they represented in a different model of the rat brain; i.e. a different atlas. It is quite possible to approximate where the data might fit in another atlas than the one they are mapped to, but this requires some amount of time and experience and is necessarily imprecise.

This makes it difficult to evaluate data mapped to one atlas, in light of data mapped to another. A central injection site associated with a particular elicited behavior and mapped to the Paxinos & Watson atlas may look as though it could potentially overlay a given fiber system that was traced and mapped to the Swanson atlas, but one cannot be sure without reconciling the Paxinos & Watson model with the Swanson model – especially if the data lie in a brain area that is conceptualized differently in each atlas.

An added difficulty arising from the use of multiple, siloed brain models to record data, is that these models may fall out of use, and all data logged within them potentially become obsolete. This deficit may be manifest in the need to repeat past experiments (witness Aim 1 of the present work), or simply in missed opportunities – a fiber system hit by a central injection in by-gone years that revealed its function, yet the mapped data languish anonymously within the confines of an old-fashioned brain model, effectively revealing – nothing.

There is one further unfortunate consequence of this situation, which is that it retards the development of a rat brain model that incorporates all mapped data, or as much of them as possible; or the reconciliation of all information about the rat brain that can be tied to its anatomy within a single conceptual framework.

A means of migrating data between atlases, therefore, would be of great utility. Since many atlases of the rat brain are based on a shared coordinate system (stereotaxic coordinates), it seems that the development of a methodology for transferring mapped data from one such atlas to another should be feasible. In the stereotaxic coordinate system, axis origins are located with reference to the skull of the animal in question, and are determined using the stereotaxic instrument employed to fix an animal in flat-skull position during neurosurgery. Although many atlases of the rat brain have made use of this system [121], today only two are in wide use: The Rat Brain in Stereotaxic Coordinates, by Paxinos & Watson [122, 123]; and Brain Maps: Structure of the Rat Brain, by Swanson [4]. If these reference spaces could be reconciled, a vast amount of data would gain new context, and the goal of realizing a unified model of the rat brain would be that much more feasible. Therefore the Khan lab has undertaken to address this issue; and in Specific Aim 2 I have assayed an attempt at creating a systematic methodology useful for migrating data between these atlases, and begun an effort to assess the degree to which the atlases differ using statistical analyses.

Specific Aim 1: Contribute To A Chemoarchitectural Atlas Of The Rat Hypothalamus

Objective

The goal of this specific aim is to begin a massive hypothalamic mapping endeavor. When complete, the hypothalamic chemoarchitectural atlas will provide information on the distributions of many neurotransmitters and neuropeptides; whether they co-localize with each other and where such colocalized populations are to be found; and where synapses between different chemically defined populations are located. This will improve upon existing maps of neurotransmitters in the hypothalamus by being more comprehensive, more detailed, and including information on circuitry (location of synapses). It will also be available digitally, in the form of Adobe Illustrator files, which will allow other investigators to easily manipulate it, and in the form of archived information in the online neuroanatomical database, Brain Architecture Management System 2 (BAMS2).

This particular chapter of the endeavor is focused on providing detailed information on the distribution and colocalization of the neuropeptides α-MSH and MCH, and the enzyme nNOS, as well as information regarding locations where a search for synapses between neurons of the studied chemical systems may be more likely to bear fruit. We have nominated such regions possible synaptic interaction zones (PSIZ).

Materials and Methods

Figure 2.1 provides an overview of the methodology used to complete this Specific Aim.

Animals

Adult male Sprague-Dawley rats, in the weight range of 290–315 grams, were used for these studies. Animals were maintained on a 12-hour light/dark cycle (‘daytime’ from 7:00 am to 7:00 pm), and provided free access to food and water. The University of Texas at El Paso Institutional Animal Care and Use Committee approved the methodology of all experiments described herein.

Tissue Processing

Animals were sacrificed upon reaching an appropriate weight, following the procedures described in [124]. While sedated with inhaled isoflurane, animals were perfused first with 0.01 M sodium phosphate-buffered saline (pH 7.4 at room temperature), and then with cold 4% para-formaldehyde in sodium tetraborate decahydrate buffer (pH 9.5 at 4°C). Animals were then swiftly decapitated using a guillotine, and brains were dissected out of the skull. Brains were fixed at 4°C in 20% sucrose, 4% para-formaldehyde buffered in sodium tetraborate decahydrate until saturated, then frozen in hexane over dry ice and stored at –80°C. Sectioning was carried out using a sliding microtome equipped with a freezing stage packed with dry ice. 20 μm-thick coronal sections were collected as six 1-in-6 series from levels 14 to 38 in the Swanson atlas, or else as five 1-in-5 series from level 14 to 38 in the Swanson atlas. Series were stored in cryoprotectant at –20°C.

Immunofluorescence Histochemistry

Immunofluorescence histochemistry was performed after [125] (excepting the substitution of DAPI for NeuroTrace). Each fluorescently stained series contains four labels: three directed against various molecules involved in neurotransmission, and one directed against cellular nuclei (DAPI). Antibodies and conjugates used are described in **Table 2.1**.

Sections were rinsed in Tris-buffered saline (TBS; pH 7.4 at room temperature) in a set of 5x5 washes (5 washes lasting 5 minutes each), prior to incubation with blocking solution (BS; 2% normal donkey serum and 0.1% Triton-X in TBS) for 1–2 hours at room temperature. Subsequently, sections were incubated with primary antibody solution prepared in BS for 14–16 hours at 4°C. Tissue underwent a 5x5 wash before incubation with secondary antibody solution prepared in BS for 4–6 hours at room temperature in the dark. From this point onward all incubations and washes were conducted in the dark (using the expedient of a piece of foil). Another 5x5 wash preceded incubation with 1:500 parts Alexa Fluor 488-conjugated streptavidin and 1:1,000 parts DAPI in BS for 1 hour at room temperature. Stained sections were mounted on

SuperFrost Plus slides, coverslipped in sodium bicarbonate-buffered glycerol sealed with nail polish, and stored at 4°C wrapped in foil.

Nissl

Sections were mounted on slides subbed with gelatin for improved tissue adherence, and dried overnight at 60°C. Mounted sections were dehydrated in successive alcohol concentrations (0%, 50%, 70%, 95%, and 100% alcohol in deionized (DI) water), defatted in xylene, rehydrated, stained in 0.5% thionin, differentiated in 0.4% acetic acid, rinsed 3x in DI water, dehydrated, and cleared in xylene. All incubations lasted 3 minutes except those in xylene (10–15 minutes) and the thionin, acetic acid, and rinse steps ('to taste'). Slides were coverslipped in DPX without being allowed to dry.

Imaging

Sections were imaged at 20x resolution using an AxioImager M2 upright fluorescence microscope fitted with a motorized stage and appropriate filters. Single 20x shots were stitched together with Volocity 6.1.1 to generate high-resolution, wide-field images. An LSM 700 confocal microscope with a motorized stage and 405 nm, 488 nm, 555 nm, and 639 nm wavelength lasers was used to image some sections at 63x, and to take *z*-stacks.

Mapping

The fluorescent staining was mapped to the 2004 Swanson atlas of the rat brain [4] using Adobe Illustrator CS6 and a Wacom Bamboo pen tablet. **Figure 2.2** provides an overview of the steps involved in this process. The Nissl series is the basis for such maps, and because there is a maximum of 120 μM between the Nissl series and any fluorescent series, the Nissl is an almost-exact copy of all other series. The following is a detailed description of the methodology and considerations involved.

Firstly, the plane of section difference between the atlas and the experimental brain must be accounted for. Failure to do so results in errors wherein staining occurring in one nucleus is mistakenly mapped to a nucleus anteriorly or posteriorly adjacent to it (with coronal sections). It

is possible to quantitate the medial-lateral plane of section difference between two tissue sets using trigonometry, as shown in **Figure 2.3**. One must choose a fiducial (that is, a structure that can serve as a landmark) to use as the basis for the determination – this fiducial must be highly symmetrical, be near the area of interest and as far as possible from the midline, and must possess an easily defined feature that is restricted in its spatial extent and is present in different sections on the two hemispheres. The two instances of this fiducial (one in each hemisphere) describe a right triangle, wherein the distance between the fiducial's defined feature in each hemisphere in a perfect plane of section (assuming symmetry pertains) forms the hypotenuse of the triangle and the distance between the sections in which the fiducial's defined feature occurs forms the opposite side. The distance between the fiducial's defined features in the actual plane of section of the tissue forms the adjacent side. Since the section thickness is known, the opposite side is known, and the adjacent side may be estimated by measuring the distance between the fiducial's defined feature and the midline in each of the two sections and adding. The inverse tangent function allows derivation of the desired angle (see **Figure 2.3**). The estimation may be refined by successive iterations, in which the approximate plane of section is used to improve the estimate of the adjacent side's length, which is then used to obtain an updated value for plane of section, etc. The same method, with slight adaptations, may be used to compare the dorsal-ventral plane of section between two brains, but not to find an absolute plane of section error, due to lack of an appropriate axis of symmetry. For brains wherein only one series is Nissl-stained, the Nissl sampling frequency is often too low to permit such calculations, as it is unlikely that a fiducial's defined feature will be present in different sections in the same series. Therefore, alternative accommodations must be made.

A careful examination of the structures in the Nissl versus those in the atlas will allow one or more atlas levels to be assigned to each Nissl section. This method is robust to asymmetries present in fiducials, as so many are considered that an overall trend of greater development of fiducials on one side or the other will emerge – for instance, it may be found that the right hemisphere is caudal to the left, and so in many sections the right-most side may

correspond to the atlas level immediately posterior to that level which the left-most side corresponds to. Where exactly the boundary between atlas levels represented in the section lies must be estimated and can be represented with a line(s) drawn onto the section, as shown in **Figure 2.4**. Note, however, that much of the section will perforce lie between atlas levels, and there may be areas wherein elements distinctive of one level intermingle with elements deriving from another. Therefore, it is unwise to regard the line separating atlas levels on a section as a hard and fast rule – viewing it as a guideline that may be overlooked if warranted is a more effective strategy. The boundary distinguishing regions of a section mapped to one atlas level from regions mapped to another may thus be meandering. This method will greatly reduce but cannot completely remedy errors resultant from plane of section differences between brains.

The next item in the methodology is the parcellation of the Nissl sections, based on the assigned atlas level(s) – this simply means to draw lines in Adobe Illustrator in a layer over the Nissl that delineate the boundaries of structures therein (**Figure 2.5**). In actual practice, it is advisable to parcellate at least some structures simultaneously with or even before assigning atlas levels, to avoid bias (that is, to be led more by the cytoarchitecture present in the sections than by the layout of the atlas). Level assignments and parcellations are reciprocal processes. Cellular morphology, density, and variety are the principle determinants of cytoarchitectural parcellation. It should be borne in mind that the disposition of assignments, and in particular boundaries between parts of a section that map to different levels, may be refined based on parcellations, such that level assignations/plane of section corrections and the structures in the Nissl is only relevant insofar as it sheds light on the disposition of the structures in the fluorescent staining – thus any 'outlier' cells in the Nissl should be ignored when parcellating because they will not be present in the other series. Additionally, smooth lines are to be preferred – not for aesthetic reasons but because they are more likely to represent the overall trajectory of the boundary across multiple sections. Some structures, and particularly substructures, may be exceptionally subtly distinguished from each other and the surround. Dashed lines (or some such) may be

employed to convey differences in confidence regarding certain parcellations. This qualification is not standard practice in mapping, but increases the honesty of reporting.

A couple of additional considerations apply during parcellation. It is important to note the orientation of the brain during cutting, as the tissue which first encounters the microtome blade will be compressed. Therefore it is advisable to orient the brain on the stage such that the region of interest faces away from the blade; however, this may not always be possible, and in such cases one should recognize that some nuclei near the edge of the brain may appear denser and their cells more compact than is natural. Additionally, the thickness of the brain sections collected must be taken into account as thicker sections will appear more densely cellular than thinner sections – therefore it is good practice to select a fixed section thickness for a project. In general parcellations may be easier with thicker sections.

The analysis up to this point will allow determination of which sections most closely correspond to each atlas level under consideration. It is not necessary to proceed with sections that map to areas of atlas levels that are better represented by other sections.

At this point it becomes necessary to align the Nissl sections with the corresponding fluorescently stained sections. Although the sections are only from 20–120 μm apart, due to distortions arising in histological processing (most notably in mounting) they will not have the same shape once stained and mounted. To align the sections a landmark is required that is located internally, is relatively stable in the face of processing distortions, can be unambiguously identified, and maintains a consistent arrangement or location in successive sections. Blood vessels meet these requirements. The overall strategy for alignments is thus to import images of successive sections into a single Illustrator file (images needed are of the Nissl, the fluorescent series being analyzed, and any series that lie between them), to identify and outline blood vessels appearing in multiple sections, and to arrange the outlines (images moving along with them) such that vessels in different sections assume a logical spatial relationship. It is preferable to outline a large number of vessels, since some may be more distorted than others – in this way a general consensus may be taken and a ‘best-fit’ alignment arrived at. When making the

alignments, it should be borne in mind that vessels caught running in the plane of section of the tissue provide more information (fewer degrees of freedom) than vessels running more or less orthogonal to the section plane, and that vessels caught branching provide more information still. These vessels should be given more weight in the consensus alignment (**Figure 2.6**). In order to maximize the facility of identifying vessels in fluorescent sections, the image brightness may be increased and the contrast decreased, thereby enhancing the background staining (**Figure 2.7**). If there are areas of the sections in which the quality of the vessel alignments is decreased (so that quality in other areas may be increased), these should be marked so that in the next step it can be recalled that correspondence in that area between the Nissl and the fluorescent section is diminished. **Figure 2.8** demonstrates the higher quality of alignments based on blood vessels versus based on section outlines.

Now the Nissl parcellations may be transferred to the fluorescent sections. Because the boundaries of many well-defined nuclei may be surprisingly inconstant from section to section, it is wise to pull any and all structural information present from the fluorescent sections. White matter tracts are generally quite easily visualized in fluorescent staining, based on differences in background (see **Figure 2.7**). The DAPI stain, which is the fourth label in all fluorescent series used, is useful for determining regional differences in cellular density, and can be used to parcellate a number of structural nuclei. A partial parcellation of the fluorescent sections should be made based on these sources (**Figure 2.9a**). The Nissl parcellation is fitted on top of it in Illustrator, and is transferred as appropriate – which elements of the Nissl parcellation are transferred directly and which are tweaked to better fit the partial fluorescent parcellation will depend on a variety of factors: the completeness of the partial parcellation, the quality of correspondence between the Nissl and fluorescent section from region to region as determined during vessel alignments, the apparent match or mismatch between the Nissl and fluorescent parcellations in each area, and the mapper's professional judgment (**Figure 2.9b, c**). Again, dashed lines or the like may be used to distinguish areas of high confidence from those of lesser confidence and greater ambiguity, along with color-coding to indicate which elements of the

transferred parcellation derive from information present in the fluorescent sections themselves, and which derive from the Nissl and therefore have lesser confidence.

This produces fully parcellated fluorescent sections that form the basis for the maps. A representation of the staining patterns may now be made on the relevant digital atlas plate(s) in Illustrator. For cell bodies, distribution and density should be represented; for fibers, distribution, density, length, and orientation. Diffuse staining (which likely belongs to neuropil) can also be shown (**Figures 2.12–2.33**). It is not necessary or feasible to create a map with a one-to-one correspondence between mapped cell bodies/fibers and those present in the section. Instead, relative densities/amounts should be conveyed. Standards should be established regarding how different densities are denoted, to reduce subjectively generated variance (especially since it is not possible to complete this task within a day or anything near it). Different colors may be employed to mark differences in confidence, or if images of the parcellated data series are shown uncertainty may be conveyed in these.

In this stage it becomes necessary to determine what staining is signal and what staining is background noise. Many faint fibers and cell bodies are likely to be visible in various brain regions. Because the occurrence of these dim elements is generally patterned, they are unlikely to represent autoflorescence of the tissue. They are more likely the result of nonspecific antibody binding, or they may reflect the presence of very small amounts of antigen – especially when the antigen is a neuropeptide in tissue not treated with colchicine, due to efficient axonal transport which may result in very little neuropeptide being present in soma [126, 127]. Controls for antibody specificity may only partially address the question. The interpretation of faint staining is thus subjective, and can have a large impact on the appearance of the final map.

Additionally, the influence of imaging artifacts and processing must be taken into account. After imaging it is generally necessary to alter the white or black points and the gamma correction, to reveal faint staining while reducing background. Generally it is advisable to capture images with a relatively low exposure time, so that the brightest elements in the image will not appear saturated, which bloats their size and ablates any details that might be present.

This practice frequently obligates the use of these image processing tools, especially if the exposure time is not altered between different images. However, different images will require different degrees of processing, for instance resulting in inconsistencies in the brightening of the images – thus faint labeling in a given image that was brightened more than another given image may in actuality be much more faint than faint staining in the other image. While not necessarily consequential, effects of this sort should be borne in mind while creating final maps.

Image artifacts created by small specks of debris on the slides may mimic cell bodies, but are generally brighter and larger than most cells and can generally be distinguished from true staining. Another persistent artifact in stitched images is a tiling effect created by graduated illumination levels in each individual field captured, even with Köhler illumination. Depending on the software used for stitching, this effect is very difficult or impossible to eliminate in fluorescent microscopy, though it can be removed in brightfield microscopy more readily. The result of this tiling is that staining in some regions (the center of each field) appears brighter than in others (the edges of each field), in a manner that is unrelated to, and may obscure, actual differences in the strength of labeling that may be present. This must be corrected for during final mapping as well as possible, and may easily be overlooked by novice mappers.

Considerations regarding the thickness of sections and the orientation of the brain during cutting discussed previously for Nissl parcellations apply to final mapping as well. If the region of interest is near the edge of the brain, and this edge faced the blade in cutting, some tissue will be compressed, and the fluorescent staining will appear artificially dense. One may refer to the degree of compression and density-alteration present in the Nissl material to approximate the degree of distortion, and mapped densities should be altered accordingly. Additionally, thicker sections will appear denser than thinner sections. While thicker sections are likely to be preferable during Nissl parcellations, they are less advantageous for final mapping, especially if fibers are being mapped, because fibers outside the plane of focus during imaging may appear so blurry they are mistaken for image artifacts or not seen at all. A thicker section will have more fibers that fall above or below the plane of focus than a thinner section.

While mapping cell bodies, colocalization between different antigens must be scrupulously checked by importing a single-channel image for each antigen stained for in that series, aligning the images, and switching the visibility on and off (**Figure 2.10**). Ideally colocalization will be visible in a merged image as a combination between the colors of the fluorophores involved; however, if the intensity of labeling for one antigen very much exceeds that of the other, the weaker labeling will frequently not be apparent. In some of these cases a decision must be made as to whether the weaker labeling is in fact signal, or if it is background.

In some cases wherein an atlas level spans multiple sections, the fluorescent staining on the rostral section representing that level may differ from the staining on the caudal section. It is likely in these cases that at least one of the sections in question falls just rostral or caudal to the classical atlas level, yet lies much closer to the level selected than to any other level. These discrepancies must be resolved through reliance on the mapper's professional judgment on a case-by-case basis. In general, any interesting elements in the staining on either section should likely be represented on the final map. A note in the text may indicate which staining lies rostrally and which caudally.

A final difficulty consists in the resolution of discrepancies between the atlas parcellation and the fluorescent parcellation (see **Figure 2.11**). Especially for subparcellations of the LHA, whose cytoarchitectural structure is exceptionally subtle, there may be some considerable difference between the exact shape of the subregions in the atlas and in the experimental sections. It should not be forgotten that any brain atlas is a hypothesis regarding brain architecture rather than confirmed fact, and Larry Swanson himself has said that the LHA subparcellation is highly variable from brain to brain and that his parcellation is not necessarily present in all tissue sets [personal communication]. This leads to an interesting philosophical quandary: should the integrity of observed neuronal populations be preserved at the expense of that of the subparcellation, or vice versa? In **Figure 2.11**, the circled population of MCH-immunoreactive cells falls in an area wherein my parcellation differs from that of the Swanson atlas. In the corresponding MCH map, I have split this population, distorting its arrangement in

the actual tissue such that it is mapped to the substructures in which I observed it (preservation of the integrity of the subparcellation at the expense of that of the population). The advantage of doing it this way is that users of the chemoarchitectural atlas will know what substructures they can expect to find the population in, while the disadvantage is that users will not realize that it is a single population rather than two (unless I specify this and they trouble to read all such specifications). I have recently reconsidered this decision, and will follow the alternate course in future mapping. I have reproduced this map here as an example. My reasoning is as follows: whether or not preserving the subparcellation versus populations is more accurate is likely dependent on whether the subparcellation is, in fact, correct. As it stands, it is a hypothesis (based upon evidence [4]) awaiting further experimental validation. Chemoarchitectural information is one type of data that might be used to endorse or dispute the hypothesized subparcellation. As pertinent data should be used to shed light on a hypothesis, rather than using the hypothesis to color representation of the data, it is more appropriate to show populations as they are, regardless of whether representation of the substructural location of the population is altered by this. Of course, there is also the possibility that the atlas subparcellation is correct but that my parcellation is not (that is, that the difference between the two is the result of a mistake on my part and in actuality there is either no difference or a different difference), in which case it were also preferable to represent the population as is. These sorts of considerations are a major reason why it is much more honest and useful to other investigators to distinguish between areas of high confidence and low confidence in the maps.

Table 2.1: Antibodies and Conjugates Used in Immunofluorescence Histochemistry.

Antigen/Conjugate	**Species**	**Manufacturer (Catalogue #)**	**Concentration**
α-MSH	sheep polyclonal	Millipore (AB5087)	1:20,000
MCH	rabbit polyclonal	Phoenix Pharmaceuticals (H–070–47)	1:20,000
nNOS	mouse monoclonal	Santa Cruz Biotechnology (sc–5302)	1:5,000
mouse IgG-cy3	donkey	Jackson ImmunoResearch (715–165–150)	1:500
rabbit IgG-cy5	donkey	Jackson ImmunoResearch (711–175–152)	1:500
sheep IgG-biotin	donkey	Jackson ImmunoResearch (713–065–147)	1:500
streptavidin-Alexa Fluor 488	n/a	Jackson ImmunoResearch (016–540–084)	1:500

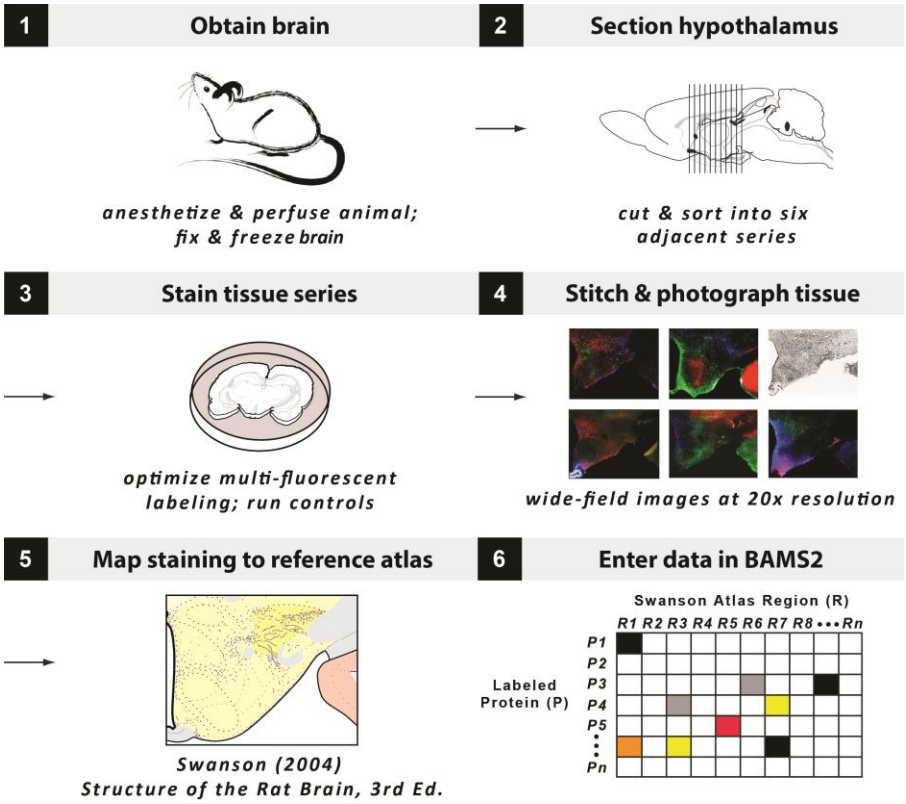

Figure 2.1: Workflow for Specific Aim 1.

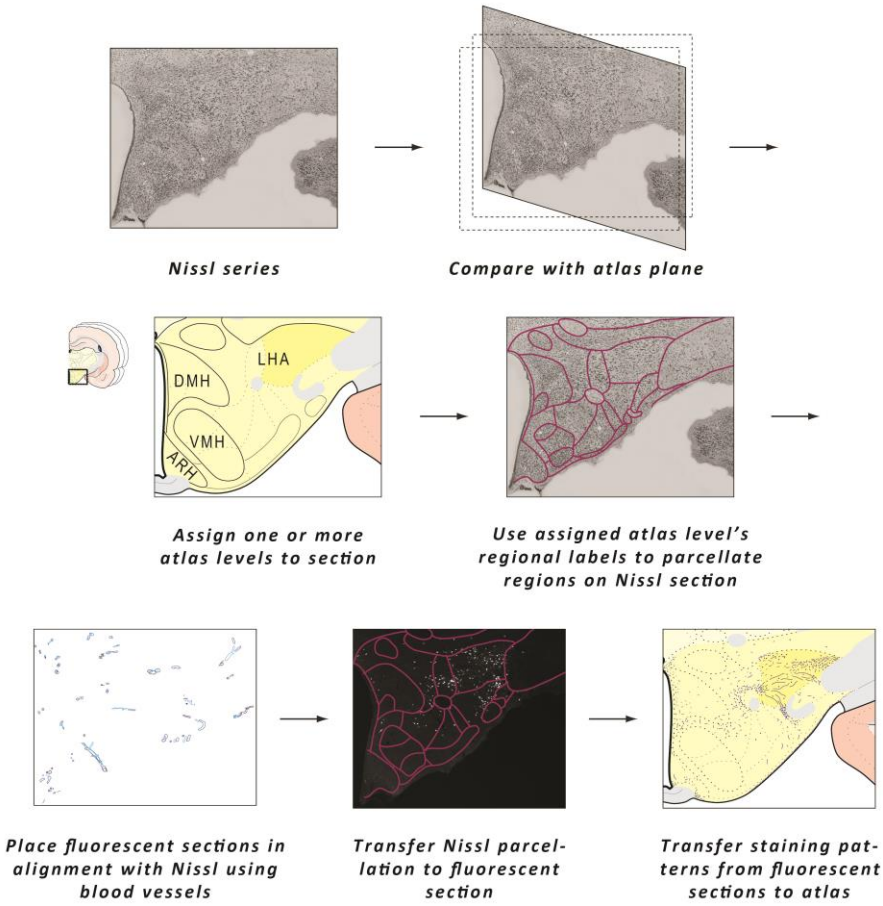

Figure 2.2: Overview of the Mapping Process.

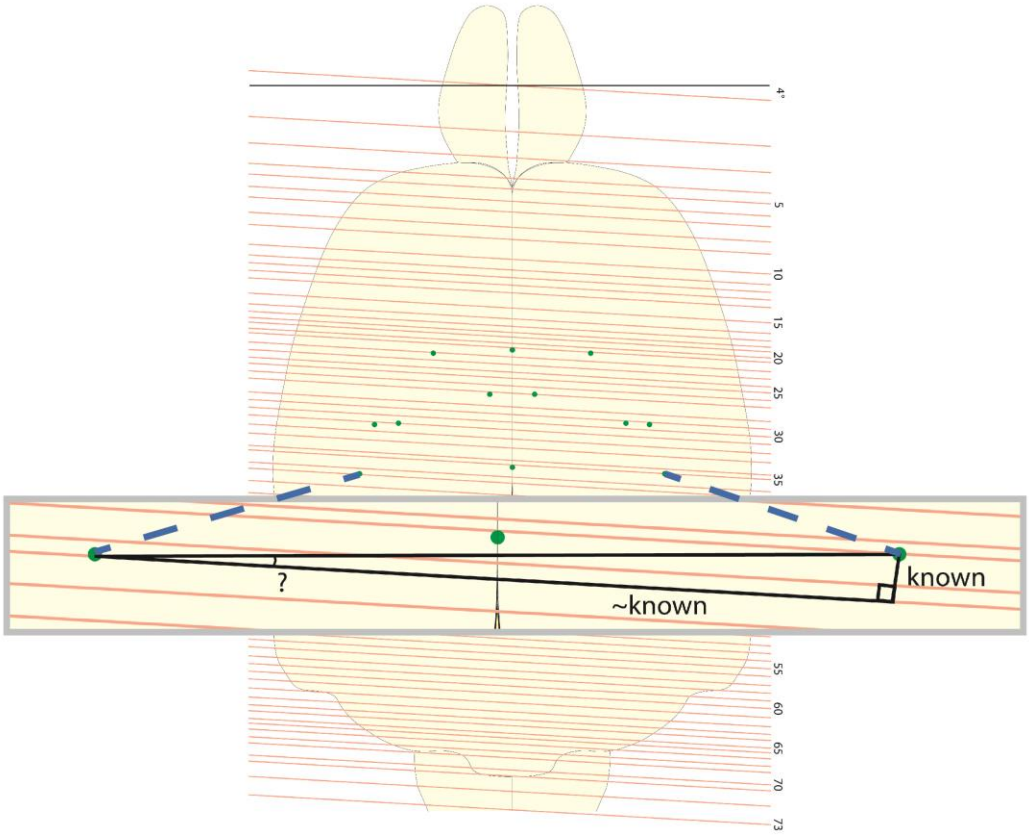

Figure 2.3: Determination of Plane of Section.

Transverse view of the brain used to create the Swanson atlas, with atlas levels shown as red lines. Green dots represent fiducials chosen to calculate the medial-lateral plane of section difference of the atlas brain from a true coronal section. The orientation of the atlas levels shows the plane of section error, found to be 4°. The enlargement shows the trigonometric determination of plane of section error. Adapted from Swanson [4].

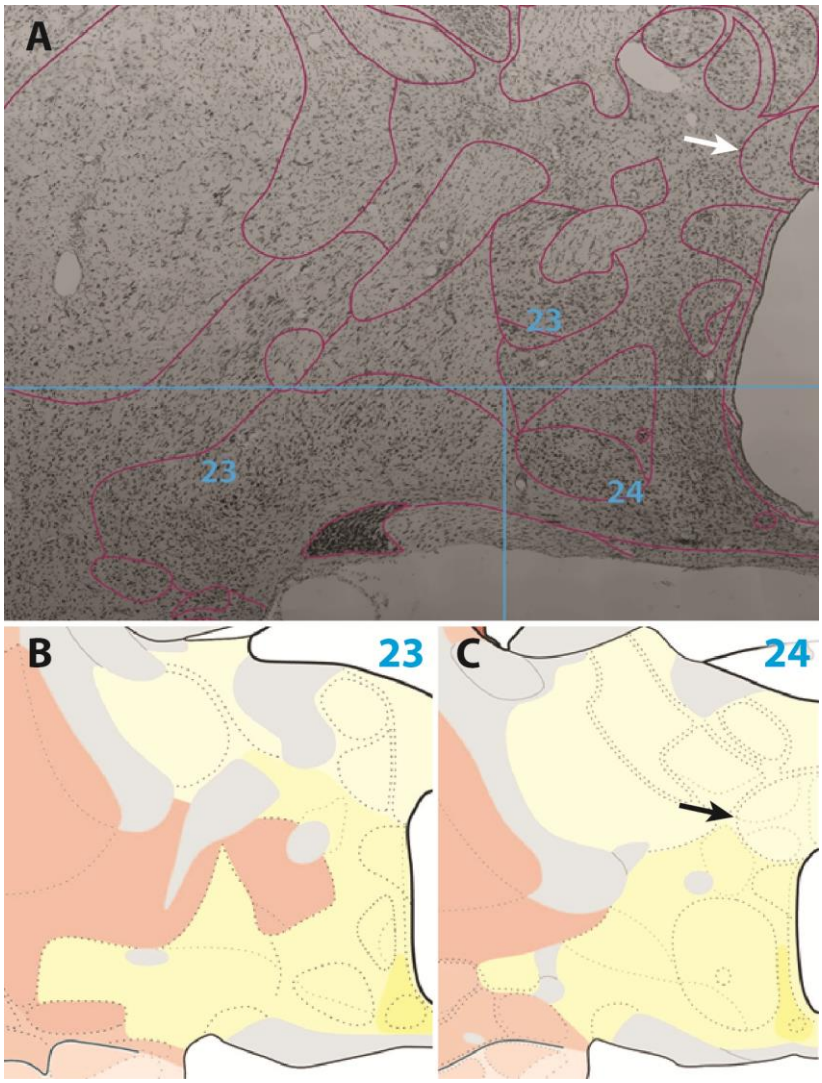

Figure 2.4: Accounting for Plane of Section in Mapping.

(A) A Nissl-stained section mapped to levels 23 and 24 of the Swanson atlas. Blue lines indicate, roughly, the boundaries between levels. The arrows indicate a structure (the nucleus reuniens) in the Nissl which corresponds to level 24, although the surrounding structures more closely match level 23. **(B)** Level 23 of the Swanson atlas. Reproduced from [4]. **(C)** Level 24 of the Swanson atlas. Reproduced from [4].

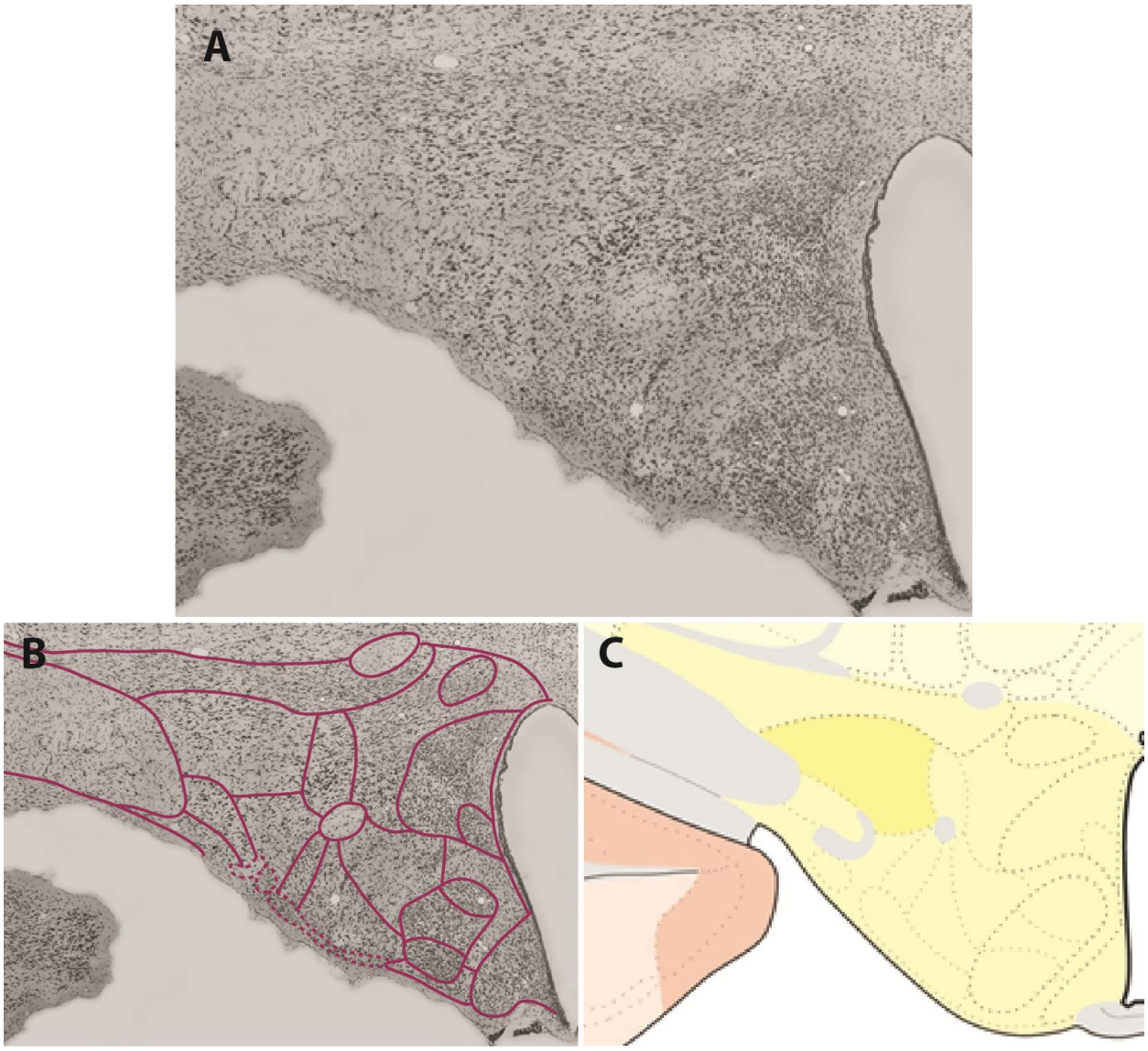

Figure 2.5: Nissl Parcellation

(A) Unparcellated Nissl section assigned to level 29 of the Swanson atlas. **(B)** Parcellation of the section in **A** based on **C**. **(C)** Level 29 of the Swanson atlas, reproduced from [4].

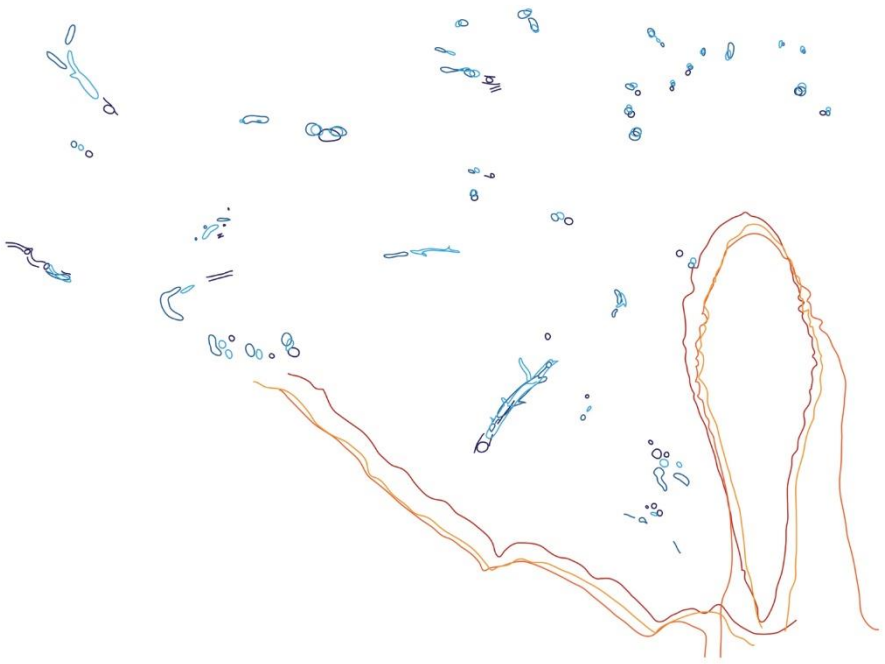

Figure 2.6: Vessel Alignments.

Corresponding sections from series 2 (α-MSH, MCH, nNOS staining – same section as that shown in **Figure 2.5**), series 3 (intervening series), and series 4 (Nissl stain) of one brain. Blood vessels and the bottom/third ventricle of the sections have been outlined in Illustrator (darker colors – Nissl section; lighter colors – α-MSH, MCH, nNOS section) and the vessels have been used to align the sections. Note that the logic of the arrangement is heightened for vessels traveling in the plane of section/caught branching, at the expense of the arrangement of vessels traveling roughly orthogonal to the plane of section. Note also that the quality of the arrangement is reduced at the lower right but maximized elsewhere.

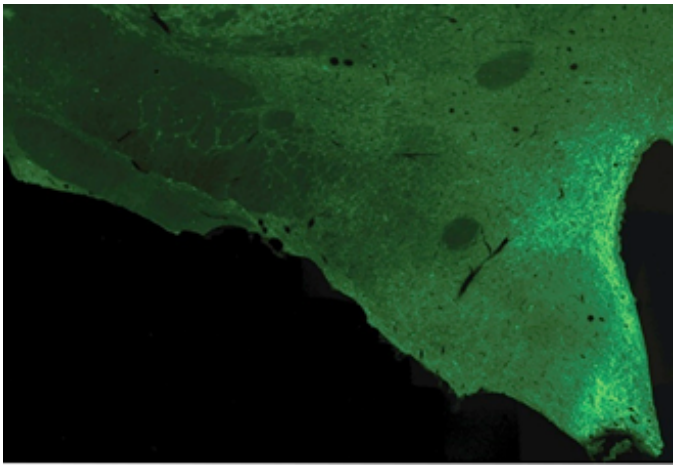

Figure 2.7: Increasing Background Visibility for Vessel Alignments.

Single-channel view (α-MSH) of the section from **Figures 2.5–2.6**, with the background staining increased for easy viewing of vessels and white matter.

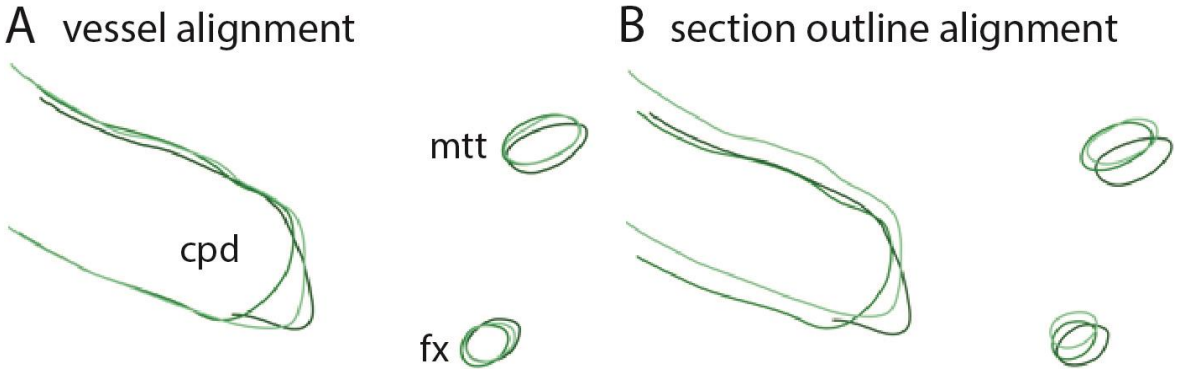

Figure 2.8: Quality of Alignments.

(A) The agreement of the major white matter tracts in the sections from **Figure 2.6**, when aligned based on blood vessels. **(B)** Their agreement when aligned based on section outlines. fx – fornix, mtt – mammillothalamic tract, cpd – cerebral peduncle.

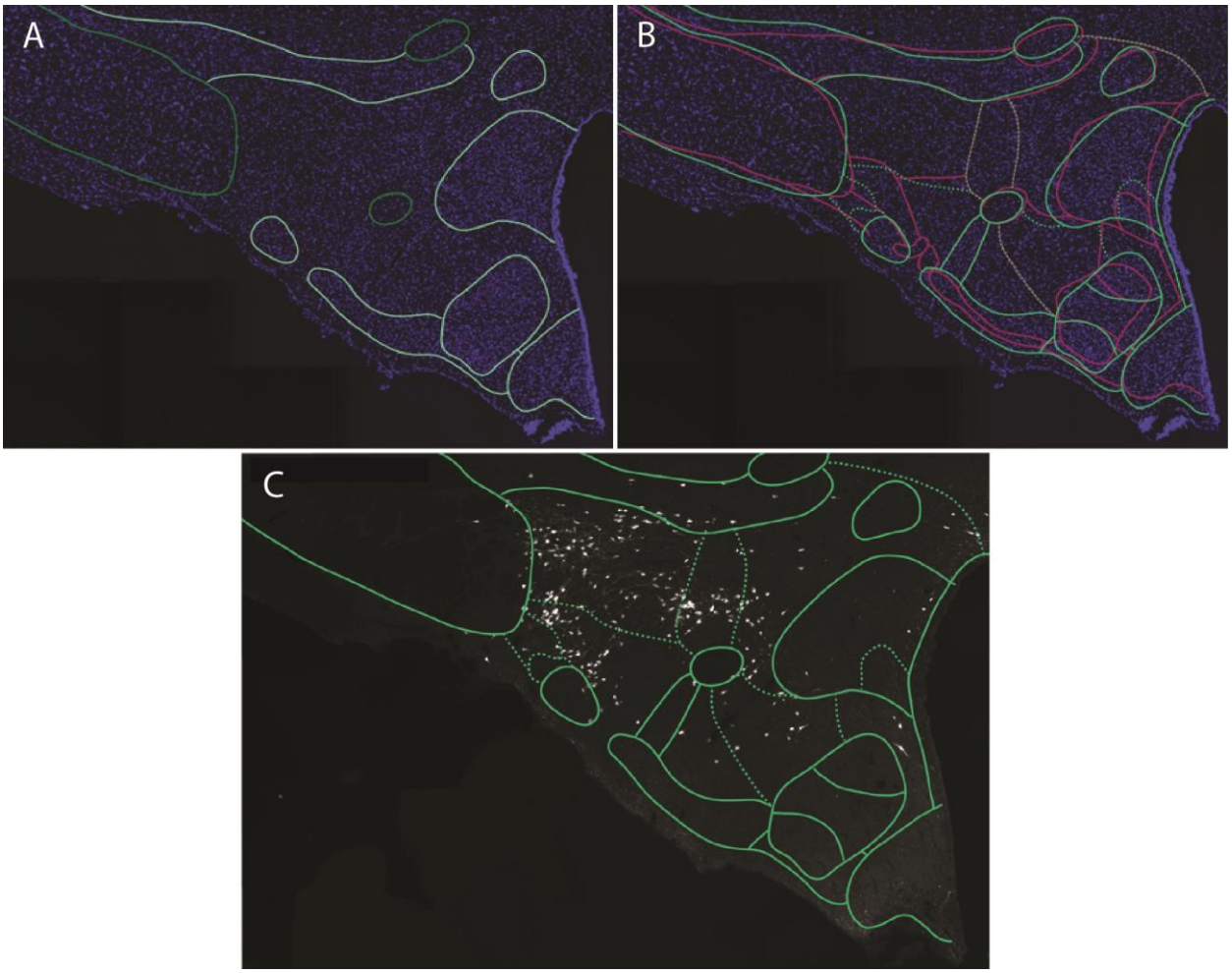

Figure 2.9: Transferring Nissl Parcellation to Fluorescent Sections.

(A) Single-channel (DAPI) view of the section from **Figures 2.5–2.8**. Structures outlined in dark green were identified based on the image in **Figure 2.8**, while structures with light green outlines were identified based on the DAPI image shown. **(B)** An overlay of the fluorescent and Nissl parcellations (alignment was determined by blood vessel analysis). The fluorescent parcellation has been completed by copying the Nissl parcellation and, where appropriate, modifying it to agree with the structure outlines shown in **A**. **(C)** The fluorescent parcellation overlaid on a single-channel (MCH) view of the section.

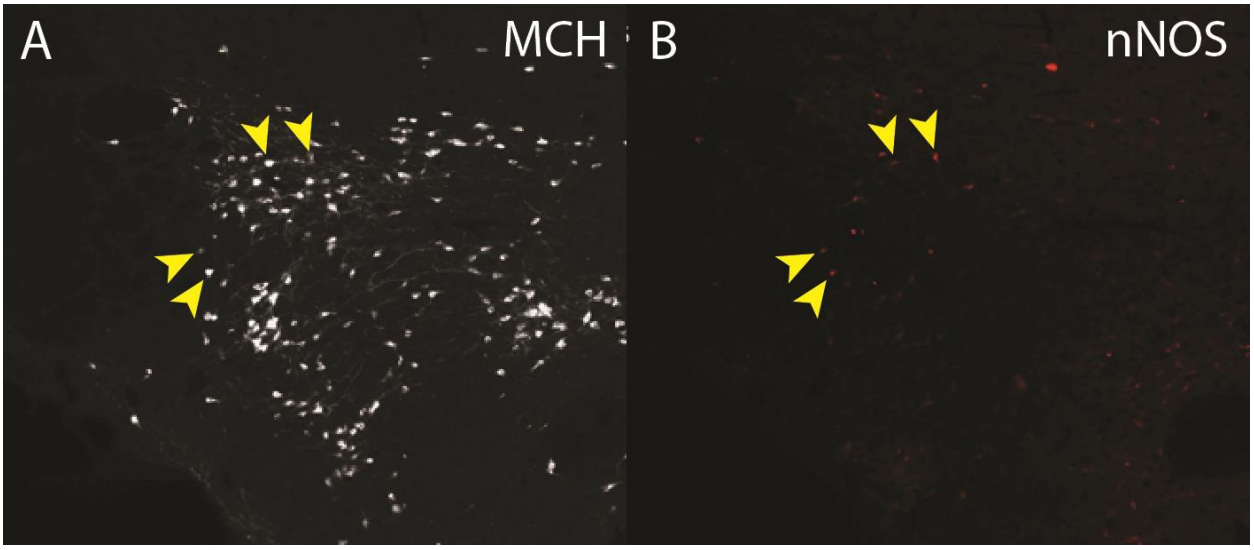

Figure 2.10: Identifying Colocalization.

(A) A single-channel (MCH) enlargement of a region of the section from **Figures 2.5–2.9**. The arrows indicate cells in which MCH is colocalized with nNOS. **(B)** nNOS staining in the same enlarged region of the same section. The cells indicated in **A** are so in **B** as well. Notice that two of them are quite faint.

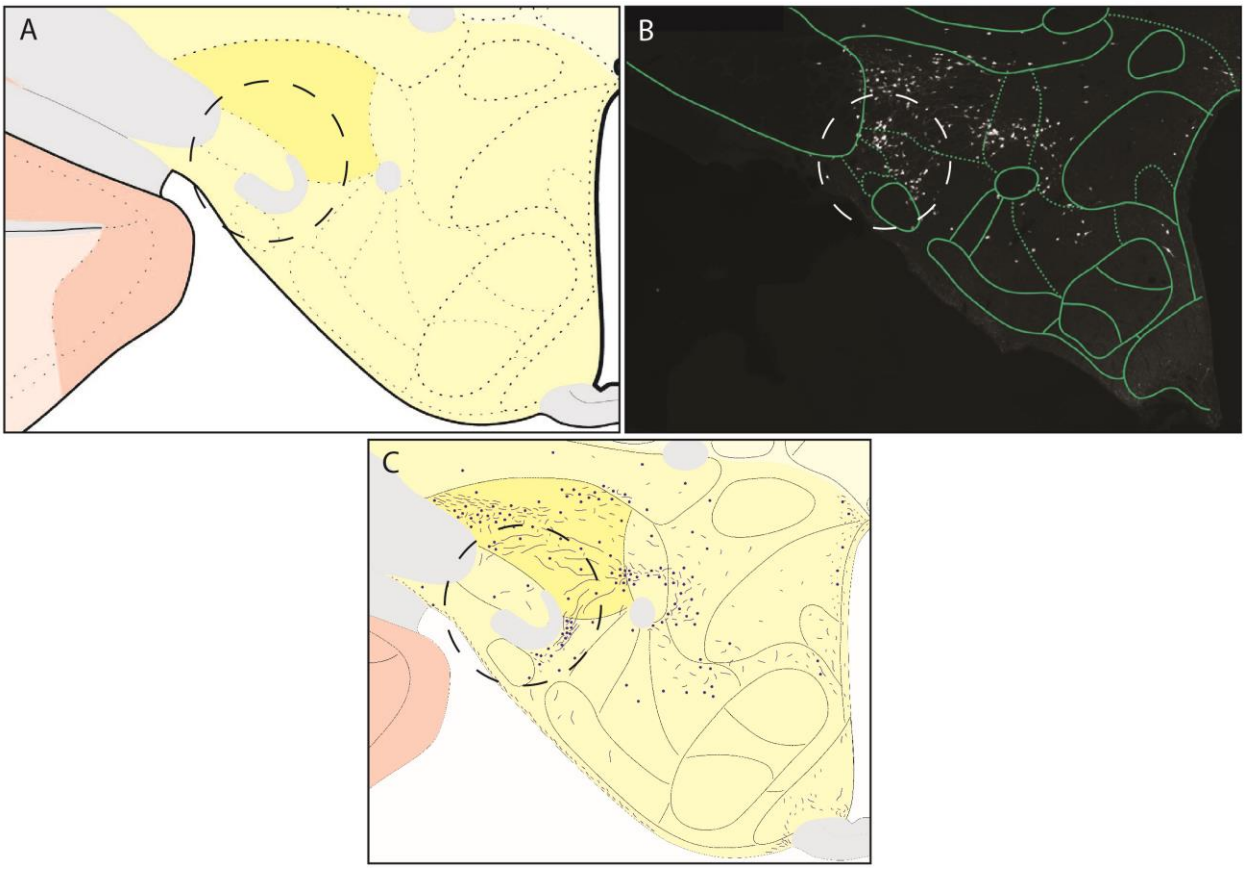

Figure 2.11: Resolving Conflicts between Reference and Experimental Parcellations.

(A) Level 29 of the Swanson atlas. The circle indicates a region of low correspondence between the atlas and the fluorescent parcellation. **(B)** The fluorescent parcellation from **Figure 2.9**, showing MCH. **(C)** A map of MCH cell bodies and fibers to level 29, in which the population of cells circled in **B** has been split into two, in order to avoid altering the structure they are reported in.

Results

Working with Steven Michelmann, I have created maps of α-MSH, MCH, nNOS, and their PSIZs in the hypothalamus in brain 13–082 (**Figures 2.12–2.33**); and such maps in the hypothalamus for levels containing the LHA in brain K10–053 (**Figures 4.1–4.13** in the Appendix). **Table 2.2** contains a legend for reading the maps; and **Figure 2.34** is a graphical summary of staining patterns for each antigen at each LHA-containing level of the Swanson atlas (levels 22–34), based on brain 13–082.

All maps of cell bodies, PSIZs, and diffuse staining were created by me. Additionally, all Nissl parcellations, vessel alignments, and parcellation transfers were performed by me. In brain 13–082 some maps of fibers were created by me, and some by Steven Michelmann. For **Figure 2.12**, the fiber maps shown in panel **b** were created by Steven Michelmann and edited for quality by myself; while the maps shown in panel **c** were created by me. For **Figure**s **2.13–2.15**, the fiber maps shown in panel **b** were created by Steven Michelmann and edited for quality by myself; while the maps shown in panels **c** and **d** were created by me. For **Figures 2.15–2.29**, the fiber maps shown in panel **a** were created by Steven Michelmann; while the maps shown in panels **b** and **c** were created by me. For **Figures 2.30–2.33**, the fibers maps were created by Steven Michelmann; and the map of nNOS cell bodies in **Figure 2.33** was created by me. My full maps for these levels were lost.

The following is a textual description of the mapped data at each level. It has been based on the maps in **Figures 2.12–2.33** created by me wherever possible – for levels 33–36 some of the descriptions are based on fiber maps created by Steven Michelmann, but I have attempted to account for the higher overall density of fibers in these maps, so that the textual descriptions should remain consistent.

α-MSH-ir Cell Bodies

α-MSH-immunoreactive (α-MSH-ir) cell bodies are found in the hypothalamus beginning at level 26, where there is a single cell body in the lateral ARH (**Figure 2.23a, b**). At level 27,

there are a few α-MSH-ir cell bodies in the ARH, generally located ventrally (**Figure 2.24a, b**). At level 28, there is a moderately dense cluster of α-MSH-ir cell bodies in the ARH, located ventrally and centrally with respect to its mediolateral extent. There is also a lone cell body in the TUsv just lateral to the lateral tip of the ARH (**Figure 2.25a, b**). At level 29 there are several α-MSH-ir cell bodies in the ARH, generally located ventrally and centrally with respect to its mediolateral extent; although one cell body is found dorsally (**Figure 2.26a, b**). At level 30 there is a dense cluster of α-MSH-ir cell bodies, with a moderately dense dorsal fringe, in the ARH, located laterally and centrally with respect to its dorsoventral extent (**Figure 2.27a, b**). At level 31 there is a single α-MSH-ir cell body in the PVpo, located ventrally and centrally with respect to its mediolateral extent (**Figure 2.28a, b**). At level 32 there are a few α-MSH-ir cell bodies in the ventral PVpo (**Figure 2.29a, b**).

α-MSH-ir Fibers

α-MSH-ir fibers are sparse in the LPO and BSTal at levels 15 and 16, with moderate density in the BSTam (**Figure 2.12c, d; Figure 2.13c, e**). At level 17 there are dense α-MSH-ir fibers coursing ventromedially in the AVPV and ventromedial AVP, spilling into the surrounding MPO; as well as a moderately dense band of fibers mediolaterally crossing the LPO dorsal to the MPO and terminating at the medial edge of the PS; there is also a dense cluster of α-MSH-ir fibers in the dorsolateral PS and ventral BSTam. A somewhat spare curtain of fibers spans the LPO above the afore-mentioned band, running dorsoventrally, and there is a light cluster of fibers at the border between the BSTal and BSTam. Fibers track along the medial edge of the aco, in the BSTam, and sparse fibers are also found in the MEPO. α-MSH-ir fibers largely avoid the lateral MPO and ventral LPO (**Figure 2.14c, e**).

α-MSH-ir fibers at level 18 are sparse, with the exception of a moderately dense fringe of fibers lining the third ventricle and oriented ventromedially, in the MEPO, AVPV, and PSCH; which becomes denser in the dorsal AVPV and ventral MEPO. The curtain of fibers described at level 17 is present, but sparser, as is the cluster of fibers in the dorsolateral PS and ventral

BSTam. α-MSH-ir fibers largely avoid the ADP, lateral MPO, and ventral LPO (**Figure 2.15c, e**).

α-MSH-ir fibers at level 19 are found in moderately dense clusters in the dorsal PS, in the lateral BSTfu and ventral BSTal, in the BSTam dorsal to the aco, in the central BSTov, in the LPO dorsal to the aco, in the medial LPO just ventral to the aco and the dorsomedial MPO, and lining the third ventricle in the AVPV and PSCH. α-MSH-ir fibers along the third ventricle become dense as they enter the MEPO. A few long fibers run dorsoventrally in the dorsal BSTov and dorsal BSTam. α-MSH-ir fibers largely avoid the AVP, MPN, lateral MPO, and ventral LPO (**Figure 2.16a, b**).

α-MSH-ir fibers at level 20 are dense along the third ventricle in the medial PSCH, PVpo, and ventral MEPO; with some spillage into the I, particularly dorsal and ventral to the MPN. They are moderately dense in the ventral BST (the parcellation of the ventral BST into subsections is unreliable at this level and therefore one hesitates to positively assign the staining to one subsection or another). A number of long fibers are found in the BSTal lateral to the temporal limb of the anterior commissure (act). α-MSH-ir fibers largely avoid the LPO (excepting a few ventrally located fibers), lateral MPO, SO, VLP, AVP, and MPN (excepting a few in the ventral MPNm) (**Figure 2.17a, b**).

α-MSH-ir fibers at level 21 are very dense along the third ventricle in the PVpo and medial I; spilling with moderate density into the medial MPMm, with a very dense arm stretching from the PVpo and I into the MPNm beside the MPNc. This ventricular fringe is observed to possibly intrude into the dorsal SCH, although this reporting should not be regarded as definitive, because the SCH could not be reliably identified in the Nissl at this level. Moderately dense α-MSH-ir fibers are distributed throughout the BST, with a number of longer fibers coursing either ventrolaterally (in the ventral and dorsomedial BST, continuing into the dorsal MPO), or dorsoventrally (in the dorsolateral BST). Somewhat sparse long fibers are also found in the lateral MPO and dorsal MPNl, crossing into the MPNc. α-MSH-ir fibers largely avoid the SO and LPO, excepting a few in the ventromedial LPO (**Figure 2.18a, b**).

α-MSH-ir fibers at level 22 are dense along the third ventricle in the PVpo, medial I, and PVH (thinning out dorsally and laterally in this structure); spilling with moderate density into the MPNm. Somewhat sparse fibers occur in the BST, especially in the BSTif and BSTtr. α-MSH-ir fibers largely avoid the LHA (although a few are found in the LHAai), anterior hypothalamic area (AHA), AHN, SO, and SCH (excepting a light fringe along its ventral border). In the case of the SCH, it is apparent that the density of fibers bordering the third ventricle is specifically interrupted so that this structure may be avoided (**Figure 2.19a, b**).

α-MSH-ir fibers at level 23 are dense along the third ventricle in the PVa, medial I, and PVH (thinning dorsally and laterally). Moderately dense fibers are found in the ventral MPNm and dorsal MPNl; and in the BSTif, spilling into the lateral MPO. α-MSH-ir fibers largely avoid the AHA (excepting a few, located dorsally), AHN, SCH, SO (excepting a light fringe along its ventral border), and LHA (**Figure 2.20a, b**).

α-MSH-ir fibers at level 24 are dense along the third ventricle in the PVa and PVHpv, and moderately dense in the SBPV, medial I, and medial PVHap. Sparse fibers dot the AHNc. α-MSH-ir fibers largely avoid the LHA, RCH, and SO (excepting a light fringe along its ventral border) (**Figure 2.21a, b**).

α-MSH-ir fibers at level 25 are dense along the third ventricle in the PVa and PVHpv, spilling with moderate density into the SBPV and medial RCH. Sparse fibers are located in the AHNc, AHNp, and LHAjp; and moderately dense fibers are found in the PVHdp and dorsal PVHmpd. α-MSH-ir fibers largely avoid the ZI, the rest of the LHA, the SO (excepting a light fringe along its ventral border), the AHNa, and the PVHpmm (**Figure 2.22a, b**).

α-MSH-ir fibers at level 26 are dense along the third ventricle in the ARH, PVi, and PVHpv; spilling with moderate density into the medial I, medial SBPV, and medial PVHmpd. Sparse fibers are found in the TUsv, especially ventrally. α-MSH-ir fibers largely avoid the LHA, VMH, and ZI (**Figure 2.23a, b**).

α-MSH-ir fibers at level 27 are very dense along the third ventricle in the PVi and PVHpv. They are similarly dense in the ARH in a patch located centrally and ventrally, thinning

out somewhat dorsally and medially, and thinning out significantly laterally. Moderately dense fibers are found in the medial PVHmpd, medial I, SBPV, and medial TUsv. A cluster of moderately dense α-MSH-ir fibers appears in the PVHf, LHAd just lateral to the PVHf, and ZI just dorsolateral to the PVHf. α-MSH-ir fibers largely avoid the LHA and ZI (excepting the described cluster), SOr, TU (except as described), and VMH (**Figure 2.24a, b**).

α-MSH-ir fibers at level 28 are dense to moderately dense along the third ventricle in the PVi, with a sparse patch occurring in the ARH bounded by denser regions on all sides. Dense fibers are found in a band beginning in the lateral ARH and arching laterally and ventrally to the edge of the section, passing through the ventromedial TUsv and the region ventral to it. Fibers continue in this space ventral to the TU until the SOr. Moderately dense fibers are found in a thin strip in the medial DMH bounding the PVi, while the rest of the DMH has somewhat sparsely distributed fibers that reach laterally to the fx. The cluster of fibers in the dorsal LHAd and ventral ZI described at level 27 persists at level 28 and is denser, with longer fibers; a few fibers also occur in the ventromedial ZI. α-MSH-ir fibers largely avoid the LHA lateral and ventral to the fx, the SOr, and the VMH (**Figure 2.25a, b**).

α-MSH-ir fibers at level 29 are dense along the third ventricle in the PVi and dorsal ARH, where they are continuous with a dense band of fibers stretching laterally and ventrally through the ARH and terminating at the edge of the section. Fibers are sparser immediately along the lateral edge of the ARH and in a small ventromedial patch. Moderately dense fibers fill the DMH, becoming denser medially and thinning out in small patches dorsally and ventrally; these fibers stretch laterally into the LHAjd. The cluster of fibers described at levels 27 and 28 in the dorsal LHAd and ventral ZI may shift ventrally at level 29 to be entirely contained within the LHA dorsal to the fx; or it may no longer be present if the fibers at that location belong to a different grouping. Sparse fibers are found along the ventral edge of the section in the lateral TUi and ventral to it, and continuing past it to the region ventral to the TUl. α-MSH-ir fibers largely avoid the LHA lateral and ventral to the fx (excepting along the extreme ventral edge of the section), the VMH, and the PH (**Figure 2.26a, b**).

α-MSH-ir fibers at level 30 are dense along the third ventricle in the PVi, especially towards the center of its dorsoventral extent, although they become quite sparse at the dorsal limit of the PVi. Fibers are moderately dense in the majority of the ARH, but become dense ventrally and laterally. α-MSH-ir fibers are moderately dense in the DMHa, except in its ventral tip where they are dense, and these fibers spill over into the DMHp along its medial border. A band of dense fibers stretches from the PVi across the ventral arm of the DMHp and fans out into the DMHv, thinning as it reaches the lateral border. Sparse fibers are found in the I, TUsv, TUi, and VMHvl; α-MSH-ir fibers largely avoid the ZI, STN, LHA lateral and dorsal to the fx, TUte, and TUl (**Figure 2.27a, b**).

α-MSH-ir fibers at level 31 are dense in the PVi beside the DMH; especially in the portion centrally located with respect to the dorsoventral extent of the DMHa; dorsal and ventral to this region of the PVi fibers are sparse. A cluster of dense fibers occurs ventral to the medial PVp, and another small cluster is found within the PVp, centrally along its mediolateral extent. There are moderately dense fibers in the DMHa, centrally in the DMHp with regard to its dorsoventral extent, and dorsomedially in the DMHv. Ventral to where these fibers are found in the DMHp, another group of fibers courses to the DMHp's ventral limit and slightly beyond; these are of modest length and oriented ventromedially with a slight incline. Sparse fibers are located in the LHAjvv dorsal to the DMH, which spill over into the most medial portion of the PH; sparse fibers also dot the ventral edge of the section. α-MSH-ir fibers largely avoid the ZI, STN, PSTN, LHA (except as described), TU, and PH (except as described) (**Figure 2.28a, b**).

α-MSH-ir fibers at level 32 are moderately dense in a dorsoventrally-oriented band occupying the majority of the PVp, excepting its lateral and medial margins, and TMd, and extending and expanding into the I ventrally and the I and ventromedial PH dorsally; there are also moderately dense to sparse fibers along the ventral edge of the section. α-MSH-ir fibers largely avoid the STN, PSTN, LHA (except along the section edge), TUte, and PMd (**Figure 2.29a, b**).

α-MSH-ir fibers at level 33 are dense ventral to the PVp, while being moderately dense within the PVp and a bit less so lateral to it, in the PMv, TMv, and ventral LHAp. Some fibers occur in the ventromedial PMd and the area ventral to it and to the MMme. There is a cluster of moderately dense fibers just lateral to the LHAsfpm (although the LHA subsections were generally difficult to identify in the Nissl), which thins out as it stretches dorsomedially towards the fx. Moderately dense α-MSH-ir fibers are found in the PH as well, thinning towards its lateral border, and being pointillescent ventrally and moderately long, with a dorsoventral orientation, dorsally. Sparse fibers are found in the PSTN and LHAp lateral to the fx. α-MSH-ir fibers largely avoid the dorsal LHAp and markedly avoid the area surrounding the fx, including the majority of the PMd and the LHAsfpm (tentatively) (**Figure 2.30**).

α-MSH-ir fibers at level 34 are dense along the section's ventral edge, including the ventral portion of the TMv, and moderately dense in the PVp. There is a band of moderately dense fibers running mediolaterally across the section from the dorsal portion of the TMv through the ventral LHAp to the SUMm, and some fibers in the dorsal LM, MMme, and ventral PH. α-MSH-ir fibers largely avoid the MM, smd, and the majority of the LM (**Figure 2.31**).

α-MSH-ir fibers at level 35 are moderately dense along the ventral edge of the section, including the ventral LM, thinning in the area between the LM and PVp to become denser again ventral to the mammillary recess of the third ventricle. There is a pointed band of fibers stretching mediolaterally through the SUMm and SUMl, and sparse fibers in the dorsal portion of the TMv, the medial smd, and the medial PH. α-MSH-ir fibers markedly avoid the MM, MMme, and LM (except along its ventral border) (**Figure 2.32**).

α-MSH-ir fibers at level 36 are moderately dense along the section's ventral edge, ventral to the MM, and in the SUM. There are some fibers along the ventral edge of the PH that funnel medially and rise to the dorsal PH, becoming longer and oriented ventromedially; and a small cluster of fibers in the ventral TMv. α-MSH-ir fibers largely avoid the MM (**Figure 2.33**).

MCH-ir Cell Bodies

Melanin-concentrating hormone-immunoreactive (MCH-ir) cell bodies are found in the hypothalamus beginning at level 26. Here, there are sparse cell bodies in the lateral ZI and dorsal LHAd; as well as a lone cell in the AHNc (**Figure 2.23a, b**). At level 27 their number is greatly increased, and there is a moderately dense population running in a band along the ventral edge of the ZI; and another, slightly less dense, population centered in the dorsal AHNp (avoiding the AHNd) that spills over on either side into the SBPV and LHAd dorsomedial to the fx. There are also a few scattered MCH-ir cell bodies in the LHAd lateral to the fx, including a small group in the extreme lateral LHA, dorsal to the tip of the opt. There is a lone cell in the I just ventral to the AHNc, and one in the PVi just ventral to the PVHpv (**Figure 2.24a, b**).

MCH-ir cell bodies at level 28 are moderately dense in the ZI dorsal to the hypothalamus, particularly medially and ventrally, largely avoiding the ZIda and occasionally straying dorsally into the small area between the ZI and the thalamus. This population is apparently continuous with that present in the dorsolateral LHAd; MCH-ir cell bodies continue, less densely, ventrolaterally along the lateral edge of the LHA, straying singly into the sup and SI, but it is not clear whether they belong to the same population. MCH-ir cell bodies form a sort of hemi-halo medially and ventrally around the fx, and there is a small cluster of MCH-ir cells just ventrolateral to the lateral tip of the DMHa, with a few cells extending medially in the I. There is another small cluster of MCH-ir cells in the dorsomedial tip of the DMHa and dorsomedial LHAjd (**Figure 2.25a, b**).

MCH-ir cell bodies at level 29 are sparse in the ZI, and concentrated, such as they are, medially; the population present there at level 28 appears to have shifted ventrally into the LHAs, LHAd, and LHAm (although parcellation of the LHA subdivisions was again difficult), and is particularly dense dorsal to the fx and medial to the cpd. MCH-ir cells are also scattered in the lateral and medial, but not central, LHAjd (a lone cell is present in the dorsal PH); and their density picks up slightly as they run in a band from the fx to the VMH, passing just beside the ventrolateral tip of the DMHa; a few are also found between the VMH and DMH in the I. Very

few cells are located in the DMHa, and in the ventral LHA (excepting the band previously described) (**Figure 2.26a, b**).

At level 30, the population described in the dorsal LHA at level 29 has become sparse, except for a smallish but dense cluster of MCH-ir cell bodies in the dorsolateral LHA and ventral ZI. There are a couple of additional MCH-ir cells in the ZI, dorsal to the cluster, and at its medial tip ventral to the mtt. There is another population of MCH-ir cell bodies ventral to that in the dorsal LHA, which is moderately dense and runs in a band ventomedially from the cpd to the fx; the halo of cells around the fx is complete at this level. There are a couple of cells in the LHAs, apart from the populations already described. A few cells are found in the ventral DMHa and adjacent PVi (one straddles these structures dorsally), one is found in the ventral DMHp, and a few more are located in the ventral DMHv, continuous (or at least contiguous) with the fx's halo (**Figure 2.27a, b**).

MCH-ir cell bodies at level 31 are dense in the PST, spilling over into the immediately adjacent LHA; there are sparse cell bodies along the ventral ZI beginning dorsal to the PST and traveling medially. The fx has a halo of cells around it still in the LHA and PH, but it is sparser, and there is a small moderately dense cluster of MCH-ir cell bodies just ventrolateral to the fx and another medial to it, straddling the PH and LHAjvv. There is a very small cluster of cells in the lateral PH just medial to the PST, and a few more cells scattered dorsally in the PH and dorsal LHAjvv. MCH-ir cell bodies are scattered in the DMHa and PVi dorsal to the DMH, and in the dorsal DMHv; a lone cell is in the ventral DMHp (**Figure 2.28a, b**).

At level 32, most MCH-ir cell bodies are found in two clusters; one somewhat sparse located in the LHAp dorsal and medial to the PSTN, and one moderately dense in the ventrolateral quadrant of the PH. There also a couple of cells in the LHAp lateral to the ventral tail of the mtt, a few just ventrolateral to the fx, one in the ventral LHA (possibly in the LHAsfpm), several in the TMd and I just lateral to it, and a couple in the I dorsal to the PVp (**Figure 2.29a, b**).

MCH-ir cell bodies at levels 33–36 have not yet been mapped.

MCH-ir Fibers

MCH-ir fibers at level 15 are moderately dense in the LPO; at level 16 they are sparse in the LPO, BSTam, and BSTal. The majority of MCH-ir fibers at both levels are pointillescent, excepting a few longer ones, particularly in the medial LPO at level 15, and off the medial edge of the aco at level 16 (**Figure 2.12c, d; 16c, e**).

MCH-ir fibers at level 17 are moderately dense are pointillescent in the dorsal LPO, being particularly concentrated medially and fanning out laterally. Sparse fibers are found in the BSTal dorsal to the aco; and a number of longer fibers are located in the ventromedial MPO and ventral AVPV, oriented ventromedially, and generally running parallel to shorter and denser α-MSH-ir fibers at the same location (**Figure 2.14c, e**).

MCH-ir fibers at level 18 are densely clustered and pointillescent in the dorsomedial LPO, fanning out laterally, with a few longer fibers running dorsoventrally superimposed over these in the dorsal LPO. Sparse, medial length fibers occur in the ventral MPO, ventral LPO, and lateral AVP, and are oriented ventrolaterally; a number of shorter fibers are found medial to these in the AVPV, ventral MPO, and PSCH that are oriented ventromedially and again overlap with similar but denser α-MSH-ir fibers. There is a moderately dense cluster of MCH-ir fibers in the BSTju and lateral BSTal and there are a few fibers rounding the medial edge of the aco in the BSTam. MCH-ir fibers are sparsely distributed throughout the MEPO, dorsal MPO, ADP, lateral LPO, and majority of the BST (**Figure 2.15c, e**).

MCH-ir fibers at level 19 are densely clustered and pointillescent in the LPO dorsal to the aco. They are moderately dense in the PSCH, ventral AVPV, and medial MPO, and have lost the dominant orientation they exhibited in this region at levels 17 and 18. There are a few longer fibers in the dorsal BSTam running ventromedially; and a couple longer fibers in the ventral MPO just dorsal to the lateral end of the och, and ventral to the AVP, oriented mediolaterally. Sparse MCH-ir fibers are found in the MEPO ventral to the aco, MPO, LPO, and the majority of the BST. MCH-ir fibers largely avoid the PS, ADP, MPN, and BSTfu (although the BST parcellation is relatively low-confidence in this area) (**Figure 2.16a, b**).

Modestly long, sparse MCH-ir fibers are found at level 20 in the BST near the st (in the BSTpr, BSTrh, and dorsal BSTal); in a line running from the dorsomedial LPO, through the dorsal MPO, into the ADP (oriented ventrolaterally); and more densely running along the dorsal border of the och through the ventral MPO, AVP, and PSCH, oriented shallowly ventrolaterally. There is a cluster of somewhat sparse MCH-ir fibers in the ventral LPO just medial to the NDB. MCH-ir fibers are scattered sparsely throughout the majority of the hypothalamus and BST (**Figure 2.17a, b**).

MCH-ir fibers at level 21 are dense to moderately dense near the ventral edge of the third ventricle, in the ventromedial MPO; moderately dense in the ventral MPO and LPO in a cluster centered dorsal to the SO; and moderately dense in a band running mediolaterally across the LPO just dorsal to the NDB. There is a moderately dense cluster of fibers dorsal to the band described in the LPO, and another at the dorsal tip of the LPO that spills over into the lateral MPO. MCH-ir fibers are also moderately dense in the BAC. Sparse fibers are distributed along the PVpo and adjacent MPO, dorsal MPO, AHN, PD, and majority of the BST including some longer fibers. MCH-ir fibers largely avoid the MPN (excepting a couple at the ventral, lateral, and dorsal edges), and are less dense in the BSTpr than elsewhere in the BST. They may be less dense in the BSTmg as well, but this area was parcellated with low-confidence (**Figure 2.18a, b**).

MCH-ir fibers at level 22 are moderately dense in an elongated cluster in the LHAav where it forms the ventral edge of the section, and sparse in the LHAai and PVpo. They are moderately dense along the lateral and ventral edges of the BST and sparse elsewhere in the BST. They largely avoid the SO, SCH, AHN, MPNl, and PVH except between the fingers of the mct (**Figure 2.19a, b**).

MCH-ir fibers at level 23 are moderately dense in a cluster in the LHAav where it forms the ventral edge of the section, and sparse in the PVpo and BST. They largely avoid the SO, SCH, AHN, MPN, PVH, LHAjp, and MPO dorsal to the fx (**Figure 2.20a, b**).

MCH-ir fibers at level 24 are sparsely distributed throughout the PVa, PVH, AHNc, and SBPV and I where they lie between the AHN and PVpo. There are a few fibers in the ventral LHAav where it forms the ventral edge of the section. MCH-ir fibers largely avoid the SO, AHNa, RCH, SCH, and LHA except as described and for a few fibers in the vicinity of the fx (**Figure 2.21a, b**).

MCH-ir fibers at level 25 are moderately dense in a cluster in the RCH ventral to the third ventricle, and somewhat sparse in a cluster centrally located in the ZI. Somewhat sparse MCH-ir fibers run along the dorsal border of the hypothalamus, beginning just ventral to the ZI, passing through the LHAjp, avoiding the PVHdp, and terminating at the PVHpv. Sparse fibers are scattered in the AHNc and AHNp, PVa and adjacent SBPV, LHAav, and LHA around the fx. MCH-ir fibers largely avoid the SO, AHNa, and LHAai except beside the fx (**Figure 2.22a, b**).

MCH-ir fibers at level 26 are moderately dense in a thin strip running just dorsal to the sup, from the ME to the lateral tip of the TUsv and slightly beyond. They are sparsely distributed in the PVi, PVHpv, SBPV, and medial AHN, and a few fibers occur in the ZI and LHAav near the MCH-ir cell bodies present at those locations. They largely avoid the VMH, ARH, LHA ventral to the fx (except as described), and PVH aside from the PVHpv (**Figure 2.23a, b**).

MCH-ir fibers at level 27 are somewhat sparse near MCH-ir cell bodies in the ventromedial ZI and SBPV; and sparse in the PVi, medial PVHmpd, and along the ventral edge of the section, ventral to the TUsv. MCH-ir fibers largely avoid the VMH, TU, ARH, LHA, AHNd, AHNc, and PVH except as described (**Figure 2.24a, b**).

MCH-ir fibers at level 28 are moderately dense in the ventral and medial ZI and lateral LHA, near MCH-ir cell bodies, and being dominantly oriented either ventrolaterally or mediolaterally; and in the ventromedial TUsv and the area just ventral to it – these fibers are shorter than those in the ZI and LHA. Sparse fibers are found in the TUi near its lateral edge. There are additional fibers in the medial and dorsal DMH, dorsomedial LHAjd, dorsal I, and LHA in a hemi-halo around the fx that stretches medially to meet the I; these for the most part

accompany MCH-ir cell bodies. MCH-ir fibers largely avoid the VMH, ARH, PVi, and ZIda (**Figure 2.25a, b**).

MCH-ir fibers at level 29 are dense to moderately dense in the lateral LHA and in a column in the LHA dorsal to the fx, near MCH-ir cell bodies. Short fibers form a moderately dense fringe just lateral to the ME, in the ventrolateral ARH and the area ventral to it, and are primarily oriented ventromedially. MCH-ir fibers are moderately dense in the medial LHAjd and dorsomedial DMHa as well. Sparse fibers track along the ventral edge of the section from the ME to the area ventral to the TUl; and accompany MCH-ir cell bodies in the LHA just medial to the fx, traveling ventrally and around the lateral tip of the DMHa to finish in the dorsal I. MCH-ir fibers largely avoid the VMH, PVi, TU (although parcellation of the TUl is low-confidence), PH, and DMH except as described (**Figure 2.26a, b**).

MCH-ir fibers at level 30 are short and moderately dense near MCH-ir cell bodies in the dorsolateral LHA, spilling over into ventral ZI, and continuing in a band medially to a point dorsal to the fx. Moderately dense fibers are also found in the ventrolateral ARH and the area just ventral to it, where they form a fringe around the ME, and are primarily oriented ventromedially or mediolaterally. Sparse MCH-ir fibers occur near MCH-ir cell bodies in the LHA lateral to the fx and in a halo around it, and without cell bodies along the ventral edge of the section from the ME to a point ventral to the medial end of the TUl. Sparse fibers are also found in the PVi, the DMHv near MCH-ir cell bodies, and ventral DMHa near cell bodies. MCH-ir fibers largely avoid the VMH, TU, PH, and ZI except as described (**Figure 2.27a, b**).

MCH-ir fibers at level 31 are dense in a cluster near MCH-ir cell bodies in the PST, with pointillescent fibers extending in a line laterally from the cluster and terminating in the ventral ZI; and moderately dense near cell bodies in the LHA and PH ventrolateral and medial to the fx. Sparse MCH-ir fibers travel along the ventral edge of the section from the midline to the cpd, and are found in the PVi, and the DMH near MCH-ir cell bodies in the DMHa, central DMHp, and dorsal DMHv. Sparse fibers are also found in the dorsal PH and the LHA dorsal to the

DMH, mostly near MCH-ir cell bodies. MCH-ir fibers largely avoid the TU and ZI except as described (**Figure 2.28a, b**).

MCH-ir fibers at level 32 moderately dense in the lateral LHAp near MCH-ir cell bodies, and forming a line of pointillescent fibers that travel from the dorsal margin of the cell bodies laterally to the ventral ZI. Sparse to moderately dense fibers travel along the ventral edge of the section from the midline to the cpd, and sparse fibers occur in the ventral PH, some of them being near cell bodies in the ventrolateral PH. Sparse fibers are found in the I, dorsal PVp, TMd, and dorsally in the area immediately medial to the PH, being shorter dorsally and longer ventrally; long sparse fibers are distributed infrequently throughout the ventromedial hypothalamus medial to the fx and ventral to the PH. MCH-ir fibers largely avoid the PMd, PSTN, and TUte (**Figure 2.29a, b**).

MCH-ir fibers at level 33 are moderately dense in the PSTN and lateral LHAp, and dorsal PH; and dense in the ventral PVp and area ventral to it. Sparse fibers travel along the ventral edge of the section from the midline to the cpd, becoming very sparse in the area ventral to and in between the TMv and PMv. Sparse fibers are found in the TMv, ventral PMv, dorsal PVp, area immediately dorsal to the mammillary recess of the third ventricle and spilling into the ventral MMme, LHAp, LHA ventral to the PSTN, and PH; a couple of fibers occur in the lateral SUMl and medial PMd. MCH-ir fibers largely avoid the LHA immediately surrounding the fx, and PMd except as described (**Figure 2.30**).

MCH-ir fibers at level 34 are moderately dense surrounding the mammillary recess of the third ventricle, in the PVp and spilling over into the ventromedial MM, and along the ventral edge of the section, from the midline to the cpd and including the TMv and ventral and lateral margins of the LM. There is a somewhat sparse cluster of fibers in a triangular shape in the SUMl dorsal to the fx, and sparse fibers in the lateral LHAp and SUMl except for its ventral portion situated dorsal to the mp. Short sparse fibers fill the smd, SUMm and SUMl just lateral to it, and PH, becoming longer in the dorsal PH and ringing the mtg. Sparse fibers are also found

in the MM along the midline. MCH-ir fibers largely avoid the MM, MMme, and LM, except as described (**Figure 2.31**).

MCH-ir fibers at level 35 are moderately dense along the ventral edge of the section from the midline to the cpd; straying into the lateral LM, being interrupted ventral to the lateral MM, including the PVp and the area surrounding the mammillary recess of the third ventricle, and straying into the MM at discrete sites located at its lateral edge and dorsal to the PVp. A couple of fibers occur in the TMv, although the band of fibers lining the ventral section edge is interrupted here. Sparse fibers are found in the SUMm and extend laterally in a band through the SUMl located centrally with regard to its dorsoventral extent and terminating dorsal to the mp; and in the medial smd and the PH except for its lateral and dorsal extremities. MCH-ir fibers largely avoid the LM and MM, except as described (**Figure 2.32**).

MCH-ir fibers at level 36 are dense along the ventral edge of the section from the midline to the lateral edge of the MM, spilling over into the ventral MM and thinning out somewhat; the majority of the MM contains sparse fibers, although the lateral MM has very few. MCH-ir fibers are moderately dense in the SUMl and somewhat sparse in the SUMm and ventral PH. Sparse fibers occur along the midline in the PH, being dominantly oriented dorsoventrally, thinning out in the dorsal limb of the PH. Somewhat sparse fibers are located in small clusters in the ventral TMv, between the TMv and mp at their lateral edges, and between the mp and PH; sparse fibers fill the remainder of the unnamed space between structures in the lateral hypothalamus at this level (**Figure 2.33**).

nNOS-ir Cell Bodies

A lone neuronal nitric oxide synthase-immunoreactive (nNOS-ir) cell body is found in the lateral LPO at level 15, while a couple occur at the lateral and medial edges of the LPO at level 16. A lone cell body is located in the BSTam dorsal to the aco at level 16 (**Figure 2.12c, d; 16c, e**).

nNOS-ir cell bodies at level 17 are densely clustered in the medial AVP, spilling over into the area just medial to it, and moderately dense throughout the remainder of the AVP and in the MEPO. Dense nNOS-ir cell bodies line the third ventricle in the AVPV, MEPO, and OV. Moderately dense cell bodies occur in a band crossing the dorsal LPO mediolaterally just dorsal to the MPO, thinning out laterally. Sparse cell bodies are found in the MPO, LPO dorsal and ventral to the band previously described, PS, and BST, with only a couple of cells found in the BST dorsal to the aco (**Figure 2.14c, e**).

nNOS-ir cell bodies at level 18 form a very dense band traveling ventrolaterally from the ventral MEPO to the ventral AVP, adhering to its medial edge. A couple of cell bodies are found in the area medial to this band, one being in the dorsolateral AVPV. Dense cells travel in a line vertically along the midline in the MEPO, and moderately dense cells occupy the lateral MEPO. Dense cell bodies are diffusely clustered in the dorsal LPO dorsal to the ADP, and moderately dense cell bodies are located in the dorsomedial LPO. Sparse cell bodies fill the AVP except as described, MPO, and PS; and are located in dorsal BSTam and central ADP. A couple of additional cell bodies are found in the BSTam just dorsal and ventral to the aco and in the LPO medial to the PS. nNOS-ir cell bodies largely avoid the PSCH, ventral LPO, and lateral and ventral BST (**Figure 2.15c, e**).

nNOS-ir cell bodies at level 19 are dense in the MEPO and moderately dense in the dorsomedial ADP and ventral and dorsal AVP; they are sparse in the MPO, medial LPO, remainder of the ADP, and PS. A couple of cell bodies are present in the dorsal AVPV, and a few are scattered in the BSTam and BSTal. One is found in the PSCH. nNOS-ir cell bodies largely avoid the MPN, AVPV except as described, lateral BST, and lateral LPO (**Figure 2.16a, b**).

nNOS-ir cell bodies at level 20 are dense in the MEPO and SO. Somewhat sparse clusters of cell bodies are found in the medial ADP and adjacent MPO, dorsal AVP and adjacent MPO, and lateral LPO. A few cell bodies are located in the MPNm, ventral BST, and MPO just lateral to the MPN and ADP. Lone cells occur in the dorsal MPNl, dorsal MPNc, PSCH, and ventral

LPO. nNOS-ir cell bodies largely avoid the PVpo, VLP, BSTpr and lateral BST, and LPO except as described (**Figure 2.17a, b**).

nNOS-ir cell bodies at level 21 are dense in the MEPO and SO; and are found in moderately dense clusters in the lateral LPO, straddling the medial LPO and lateral MPO, ventromedial MPNl spilling over into the MPNm, and dorsal MPO. Several small, moderately dense groupings of nNOS-ir cell bodies occur in the BST; in the medial BST (tentatively localized to the medial BSTdm), dorsal BSTpr, just medial to the ventromedial BSTpr, just ventral to the BSTpr, lateral to the dorsal fx, straddling the BSTam and BSTal (tentatively localized), in the BSTal just medial to the BSTrh and spilling over into it (tentatively localized), and in the dorsal BSTal. Additional nNOS-ir cell bodies are scattered sparsely throughout the BST. Sparse cell bodies also occur in the dorsal LPO, central and ventral MPO, and AHN. A single cell is found in the SCH. nNOS-ir cell bodies largely avoid the PVpo (**Figure 2.18a, b**).

nNOS-ir cell bodies at level 22 are dense in the SO and dense to moderately dense in two small clusters in the PVH; one in the PVHpv and medial PVHap between the fingers of the mct, and one in the lateral PVHap and dorsolateral PVHam and spilling over into the adjacent MPO. Cell bodies are also moderately dense in the lateral LHAav dorsal to the MA, being distributed somewhat sparsely throughout the remainder of the LHA. A couple of cell bodies are found in the PVpo adjacent to the MPN, and in the MPO, AHA, and SBPV (or possibly in the I instead). nNOS-ir cell bodies avoid the MPN, AHN, and SCH (**Figure 2.19a, b**).

nNOS-ir cell bodies at level 23 are dense in the SO and in the dorsal PVHpv. They are moderately dense in the dorsal and lateral PVHap, and in the MPO between the LHAjp and PVH – these appear to be distinct groupings as the cells in the MPO are denser towards the LHAjp than towards the PVH. The remainder of the PVHap contains somewhat sparse cell bodies. nNOS-ir cell bodies are also moderately dense in a cluster in the LHAav dorsal to the SO, and in a small cluster in the LHAav ventral to the vlt (although this tract was parcellated with low confidence). The remainder of the LHA contains sparse cell bodies (excepting the LHAjp). Several cell bodies occur in the ventromedial AHNc, the lateral AHA just ventral to the BST,

and the MPO dorsal to the fx. Single cells are found in the medial LHAjp, the central MPNl, the I between the MPN and AHN, and the RCH ventral to the AHN; a couple of cells are located in the ventral PVa. nNOS-ir cell bodies avoid the MPNm, AHNa, and SCH (**Figure 2.20a, b**).

nNOS-ir cell bodies at level 24 are dense in the SO; moderately dense in the LHAjp; and form a moderately dense band in the lateral LHA that begins dorsolateral to the fx and terminates dorsal to the SO and medial to the sm (where it runs alongside the vlt), widening as it progresses ventrolaterally and fanning out as it terminates. Another small cluster of moderately dense cell bodies is found in the LHAav just ventromedial to the vlt, and somewhat sparse cells occupy the LHAav lateral to the sm and vlt, and the PVHap. A couple of cell bodies are located in the PVHpv, PVa, medial AHNc, and the LHAav or RCH ventrolateral to the AHNa (it is not clear exactly where the RCH terminates laterally). A lone cell is found between the LHAjp and the PVH. nNOS-ir cell bodies avoid the AHNa, NC, I, SBPV, and SCH (**Figure 2.21a, b**).

nNOS-ir cell bodies at level 25 are dense in the SO, the majority of the PVHpmm excepting a small strip of cells along its lateral border that are less dense, and in a cluster in the LHAjp just medial to the fx. Cell bodies are moderately dense in the LHAad dorsal and lateral to the fx, and in the LHAav dorsal to the vlt, and are somewhat sparse in a wide band in between, being sparser laterally and medially and less sparse centrally. In the lateral LHAav ventral to the SI, cells are somewhat sparse along the LHAav's ventral, lateral, and dorsal borders and are absent centrally. nNOS-ir cell bodies are moderately dense in the majority of the PVHmpd, except an empty strip along its lateral edge. A few cells are found in the dorsal PVHdp, lateral LHAjp, and the area between the LHAjp and the PVH; and single cell bodies are located in the ventral PVHpv, dorsal PVa, medial RCH, and dorsal AHNc. nNOS-ir cell bodies avoid the AHNa, AHNp, SBPV, and ZI (**Figure 2.22a, b**).

nNOS-ir cell bodies at level 26 are dense in the SO, PVHpml spilling over into the PVHmpv ventrally, and in a small strip straddling the border between the PVHmpv and PVHmpd. They are moderately dense in the dorsomedial PVHpv, in the PVHmpd lateral to the strip previously described, and in a cluster in the LHA dorsal to the fx and spilling over into the

ventral ZI. Sparse to somewhat sparse cell bodies form a wide band in the lateral LHA beginning just lateral to the cluster previously described (spilling over into the ventral ZI) and terminating dorsal to the vlt; this band fans out ventrally to occupy the lateral extent of the LHAav and has an empty space located centrally within it in the LHAav dorsal to the vlt. A couple of cells are found in the dorsal PVa, and lone cell bodies are found in the dorsomedial PVHmpd and I medial to the VMH. nNOS-ir cell bodies avoid the ARH, TU, VMH, AHN, PVHdp, and LHA medial to the fx (**Figure 2.23a, b**).

nNOS-ir cell bodies at level 27 are dense in the majority of the SOr, thinning out laterally; and moderately dense in the PVHmpd (excepting its lateral extremity), medial PVHlp, lateral PVHf, and ventrolateral VMHvl. Cell bodies are somewhat sparse in the PVHpv, medial tip of the ZI, and laterally and medially adjacent to the cluster in the lateral PVHf in the medial PVHf and LHAd. Sparse cell bodies are distributed throughout the remainder of the LHAd and the ventral LHAsfa. A couple of cell bodies are found in the dorsal PVHlp. nNOS-ir cell bodies avoid the LHA medial to the fx, the TU, the ARH, the PVi, I, and ZI except as described (**Figure 2.24a, b**).

nNOS-ir cell bodies at level 28 are dense in the SOr, thinning out laterally and straying into the TUi; and moderately dense in a band straddling the lateral and ventral borders of the VMHvl with the LHA, TUi, and TUsv. Somewhat sparse cell bodies are distributed throughout the LHA, except in the medial LHAjd dorsal to the DMH, which is empty; in several LHA locations there are small groupings of denser cell bodies; dorsomedial to the fx, ventromedial to the cpd, medial to the lateral tip of the TUi, and ventrolateral to the lateral tip of the ZIda. Sparse cell bodies occur in the medial TUsv, medial DMH and dorsal PVi, and ventral ZI dorsal to the medial cpd and lateral LHA; several additional cell bodies occur in the ventromedial ZI. A single cell body is located in the central and lateral ARH, and a couple are in the lateral VMHc. nNOS-ir cell bodies avoid the VMHdm and ZIda (**Figure 2.25a, b**).

nNOS-ir cell bodies at level 29 are dense to moderately dense in the ventrolateral VMHvl and adjacent LHA; and moderately dense to somewhat sparse in the LHA and ventromedial ZI,

denser near the fx and sparser around the LHA's borders. Cell bodies are somewhat sparse in the medial DMHa; and lone cell bodies are found in the lateral ZI, dorsolateral PH, ventral I, lateral ARH, dorsal VMHdm, TUsv ventral to the VMHvl, medial TUi, lateral TUi, and TUl (although the identification of this structure was tentative). nNOS-ir cell bodies avoid the VMHc, DMHp, and PVi (**Figure 2.26a, b**).

nNOS-ir cell bodies at level 30 are dense in a small cluster in the lateral DMHv, and moderately dense surrounding this cluster and stretching laterally into the LHA just medial to the fx. The population of nNOS-ir cell bodies in the VMH is absent; only a couple of cell bodies remain in the ventral VMHvl. A line of cells stretches ventromedially in the ventral LHA, beginning just dorsal to the lateral tip of the TUl and finishing just dorsal to the TUte (although the TUl was parcellated with low confidence). A couple of cells are found in the ventral ZI dorsal to the LHAm, and a few occur in the ventromedial DMHp. Single cell bodies are located in the ventral PH, LHA just ventrolateral to the cells in the ZI, dorsal TUte, medial TUi, and ventral LHA just dorsal to the cell in the TUi. nNOS-ir cell bodies avoid the ARH, TUsv, TUl, VMHc, I, PVi, and DMHa (**Figure 2.27a, b**).

nNOS-ir cell bodies at level 31 are dense in a small cluster in the ventrolateral DMHp, spilling over into the adjacent DMHv. They are somewhat sparse in the LHA and PH ringing the fx dorsally; in the LHA, TUte, and TUi ventrolateral to the fx (although the TUi was parcellated with low confidence), in the DMHv and LHAjvv traveling dorsomedially from the cluster previously described; in the LHA ringing the PST dorsally, medially, and ventrally; and in a band beginning in the PVi dorsal to the DMH and traveling roughly mediolaterally through the LHAjvv, PH, and ventral ZI. Lone cell bodies are found in the dorsal PH, the LHAjvv ventromedial to the fx, the medial DMHp, and the central DMHa. nNOS-ir cell bodies avoid the PVp, TUl (parcellated with low confidence), PST, and I (**Figure 2.28a, b**).

nNOS-ir cell bodies at level 32 are dense in the lateral PMv, and moderately dense in two limbs extending laterally and dorsally from this population, into the LHAvm and TUte, and I medial to the PMd and ventral PH. There are somewhat sparse cell bodies in the ventrolateral

PH, intermingling with the MCH-ir cells in that location, and also lining the PH's lateral and dorsal borders. Two small clusters of dense cell bodies are found in the LHA just medial to the vlt (identified with low confidence) and ventral to the PSTN (identified with low confidence as well). Moderately dense to somewhat sparse cell bodies line the ventral half of the dorsal opening of the hypothalamic recess of the third ventricle; and somewhat sparse cells occupy the lateral LHAp lateral to the mtt, thinning out medially and ventrally. Several cell bodies are found in the ventromedial ZI, and lone cell bodies occur in the ventral PVp, dorsal I, dorsal LHAp just lateral to the PH, and ZI dorsal to those previously described there. Two cells lie in the PMd. nNOS-ir cell bodies avoid the TMd (**Figure 2.29a, b**).

nNOS-ir cell bodies have not yet been mapped at levels 33–36.

nNOS-ir fibers

nNOS-ir fibers at level 15 are sparse in the lateral LPO, and at level 16 are sparse in the lateral and medial LPO, while avoiding the structure's center. Sparse fibers at level 16 are also found in the BSTal, spilling over into the BSTam along its border with the BSTal; and there are a couple of longer fibers in the BSTam just medial to the aco. Diffuse nNOS staining, not possessing distinguishable features or structural characteristics beyond a vague reticular quality and interpreted as nNOS-ir neuropil, is found at level 16 in the LPO and the dorsal and medial BSTam, ceasing where the BSTam runs ventral to the aco (**Figure 2.12c, d; 16c, e**).

nNOS-ir fibers are moderately dense in a wide band that runs mediolaterally and spans the dorsal LPO and dorsal tip of the MPO and terminates in the BSTam medial to the aco; being shorter laterally and thinning out just ventral to the MS. Somewhat sparse fibers occur in the PS, and in the ventromedial AVP and MPO ventral to the AVP; and sparse fibers are found in the MEPO, MPO just lateral to the AVP, ventral LPO, and BSTal and BSTam along their lateral borders and immediately dorsal to the aco. nNOS-ir neuropil is found in the BSTam, except its ventral tip; in the BSTal, except along its lateral border; in a band crossing the LPO mediolaterally, being located in the dorsal portion of the band of nNOS-ir fibers previously

discussed; in the MEPO, except along its dorsolateral border; and in the dorsomedial AVP. nNOS-ir fibers largely avoid the AVPV (**Figure 2.14c, e**).

nNOS-ir fibers at level 18 are somewhat sparse in a band that travels mediolaterally across the dorsal LPO; they are dominantly oriented dorsoventrally, and are longer and denser medially. nNOS-ir fibers are also somewhat sparse in the medial MEPO, and in a line running along the medial border of the AVP and extending slightly into the MPO dorsal to it. Fibers are sparse in the BST along the edges of the aco and act, some of them being long; there are a few fibers scattered elsewhere in the BST; and a few fibers in the ADP, notable because one is long. nNOS-ir neuropil is found in a wedge at the section's midline, beginning in the dorsal MEPO and extending dorsally through the MPO into the LPO to terminate just short of the ventral border of the MS; and in the BSTam dorsal and medial to the aco, extending into medial BSTal immediately dorsal and ventral to the act. nNOS-ir fibers largely avoid the ventral LPO, AVPV, PSCH, and AVP and MPO except as described (**Figure 2.15c, e**).

nNOS-ir fibers at level 19 are moderately dense in the MEPO, in the LPO dorsal to the aco, and in a wedge extending laterally from the MEPO, through the dorsomedial MPO and dorsomedial ADP into the dorsal LPO just ventral to the aco. nNOS-ir fibers are somewhat sparse in the AVP, excepting its lateral edge, the MPO dorsal to the AVP, and the ventromedial MPN. They are sparse in the PS and BST, being nearly absent from the lateral and ventral extremities of the BST, and denser along the border of the act and aco; those along this border are dominantly oriented parallel to it. nNOS-ir neuropil exists in the MEPO, spilling over into the LPO dorsal to the aco; and in the BST, again being absent from its lateral and ventral extremities, except in a horn extending to the ventrolateral corner of the BST and apparently parallel to the tip of the act and aco. nNOS-ir fibers largely avoid the ventral LPO, AVPV, and PSCH (**Figure 2.16a, b**).

nNOS-ir fibers at level 20 are moderately dense in the MEPO, and in the dorsal MEPO are long and oriented dorsoventrally. Fibers are also moderately dense in a cluster near nNOS-ir cell bodies in the lateral extremity of the LPO; and are somewhat sparse near cell bodies in the

dorsomedial MPO, dorsal to the MPN and medial to the ADP. Fibers are sparse near nNOS-ir cell bodies in the ventral MPO and dorsomedial AVP, in the ventral MPNm and MPNc, and in the MPO lateral to the MPN. A few fibers are scattered throughout the BST. nNOS-ir neuropil occurs in the MEPO and in the BST, beginning in the BSTpr and extending ventrally through the medial BSTal, terminating in the dorsolateral BSTam and BSTmg (although BST parcellations ventral to the aco are low-confidence). nNOS-ir fibers largely avoid the PVpo, PSCH, VLP, SO, LPO except as described, and MPNl (**Figure 2.17a, b**).

nNOS-ir fibers at level 21 are dense in a band stretching mediolaterally from the BST ventral to the act to the lateral MPO ventral to the aco; these fibers are denser and longer and dominantly oriented ventrolaterally in the BST, while in the lateral MPO they are shorter, less dense, more widely distributed (that is, the band fans out dorsally and ventrally), and less likely to be oriented ventrolaterally. Fibers are moderately dense in the dorsal MPNl and MPNm, spilling over into the MPO laterally; in a band in the ventral MPNl and MPNm, spilling into the MPO laterally; in a cluster in the lateral extremity of the LPO; in the dorsomedial MPO and MEPO ventral to the aco; along the dorsal and medial borders of the BSTpr, spilling over into the area ventromedial to the BSTpr and becoming more dense; and near nNOS-ir cell bodies in the dorsal BSTal. Fibers are somewhat sparse throughout the majority of the remainder of the BST, excluding empty regions in the dorsolateral BSTpr, ventral BSTrh, and central BSTam, although with the exception of the BSTpr these areas are parcellated with low-confidence. nNOS-ir fibers are also somewhat sparse in the AHN and near nNOS-ir cell bodies straddling the boundary between the LPO and MPO, centrally located with respect to the boundary's dorsoventral extent. Sparse fibers accompany cell bodies in the dorsal LPO, and are found in the ADP. nNOS-ir neuropil occurs in the majority of the BST, spilling over into the MPO along the BST's ventromedial border; and except for the area along the lateral border of the BST, the dorsal BSTpr, and the BST dorsal to the ADP and ventral to the act and aco. nNOS-ir fibers largely avoid the SCH and PVpo (**Figure 2.18a, b**).

nNOS-ir fibers at level 22 are dense in the lateral BST and along the ventral edge of the section in the SO, being dominantly oriented ventrolaterally; and moderately dense in the lateral LHAav. They are somewhat sparse in the medial BST, except the BSTv which is largely unoccupied by nNOS-ir fibers (although the BSTv was parcellated with low-confidence); medial LHAav; LHAai; majority of the SO except as described; and near nNOS-ir cell bodies in the lateral PVHap and dorsolateral PVHam. nNOS-ir fibers are sparse in the MPO and AHA, and in the PVHpv and PVHap between the fingers of the mct. nNOS-ir fibers largely avoid the AHN, SCH, MPN, PVpo, SBPV, and I (**Figure 2.19a, b**).

nNOS-ir fibers at level 23 are dense along the ventral edge of the section in the SO, being dominantly oriented ventrolaterally; and moderately dense in a cluster near cell bodies in the LHAav dorsal to the SO; in the medial LHAjp, dorsal PVHap, and MPO in between these two structures; and in the BST, spilling over dorsally into the MPO. Fibers in the LHAjp are dominantly oriented mediolaterally. nNOS-ir fibers are somewhat sparse in the SO, except as described, and LHAav ventral to the vlt (although the vlt was parcellated with low-confidence); and are sparse laterally in the LHAav, in the LHAai, and in the PVHpv. nNOS-ir neuropil is found in the BST and spills over ventrally into the LHAai and AHA. nNOS-ir fibers largely avoid the AHN, MPN, SCH, PVpo, RCH, SBPV, I, and AHA except as described (**Figure 2.20a, b**).

nNOS-ir fibers at level 24 are dense along the ventral edge of the section in the SO; and along a small portion of the ventral border of the LHAav medial to the MEAad, and extending from the edge of the section to a point roughly halfway to the vlt along the LHAav border (although the vlt was parcellated with low-confidence), being denser towards the interior of the section and becoming sparse towards the ventral edge of the section. These fibers are all oriented dominantly ventrolaterally. Fibers are moderately dense to somewhat sparse in the LHAjp; and are moderately dense in a band running from the lateral edge of the LHAjp immediately dorsal to the fx in the LHAad, through the LHAai, and terminating in the LHAav dorsal to the SO and medial to the vlt and sm. This band is thinner dorsally and widens ventrally, and dorsal to the fx

the fibers within it are denser, shorter, and dominantly oriented mediolaterally. Additional nNOS-ir fibers in the LHAav are found near cell bodies in a ventrally-located cluster and along the borders of the LHAav lateral to the vlt and sm; these fibers are somewhat sparse to moderately dense. Somewhat sparse fibers also occupy the PVHap, becoming sparse laterally; and sparse fibers are located in the PVHpv and dorsal PVa, and in the lateral AHN. A group of fibers straddling the boundary between the AHNa and AHNc are moderately long and oriented ventrolaterally. nNOS-ir neuropil is found in the LHAjp, and stretches ventrally in a band that occupies the lateral AHNc, terminating just dorsal to the AHNa and lateral to the NC. nNOS-ir fibers largely avoid the SCH, RCH, SBPV, and I (**Figure 2.21a, b**).

nNOS-ir fibers at level 25 are dense along the ventral edge of the section in the SO, being dominantly oriented ventrolaterally; moderately dense in the PVHpmm, becoming somewhat sparse in the PVHmpd and PVHdp; and moderately dense in a cluster near nNOS-ir cell bodies in the lateral LHAjp just medial to the fx. A somewhat sparse band of fibers stretches from the LHAad dorsal to the fx and just lateral to the LHAjp, through the LHAai, into the dorsal LHAav; these fibers are dominantly oriented ventrolaterally and are denser dorsally. Somewhat sparse fibers are also found along the borders of the lateral LHAav ventral to the int. There is a small moderately dense cluster of fibers in the dorsal PVa, and sparse fibers in the SO. nNOS-ir fibers largely avoid the ZI, AHN, PVa except as described, I, SBPV, and RCH (**Figure 2.22a, b**).

nNOS-ir fibers at level 26 are moderately dense in a cluster in the lateral LHAjp dorsal to the fx, and spilling over into the ventral ZI; and are somewhat sparse in a band running from the lateral edge of the cluster previously described, through the LHAad, terminating in the LHAai, and spilling over into the ventral ZI and lateral LHAjp. Fibers in this band are dominantly oriented ventrolaterally. nNOS-ir fibers are somewhat sparse in the ventrolateral LHAav, PVHpml, PVHmpd, and PVHpv; they are sparse in the PVHmpv. nNOS-ir fibers largely avoid the ZI except as described, AHN, LHA medial to the fx, VMH, TU, ARH, PVi, I, and SBPV (**Figure 2.23a, b**).

nNOS-ir fibers at level 27 are moderately dense in a cluster in the PVHf, and in the PVHmpd, excepting its lateral extremity. They are somewhat sparse in a small cluster in the LHA immediately dorsal to the sup, and ventromedial to the vlt, although the vlt was parcellated with low-confidence; and in a small fringe ventromedial to the TUsv and immediately lateral to the ME. Sparse fibers are located in PVHpv, medial PVHlp, medial ZI, and LHA lateral to the fx. nNOS-ir neuropil is found in the VMHvl and in a band along the border of the ME, in the ARH and the area ventromedial to the TUsv. nNOS-ir fibers largely avoid the TU, VMH except as described, LHA medial to the fx, AHN, ARH except as described, I, SBPV, PVi, and ZI except as described (**Figure 2.24a, b**).

nNOS-ir fibers at level 28 are dense to moderately dense near nNOS-ir cell bodies straddling the lateral and ventral border of the VMHvl with the LHA and TU, being denser ventrally; and in a band in the ventral ARH, medial TUsv, and the area ventral to the TUsv. Moderately dense groupings of fibers occur in several locations in the LHA; in the ventrolateral LHA dorsal to the lateral tip of the TUi, in the lateral LHA just ventromedial to the cpd, in the LHAjvv (although the LHA subparcellations are low-confidence), and in the in dorsomedial LHA dorsal and medial to the fx; elsewhere in the LHA nNOS-ir fibers are somewhat sparse, except in the LHAjd dorsal to the DMH, where they are sparse. Somewhat sparse fibers are also found in the ZI lateral to the ZIda and medial to the em, where they are dominantly oriented ventromedially; along the ventral, lateral, and dorsal edges of the DMH; and in the medial TUsv, VMHc, and ventral I. nNOS-ir neuropil is located in the VMHc, in the dorsal VMHdm, and in a band in the ventral ARH and the area ventral to the TUsv lateral to the ME. nNOS-ir fibers largely avoid the TUi, ARH except as described, PVi, and VMHdm except as described (**Figure 2.25a, b**).

nNOS-ir fibers at level 29 are moderately dense in a small cluster in the lateral LHA and lateral vlt, although the vlt was parcellated with low-confidence. They are moderately dense to somewhat sparse near nNOS-ir cell bodies in the LHA beginning just ventromedial to the fx and travelling ventromedially to terminate in the lateral and ventral VMHvl; additional somewhat

sparse fibers ring the fx in a halo. Somewhat sparse fibers are also found in the lateral LHA just medial to the cpd; in the medial TUl, although this structure was parcellated with low-confidence; in the DMHa; and in the dorsal ZI dorsal to the medial tip of the cpd, where they are short and oriented ventromedially. nNOS-ir neuropil occurs in the VMHdm, spilling over into the I and LHAjvd dorsally and the VMHc ventrally and terminating short of the VMHdm's medial border; and in a band in the ventral ARH just lateral to the ME. nNOS-ir fibers largely avoid the TU, except as described; VMHc, except as described; I, except as described; PVi; and DMHp (**Figure 2.26a, b**).

nNOS-ir fibers at level 30 are somewhat sparse near nNOS-ir cell bodies in the lateral DMHv and LHA medial to the fx; and near nNOS-ir cell bodies in the lateral VMHvl, medial TUi, and ventral LHAjvv. Fibers are sparsely distributed in the PH, ZI, LHA dorsal to the fx, DMHa, and along the ventral and lateral borders of the DMHp. nNOS-ir neuropil occurs in one cluster in the medial VMHvl and VMHc, medial TUsv, ventral I, and lateral ARH; and in a particularly brightly-staining band in the ventral ARH just dorsal to the ME. nNOS-ir fibers largely avoid the TU, except as described; LHA lateral to the fx; dorsal I; and PVi (**Figure 2.27a, b**).

nNOS-ir fibers at level 31 are dense and short in a cluster in the LHAjvv and PVi at the dorsal end of the hypothalamic recess of the third ventricle; and in a small cluster at the ventral edge of the section in the LHA ventral to the fx. Moderately dense fibers are found near nNOS-ir cell bodies in a band beginning in the medial ZI ventral to the mtt and traveling mediolaterally to the medial border of the PH; and in a small cluster in the LHAjvv just lateral to the dorsal tip of the DMHv. Sparse fibers are located in the LHA and PH medial to the fx in a partial ring around the fx; in the ventral LHA dorsal to the TUte; and in the ventral DMHv and ventrolateral DMHp. nNOS-ir neuropil occurs in a small cluster near nNOS-ir cell bodies in the ventrolateral DMHp; and in a wide band in the PVp and the area ventral to the PVp and lateral to the MEin. nNOS-ir fibers largely avoid the TU, PST, I, and PVi except as described (**Figure 2.28a, b**).

nNOS-ir fibers at level 32 are moderately dense and pointillescent in the dorsal I and medial PH along the dorsoventral extent of the dorsal portion of the hypothalamic recess of the third ventricle, being denser dorsally; and in a small cluster in the PH dorsomedial to the mtt. Fibers are somewhat sparse in the ventral PH; near nNOS-ir cell bodies in the dorsal TUte, LHAvm just dorsal to the TUte , lateral PMv, and I dorsal to the PMv; in small clusters near nNOS-ir cell bodies in the LHAvm just medial to the vlt (parcellated with low-confidence) and in the medial LHAvl (parcellated with low-confidence); in the lateral LHAp; and in a small cluster in the dorsomedial LHAp. nNOS-ir neuropil is found in the TUte, PMv, and I dorsal to the PMv, spilling over into the LHAvm dorsal to the TUte, and terminating short of the ventral border of the TUte and ventral and medial borders of the PMv. nNOS-ir fibers largely avoid the ZI, PSTN, I except as described, TMd, and PVp (**Figure 2.29a, b**).

nNOS-ir fibers at level 33 are moderately dense in the dorsal PH; in the PH along the lateral border of the hypothalamic recess of the third ventricle; in a small cluster in the PH ventral to the SPFm; in the ventral PMd and the LHAp just lateral to it; in the medial PMv; in a small cluster just dorsal to the mammillary recess of the third ventricle; and in the ventrolateral SUMl. Somewhat sparse fibers are present in the ventral PH and ventral MMme; while sparse fibers are located in the remainder of the PH, in the LHA immediately lateral to the fx, and in a semi-circle ringing the fx at a distance in the lateral LHA, beginning just lateral to the fibers in the ventrolateral SUMl and terminating in the ventral LHAsfpm (although the LHAsfpm was parcellated with low-confidence). nNOS-ir fibers largely avoid the dorsal LHAp and PSTN. nNOS-ir neuropil has not been mapped at this level (**Figure 2.30**).

nNOS-ir fibers at level 34 are moderately dense in the dorsomedial PH, the SUMm, and the PVp and the area immediately surrounding it; they are somewhat sparse in a small cluster in the central LHAp. Sparse fibers are found in the SUMl except for its ventral lobe, the remainder of the LHAp, the remainder of the PH except for a small empty region dorsolateral to the mtg, the smd, the medial TMv, and a thin band traveling dorsoventrally from the dorsal MMme to the ventral MM; a few fibers are located in the lateral MM. nNOS-ir fibers largely avoid the LM,

lateral TMv, and the medial MM except as described. nNOS-ir neuropil has not been mapped at this level (**Figure 2.31**).

nNOS-ir fibers at level 35 are moderately dense in a cluster straddling the border between the SUMm and SUMl, and in a cluster in the lateral PVp and the area immediately surrounding it. Somewhat sparse fibers are found in the medial PH, smd, lateral border of the SUMl and the area immediately lateral to it, and ventral TMv. Sparse fibers occupy the remainder of the SUMl, and the lateral MM; a few fibers are located in the dorsolateral PH and form a line traveling dorsoventrally along the midline from the area just dorsal to the MM to the area just ventral to it, being denser ventrally. nNOS-ir fibers largely avoid the LM and medial MM except as described. nNOS-ir neuropil has not been mapped at this level (**Figure 2.32**).

nNOS-ir fibers at level 36 are somewhat sparse in the medial PH, where they are long and oriented dorsoventrally; along the ventral border of the PH; in the ventral SUMl and SUMm; and along the ventral edge of the section in the area ventral to the MM, from the midline to its lateral extent. Sparse fibers are found in the TMv, dorsal PH, near nNOS-ir cell bodies in the dorsolateral MM, and in the area between the TMv, SUMl, and PH. A few fibers are found in the lateral PH. nNOS-ir fibers largely avoid the MM, except as described. nNOS-ir neuropil has not been mapped at this level (**Figure 2.33**).

MCH/nNOS-ir cell bodies

A population of cell bodies immunoreactive against both MCH and nNOS antibodies appears at level 28; it is located in the dorsolateral LHA, extending ventrally to the vlt (parcellated with low confidence) and laterally to the fx and spilling over into the cpd, and being dense dorsolaterally and somewhat sparse ventrally and medially (**Figure 2.25c**). At level 29 MCH/nNOS-ir cell bodies are dense to moderately dense in a cluster in the LHA just medial to the medial tip of the cpd; somewhat sparse cell bodies continue medially to the fx (**Figure 2.26c**). At level 30 somewhat sparse MCH/nNOS-ir cell bodies are found in the dorsolateral LHA, while a couple of cell are in the LHA dorsal to the fx, and one is in the ventral ZI dorsal to

the medial tip of the cpd (**Figure 2.27c**). At level 31 there is a cluster of somewhat sparse MCH/nNOS-ir cell bodies in the ventral PST and the LHA just ventral to the PST; and a lone cell body in the area dorsal to the PST and ventral to the ZI (**Figure 2.28c**). At level 32 there are a few MCH/nNOS-ir cell bodies scattered in the lateral LHAp. This is the caudal-most level at which such cells are present (**Figure 2.29c**).

Potential Synaptic Interaction Zones (PSIZs)

No PSIZs are identified at level 15. At level 16, there is a PSIZ involving α-MSH and nNOS occupying the majority of the BSTam medial and dorsal to the aco, and another involving MCH and nNOS occupying the majority of the LPO (**Figure 2.13d**).

At level 17 there are two PSIZs involving α-MSH and nNOS; one that stretches from the medial AVP and the MPO medial to the AVP dorsally to occupy the majority of the MEPO, excepting its ventralmost and dorsalmost reaches; and one that begins as a band running ventromedially across the LPO from the midline dorsal to the MPO to the BSTam, and then widens to occupy the BSTam dorsal and medial to the aco and the medial BSTal dorsal to the aco – this may be a continuation of the PSIZ for α-MSH and nNOS at level 16. There is one PSIZ involving MCH and nNOS that fills the majority of the dorsal LPO, excepting its ventral and dorsal margins; this may also be a continuation of the PSIZ for MCH and nNOS at level 16 (**Figure 2.14d**).

At level 18 there are three PSIZs involving α-MSH and nNOS, which may be remnants of the PSIZ described for α-MSH and nNOS at level 17 in the AVP, MPO, and MEPO; one lies in the medial AVP, another in the ventral MEPO, and the third in the dorsal tip of the MEPO. There are two PSIZs involving MCH and nNOS, which also may be remnants of the PSIZ described for MCH and nNOS at level 17; one is in the dorsomedial LPO, the other in the dorsolateral LPO. A PSIZ involving α-MSH and MCH lies along the lateral border of the preoptic recess of the third ventricle, in the medial AVPV and the PSCH excepting its lateral tip (**Figure 2.15d**).

At level 19 there are two PSIZs involving α-MSH and nNOS; one in the dorsal ADP, and one in the MEPO ventral to the aco, which may or may not be continuous with those described in the MEPO at level 18. There is one PSIZ involving MCH and nNOS, in the dorsal LPO dorsal to the aco, which may be a continuation of those described for MCH and nNOS at level 18. And there are two PSIZs involving α-MSH and MCH; one in the PSCH and ventromedial AVPV, and one in the ventromedial MEPO and dorsomedial AVPV along the third ventricle; it is possible that the PSIZ described for α-MSH and MCH at level 18 has split in two at level 19 (**Figure 2.16c**).

At level 20 there are two PSIZs involving α-MSH and nNOS; one along the lateral border of the MEPO dorsal to the aco, and one in the MEPO ventral to the aco that sends a limb into the MPO dorsal to the MPN and ventral to the ADP; this limb may be continuous with the PSIZ for α-MSH and nNOS described at level 19 in the ADP, while the MEPO PSIZ(s) is obviously potentially continuous with that from level 19. There are also two PSIZs involving MCH and nNOS; one in the lateral extremity of the LPO, and one along the lateral and ventral borders of the MEPO dorsal to the aco; neither is likely to be continued from level 19 PSIZs. There is one PSIZ involving α-MSH and MCH; which runs along the dorsal border of the och in the MPO, ventromedial AVP, and PSCH; and continues along the lateral border of the third ventricle, in the PSCH, MPO, and PVpo, terminating ventral to the MPNc; this may be a continuation of the ventral PSIZ involving α-MSH and MCH at level 19, as both appear centered on the PSCH (**Figure 2.17c**).

At level 21 there is one large, novel PSIZ involving MCH and nNOS occupying the majority of the BST, excepting its dorsal, lateral, and medial edges, and spilling over into the LPO ventral to the PD. There is also a PSIZ involving α-MSH and MCH, along the ventral and lateral borders of the third ventricle in the PVpo and MEPO, terminating dorsal to the AHN; this may be continuous with the PSIZ for α-MSH and MCH at level 20 (**Figure 2.18c**).

At level 22 there are three PSIZs involving α-MSH and nNOS in the PVH; one in the lateral PVHap and dorsolateral PVHam, one in the PVHpv and medial PVHap beginning just

ventral to the first branching of the mct into fingers and extending ventrally approximately halfway along their length, and one small one in the PVHap amongst the fingers of the mct (**Figure 2.19c**).

At level 23 there is one PSIZ involving α-MSH and nNOS occupying the majority of the PVH, excepting its ventral tip, which may represent a consolidation of the PSIZs described at level 22 (**Figure 2.20c**).

At level 24 there is one PSIZ involving α-MSH and nNOS occupying the majority of the PVH, excepting its ventral and dorsal tips and its lateral border, which is likely continuous with the PSIZ described at level 23 (**Figure 2.21c**).

At level 25 there are two PSIZs involving α-MSH and nNOS; one in the PVHdp and dorsal and medial PVHmpd; and one small one straddling the boundary between the PVHpv and the PVa; these may be continuous with the PSIZ described at level 24. There is also a PSIZ involving α-MSH and MCH in the medial RCH, ventral to the third ventricle and dorsal to the sup (**Figure 2.22**).

At level 26 there is one PSIZ involving α-MSH and nNOS in the PVHpv, spilling over ventrally into the PVi; this may represent a consolidation of the PSIVs for α-MSH and nNOS described at level 25, or might be continuous with only one of them, likely the ventral one. There is a PSIZ involving α-MSH and MCH in the PVi and the adjacent SBPV, which may be continuous with the PSIV for α-MSH and MCH described at level 25 or may be novel, as it is located in the same structure but has shifted, with the PV, dorsally, possibly to avoid the emerging ARH (**Figure 2.23c**).

At level 27 there is one PSIZ involving α-MSH and nNOS in the PVHpv, excepting its ventral and dorsal tips, and the PVHmpd, excepting its lateral tip and spilling over dorsolaterally into the PVHlp; this may or may not be continuous with the PSIZ described for α-MSH and nNOS at level 26 (**Figure 2.24c**).

At level 28 there is one PSIZ involving α-MSH and nNOS in the ventral ARH and the area ventral to the ARH, which forms a band just lateral and dorsal to the ME. There is one PSIZ

involving MCH and nNOS in the dorsolateral LHA and ventral ZI. There are also two PSIZs involving MCH and α-MSH; one straddling the border between the LHA and the ZI dorsal to the fx; and another in the ventral TUsv, ventrolateral ARH, and the area ventral to the TUsv and ARH, just lateral to the ME (**Figure 2.25c**).

At level 29 there are two PSIZs involving α-MSH and nNOS; one forming a band that stretches mediolaterally across the DMH from its lateral tip to the PVi, and the other forming a band in the ventral ARH and the area ventral to the ARH just lateral and dorsal to the ME; this is likely continuous with the PSIZ for α-MSH and nNOS described at level 28. There are also two small PSIZs involving MCH and nNOS; one in the dorsal LHA lateral to the fx that spills over into the ventral ZI and may be continuous with the PSIZ described for MCH and nNOS at level 28, and one in the LHA just medial to the fx. There is a single PSIZ involving α-MSH and MCH in the ventrolateral ARH and the area ventral to the ARH, just lateral to the ME (**Figure 2.26c**).

At level 30 there are three PSIZs involving α-MSH and nNOS; one in the lateral DMHv spilling over laterally into the LHA that might be continuous with the PSIZ for α-MSH and nNOS described in the DMH at level 29, one in the ventrolateral VMHvl, and one forming a band in the ventral ARH and the area ventral to the ARH just lateral and dorsal to the ME; the latter PSIZ may be continuous with that described for α-MSH and nNOS in the ARH at level 29. There is one PSIZ involving MCH and nNOS in the LHA medial to the fx and the lateral DMHv, from which a limb extends that wraps around the fx dorsally; this may be continuous with the small PSIZ for MCH and nNOS described as being medial to the fx at level 29. There are three PSIZs involving α-MSH and MCH as well, one being located along the ventral edge of the section ventral to the TUi. One roughly forms a band in the ventral and lateral ARH, ventromedial TUsv, and the area ventral to the ARH, just lateral and dorsal to the ARH PSIZ for α-MSH and nNOS at this level; this PSIZ may be continuous with the ARH PSIZ for α-MSH and nNOS described at level 29. And the third is large and irregularly shaped, occupying the dorsal ARH, PVi, medial I, medial DMHa, and ventral DMHp; with a limb extending mediolaterally

across the DMHa (centrally located with respect to its dorsoventral extent) and into the LHA (**Figure 2.27c**).

At level 31 there are three PSIZs involving α-MSH and nNOS; a small one in the ventral TUte, one in the dorsal PVi stretching laterally through the LHAjvv into the medial PH, and one in the ventrolateral DMHp and medial DMHv that extends a limb dorsally along the border between the DMHp and DMHv into the LHAjvv; the last may be continuous with the PSIZ for α-MSH and nNOS described in the DMH at level 30. There are six PSIZs involving MCH and nNOS; three small ones ventral to the TUte, ventral to the TUi, and dorsolateral to the PST; one forming a band stretching from the medial DMHp dorsally through the DMHa, PVi, and LHAjvv, where it widens into the PH; one in the PH surrounding the fx medially and dorsally; and one forming a band that stretches from the lateral DMHp dorsolaterally through the dorsal DMHv into the LHAjvv; these last two PSIZs, especially the second-to-last, may be continuous with the PSIZ for MCH and nNOS described in the DMH and LHA near the fx at level 30. There are three PSIZs involving α-MSH and MCH; one along the ventral edge of the section ventral to the TUte and TUi; one along the ventral edge of the section ventral to the PVpo and extending dorsally into the PVpo centrally along its mediolateral extent, that may be continuous with the PSIZ for α-MSH and MCH described at level 30 in the ARH; and one large one occupying the dorsomedial DMHv, the majority of the DMHp, the DMHa, the majority of the PVi, the medial LHAjvv dorsal to the DMH, and extending laterally into the medial PH; this last PSIZ may be continuous with the PSIZ for α-MSH and MCH described in the DMH and PVi at level 30 (**Figure 2.28c**).

At level 32 there are five PSIZs involving α-MSH and nNOS; a small one in the ventral PVpo; a small one in the PH dorsolateral to the mtt; one along the ventral edge of the section in the LHA ventral to the TUte; one located centrally in the PMv; and one and irregularly shaped one that consists of two limbs connecting to each other in the PH, one stretching dorsoventrally in the dorsomedial PH and the area medial to the PH and lateral to the dorsal portion of the hypothalamic recess of the third ventricle and one beginning in the I dorsal to the PMv and

stretching dorsoventrally into the ventral PH. It is possible this last PSIZ is continuous with the PSIZ for α-MSH and nNOS described in the PVi and PH at level 31. There are three PSIZs involving MCH and nNOS; one small one in the LHA ventral to the TUte; one forming a short band stretching mediolaterally in the lateral LHAp ventral to the ZI; and one large and irregularly shaped one roughly mirroring the dorsal limb and connecting point of the large PSIZ for α-MSH and nNOS at this level, but also extending laterally in the ventrolateral PH to the mtt. This last PSIZ may be continuous with the PSIZ for MCH and nNOS centered on the PVi described at level 31. There are also three PSIZs involving α-MSH and MCH; one stretching along the ventral edge of the section in the LHA and I from the midline to the cpd; one forming a short band in the lateral LHA just dorsal to the PSTN; and one large and irregularly shaped one in the dorsal PVpo, TMd, dorsomedial I, medial PH, and the area medial to the PH and lateral to the dorsal portion of the hypothalamic recess of the third ventricle. This last PSIZ may be continuous with the PSIZ for α-MSH and MCH described in the DMH, PVi, and LHAjvv at level 31; while the first PSIZ for α-MSH and MCH may be continuous with those described at level 31 that lie along the ventral edge of the section (**Figure 2.29c**).

PSIZs have not yet been mapped at levels 33–36.

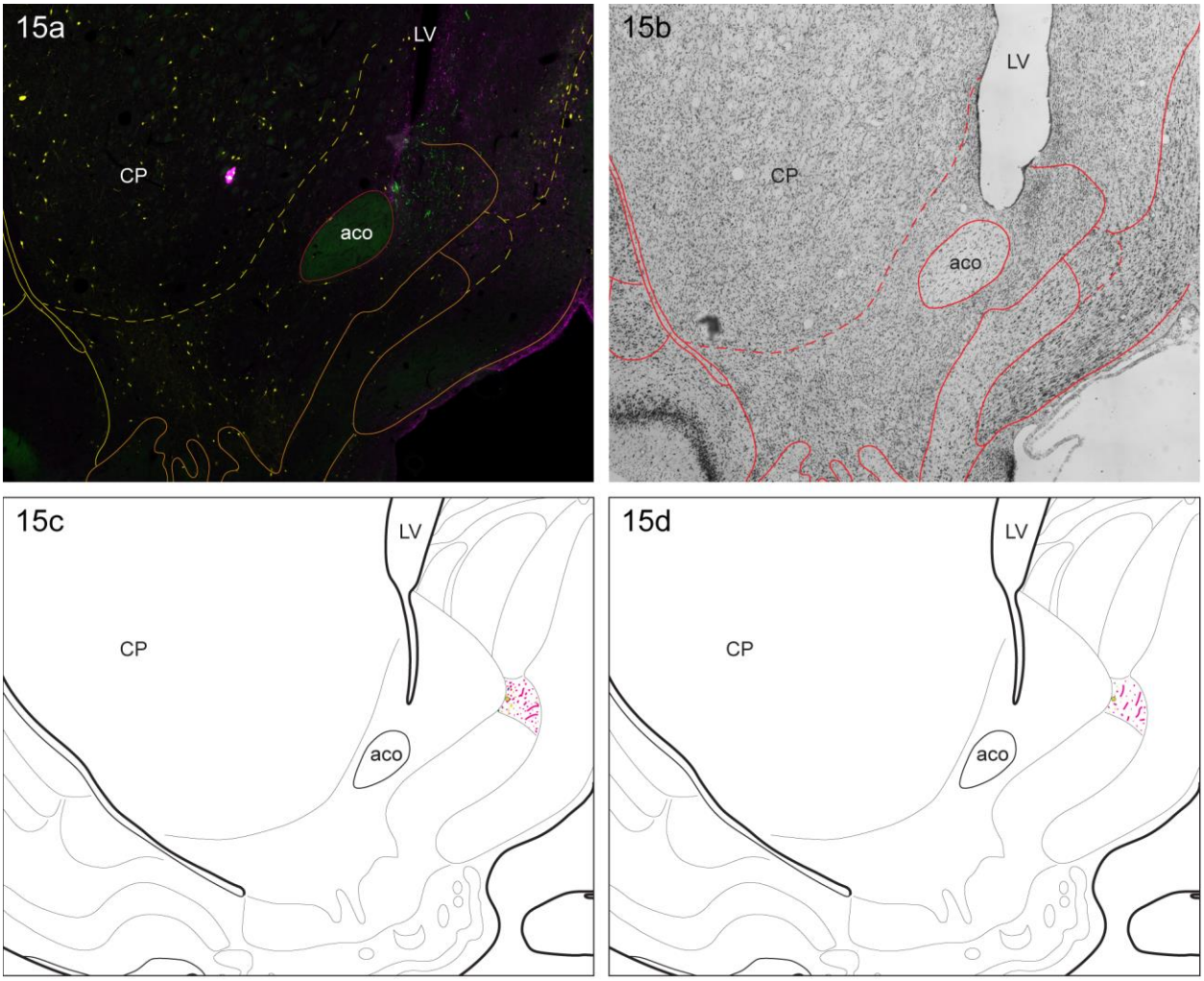

Figure 2.12: Level 15 Maps.

Table 2.2: Legend for Maps.

	Cell Bodies	Fibers	Diffuse	PSIZs
α-MSH				
nNOS				
MCH				
MCH/nNOS cell bodies				
α-MSH/nNOS				
α-MSH/MCH				
MCH/nNOS				

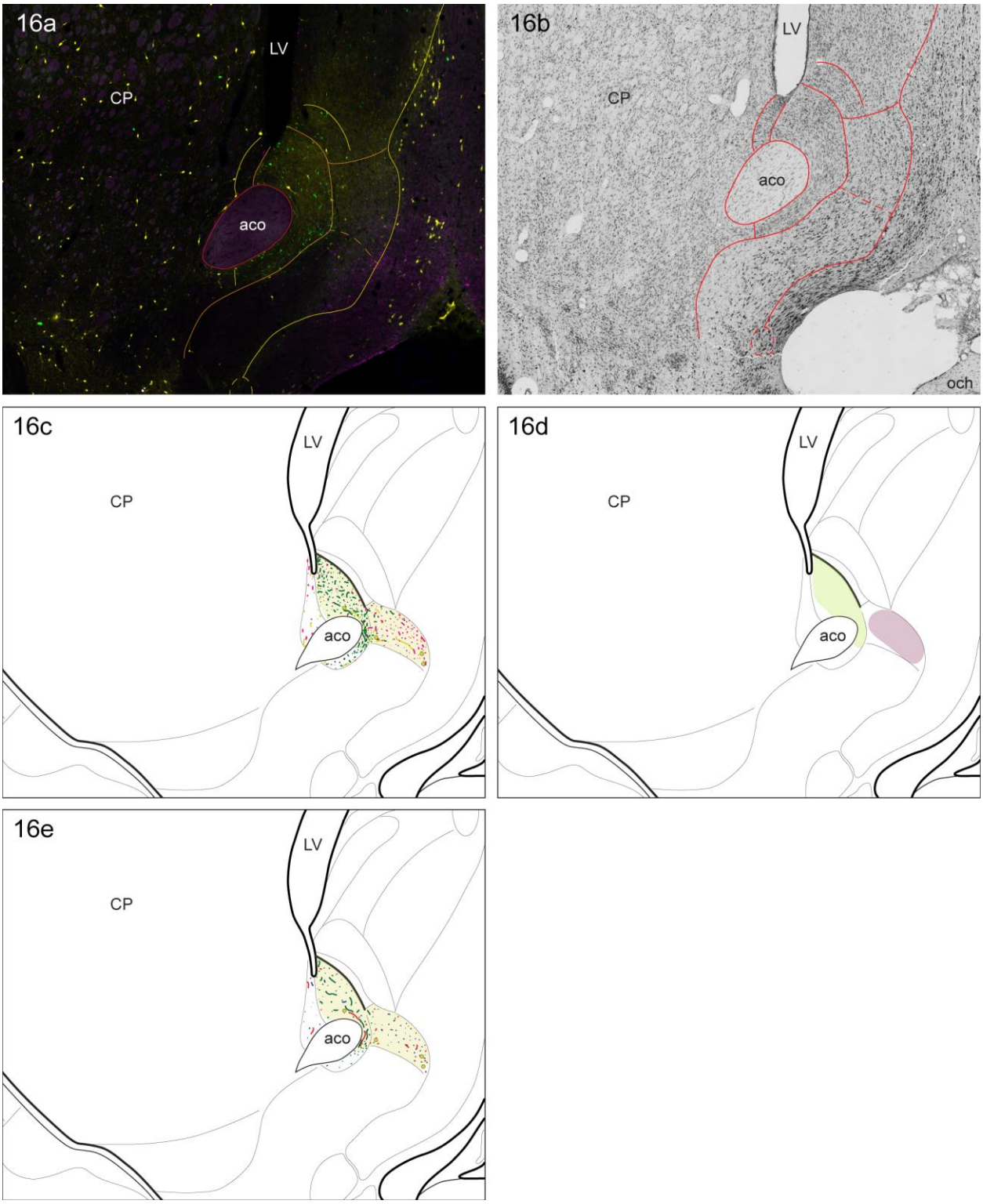

Figure 2.13: Level 16 Maps.

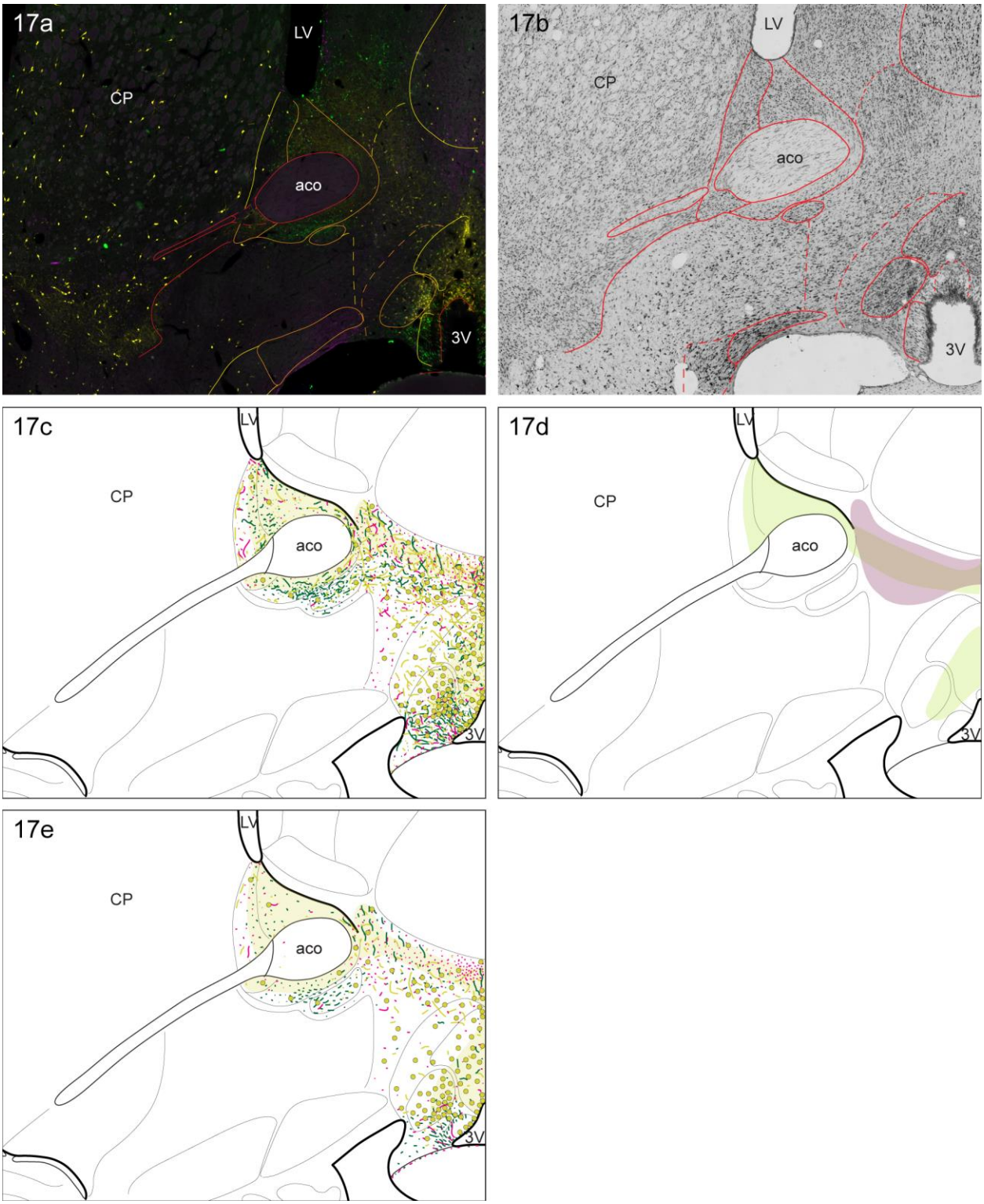

Figure 2.14: Level 17 Maps.

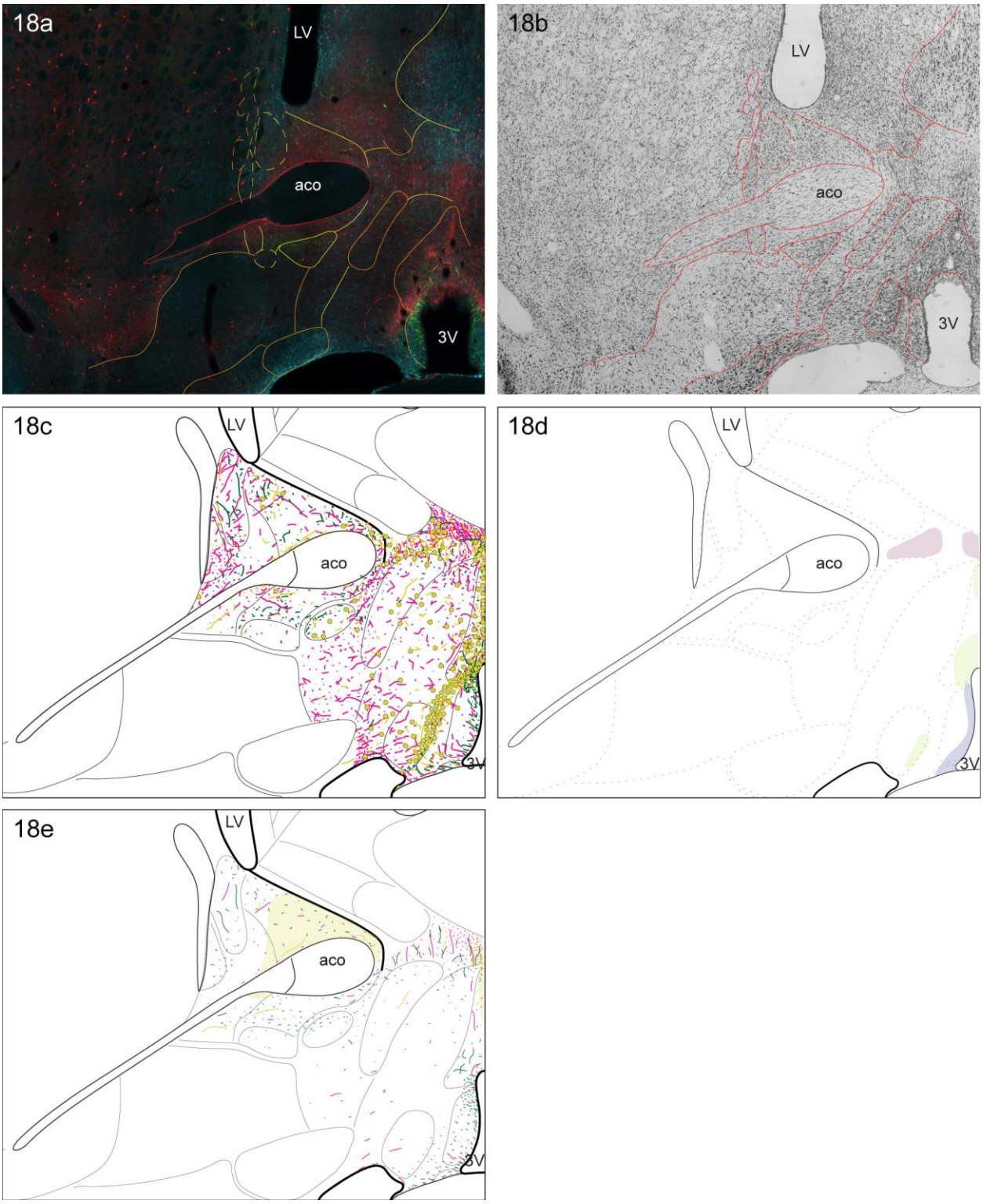

Figure 2.15: Level 18 Maps.

Figure 2.16: Level 19 Maps.

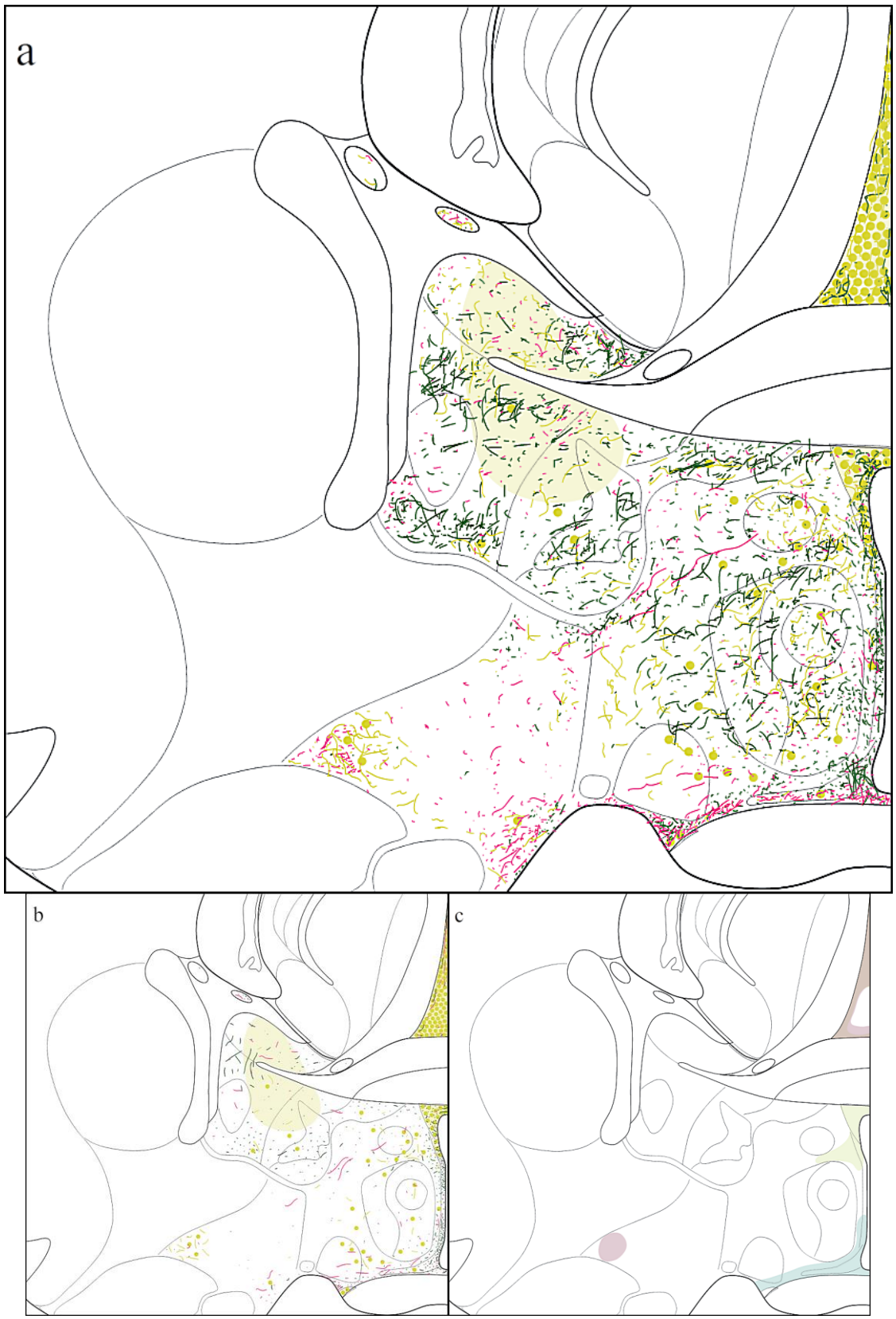

Figure 2.17: Level 20 Maps.

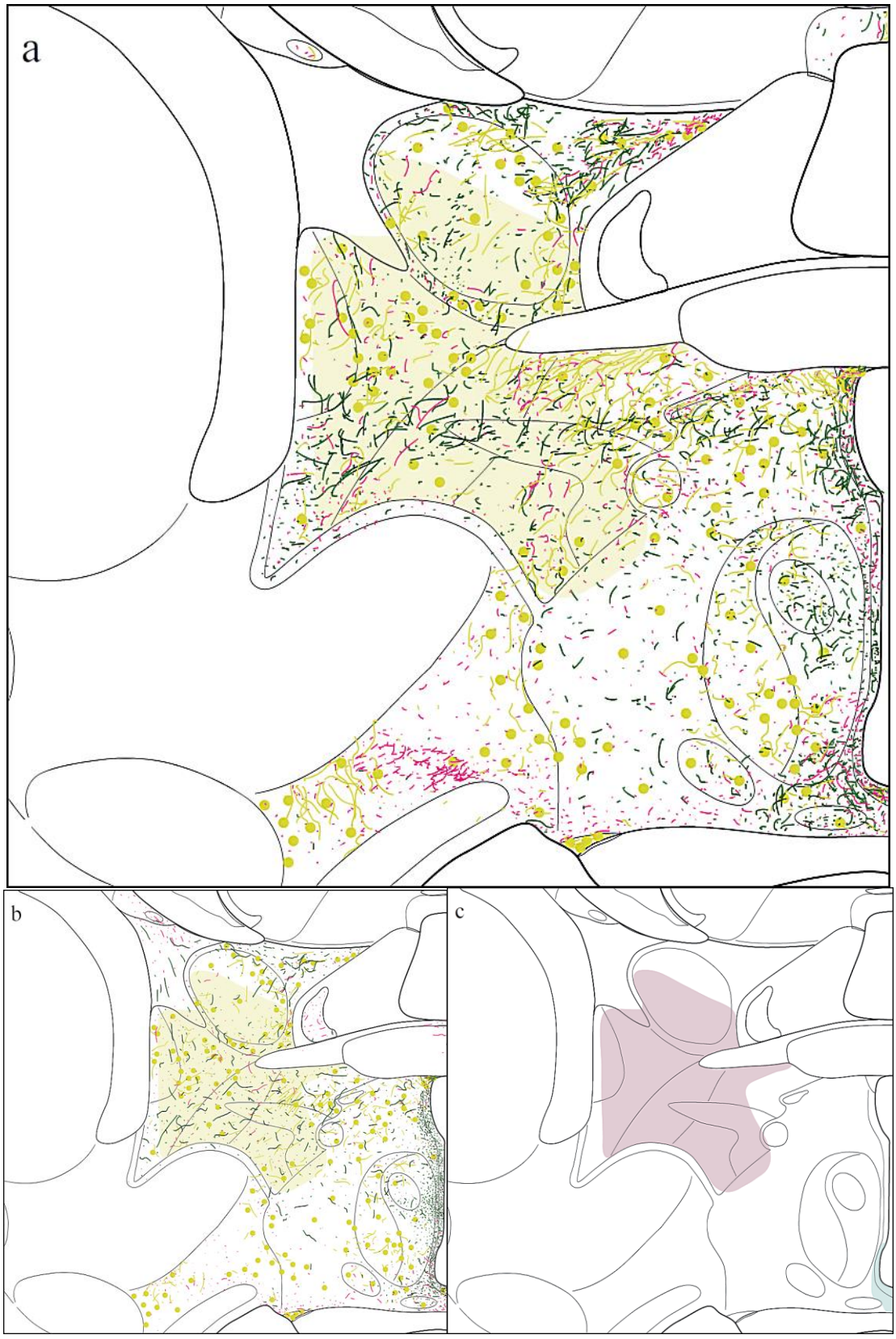

Figure 2.18: Level 21 Maps.

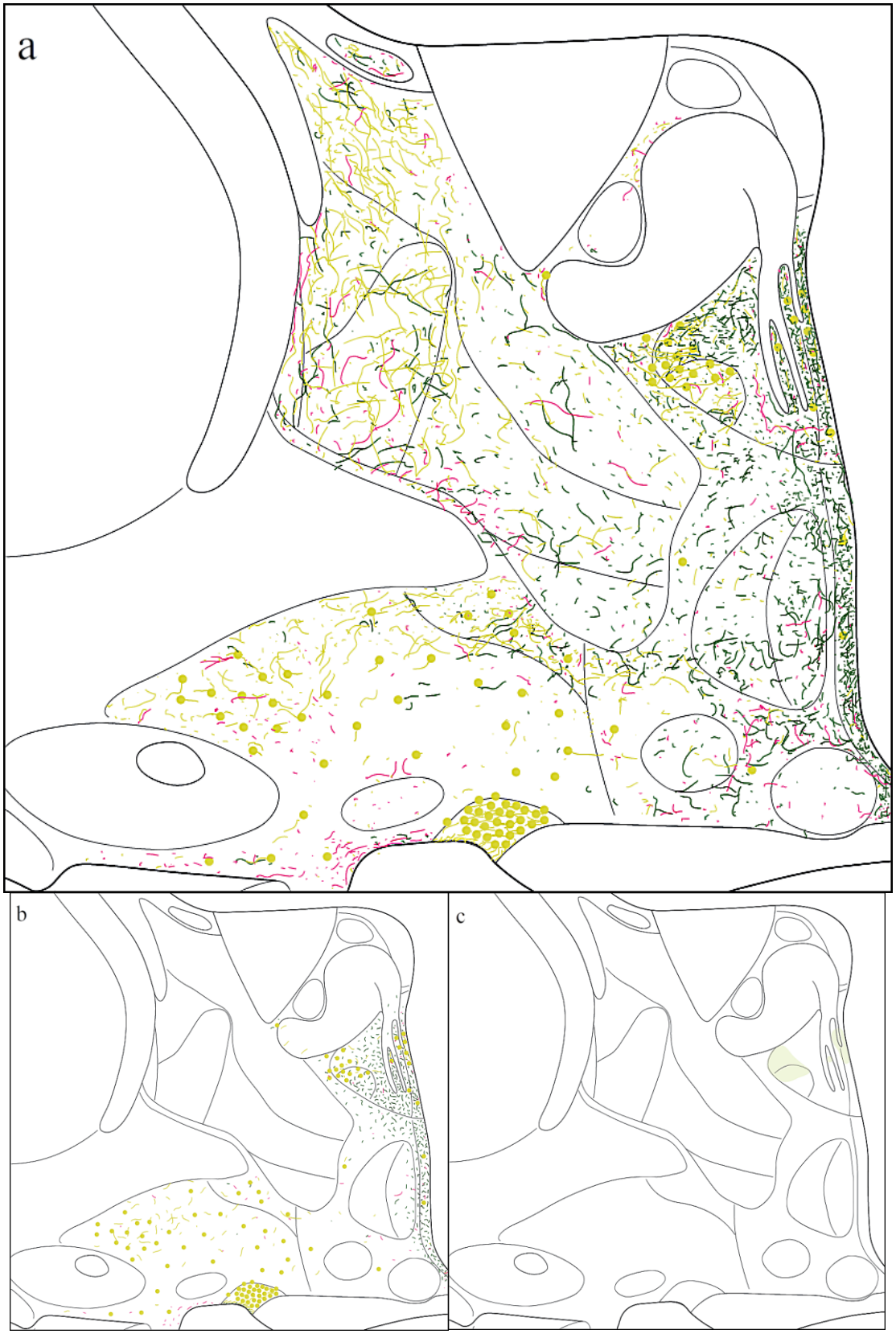

Figure 2.19: Level 22 Maps.

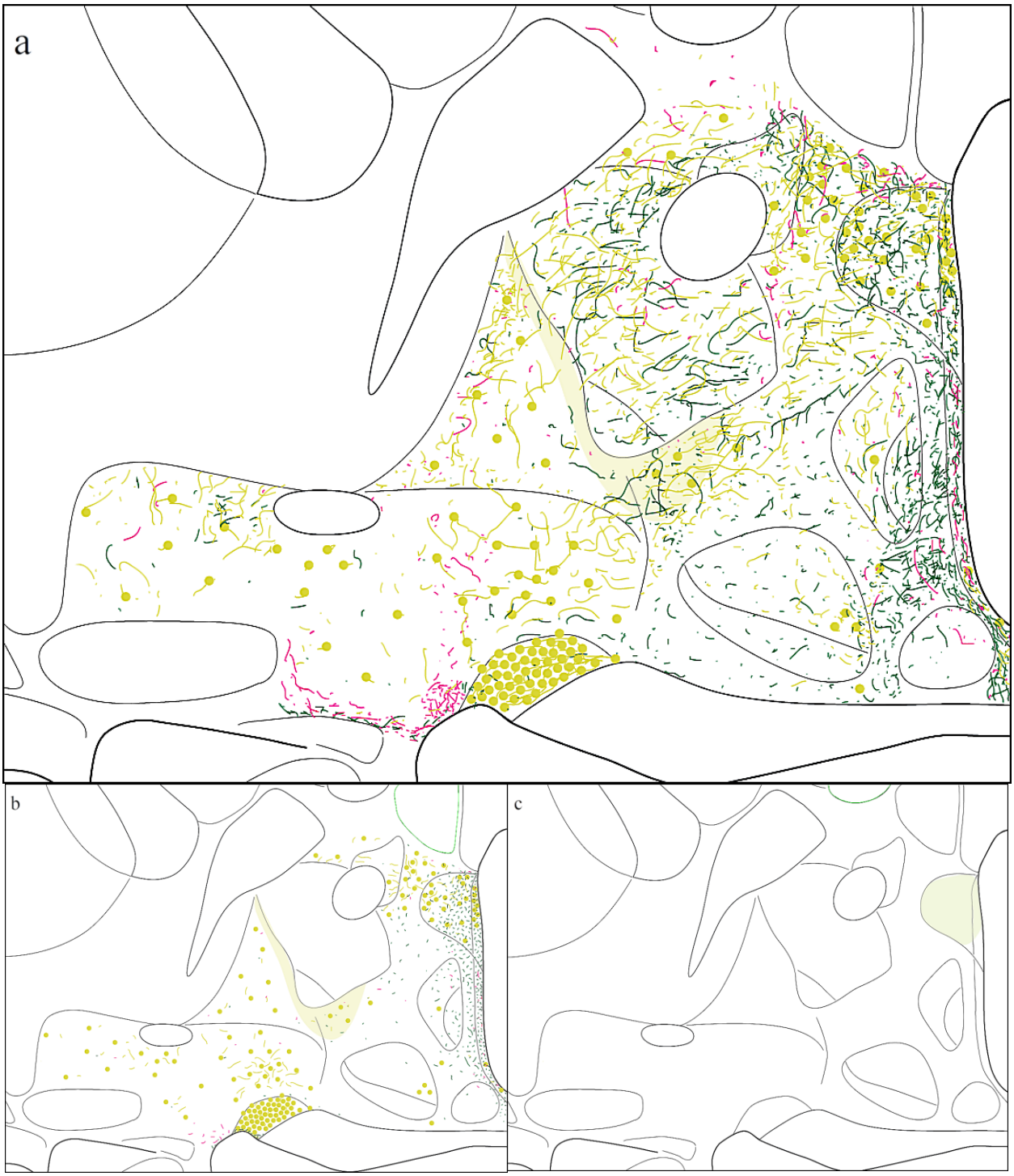

Figure 2.20: Level 23 Maps.

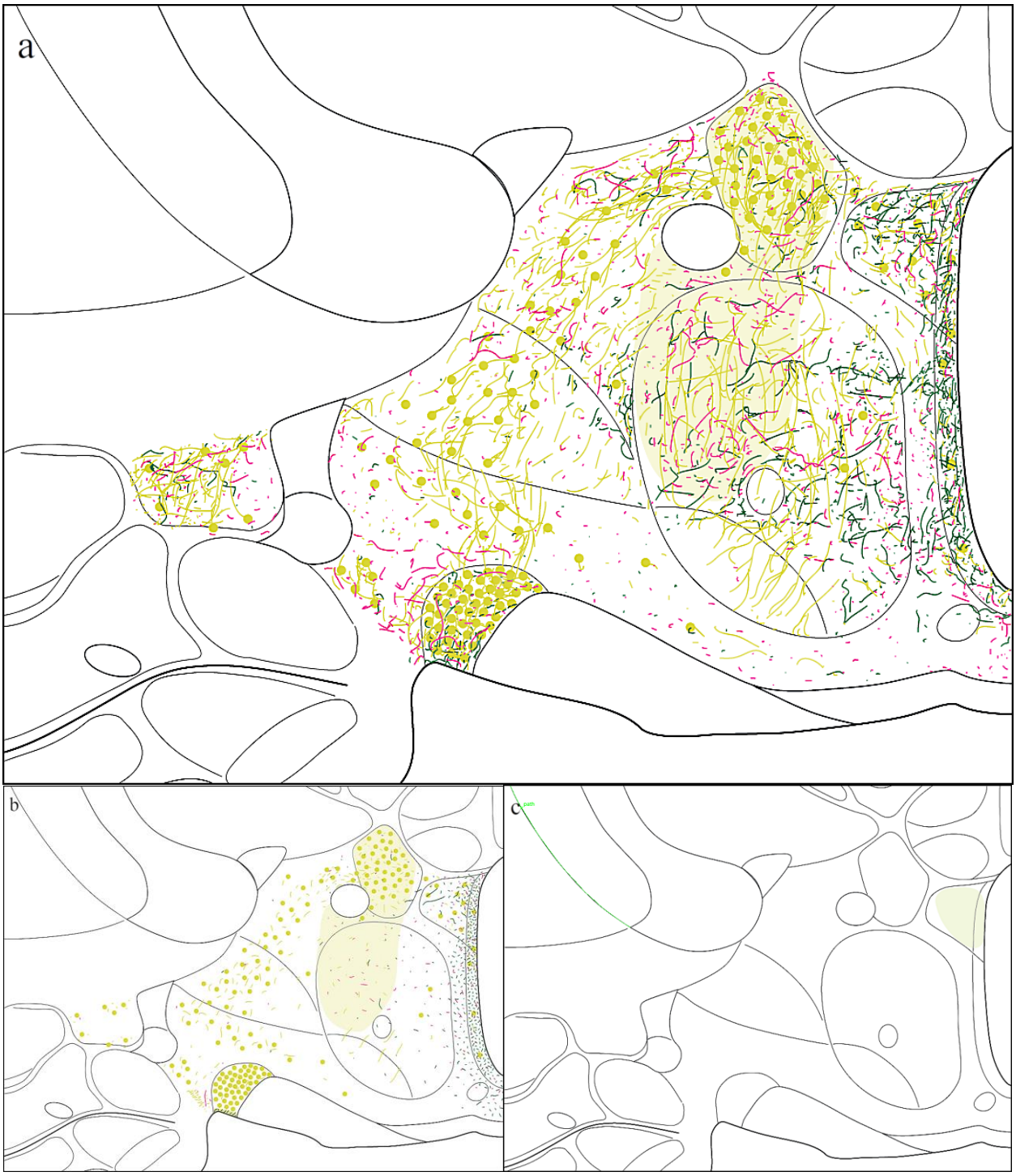

Figure 2.21: Level 24 Maps.

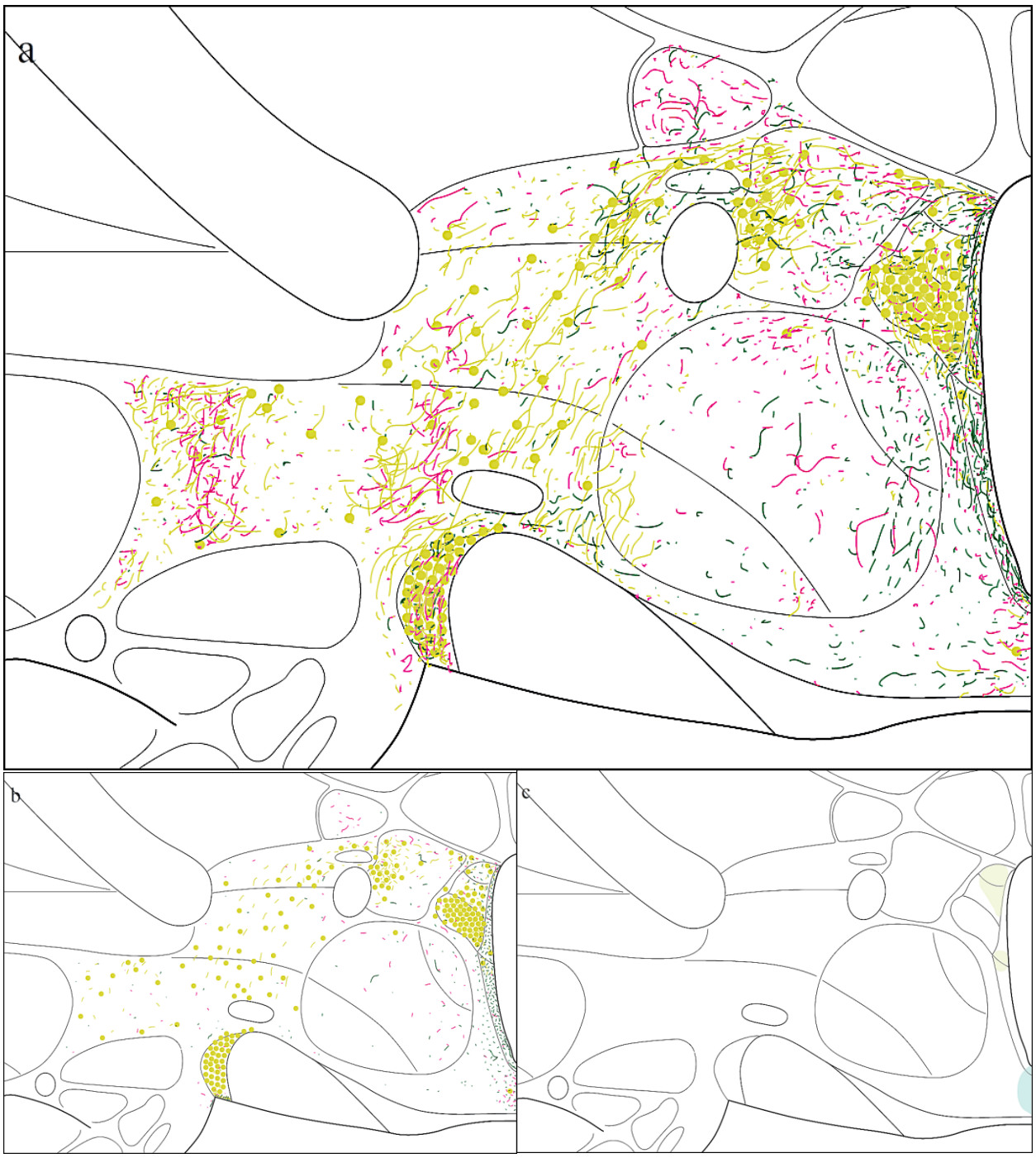

Figure 2.22: Level 25 Maps.

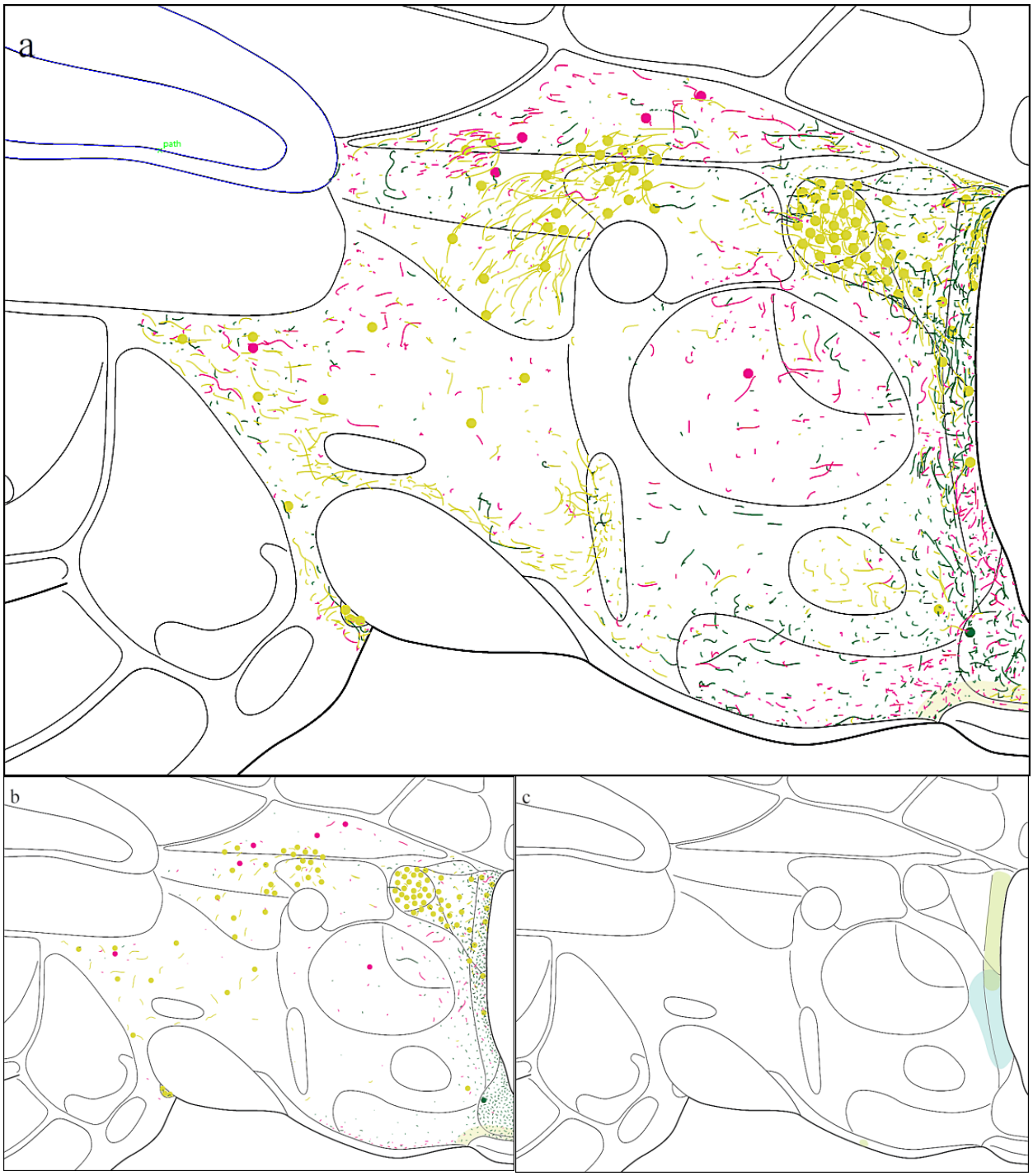

Figure 2.23: Level 26 Maps.

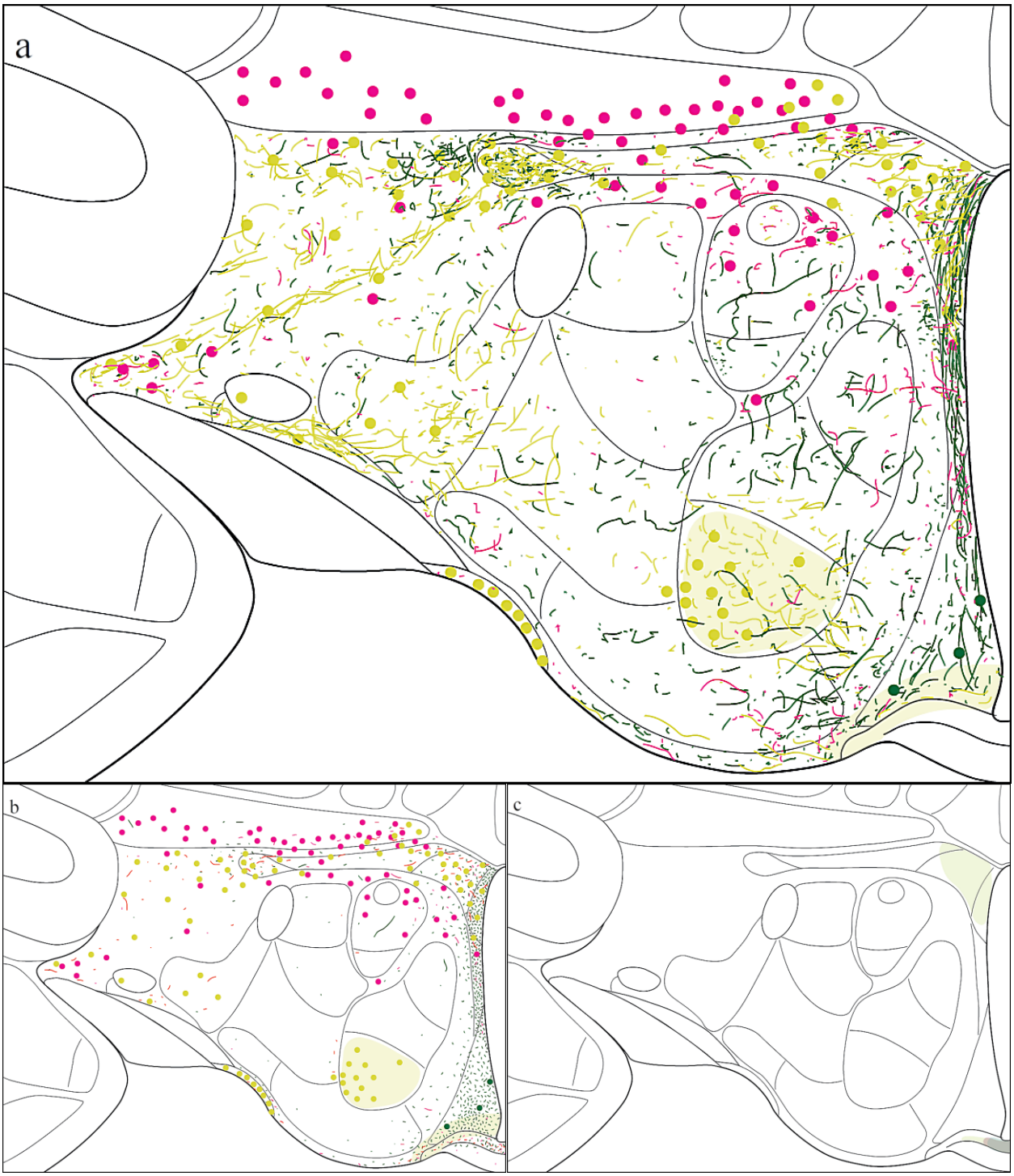

Figure 2.24: Level 27 Maps.

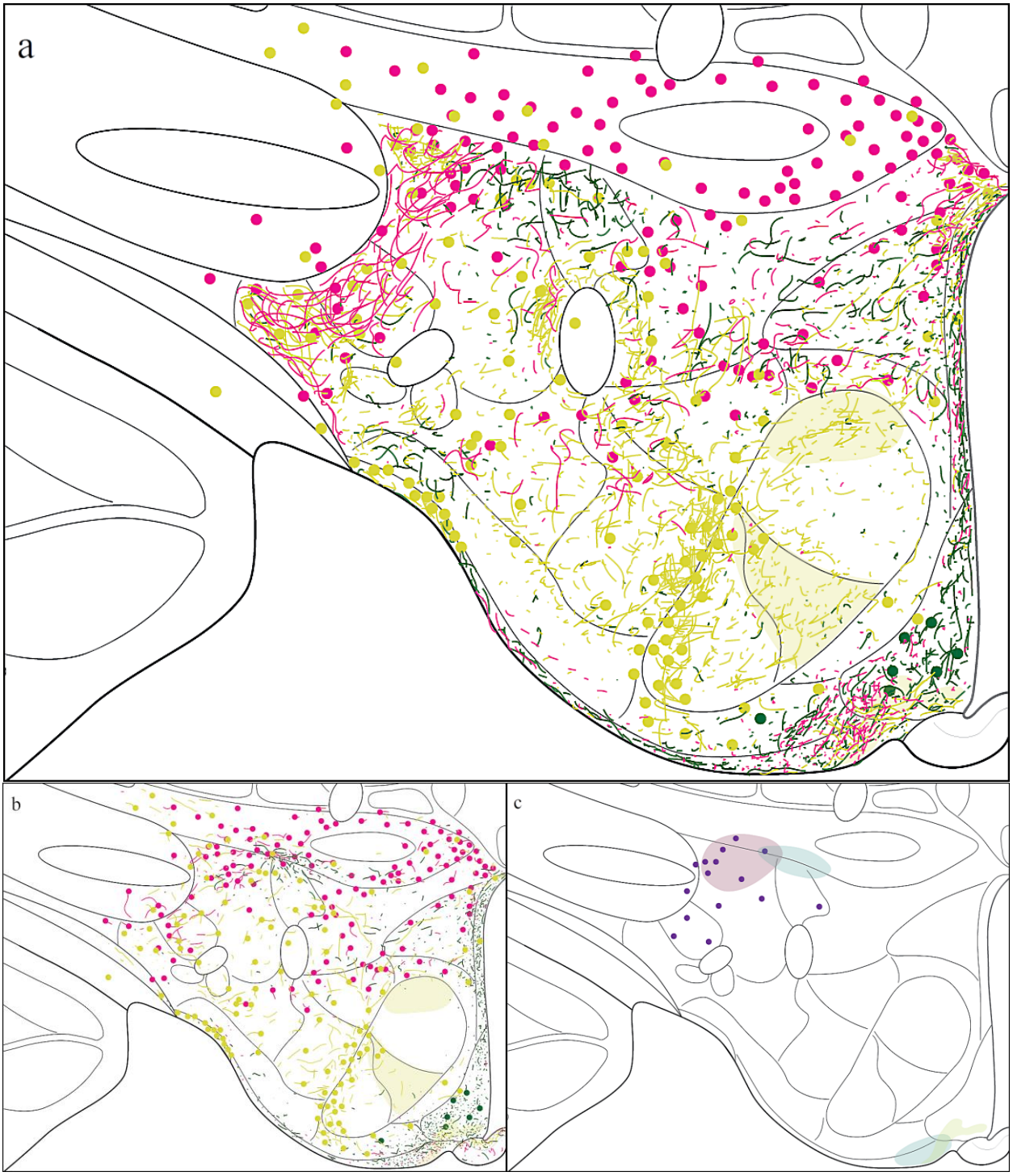

Figure 2.25: Level 28 Maps.

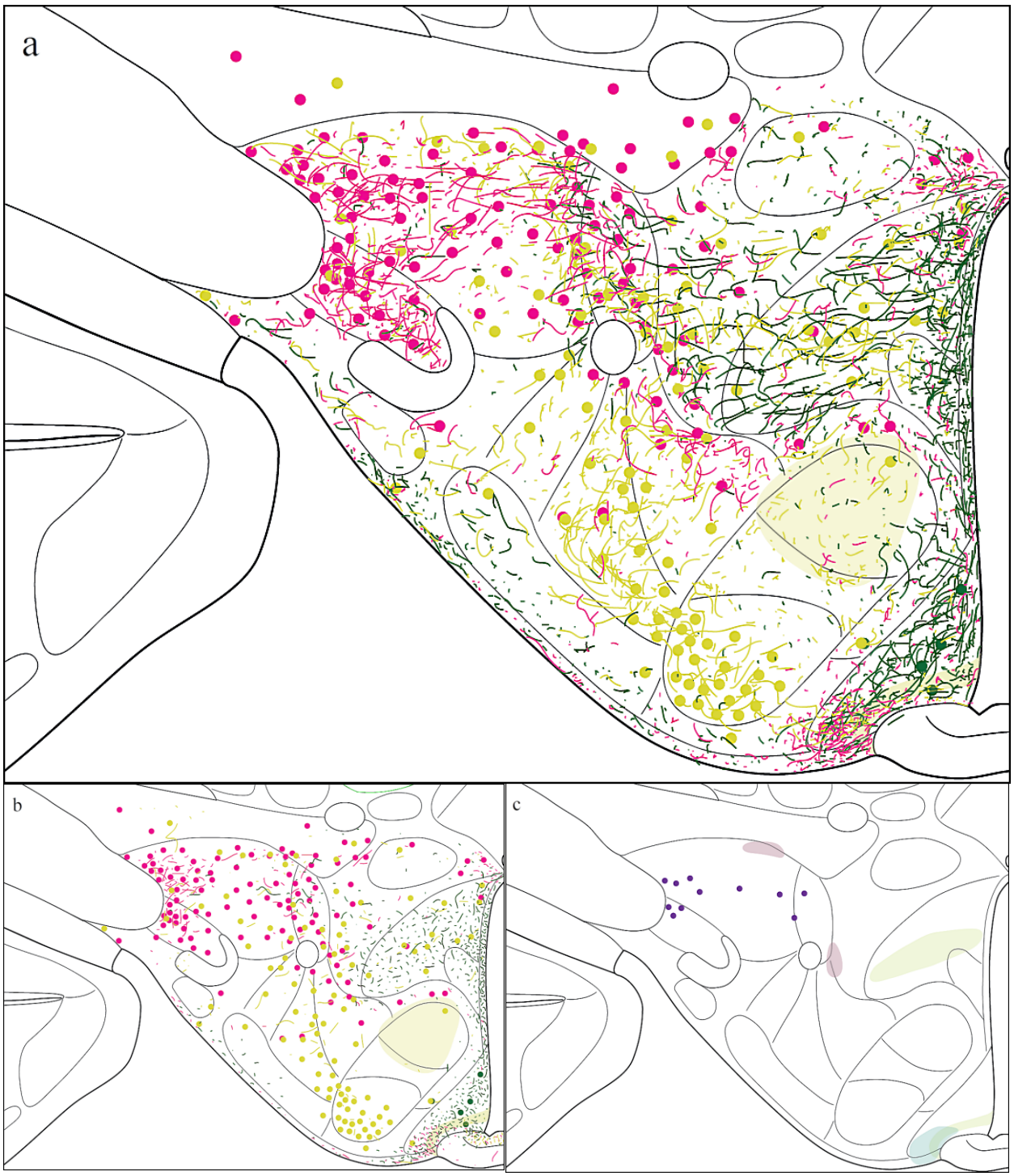

Figure 2.26: Level 29 Maps.

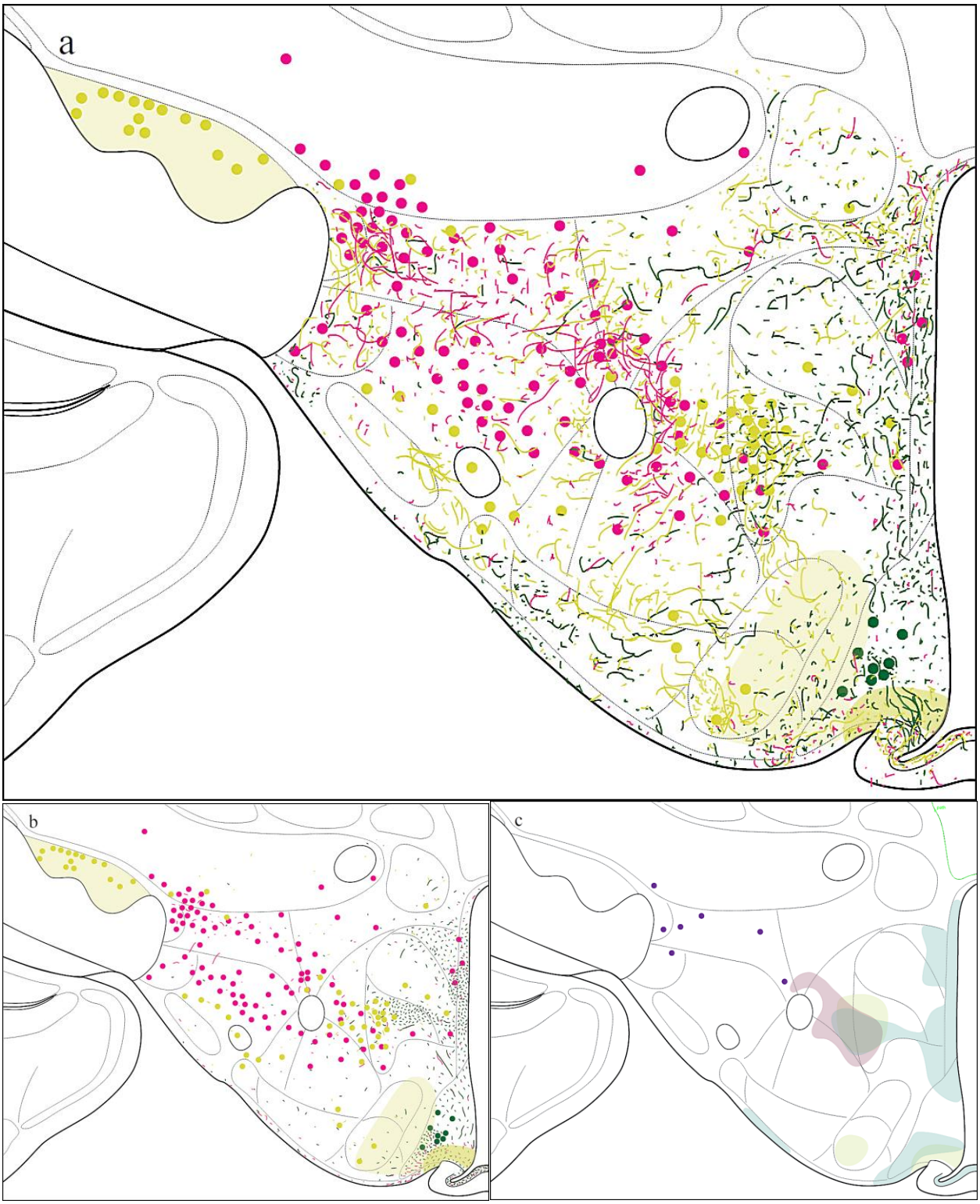

Figure 2.27: Level 30 Maps.

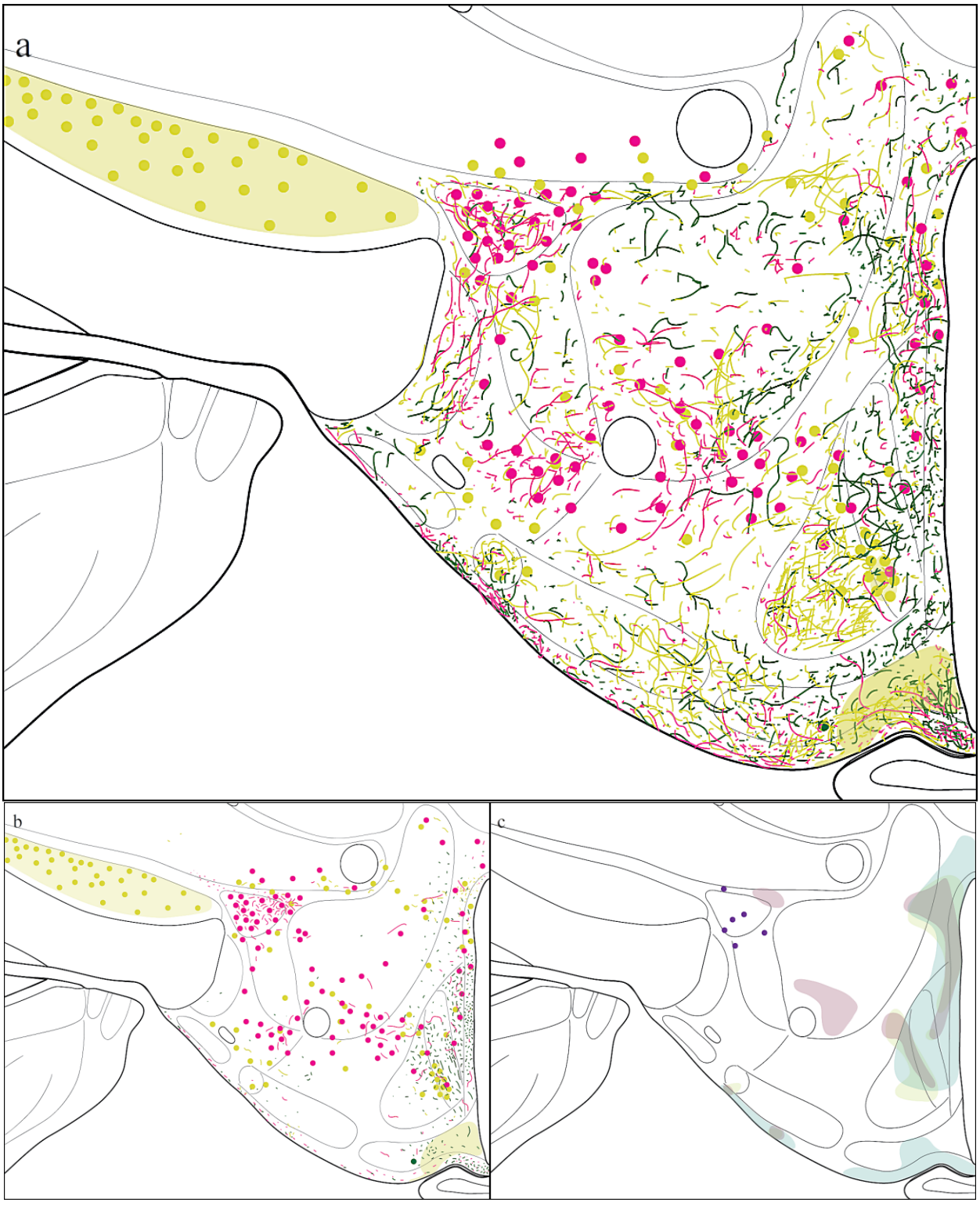

Figure 2.28: Level 31 Maps.

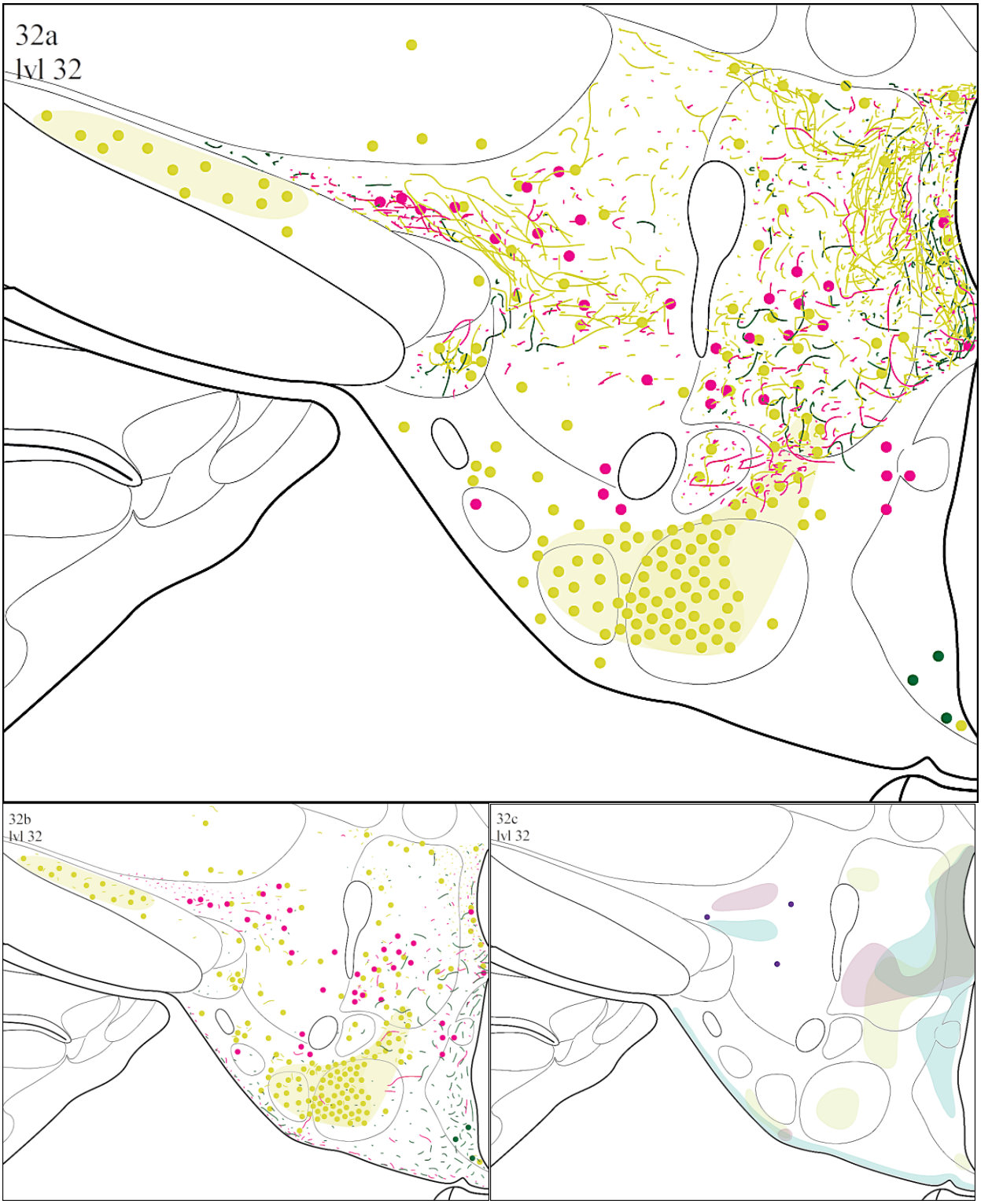

Figure 2.29: Level 32 Maps.

Figure 2.30: Level 33 Maps.

Figure 2.31: Level 34 Maps.

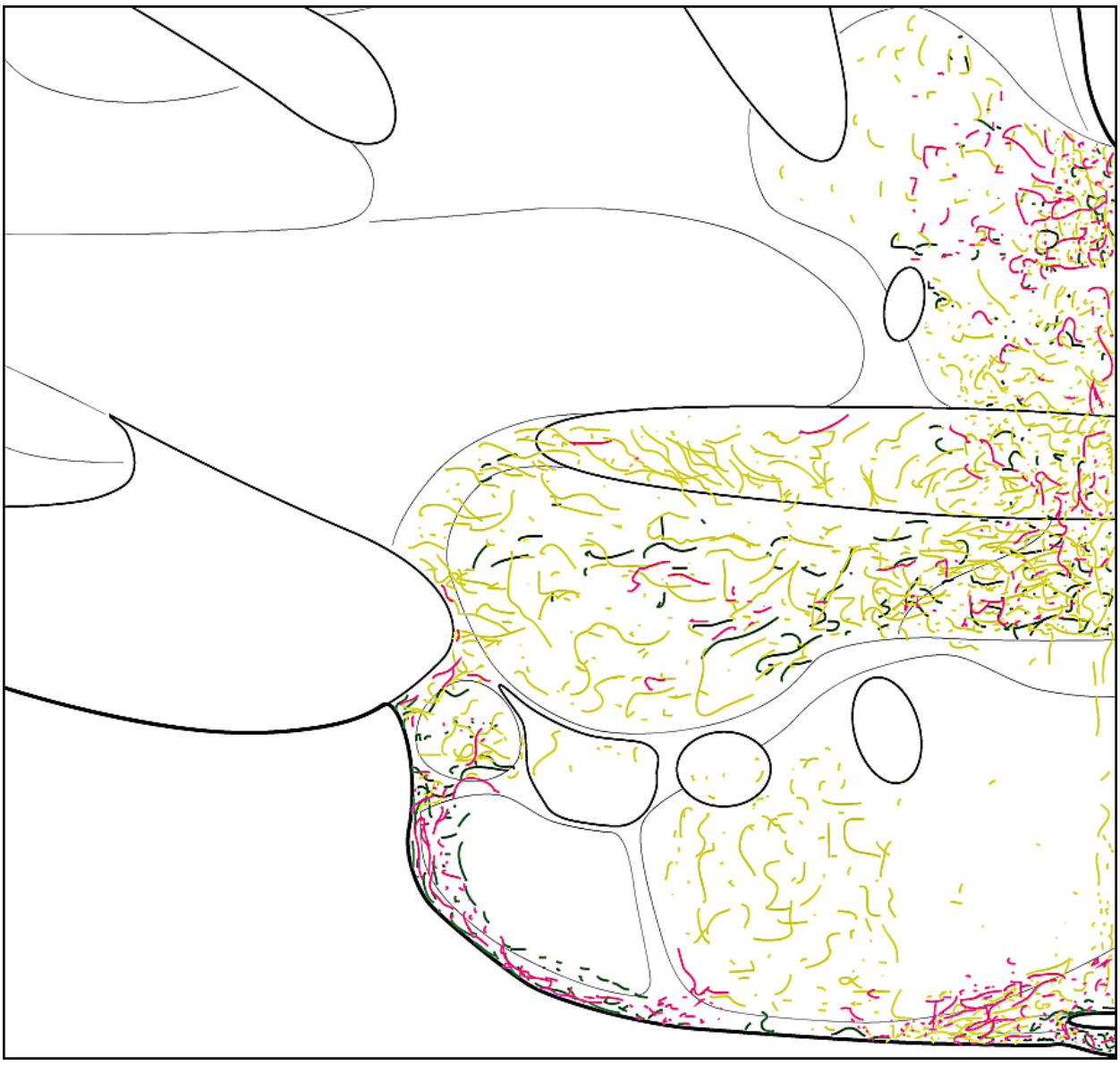

Figure 2.32: Level 35 Maps.

Figure 2.33: Level 36 Maps.

Figure 2.34: Graphical Summary of α-MSH, MCH, and nNOS Distributions and Interactions at Selected Levels for Selected Structures in the Rat Hypothalamus.

Discussion

Regarding Results

Previous reports of the distributions of α-MSH, MCH, and nNOS [61-66, 98-100, 102, 103, 116-120] were confirmed by the present results. The staining also revealed a previously unidentified population of nNOS/MCH cells located in the dorsolateral LHA through levels 28–32 in the Swanson atlas, the abundance of which is greatest at levels 30 and 31. Kenichiro Negishi of the Khan lab has found that some of these colocalized cells project to the prefrontal cortex [personal communication]. A subset of MCH cells has also been found to project directly to motoneurons in the trigeminal motor nucleus in the guinea pig, and it has been confirmed that none of them express nNOS (a separate subset of nNOS cells located in the PV medial to the DMH does project to trigeminal motoneurons) [128]. Since nNOS has been shown to affect food intake [107], as does MCH [79, 81], and since both the LHA and the prefrontal cortex participate in networks controlling feeding [33, 129], perhaps these neurons containing both MCH and nNOS function in the regulation of ingestive behavior. Specifically, they may modulate the tension between metabolically necessary and metabolically unnecessary eating, since the prefrontal cortex plays a role in binge eating [129] while the LHA senses nutritive status [34]

The potential synaptic interaction zones (PSIZs) reported here are mainly of uncertain import. A region was only included as a PSIZ if the staining for two antigens was at least moderately dense in that location; thus, potential synaptic contacts between the cells expressing the studied molecules in sparse regions are omitted. However, such contacts might figure just as prominently in a functional circuit. Also, a not inconsiderable amount of volume transmission takes place in the hypothalamus, and is not captured in the PSIZs [15, 130]. And most regions in the hypothalamus are also in contact with the CSF, another form of volume transmission [22]. Finally, a PSIZ is only worthwhile if another investigator uses it as a clue, and searches the area for synapses between neurons expressing α-MSH, MCH, and/or nNOS.

While the maps presented in this study are either more detailed or easier to use (because they exist as freely available Illustrator files), or both, than previous maps of α-MSH, MCH, and

nNOS; and while additional information has been gained by the use of triple-labeling staining techniques; perhaps the most important advance offered in this study is the minute description of the methodology used to generate the maps. The mapping process is generally stringently summarized and glossed over in scientific articles that show maps. This is likely the result of multiple factors: mapping is a subjective process, and subjective methods may be uncomfortable for scientists to write about; mapping is a relatively amorphous process that may seem to lack discrete, easily stated steps; mapping is a highly individualized process, especially compared with techniques like histological staining or Western blotting that are done in almost the same way across time and institutions; and mapping is a frequently overlooked and undervalued technique – so why should not the description of it be as well? It is my hope that the detailed explanation of my methods may serve as a useful reference to those seeking to learn to map or to better understand how published maps have been created.

Some Issues of Representation in Mapping

I have noticed successive refinements, and successive differentiations, in my mapping. Revisiting some of my earliest Nissl parcellations, I have noted that, while I approached these parcellations with the utmost in somber care, all too often my parcellations took into account spurious artifacts such a little 'lines' of cells and empty spaces. It is only natural that the mind should seize upon these as 'borders'; but in truth they are meaningless. I knew this even then, but was unable to disallow their influence upon my parcellations, which I believe crept in unconsciously, and in the absence of a sounder basis for the placement of bounding lines. Having matured somewhat in my craft and returned to these parcellations, I was able to see things in the Nissl-stained tissue which before I had not: I found myself noting the subtly-distinguished morphologies of cells, and not merely the densities of their distributions and the most grossly obvious differences in cellular morphology and/or orientation. While this development clearly qualifies as a refinement, the next may only be a difference.

For quite a long time, in all of my fiber maps, I did not allow one drawn 'fiber' to cross another. I have no reason for this. It is simply how I proceeded. It did not occur to me that this was a choice I was making in how I represented the staining that had implications or might be significant. And then for a long time, I did not map; being busy with other things, and chiefly with the training of a cohort of undergraduates in mapping. When next I did, I noticed two things had changed: I was able to parcellate very quickly, having learned both to better 'see' in the Nissl, and to recognize and avoid parcellating structures I could not 'see' (for such parcellations are little better than lies); and I drew 'fibers' in my maps that sometimes crossed one another. At first it struck me that of course fibers do cross in the brain, and so to draw them that way is superior. But now I am not so sure: when one sees crossing fibers in stained tissue, are not these fibers most often passing by each other in three-dimensional space without touching, or even coming exceptionally close? So then if I draw them as crossing, am I perhaps implying something about them that is not true? But if I draw them as never crossing, am I not implying a different thing about them that is not true (that they never pass by each other depth-wise)? Perhaps my original predilection would be the better, if I were then to specify that I had merely used a representational motif that did not reflect the exact disposition of all fibers in the area…or perhaps not. I am of two minds about it.

In any case, this change caused me to feel I should update all my old fiber maps for brain 13–082. I encountered difficulties while doing so that led me to recruit Steven Michelmann to my aid, and so it came to pass that all my fiber maps were twinned with the addition of his (except those which were lost). His maps differ from mine in two key respects: he represented fibers more densely than I (that is, the ratio of drawn 'fibers' to real, stained fibers in his maps is higher than in mine), and he chose to view more faint fibers as real, stained fibers (and not as background staining) than I. The result is that his maps are considerably busier than mine. While I have not edited the majority of his maps for quality, I cannot say that his choices were invalid; they are merely different from my own. In all likelihood, the truth of the staining lies somewhere between his fiber maps and mine.

An additional point of interest may here be observed: Steven Michelmann's fiber maps to the earlier Swanson atlas levels were created when he was relatively inexperienced, while his maps to the later Swanson levels were created once he had obtained rather more practice. While his very earliest maps I have corrected, beginning with **Figure 2.16a**, one may study the development of his technique through time.

Limitations of the Technique

While the importance of mapping as a modeling tool may be difficult to argue, the technique nonetheless suffers from several limitations. Chief among these is this: in my opinion, mapping possesses characteristics that together repel the human interest. It is always tedious and always unsure. It requires the attentions of an active mind, yet rewards them but poorly, with monotony. It demands a careful self-reflection, and a constant questioning of one's littlest representational choices; yet offers no unambiguous answers, which may undermine the mapper's self-confidence. Boredom, too, presents a challenge to confidence. And because mapping is a subjective technique, self-confidence; that is, the measured confidence in one's judgment, knowledge, and experience; is crucial, as a keystone in an arch.

There are limits to the resolution of mapping that are not always obvious – that is, although the underlying histology permits an examination of individual cells, it is frequently not possible to propagate that single-cell resolution into the final map. A neophyte in particular may struggle with this constraint: while learning the technique, often I would feel the great weight of Truth bearing down upon me as I wrestled with the assignation of *this* cell body to *this* nucleus or to *that* adjacent area. With the boon of experience, gradually I became aware that it is not meaningful, in most cases, to assign a specific cell body, being near to a border, to a structure on either side. In reality, the brain is not organized along abrupt boundary lines, but as a genetically and environmentally choreographed intermingling of many hazes, and each haze is a particular neuronal population, defined as a unique intersection of chemical, connective, functional, morphologic, and geographic identities. To parcellate such a morass, is to simplify its

complexity, and to lose single-cell resolution; especially along borders. And as mentioned above, such simplification may engender mental stresses in the unexperienced that are another drawback of the technique. And of course, the resolution restrictions discussed above pertain only mediolaterally and dorsoventrally; the anteroposterior resolution is much more severely limited by the number of levels present in the atlas being mapped to.

Mapping also suffers significantly from the law of diminishing returns, in that large gains in a mapper's experience may be manifest by small gains in the detail and accuracy of his or her maps. This effect is evident during the final stage of mapping, in which staining patterns are symbolically represented upon an atlas plate. At one point in my studies I trained a cohort of underclassmen in mapping, and observed that all the principal characteristics of the stained, parcellated material appeared in their maps; though I had devoted myself to the cultivation of these skills for some few years, while they had accrued only a few months of practice. A number of details were omitted from these relatively untutored maps, but whether this matters might be debated – some labs may prize detail highly, while others might judge it not worth the investment in training. In my opinion, possessing a depth of experience is of great benefit for performing Nissl parcellations and for transferring these parcellations to images of the data series (here, fluorescently stained); but is less valuable for performing vessel alignments and for creating the final map.

Future Directions

Probabilistic Maps

During the course of these studies, I had the opportunity to observe differences in the distribution patterns and densities of immunoreactive cells and fibers amongst a number of individual rat brains. While the major characteristics of these patterns were observable in all brains examined, the finer details varied from brain to brain (see **Figures 4.1–4.13** in the Appendix, as compared to **Figures 2.19–2.31**). Occasionally a significant variation was present – notably, one brain had unaccountably higher quantities of MCH-ir fibers throughout the tuberal

hypothalamus than any other (data not shown). Since all animals used in this study were of the same strain and sex, similar in weight and age, and handled and lodged in the same manner; it seems imminently possible that this difference was part of a natural variation in MCH circuitry amongst the brains of similar individuals. Typically the specter of individual variation is ignored in chemoarchitectural and connectional (tract tracing) anatomical investigations, as accurately and thoroughly documenting such variation is a daunting task that necessarily hyper-inflates the scale of any experiment attempting to take individual differences into account. Especially in the case of tract tracing studies, and any other studies reliant on the improbable placement of an injection into a discrete brain structure, the difficulty must be considered prohibitive. However, attempts to document individual variation are clearly warranted; and it must be concluded that the most appropriate chemoarchitectural map does not consist of markings representing fibers and cells, but of clouds and shadings (perhaps) representing the probability of particular features occurring in particular locations. That is, the chemoarchitectural brain maps of the future are to be probabilistic.

The Great Atlas

Not all are in agreement that mapping one's data is the best means of reporting them. Photomicrographs are the most strictly honest way to report data that might be mapped, and are the form in which much of the previous work on α-MSH, MCH, and nNOS distributions has been reported. They are very much simpler to produce, as well. Photomicrographs may serve many of the purposes of mapping, with regard to hypothesis construction and data interpretation – mapping merely makes the possible connections between different data sets (mapped to the same atlas) easier to see. Still a map is, to my mind, superior to an annotated photomicrograph – but only insofar as it is valuable as a model; for models aid the understanding, and the brain is complex. And what is lacking in neuroscience, and not contributed by any map, is a single, comprehensive model of the brain. I believe such a model might take the form of an atlas: a cytoarchitecturally-based, communally accepted, realistic and centralized repository of all

neurological data of any sort that can be tied to the anatomy. A great atlas, containing many maps.

I envision this atlas taking as its subject the rat, so to benefit from the long history of anatomical work performed in the rat; and being based on the Swanson atlas for the elegance of its hierarchical parcellations and the willingness of its creator to use a free, online format in future editions [personal communication]. While the newest editions of the Paxinos & Watson atlas (2005 and 2007) contain many more levels, and therefore much greater anteroposterior resolution, than any previous atlases in the rat (see **Figure 2.1**), still I judge it that the importance of a hierarchical parcellation – lacking in Paxinos & Watson – outweighs this gain in resolution; for it is essential that a model be well-organized.

If such an atlas is to be born, I believe the following precepts are true: it must dispense with the techniques used in this dissertation, as too time-consuming and inaccessible to the average neuroscientist. When it is first glimpsed by the world at large, it must be sufficiently well-formed to immediately appear useful to almost any neuroscientist working in the rat. And it must be formatted and constructed in such a way that any neuroscientist who uses it will feel confident in adding their data to it – confident that they are capable of doing so, and confident that doing so matters.

To this end, I have cogitated upon a stripped-down mapping methodology that might meet the requirements of this atlas. Many elements of fine detail and some of accuracy are sacrificed in this method, but speed and accessibility are gained. Only Adobe Illustrator and a Nissl-stained series are required.

Firstly, the Nissl parcellation is to be abbreviated; only those structures, and occasionally substructures, which are immediately apparent (with some small modicum of practice) in the Nissl are to be parcellated. For the hypothalamus, these structures include (but may not be limited to): the aco, och/opt/sup, fx, int/cpd (usually; sometimes the medial border is vague), mtt, pm, mp, fr, portions of the MS and ACB, the LSr.vl.v and LSv, portions of the BST, the MEPO, sometimes the AVP or AVPV, the ADP, sometimes the MPN and usually the MPNc, the SCH,

AHNd, sometimes the AHN, the SO, SOr, PVH, PVHam, PVHpmm, PVHpml, PVHlp, sometimes the PVHmpd, the NC, ARH, VMH, VMHdm, VMHvl, ME, ZIda, DMHp, TUte, STN, much of the PVp, the TMd, sometimes the PMd and PMv, the MM, MMme, the TMv and LM although they are easily confused with each other, portions of the SUM, and sometimes portions of the PH. For the thalamus, usually the mtt, fr, sm, RE and REm, AD, AV, LD, VAL, MH, LH, and sometimes the RH are readily identified; though this is not to be considered a complete list as I have not worked in the thalamus but only chanced frequently to observe it. If only a small part of a structure's border is clear in the Nissl, it is to be drawn in the parcellation; incompleteness is no fault. Level assignment/plane of section error are to be determined based upon the parcellation and not as a separate step.

Second, the vessel alignment is to rely on very few vessels; only one or two in each quadrant, where applicable (for instance, in much of the tuberal and mammillary hypothalamus, one quadrant is mainly occupied by empty space and by the amygdala, disconnected from the hypothalamus). Alternatively, an alignment can be conducted based only on white matter tracts which are readily visible in the Nissl and in the background staining in the data series.

The Nissl parcellation is to be transferred similarly to how it is done in the full mapping methodology, but with less care and no documentation regarding which bit is from where. Also, since the Nissl parcellation itself is bare-bones, this step will be faster.

Finally, the final mapping is not to be performed by the placement of circles and drawn 'fibers'; rather, a series of simple shapes is to be drawn in the locations of the salient staining features, and filled in as appropriate with a simple symbolism. A pattern of circles may indicate cell bodies; several patterns may be prepared of varying circle density to represent different densities of cells. A pattern of lines may represent fibers; again an array of patterns may be prepared, with intersecting values for line density, length, and direction (some should have lines in random directions). Additional patterns can be created to represent injection sites, diffuse staining, and the like. These patterns can be saved in Illustrator, so that they need only be created once and can then be distributed online and simply and quickly selected as warranted. A mapper

should not struggle overmuch to create separate filled shapes for every little variation in fiber character or cell density in an area, but rather should endeavor to capture only the highlights of this information – all small variations should be discarded and summarized using a single most-appropriate pattern.

The above methodology is only a proposal, and may prove to require some amount of optimization for real use. It is my hope that this or a similar method may allow many more researchers to map their data using a unified format, to the great atlas, so that a comprehensive brain model may be created. Furthermore, I envision previously published results of all types – maps to various atlases and even photomicrographs of tract tracing, chemoarchitecture, central injection, and genetic manipulation results/anatomical verifications – being updated using the above format, and placed in their rightful places in the comprehensive model. Discussion of how to migrate previously published maps to different atlases appears in the Discussion section of Specific Aim 2. Photomicrographs may in some cases be 'mapped' if some structures are visible or even merely annotated in them; parcellation would then be performed on the photomicrograph itself, an appropriate atlas level selected, and the data rendered as described above. These 'maps' will necessarily be quite low in detail and quality (and should be marked accordingly in the atlas); however, perhaps not worthlessly low, considering the value of incorporating the information they contain in the model presented in the atlas, which aspires to be comprehensive.

Of course, there is one, indispensably important need of the great atlas that cannot be met by an anatomist: its actual incarnation online. I imagine the atlas being searchable by structure, molecule, or function. I imagine that in cases where more detailed maps were available, a simple click would bring these up as a separate image. I imagine that behavioral and other types of interventional data might be similarly linked to their anatomical documentations, such as injection sites, in the atlas. Only a computer scientist can bring this dream to fruition.

Finally, I imagine all files being available for download, including a suite of template files and corresponding instructions so that other investigators may create maps of their data and submit them to the atlas, along with images and other files the maps are based on. I imagine a

small team of atlasers (anatomists and computer scientists) carrying the responsibility for briefly reviewing these maps and slotting them in as appropriate; or in some cases accepting the raw data files and creating atlas maps themselves; as well as trawling the literature for previously published results that might be incorporated.

Specific Aim 2: Develop Techniques For Data Migration Among Atlases

Objective

The goal of this specific aim is twofold: to create a systematic methodology for migrating data mapped in any one of these atlases to any other, and to investigate the differences between three atlases of the rat brain – Swanson 2004 (S) [4], Paxinos & Watson 1998 (PW2) [122], and Paxinos & Watson 2005 (PW3) [123] – using statistics. Specifically, as regards the first portion of the goal for Specific Aim 2, an attempt was made to create a systematic (stepwise) method to transfer maps of central injections from Paxinos & Watson atlases to the Swanson atlas. These maps could then be viewed in the context of the Khan lab's chemoarchitectural data also mapped to the Swanson atlas, and in the context of the great quantities of connectional data mapped to Swanson; possibly leading to hypotheses concerning the chemical identities and connectional profiles of the neuronal populations targeted by the legacy injections. Difficulties encountered while laboring towards the completion of this first goal engendered the addition of the second goal, partially a means of investigating the basic feasibility of data migrations between atlases in the first place.

Materials and Methods

Description of Unpublished Legacy Dataset

Unpublished maps of injection sites from two previously published studies in the Glenn Stanley lab were used as cases on which to test the migration methods being developed. In one of these studies, protein-tyrosine kinase inhibitors (PTKI) were injected into the LHA lateral to the fx, in order to determine the role of protein-tyrosine kinases in driving *N*-methyl-D-aspartic acid (NMDA)-elicited feeding behavior [131]. In the other, ifenprodil was injected into the LHA lateral to the fx in order to investigate the role of NMDA subunits NR2A and NR2B in NMDA-elicited feeding behavior [132]. Maps of the injection sites were made to the Paxinos & Watson 1998 [131] or Paxinos & Watson 1986 [132] atlas using a Bausch & Lomb Microprojector projection microscope and photocopies of the relevant atlas levels. A total of 45 mapped

injection sites at three different levels (26, 31, and 33 in the Paxinos & Watson 1998 atlas) were suitable for use in this study.

Atlas Plate Preparation

Original maps of the injection sites to the Paxinos & Watson 1986/1998 atlas from the lab of Dr. Glenn Stanley were scanned and imported into Adobe Illustrator CS5 (Adobe Systems Inc., San Jose, CA) files (**Figure 3.2a**). The corresponding plate from the Paxinos & Watson 1998 atlas was imported into the files and each map was lined up with it (**Figure 3.2b–c**). This was done such that the agreement at and immediately surrounding the LHA was maximized, at the expense of the alignment of more distal structures. The injection site maps were then digitalized (**Figure 3.2d**). The chart shown in **Figure 3.1** was used to identify the levels of the Swanson 2004 atlas corresponding to the Paxinos & Watson levels, and the Swanson levels were imported into each file, centered in the horizontal axis, and scaled such that the stereotaxic units of the horizontal axis were the same length for each atlas. The agreement of the Swanson and Paxinos & Watson plates was visually inspected and additional Swanson plates were imported and centered as appropriate to correct for dorsoventral plane of section differences between the atlases. Mediolateral plane of section differences were less than one level (although this determination is complicated by the fact that only one hemisphere of the brain is mapped in the Swanson atlas). The determination of which Swanson plates to use and where to place the cutoff points was based solely on the Paxinos & Watson 1998 plate, and not on the Nissl staining in the original tissue set, because the goal of the project was to compare the Swanson and Paxinos & Watson atlases. The fiducials on the Nissl indicate a different placement of the boundary between Swanson plates. The Swanson plates were cut and combined to create a single composite Swanson plate for each file.

At this point two different methods of manipulating the Swanson plate were employed, with equivalent results. In the first method the Swanson plate was stretched anisotropically such that the stereotaxic grid exactly matched that of the Paxinos & Watson plate. In the second

method, the Swanson plate was scaled by 139% in the horizontal axis and 161% in the vertical axis as per Swanson to yield stereotaxic units of a length consistent between both axes (**Figure 3.2e**) [4]. The Paxinos & Watson plate and injection maps were scaled to match the composite Swanson plate as closely as possible with a uniform scaling factor – 139.5% in both axes gave stereotaxic units in good agreement between the atlases. This factor is useful for all levels of Paxinos & Watson used in this study (levels 26, 31, 33) but possibly would not pertain to different versions of either atlas (i.e., any combination other than Paxinos & Watson 1998/Swanson 2004). The difference between the two methods of scaling the Swanson plate is 0.4% in the horizontal axis and 0.1% in the vertical axis.

Nearest Neighbor Migration Method

The strategy of this method is to replicate the relationship between the injection site and nearby fiducials on the atlas transferred to.

The boundaries of each original injection site were defined with lines which were then used to locate the 'center' of the site (**Figure 3.3a**). The choice of where to place the boundaries inevitably influences the quality of the final transformation in a level-dependent manner. Two fiducials near the injection site in Paxinos & Watson were chosen and their boundaries defined with lines (**Figure 3.3b**). Chosen fiducials were interior to the target area (for the LHA, medial and dorsal), as it was assumed more interior fiducials would suffer less distortion during processing than those on the edges of the sections. However, for some levels it may be appropriate to choose an exterior fiducial if internal fiducials vary greatly between the atlases. If the fiducials' appearance markedly differed between the two atlases, attempts were made to correct for this. For example, the fx is considerably more eccentric on the Paxinos & Watson plate than on the Swanson composite plate, and is tilted diagonally rather than being oriented vertically. Therefore the center of the fx was identified and used as the reference point for measuring distances from the site boundaries to the fx. The distance between the site's center and the fiducials was measured on the Paxinos & Watson plate (**Figure 3.3c**). The boundaries (or

relevant reference points) of the fiducials were defined on the Swanson composite plate and the measured distances were replicated (**Figure 3.3d**). As the length of the stereotaxic units corresponded very closely between the atlases after scaling, the lines representing the distances were simply cloned and repositioned as appropriate – however, if the units were not equivalent, a conversion factor could be calculated by measuring the length of each unit in mm in Illustrator (the conversion factor might well be different for the horizontal and vertical axes). The injection site was then transferred to the Swanson plate and repositioned such that its center aligned with the replicated distances (**Figure 3.3e**).

Nearest Neighbor Warped Migration Method

This is the same as the nearest neighbor migration method, except that distances were measured from the nearest fiducials to the site's boundaries rather than its center; and during the final step when the injection site was transferred to the Swanson plate, it was warped such that its boundaries conformed to the replicated distances (**Figure 3.4**).

Stable Fiducial Migration Method

The rationale behind this method is that stable fiducials are more likely to be consistent between atlases, and are therefore the appropriate reference points to use for transformations. This is in contrast to the idea that highly variable fiducials capture the most information about the differences between atlases and thus are more suitable for use as reference points.

Dr. Rick Thompson's identification of stable fiducials was used to identify fiducials at the relevant levels whose positions are relatively invariant across different brains, and of these only those appearing on the pertinent plates of both Paxinos & Watson and Swanson were selected for use [personal communication]. One fiducial met these criteria for Paxinos & Watson levels 26 and 33; level 31 had no qualifying fiducials.

The center of each site was defined as described for the nearest neighbor method (**Figure 3.3a**), and the horizontal and vertical distance from the center to the stable fiducial was

measured. These distances were reproduced on the Swanson composite plate and used to reposition the site.

The downfall of this method is that it is not robust to large differences in the fiducials between atlases, due to the small number of fiducials meeting the selection criterion.

Average Migration Method

The strategy of this method is to approximate the degree of difference in the target area between atlases at the appropriate level and use it to alter the injection site map.

The distance between various fiducial pairs near the LHA was measured for both atlases (**Figure 3.5a–b**) and the percent difference calculated for each pair (**Table 3.1** contains the data for level 26 in Paxinos & Watson and level 25 in Swanson). For each pair used, distance was measured in either the horizontal or vertical axis only. All percent differences were averaged to give a factor by which to scale the injection site in each axis. The injection site was scaled by the calculated factors on the Paxinos & Watson plate (**Figure 3.5c**), and transferred to the Swanson plate. These factors were: 89.38%, 61.96% (x, y for level 26 in Paxinos & Watson 1998 versus level 25 in Swanson); 95.81%, 79.52% (x, y for level 31 in Paxinos & Watson versus level 29 in Swanson); and 115.51%, 94.21% (x, y for level 33 in Paxinos & Watson versus level in 31 Swanson).

As this does nothing to position the transferred site appropriately, it was then necessary to move the site. The boundaries of each original injection site were defined with lines which were then used to locate the 'center' of the site (**Figure 3.5d**). The distance from the site's center to two nearby fiducials on the Paxinos & Watson plate was measured (**Figure 3.5e**) in a manner similar to that used in the nearest neighbor migration method (**Figure 3.3a–c**). Chosen fiducials were interior to the target area (for the LHA, medial and dorsal), as it was assumed more interior fiducials would suffer less distortion during processing than those on the edges of the sections. However, for some levels it may be appropriate to choose an exterior fiducial if internal fiducials

vary greatly between the atlases. The measured distances were then replicated on the Swanson composite plate (**Figure 3.5f**) and used to reposition the scaled injection sites (**Figure 3.5g**).

In another iteration of this method, distances were measured to the boundaries rather than the center of the sites, and sites were repositioned accordingly. However, proceeding in this fashion skews the transformations to one side or another, as, for instance, their right and upper boundaries remain fixed and unchanging even when different scaling factors are used.

Average Closest Migration Method

This is the same as the average method, except that only fiducial pairs very close to the LHA were used to calculate the scaling factors. Similar to the stable fiducial migration method, this method was hampered by the possibility of large differences in the fiducials between atlases, due to the small number of fiducials meeting the selection criterion. The scaling factors were: 99.69%, –28.71% (x, y for level 26 in Paxinos & Watson 1998 versus level 25 in Swanson) – due to the poorness of this method it was not pursued for additional levels.

Average No Outlier Migration Method

This is the same as the average method, except that a histogram was made of the percent differences for each axis and any outliers were excluded from the average calculations (**Figure 3.6**). The open source statistical software environment R (R Foundation for Statistical Computing) was used to generate the histograms. The scaling factors were: 88.83%, 80.65% (x, y for level 26 in Paxinos & Watson 1998 versus level 25 in Swanson); 86.01%, 79.52% (x, y for level 31 in Paxinos & Watson versus level 29 in Swanson); and 94.71%, 85.50% (x, y for level 33 in Paxinos & Watson versus level in 31 Swanson). For the percent differences in distances between fiducial pairs in the y-axis at level 31 in Paxinos & Watson and level 29 in Swanson, there were no outliers detected by histogram, so the value from the average migration method was used.

Systematic Comparison of Three Reference Spaces

Starting with level 1 of Swanson 2004, Paxinos & Watson 1998, and Paxinos & Watson 2005, Nissl staining forming the basis of each atlas, as reported in that atlas, was compared between Swanson, Paxinos & Watson 1998, and Paxinos & Watson 2005. The goal of this comparison was to identify whether the levels being considered were sufficiently similar in their cytoarchitectural features to permit a migration of data between them. If the reported Nissl-stained tissue sections were closely similar, they were deemed to correspond and the next stage of the analysis was performed. However in many cases, an adequate comparison of the Nissl material was not possible, for one or more of the following reasons: the Nissl stains reported in Swanson 2004 are low-resolution and their fine features are difficult to discern; Paxinos & Watson 1998 and Paxinos & Watson 2005 are based both on a Nissl-stained series and a series stained for AChE, and the Nissl is reported only for every other level, with the AChE staining being reported for levels in between; and Paxinos & Watson 1998 reports staining only for every other level beginning at level 10, such that a Nissl is reported only once every four levels [4, 122, 123]. Thus the levels themselves were frequently used as proxies for the Nissl, and comparison proceeded based either partially or wholly upon the structures in the atlas levels as drawn (see **Figure 3.8**). In cases wherein an atlas level in Swanson 2004 was similar to a level in only one of the Paxinos & Watson atlases, the levels were omitted from the analysis, as it would not be possible to assess their statistical similarity without three independent observations (levels in three atlases).

In the next stage of the analysis, levels identified as corresponding were imported into an Illustrator file (Adobe Illustrator CC), along with their stereotaxic coordinate grids. Rulers were shown on the file and set to measure in millimeters, and the Smart Guide option turned off. Each atlas level was individually resized so that the stereotaxic grid aligned with the file rulers and the origin points matched. If this obliged that the levels be scaled anisotropically, this was done. Each atlas level was then made visible individually, and in a separate layer points were added using the Pen tool at the most dorsal, ventral, lateral, and medial extremes of each structure

contained in a given atlas level (**Figure 3.7**). These points were then grouped and hidden so that the same process could be completed for the other atlas levels in the file. Illustrator CC was preferred over Illustrator CS6 for this portion of the project, because it allows a higher zoom – once the atlas levels are shrunk to match the file rulers, they become very small indeed.

A Microsoft Excel spreadsheet was created, and the structures appearing in the atlas levels were listed therein, arranged by level. Swanson 2004 structures occupied one column, with Paxinos & Watson 1998 structures were listed in the next, and Paxinos & Watson 2005 structures in the next. The lists were arranged such that structures that were determined to correspond between one or more atlases (such as the ARH in S and the ARC in Paxinos & Watson 1998 and Paxinos & Watson 2005) appeared on the same row. Structures without a counterpart in any other atlas were listed alone in a row. Different structures that occupy the same space were listed separately and not compared, unless an examination of the Nissl indicated that they are likely to be the same structure viewed differently by different atlasers. For example, the sod in Paxinos & Watson 1998 appears rostral to its counterpart, the sup, in Swanson 2004, in an area that is at that level (25 in Paxinos & Watson 1998 and Swanson 2004) occupied by the opt in Swanson 2004; so the sod was not compared to the opt at level 25.

For structures having counterparts in all three atlases, the stereotaxic coordinates of their most dorsal, ventral, lateral, and medial points were entered into the spreadsheet, using the Info tool in Illustrator to display the coordinates of the selected points. For some of these structures, one or more bounding points could not be defined, because clear borders were not drawn in one or more atlases. Once such a point was identified, its coordinates were not entered in any other atlas at that level, because three observations of the coordinates were needed for statistical analysis. For example, in the Swanson atlas the divisions of the cortex are indicated by tick marks arranged along the dorsal and lateral edges of the brain; while in Paxinos & Watson they are completely boxed. Therefore, usually the ventral and medial or lateral bounding points of the cortex divisions could not be identified in Swanson, and were then not recorded for Paxinos & Watson at the relevant level either.

An excerpt of this dataset was prepared for preliminary statistical analysis. A selection of structures was made based on their tendency towards clarity in the Nissl, and a set of three corresponding levels was selected based on the presence of many of the chosen structures within the levels.

Statistical Analyses

The open source statistical software environment R (R Foundation for Statistical Computing) was used to develop codes for two- and one-way repeated measures ANOVA (parametric) and the Friedman rank sum test (nonparametric) to use with excerpts of the large atlas comparison dataset generated by the methods described above. This was done by Dr. Soyoung Jeon.

The code: aov(coordinate~method*position+Error(level/position)); where coordinate = the relevant coordinate for that position (x or y), method = the atlas, position = dorsal, ventral, lateral, or medial, and level = the atlas level; was used to run two-way repeated measures ANOVA on the coordinates for a selection of single structures across all levels on which they appeared, comparing them by atlas and by atlas and position (dorsal, ventral, lateral, or medial). The nonparametric Friedman rank sum test, which does not assume sphericity, was run on the same excerpt of the dataset, and compared the coordinates for single structures across all levels on which they appeared by atlas and position.

The code: aov.fit <– aov(coordinate ~ method + Error(structure), data = subset(lvlData, position==" ")); where coordinate = the relevant coordinate for that position (x or y), method = the atlas, structure = a structure present in all three atlases, lvlData = an excerpt from the large dataset containing all data collected for one level (in each atlas), and position = dorsal, ventral, lateral, or medial (the value for the position variable is meant to appear within the quotation marks); was used to run one-way repeated measures ANOVA comparing the coordinates for each position for all structures appearing on level 27 in the Swanson 2004 atlas and on its corresponding levels (level 28 in the Paxinos & Watson 1998 atlas and level 50 in the Paxinos &

Watson 2005 atlas), by atlas. Importantly, these points were not compared by structure in this analysis.

Table 3.1: Distances between Fiducial Pairs in Swanson 2004 versus Paxinos & Watson 1998.

An indication in Table 3.1 that the measurement was from the far side of a given fiducial indicates that the height or width of that fiducial was included in the measurement. Negative values indicate an inverse relationship between the fiducial boundaries chosen – for example, the lower bound of the int is above the upper bound of the fx on Paxinos & Watson 26, but it is below the upper bound of the fx on Swanson 25, resulting in a negative distance in Table 3.1.

Axis	1st Fiducial	2nd Fiducial	Paxinos & Watson level 26 (mm)	Swanson level 25 (mm)	Swanson/Paxinos & Watson (%)
x	fx	int	36.07	37.92	105.1
x	fx far side	int	54.50	49.70	91.2
x	PVH	fx	14.04	20.22	144.1
x	PVH	fx far side	32.47	31.98	98.5
x	PVH	int	68.54	69.91	102.0
x	PV	PVH	31.75	12.91	40.7
x	PV	fx	45.79	33.14	72.4
x	PV	fx far side	64.22	44.95	70.0
x	PV	int	100.29	82.81	82.6
x	AHN	int	36.92	27.87	75.5
x	AHN	CEA	79.91	71.21	89.1
x	fx	CEA	79.06	81.27	102.8
x	PV	CEA	143.28	126.21	88.1
y	fx	opt	25.92	41.48	160.1
y	fx far side	opt	52.44	59.52	113.5
y	int	fx	15.72	–21.19	–134.8
y	int	opt	68.15	38.35	56.3
y	int	fx far side	42.24	–3.19	–7.6
y	ZI	fx	12.41	9.99	80.5
y	ZI	fx far side	38.93	27.99	71.9
y	ZI	opt	64.85	69.47	107.1
y	int	AHN	95.62	53.56	56.0
y	fx far side	AHN	79.90	74.64	93.4
y	ZI	AHN	92.31	84.73	91.8
y	opt	AHN	27.47	15.20	55.4

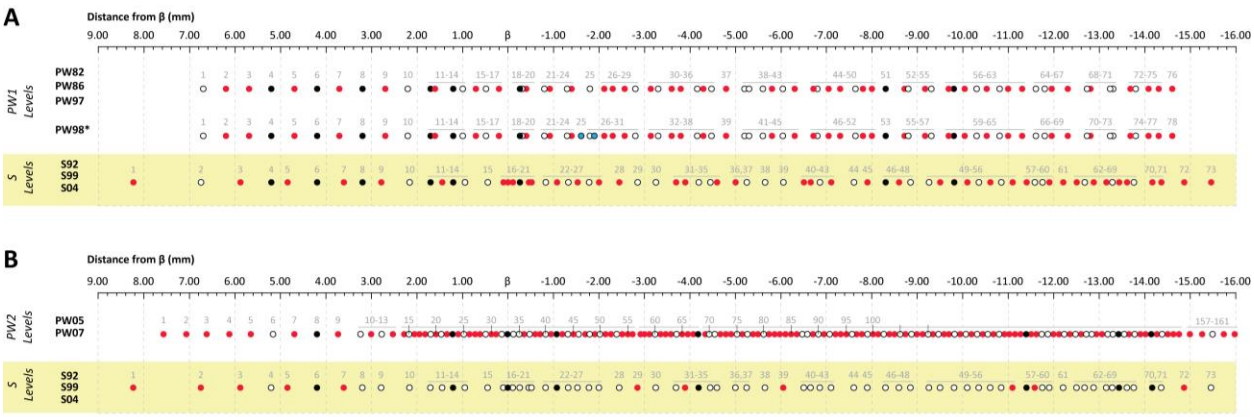

Figure 3.1: Dot Plots of Atlas Levels Calibrated to Bregma (β). Adapted from [121].

This chart compares the anteroposterior stereotaxic coordinate (distance in mm from β) for all levels in all editions of the Swanson and Paxinos & Watson atlases. Each level is represented by a circle. Red circles indicate that the level has no match in the other atlas, based on distance from β. Black circles indicate that the level has an exact match in the other atlas (i.e., the distance from β is identical). White circles indicate that the level has a match in the other atlas within 50 microns (i.e., the distance from β varies by 0.05 mm or less). 50 microns was chosen as the cutoff for classifying levels as narrowly in register because this distance is half or less the diameter of a standard brain probe [133]. The chart was created by Dr. Arshad Khan [121]. (a) The 1992, 1999, and 2004 editions of the Swanson atlas in comparison to the 1982, 1986, 1997, and 1998 editions of the Paxinos & Watson atlas. (b) The 1992, 1999, and 2004 editions of the Swanson atlas in comparison to the 2005 and 2007 editions of the Paxinos & Watson atlas. The 2005 and 2007 editions of Paxinos & Watson are based on a different brain than the previous editions of Paxinos & Watson.

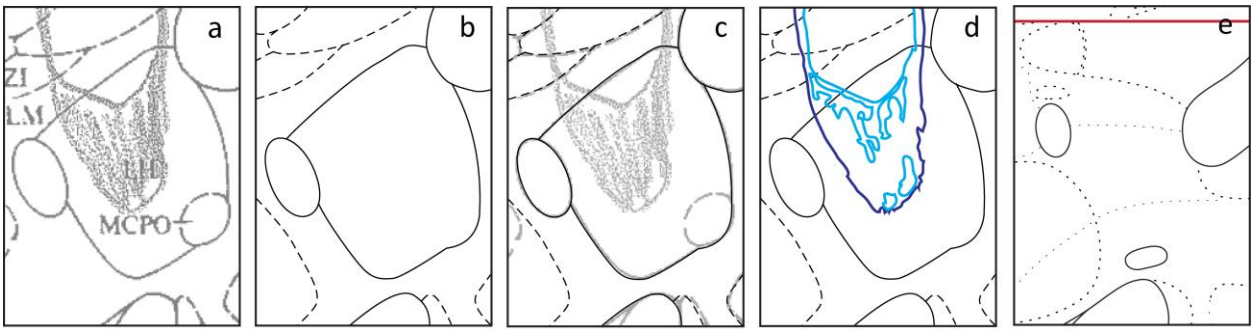

Figure 3.2: Digitization of Maps of Injection Sites (A. M. Khan, unpublished data) and Preparation of Atlas Plates.

(a) Original drawing (Khan, unpublished) onto photocopied Paxinos & Watson 1986/1998 plate. (b) 1998 plate of Paxinos & Watson. (c) Panels a and b superimposed on one another. (d) The final digital version drawn in Adobe Illustrator CS5/6. (e) Swanson 2004 composite plate, made from the Swanson 2004 plates corresponding to the Paxinos & Watson 1998 plate.

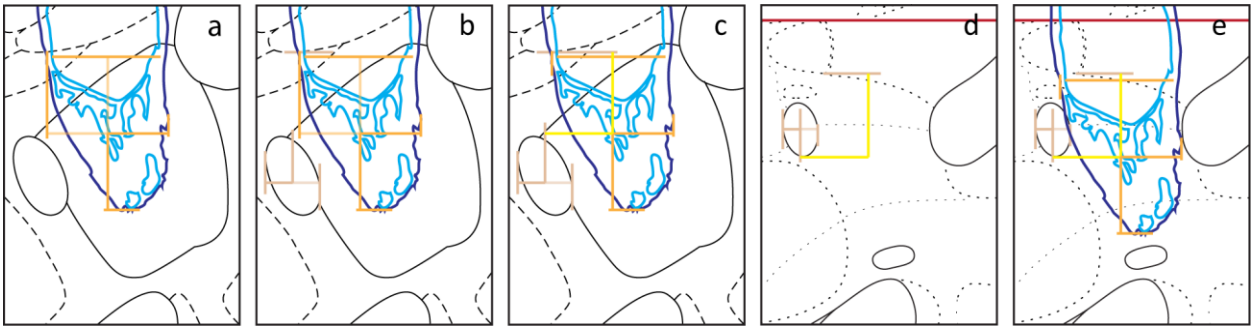

Figure 3.3: Nearest Neighbor Migration Method.

The nearest neighbor migration method, using the injection site from **Figure 3.2** as an example. (a) Digital map on Paxinos & Watson 1998 plate, with the center of the injection site defined. (b) Bracketing fiducials are defined in the same plate. (c) Distances from fiducials to the center of the site are measured. (d) Bracketing fiducials are defined on the Swanson 2004 plate, and distances measured in (c) are replicated. (e) The injection site map is transferred to the Swanson 2004 plate and positioned so that its center fits the replicated distances.

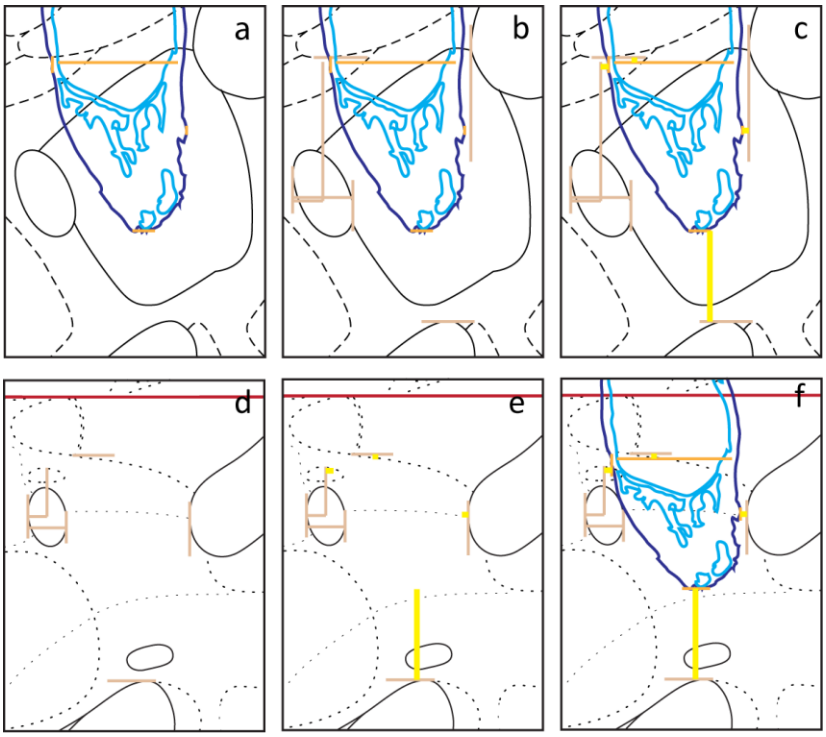

Figure 3.4: Nearest Neighbor Warped Migration Method.

The nearest neighbor migration method (which used to be known as the distance transform method), using the injection site from **Figure 3.2** as an example. (a) Digital map on Paxinos & Watson 1998 plate, with the borders of the injection site defined. (b) Bracketing fiducials are defined in the same plate. (c) Distances from fiducials to the borders of the site are measured. (d) Bracketing fiducials are defined on the Swanson 2004 plate. (e) Distances measured in (c) are replicated on the Swanson 2004 plate. (f) The injection site map is transferred to the Swanson 2004 plate and warped to fit the replicated distances.

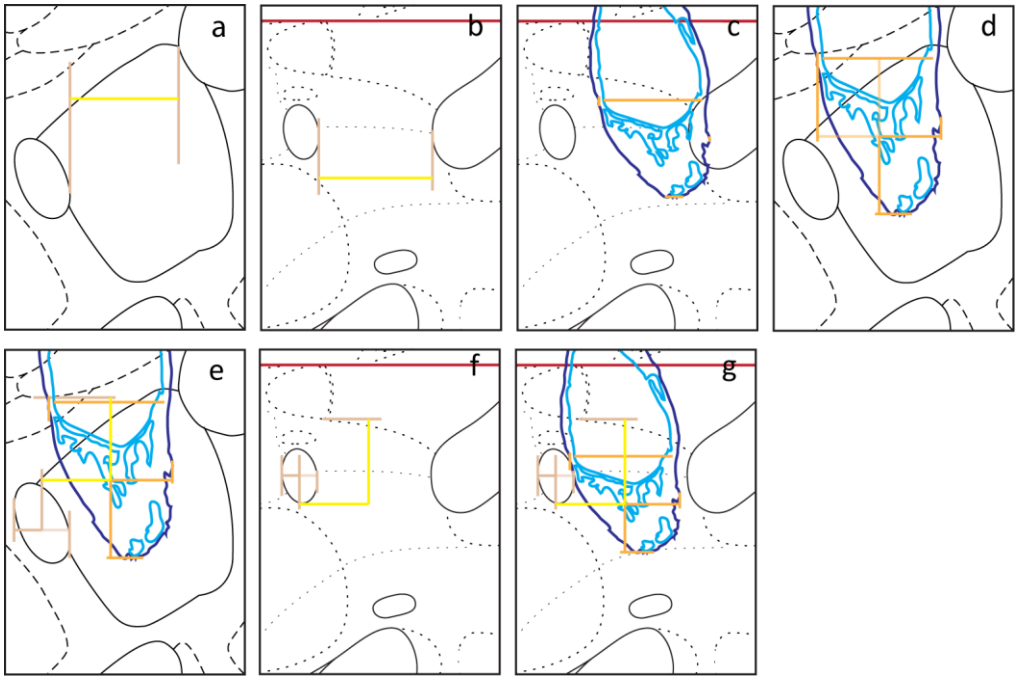

Figure 3.5: Average Migration Method.

The average migration method, using the injection site from **Figure 3.2**. (a) The distance between a pair of fiducials is measured on the Paxinos & Watson 1998 plate. (b) The distance between the same fiducials is measured on the Swanson 2004 composite plate. (c) The injection site, with defined borders, is placed on the Swanson 2004 composite plate and anisotropically scaled by the calculated factors. Its position at this point (before scaling) is stereotaxically identical to its position on the Paxinos & Watson 1998 plate. (d) The center of the original site is defined. (e) The distance from the center of the original site to two fiducials is measured on the Paxinos & Watson 1998 plate, similar to **Figure 3.3b–c**. (f) The same fiducials are defined on the Swanson 2004 plate. (g) The scaled site from (c) is repositioned such that the distances measured in (e) are replicated.

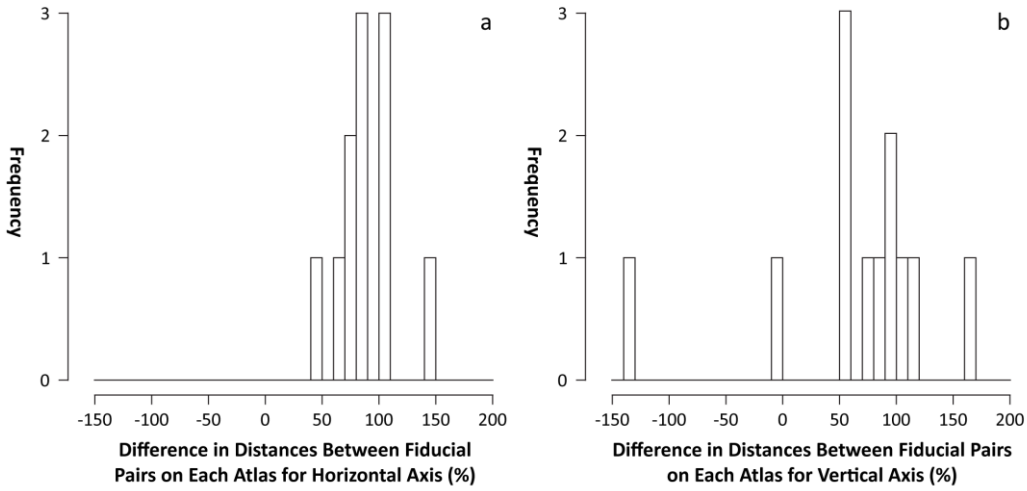

Figure 3.6: Histograms for the Average No Outlier Migration Method.

The histograms used to exclude outlier values from the averaged scaling factors for the x (a) and y (b) axes, for Paxinos & Watson 1998 level 26 versus Swanson 2004 level 25.

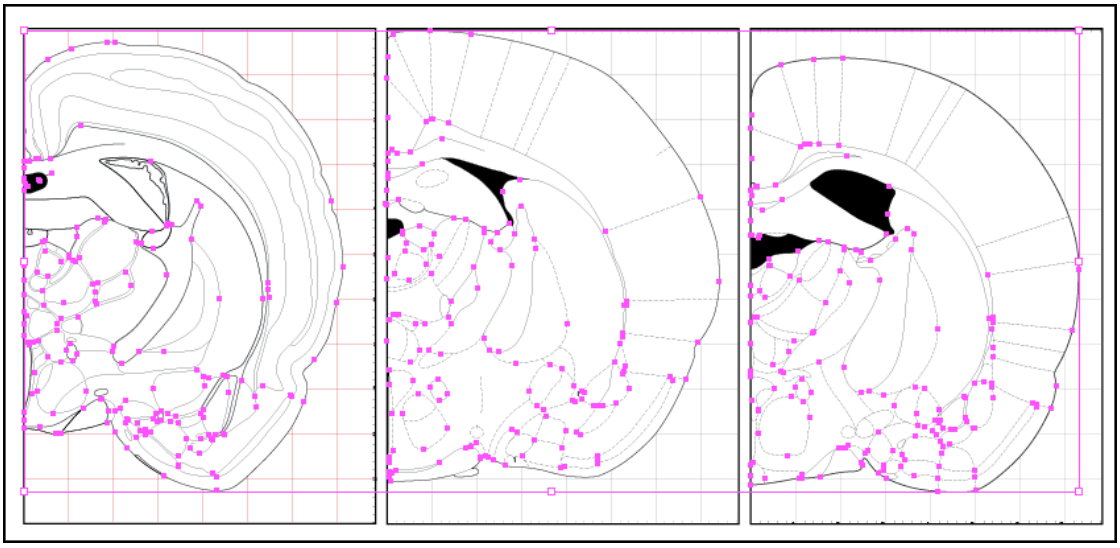

Figure 3.7: Points used for Atlas Comparison.

From left: level 25 of the Swanson 2004 atlas (–1.53 µm from β); level 25 of the Paxinos & Watson 1998 atlas (–1.6 µm from β); and level 46 of the Paxinos & Watson 2005 atlas (–1.56 µm from β). Structures identified as equivalent in all three atlases have points placed at their most dorsal, ventral, medial, and lateral extremes, where a defined border is present.

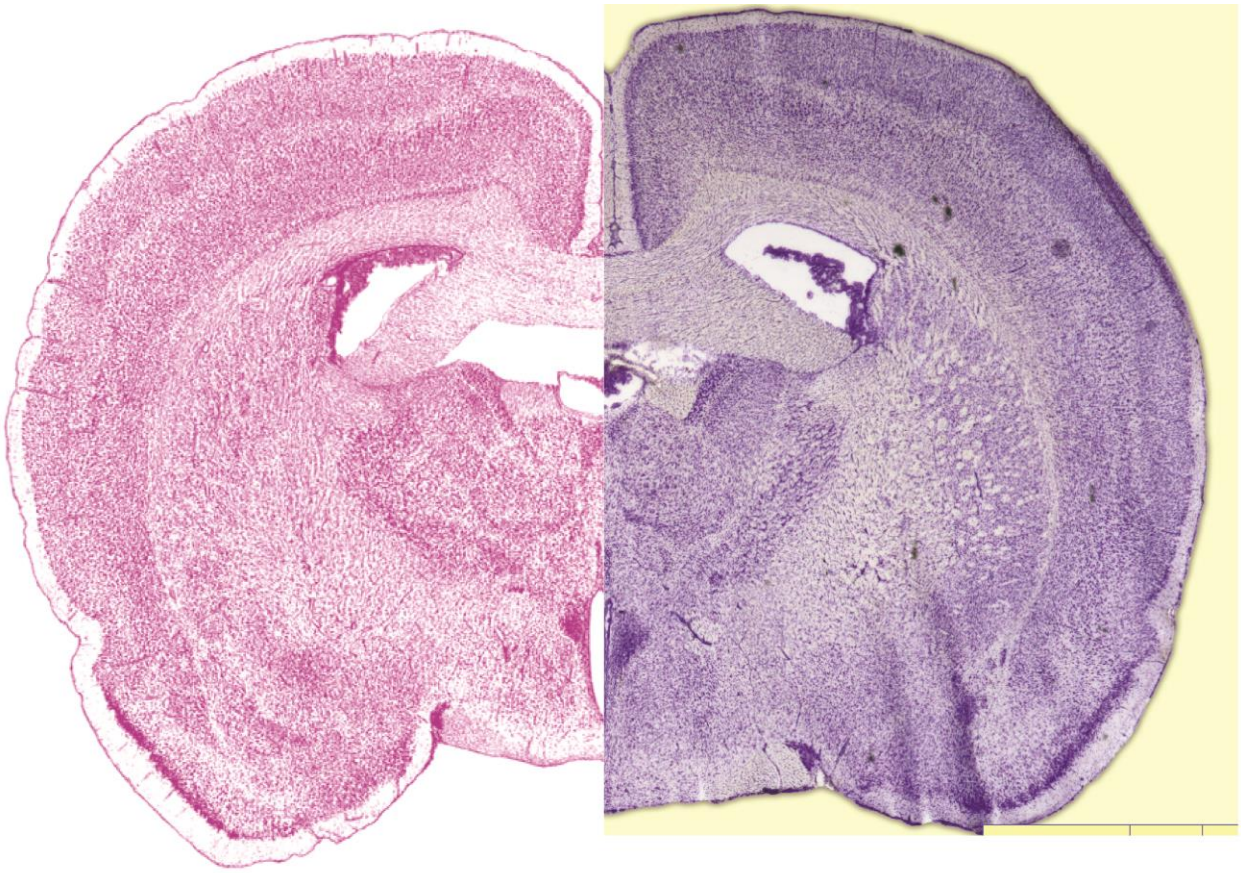

Figure 3.8: Juxtaposiing of Nissl Images for Comparison of Atlases.

From left: the Nissl reported in Swanson 2004 for level 25; the Nissl reported in Paxinos & Watson 2005 for level 46. These levels are compared in **Figure 3.7**. Paxinos & Watson 1998 does not report a Nissl for the corresponding level, level 25.

Results

Data Migration

All methods developed for systematically transferring data from one atlas to another were faulty, and failed to consistently produce reasonable transformations. The results of several of the methods are illustrated in **Figure 3.9**; of these, the nearest neighbor and average no outlier migration methods were the best, as defined by the similarity in shape, size, and position between the original mapped injection site on Paxinos & Watson 1986/1998 and the migrated map of the injection site on Swanson 2004. These were also the best methods overall, considering all 45 injection sites used, with the average no outlier migration method being slightly superior. However, every method attempted, including these, produced some strikingly poor migrations. In some cases the methodology employed led to the injection site appearing inverted on the Swanson plate, or being otherwise grossly warped in size and shape. More commonly, the migrated injection site appeared on structures it was not originally mapped onto; in particular on the white matter tracts surrounding the lateral LHA (fx, int/cpd, opt). All told, at least one acceptable migration by any method was achieved for 39% of cases (26% of cases had at least one high quality migration, usually using the average no outliers method). Mediocre migrations were achieved in 29% of cases, and only poor migrations were achieved in 34% of cases (13% of cases had only extremely poor migrations). In 79% of cases, the average no outlier migration method was judged to give the best migration.

Systematic Comparison of Three Reference Spaces

The systematic comparison of levels between Swanson 2004, Paxinos & Watson 1998, and Paxinos & Watson 2005 generated a large Excel spreadsheet, although it is not complete. Levels 1–42 in the Swanson atlas have been matched (if possible) with counterparts in the Paxinos & Watson atlases, the correspondence in their structures determined, and those structures' bounding points recorded. Levels 43–72 in the Swanson atlas remain; however, technical considerations, namely the burgeoning possibility of performing this sort of work using

computer algorithms, make the dataset unlikely to be worthwhile to complete. Due to the extremity of its size and the limited immediate utility of its contents, the record of this endeavor has been relegated to the Appendix (**Table 4.1**). Levels 43–47 in the Swanson atlas have been matched, where possible, with appropriate levels in Paxinos & Watson 1998 and 2005, and the corresponding structures in these levels have been identified. This information is also presented in the Appendix (**Table 4.2**). Finally, levels 48–73 in the Swanson atlas have been matched, where possible, with appropriate levels in Paxinos & Watson 1998 and 2005. The correspondence of all levels in Swanson with levels in Paxinos & Watson, as determined by fiducial analysis, is shown in **Figure 3.10**.

The results of repeated measures ANOVA on all coordinates of each bounding point (individually) for all structures at a selected level (level 27 in Swanson 2004, level 28 in the Paxinos & Watson 1998 atlas, and level 50 in the Paxinos & Watson 2005 atlas), were as follows: F-value = 1.028, p-value = 0.364 for the dorsal bounding point, F-value = 0.503, p-value = 0.607 for the ventral bounding point, F-value = 0.402, p-value = 0.671 for the lateral bounding point, and F-value = 0.087, p-value = 0.916 for the medial bounding point. Degrees of freedom = 2 in all cases. None of the values are significant. This means that the dorsal bounding points of structures at level 27/level 28/level 50 are not statistically different from each other, and the same statement holds true for the ventral, lateral, and medial bounding points. It is important to bear in mind that this analysis did not compare bounding points by structure, but compared all bounding points at a particular position (e.g., dorsal) for that level, that belonged to structures present in all three atlases.

The results of repeated measures ANOVA on the coordinates of selected structures, across all levels on which the structures appear, are summarized in **Table 3.2**. The results of Friedman rank sum tests on the coordinates of each bounding point (individually) for the selected structures, across all level on which they appear, are also summarized therein. Repeated measures ANOVA concluded that the coordinates for many of the structures (the AD, ARH, AV, DG, fx, PVH, and SO) were significantly different in at least one atlas; however, as this test

assumes homogeneity of variance, its appropriateness for the data is not a given. The Friedman rank sum test also concluded that the listed structures' coordinates were significantly different in at least one atlas, for at least one of their bounding points; but the p-values obtained with the Friedman test tended to be larger than with the ANOVA. The coordinates for the LD were not found to significantly differ between atlases by any test.

Table 3.2: Results of Statistical Tests for Differences in Selected Structures' Coordinates between Atlases.

Struc-ture	Repeated Measures ANOVA		Friedman Rank Sum							
			Dorsal		Ventral		Lateral		Medial	
	F-value	p-value	χ^2	p-value	χ^2	p-value	χ^2	p-value	χ^2	p-value
AD	8.21	0.002	6.5	0.039	4.7	0.097	6.5	0.039	4.7	0.097
ARH	15.44	7.5E-05	4.7	0.097	4.7	0.097	0.5	0.779	6.0	0.050
AV	3.74	0.039	6.5	0.039	8.0	0.018	3.5	0.174	6.5	0.039
DG	13.26	9.6E-06	4.7	0.097	11.2	0.004	2.7	0.264	12.0	0.002
fx	70.17	2.7E-19	18.0	1.2E-04	20.5	3.6E-05	8.2	0.017	2.0	0.368
LD	2.11	0.135	2.3	0.311	1.3	0.513	2.3	0.311	5.3	0.069
PVH	13.43	6.8E-05	7.6	0.022	6.0	0.050	6.4	0.041	4.5	0.105
SO	31.86	2.4E-08	8.4	0.015	7.6	0.022	6.4	0.041	7.4	0.024

Tests compared structures' coordinates across all levels on which they appeared in all three atlases (if there were levels at which the structure appeared in less than three atlases or had poorly defined borders, they were omitted). The repeated measures ANOVA compared coordinates for all bounding points (dorsal, ventral, lateral, medial) at once, but assumed homogenous variance (sphericity) in the data. The Friedman rank sum test did not make assumptions about the variance in the data, but was unable to compare coordinates for all bounding points at once. More significant p-values ($p<0.025$) are shaded in green, while less significant p-values ($0.05 \geq p > 0.025$) are shaded in light green. Degrees of freedom = 2.

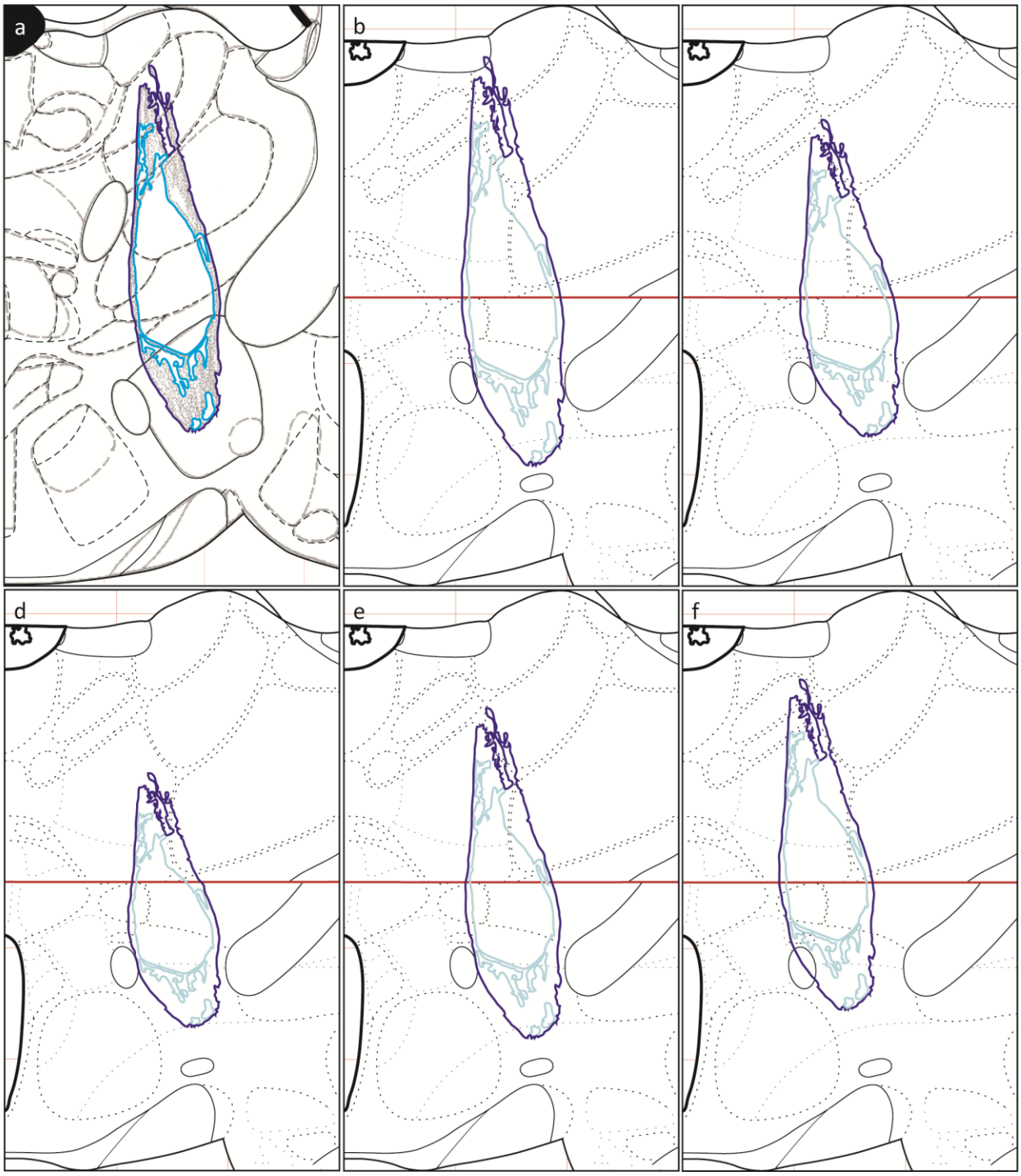

Figure 3.9: Data Migration between Atlases using Different Methods.

(a) The scanned map (Paxinos & Watson 1986/1998) of case 00/112 superimposed on the corresponding Paxinos & Watson 1998 atlas plate and digitized. (b) The migrated map on the composite Swanson 2004 plate, using the nearest neighbor migration method. (c) The migrated

map on the composite Swanson 2004 plate, using the nearest neighbor warped migration method. (d) The migrated map on the composite Swanson 2004 plate, using the average migration method. (e) The migrated map on the composite Swanson 2004 plate, using the average no outliers migration method. (f) The migrated map on the composite Swanson 2004 plate, using the stable fiducial migration method.

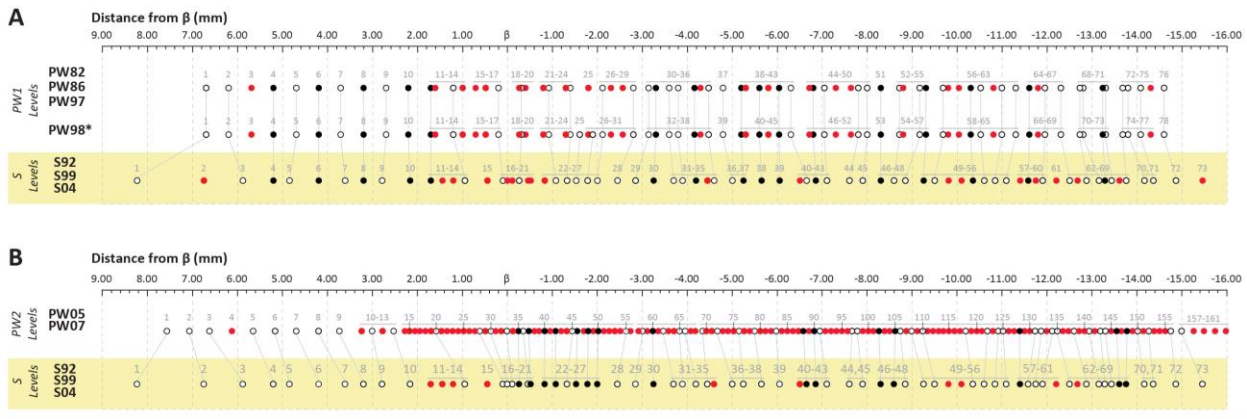

Figure 3.10: Dot Plots of Atlas Levels Matched by Fiducial Analysis. Revised from [121].

This chart is an updated version of the chart appearing in **Figure 3.1**. It displays all levels in all editions of the Swanson and Paxinos & Watson atlases, arranged by anteroposterior stereotaxic coordinate (distance in mm from β). Each level is represented by a circle, and lines between certain circles indicate that those levels are matching based on a fiducial analysis. Red circles indicate that the level has no match by fiducials in the other atlas. Black circles indicate that the level has a match in the other atlas based on a fiducial analysis and on the stereotaxic coordinates (i.e., the distance from β is 0.05 mm or less). White circles indicate that the level has a match in the other atlas based only on fiducial analysis. The original chart was created by Dr. Arshad Khan [121]. (a) The 1992, 1999, and 2004 editions of the Swanson atlas in comparison to the 1982, 1986, 1997, and 1998 editions of the Paxinos & Watson atlas. (b) The 1992, 1999, and 2004 editions of the Swanson atlas in comparison to the 2005 and 2007 editions of the Paxinos & Watson atlas. The 2005 and 2007 editions of Paxinos & Watson are based on a different brain than the previous editions of Paxinos & Watson.

Discussion

Data Migration

It proved impossible for me to develop a reliable, systematic method for transferring data among atlases. The word 'systematic' here is key – for any mapper should readily be capable of performing such transfers based upon their experience and judgment. One must place the migrating data on the new atlas in Adobe Illustrator, and position it to recapitulate its relationship with nearby fiducials in its original context. This may necessitate reorienting, rescaling or reshaping the migrating data as appropriate, and is absolutely to be done on a case-by-case basis with reliance, again, on one's professional judgment. This is, in my own professional opinion, the right way to migrate data among atlases. But such a methodology does not readily lend itself to publication, defies any attempt to speed the migration process, and is useless to untrained individuals; so a stepwise and systematic method was sought, and eluded me. The method development process, in which I had to abandon my knowledge of how to accomplish the migration task using my mapping skills, felt to me like trying to use a fork with all my digits bound together into one blunt mass. My personal feeling is that this field of inquiry is infertile. Surely if any gains are to be made here, it is not by an anatomist, but by a computer scientist; and a computer scientist would know better than I what may be possible, and when it may be so.

In my opinion, the idea that it is necessary to migrate data from Paxinos & Watson to Swanson in order to understand them in the context of chemoarchitectural or connectional data mapped to Swanson, is not wholly sound. Taking the example of the unpublished injection site maps used in this study, it is plain to see approximately where the sites must fall on Swanson (in the LHA lateral to the fx). So one might then examine chemoarchitectural and connectional maps in Swanson and identify neuronal populations and/or fibers that are also in the LHA lateral to the fx, and construct one's hypotheses. True, there is a level of detail that is clearly sacrificed by such estimations, but it is unclear how important this is. A person is not liable to find a population mapped to Swanson in the same region that is shaped like the negative of an injection site. And considering that there is a level of individual variation and idiosyncrasy among brains

that may be greater or lesser for any population but is always present and unaccounted for, it cannot be assumed that populations which narrowly avoid, or narrowly overlap, the injection site do so reliably and not spuriously.

Systematic Comparison of Three Reference Spaces

The dataset in **Table 4.1** was relatively intractable to statistical analysis, because only three observations (three brains mapped against stereotaxic coordinates) were available. However, consultation with Dr. Soyoung Jeon yielded a couple of more or less interesting and more or less valid analyses: it was possible to compare the bounding points for a single structure across all levels in which it appeared, between the three atlases, by repeated measures ANOVA. It was possible to compare one bounding point (for example, the dorsalmost point) of a single structure across all levels in which it appeared, between the three atlases, by repeated measures ANOVA and by the Friedman ranked-sum test. And it was possible to compare one bounding point (for example, the dorsalmost point) of all structures within a single level, between the three atlases, by repeated measures ANOVA. However, repeated measures ANOVA was not necessarily an appropriate test for these data because it assumes homogeneity of variance in the coordinates (sphericity); and all of the analyses had low power, due to the low number of observations.

The statistical analyses indicated that the selected corresponding levels did not significantly differ from each other, which supports the feasibility of migrating data between them, and endorses the capacity of a mapper to determine which levels correspond based on fiducials. However, it is not to be assumed that all levels identified in **Table 4.1** as corresponding do so simply or would not be identified as differing statistically. For some of these levels, it was apparent based on the fiducials that while many areas corresponded closely, some portions of the levels did not, due to plane of section differences, idiosyncrasies in the atlas brains, and possibly to differing perceptions of the atlasers. Anyone attempting to migrate data between the levels

would need to assess their correspondence in the particular region containing the data, and might find different levels that match better for that specific region, though matching less well overall.

The statistical analyses also indicated that all but one of the selected structures differed significantly over the entirety of their anterior-posterior extents between at least two of the three atlases. However, while the repeated measures ANOVA (the less valid test) found many strong differences (p-values less than 0.001), the Friedman rank sum test found that most differences were only slightly significant (p-values over 0.025) and only one structure had p-values less than 0.001, for its dorsal and ventral bounding points (indicating that the fx drifts significantly dorsally and ventrally between brains, but drifts little medially and laterally). The Friedman rank sum test results also show that structures tend to have more variation in some of their borders than in others (because while most structures had a significant p-value for one or more bounding points, none had significant p-values for all bounding points). The presence of statistically significant variations in the locations of structures between brains and atlases is expected and supported by the experience of any investigator who has done central injections – one can reliably inject at a given set of stereotaxic coordinates, but one cannot at all reliably inject into a specific brain structure.

Overall these results indicate that while most structures are fairly stable between brains and atlases, individual structures are more variable between brains and atlases than are whole levels identified as corresponding.

One additional utility of the information in **Tables 4.1** and **4.2** exists: it may smooth the path of a scientist wishing to compare the atlases or to migrate data amongst them in the future, by pointing out levels that correspond between all three atlases and structures at these levels that correspond between two or more atlases.

Future Directions

The Great Atlas

It is, however, necessary and valuable to transfer older maps to newer atlases for the sake of creating successively elaborate brain models; and the needs of the great atlas dictate that many older maps be recast in its format. For this, the following methodology would suffice.

Firstly, it must be determined which new atlas levels correspond with the relevant levels in the older atlas. This decision should not be based on stereotaxic coordinates, but on a learned visual comparison of fiducials. Only the area around the mapped data need be matched, if plane of section differences between the atlases result in only parts of the selected levels truly corresponding. If the mapped data are situated such that they span both regions that correspond well between the selected plates, and regions that do not, then the mapped data should be split accordingly. Another level in the new atlas should be found which matches the portions of the older atlas levels that contained mapped data and did not correspond to the first level identified.

The relevant new atlas level(s) should be opened in Adobe Illustrator, and the older maps imported into the files. If two or more new atlas levels had to be used, the older maps should be cut so that only the matching portions are shown in each file, or else the matching portions should be delineated with drawn border lines (it is likely that the boundary will not exist along a straight line). It is possible in Illustrator to draw an irregularly shaped border line, place it over the older map in the Layers panel, and use it to make a clipping mask that shows only its interior. The older map and the new atlas level should be arranged side-by-side.

The older map must then be studied to identify the relationship between the mapped data and the nearby fiducials, and to identify the characteristics of the mapped data themselves. The data must be redrawn onto the new atlas level using simple shapes with appropriate patterned fills, with the shapes recapitulating the relationship between the original mapped data and the nearby fiducials. This may obligate that the simple shapes differ in size or shape from the original data. For instance, if the older map shows an area of high density cells, surrounded by an area of moderate density cells, surrounded by an area of scattered cells; then three shapes should

be drawn (compound paths will be needed), and their borders should not mimic the original shape of the three fields of cell bodies, but rather the relationships between these fields and the fiducials they overlap or fall short of reaching.

Computer Algorithms in Atlas Comparison

Jose Perez has created an algorithm to compare the DG across atlases. This algorithm has been able to identify many more points in images of Nissl-stains of the DG than my paltry four, thereby achieving an altogether superior comparison; and was able to predict what level of the Swanson atlas an image of the Nissl-stained DG belonged to if the image used was from material reported in the Swanson atlas (that is, the example of the DG used was drawn in the atlas), as well what level of the Swanson atlas an image of the Nissl-stained DG corresponded with if the image used was from material reported in the Paxinos & Watson atlas. Although the DG is a very easily distinguished structure in Nissl-stained tissue, it stands to reason that in the future any truly exhaustive comparison of the atlases shall make use of algorithms to select a large number of landmarks for analysis, likely rendering the data in **Table 4.1** obsolete. This advance, along with much of my data for Specific Aim 2, are being prepared for publication [133].

Geometric Morphometrics

In the past, information on the spatial relationships between anatomical landmarks was analyzed using multivariate statistics and data including distances, angles, and ratios thereof, in the field of morphometrics, which has applications in anthropology, evolutionary biology, and other arenas. In the 1980s, this field was revolutionized by the use of Cartesian coordinates to describe these spatial relationships, in place of distances etc., and rechristened geometric morphometrics; a term coined in 1993 by F. James Rohlf and Leslie F. Marcus [134, 135]. Geometric morphometric techniques may be appropriate to the analysis of brain structures; for example, they have been used with MRI data to investigate the differences between the brains of adults exposed or not exposed to alcohol in the womb [136].

Geometric morphometrics is also subject to errors such as differing specimen orientation vis-à-vis axes (this is plane of section error in mapping) and differing specimen size, and a variety of methods are used to correct for these, the most developed of which are the Procrustes methods. Generalized Procrustes analysis requires a large number of specimens, for in this approach, the average 'configuration' (overall set of coordinates for all landmarks used in a specimen or idealized specimen) is compared to the configuration of each individual specimen; the individual configurations are rotated and translated to match more closely with the average using a least-squared method; the average is recalculated; the configurations are transformed again; etc. Analysis of the resultant data requires additional manipulation of the data set or the use of nonparametric techniques [135, 137].

Another issue is the accurate identification of landmarks, particularly when dealing with curved surfaces, such as are found in brain structures – typically these surfaces have not been studied using morphometrics, due to the difficulty of reliably finding landmarks upon them [135]. This obstacle has been addressed by the invention of sliding landmarks, also known as semilandmarks, by Fred L. Bookstein in 1991, which he applied to study, by MRI, the corpus callosum in adults with or without schizophrenia [138, 139]. Sliding landmarks are placed along the curves or curved surfaces being analyzed, and are allowed to 'slide' along vectors or planes that are tangential to the curves or surfaces during analysis, so that some statistically relevant quantity is minimized; for instance the Procrustes distances when using Procrustes methods. After sliding they are returned to the nearest point on the actual curve or surface. Thus their ultimate location, in coordinates, is determined by the method of statistical analysis. This is, again, an iterative process – tangents are thus recalculated and the landmarks re-slid, until the statistically relevant quantity is maximally minimized [135, 137].

Geometric morphometrics appears aptly suited to the sophisticated analysis of variance in brain structures across brains and atlases. However, there is one large problem: the effort required to generate a single specimen – a full rat brain drawn out in sections upon grids of stereotaxic coordinates; essentially an atlas – is enormous; and geometric morphometric

techniques benefit from the inclusion of many specimens. In his study of schizophrenic and normal brains, Bookstein used 25 brains [139]. That may be alright when gathering data using MRI, but for our present purposes such a number is nigh out of reach. Also, since the Swanson atlas uses a derived coordinate system that is actually based on the Paxinos & Watson atlas, it is questionable whether the Swanson atlas counts as an independent observation – this may introduce error into the analysis. Altogether, it seems that while techniques equal to the task of analyzing complex differences between rat brains are extant, thorough analyses must await the creation, from scratch, of additional atlas brains.

References

1. Brooks, C.M., *The history of thought concerning the hypothalamus and its functions.* Brain Research Bulletin, 1988. **20**: p. 657-667.
2. *Diencephalon*, in *Gray's Anatomy: The Anatomical Basis of Clinical Practice*, S. Standring, Editor. 2008, Elsevier.
3. Simmerly, R.B., *Organization of the Hypothalamus*, in *The Rat Nervous System*. 2015, Academic Press.
4. Swanson, L.W., *Brain Maps, Third Edition: Structure of the Rat Brain*. 3rd ed. 2004: Academic Press.
5. Paxinos, G. and C., Watson, *The Rat Brain in Stereotaxic Coordinates, Seventh Edition*. 7th ed. 2013: Academic Press. 472.
6. McCartney, C.R. and J.C. Marshall, *Neuroendocrinology of Reproduction*, in *Yen and Jaffe's Reproductive Endocrinology*. 2014, Elsevier. p. 3-26.e8.
7. Thompson, R., *Structural characterization of a hypothalamic visceromotor pattern generator network.* Brain Research Reviews, 2003. **41**(2-3): p. 153-202.
8. Bergland, R.M. and R.B. Page, *Can the pituitary secrete directly to the brain? (affirmative anatomical evidence).* Endocrinology, 1978. **102**(5): p. 1325-1338.
9. Freeman, M.E.; Kanyicska, B.; Lerant, A.; and G. Nagy, *Prolactin: Structure, function, and regulation of secretion.* Physiological Reviews, 2000. **80**(4): p. 1523-1631.
10. Trachtman, J.N., *Vision and the hypothalamus.* Optometry, 2010. **81**(2): p. 100-15.
11. de Wied, D., *Peptide hormones and neuropeptides: birds of a feather.* Trends in Neuroscience, 2000. **23**(3): p. 113.

12. Guillemin, R., *Peptides in the brain: the new endocrinology of the neuron.* Nobel Lecture, 1977.

13. Mains, R.E. and B.A. Eipper, *The Neuropeptides*, in *Basic Neurochemistry: Molecular, Cellular and Medical Aspects*, G.J. Siegel, et al., Editor. 1999, Lippincott-Raven: Philadelphia.

14. Merighi, A., *Costorage and coexistence of neuropeptides in the mammalian CNS.* Progress in Neurobiology, 2002. **66**: p. 161-190.

15. Fuxe, K.; Borroto-Escuela, D.O.; Romero-Fernandez, W.; Zhang, W.B.; and L.F. Agnati, *Volume transmission and its different forms in the central nervous system.* Chinese Journal of Integrative Medicine, 2013. **19**(5): p. 323-9.

16. McKinley, M.J.; Allen, A.M.; Burns, P.; Colvill, L.M.; and B.J. Oldfield, *Interaction of circulating hormones with the brain: the roles of the subfornical organ and the organum vasculosum of the lamina terminalis.* Clinical and Experimental Pharmacology and Physiology, 1998. **25**: p. S61-S67.

17. Blouet, C. and G.J. Schwartz, *Hypothalamic nutrient sensing in the control of energy homeostasis.* Behavioral Brain Research, 2010. **209**(1): p. 1-12.

18. Morton, G.J.; Cummings, D.E.; Baskin, D.G.; Barsh, G.S.; and M.W. Schwartz, *Central nervous system control of food intake and body weight.* Nature, 2006. **443**(7109): p. 289-95.

19. Laryea, G.; Schutz, G.; and L.J. Muglia, *Disrupting hypothalamic glucocorticoid receptors causes HPA axis hyperactivity and excess adiposity.* Molecular Endocrinology, 2013. **27**(10): p. 1655-65.

20. Hill, J.W; Elmquist, J.K.; and C.F. Elias, *Hypothalamic pathways linking energy balance and reproduction.* American Journal of Physiology, Endocrinology, and Metabolism, 2008. **294**: p. E827-E832.

21. Johren, O.; Imboden, H.; Hauser, W.; Maye, I.; Sanvitto, G.L.; and J.M. Saavedra, *Localization of angiotensin-converting enzyme, angiotensin II, angiotensin II receptor subtypes, and vasopressin in the mouse hypothalamus.* Brain Research, 1997. **757**: p. 218-227.

22. Leak, R.K. and R.Y. Moore, *Innervation of ventricular and periventricular brain compartments.* Brain Research, 2012. **1463**: p. 51-62.

23. Merchenthaler, I.; Setalo, G.; Csontos, C.; Petrusz, P.; Flerko, B.; and A. Negro-Vilar, *Combined retrograde tracing and immunocytochemical identification of luteinizing hormone-releasing hormone- and somatostatin-containing neurons projecting to the median eminence of the rat.* Endocrinology, 1989. **125**(6): p. 2812-2821.

24. Critchlow, V.; Abe, K.; Urman, S; and W. Vale, *Effects of lesions in the periventricular nucleus of the preoptic-anterior hypothalamus on growth hormone and thyrotropin secretion and brain somatostatin.* Brain Research, 1981. **222**(2): p. 267-276.

25. Morrison, S.F., *2010 Carl Ludwig distinguished lectureship of the APS neural control and autonomic regulation section: Central neural pathways for thermoregulatory cold defense.* Journal of Applied Physiology, 2011. **110**(5): p. 1137-1149.

26. Risold, P.Y.; Canteras, N.S.; and L.W. Swanson, *Organization of projections from the anterior hypothalamic nucleus: A Phaseolus vulgaris-leucoagglutinin study in the rat.* Journal of Comparative Neurology, 1994. **348**(1): p. 1-40.

27. Methippara, M.M.; Kumar, S.; Alam, M.N.; Szymusiak, R.; and D. McGinty, *Effects on sleep of microdialysis of adenosine A1 and A2a receptor analogs into the lateral preoptic area of rats.* American Journal of Physiology - Regulatory, Integrative and Comparative Physiology, 2005. **289**(6): p. R1715-R1723.

28. Schmidt, M.H.; Valatx, J.L.; Sakai, K.; Fort, P.; and M. Jouvet, *Role of the lateral preoptic area in sleep-related erectile mechanisms and sleep generation in the rat.* The Journal of Neuroscience, 2000. **20**(17): p. 6640-6647.

29. Pickard, G.E. and P.J. Sollars, *The Suprachiasmatic Nucleus*, in *The Senses: A Comprehensive Reference* (Vol. 1), A.I. Basbaum, et al., Editors. 2008, Academic Press: New York. p. 537-555.

30. Fekete, C., et al., *α-Melanocyte-stimulating hormone is contained in nerve terminals innervating thyrotropin-releasing hormone-synthesizing neurons in the hypothalamic paraventricular nucleus and prevents fasting-induced suppression of prothyrotropin-releasing hormone gene expression.* The Journal of Neuroscience, 2000. **20**(4): p. 1550-1558.

31. Onoe, H.; Watanabe, Y.; Ono, K.; Koyama, Y.; and O. Hayaishi, *Prostaglandin E2 exerts an awaking effect in the postrior hypothalamus at a site distinct from that mediating its febrile action in the anterior hypothalamus.* The Journal of Neuroscience, 1992. **12**(7): p. 2715-2725.

32. Hatton, G.I., *Nucleus circularis: Is it an osmoreceptor in the brain?* Brain Research Bulletin, 1976. **1**(1): p. 123-131.

33. Bernardis, L.L. and L.L. Bellinger, *The lateral hypothalamic area revisited: ingestive behavior.* Neuroscience and Biobehavioral Reviews, 1996. **20**(2): p. 189-287.

34. Berthoud, H.R. and H. Munzberg, *The lateral hypothalamus as integrator of metabolic and environmental needs: from electrical self-stimulation to opto-genetics.* Physiology & Behavior, 2011. **104**(1): p. 29-39.

35. Shimogawa, Y.; Sakuma, Y.; and K. Yamanouchi, *Efferent and afferent connections of the ventromedial hypothalamic nucleus determined by neural tracer analysis: Implications for lordosis regulation in female rats.* Neuroscience Research, 2015. **91**: p. 19-33.

36. Vann, S.D. and J.P. Aggleton, *The mammillary bodies: Two memory systems in one?* Nature Reviews Neuroscience, 2004. **5**(1): p. 35-44.

37. Stackman, R.W. and J.S. Taube, *Firing properties of rat lateral mammillary single Units: head direction, head pitch, and angular head velocity.* The Journal of Neuroscience, 1998. **18**(21): p. 9020-9037.

38. Kirk, I.J.; Oddie, S.D.; Konopacki, J.; and B.H. Bland, *Evidence for differential control of posterior hypothalamic, supramammillary, and medial mammillary theta-related cellular discharge by ascending and descending pathways.* The Journal of Neuroscience, 1996. **16**(17): p. 5547-5554.

39. Donato, J., Jr., et al., *The ventral premammillary nucleus links fasting-induced changes in leptin levels and coordinated luteinizing hormone secretion.* The Journal of Neuroscience, 2009. **29**(16): p. 5240-5250.

40. Cavalcante, J.C.; Bittencourt, J.C.; and C.F. Elias, *Female odors stimulate CART neurons in the ventral premammillary nucleus of male rats.* Physiology & Behavior, 2006. **88**(1): p. 160-166.

41. Canteras, N.S.; Kroon, J.A.; Do-Monte, F.H.; Pavesi, E.; and A.P. Carobrez, *Sensing danger through the olfactory system: The role of the hypothalamic dorsal premammillary nucleus.* Neuroscience & Biobehavioral Reviews, 2008. **32**(7): p. 1228-1235.

42. Markham, C.M.; Blanchard, D.C.; Canteras, N.S.; Cuyno, C.D.; and R.J. Blanchard, *Modulation of predatory odor processing following lesions to the dorsal premammillary nucleus.* Neuroscience Letters, 2004. **372**(1): p. 22-26.

43. Blanchard, D.C., et al., *Dorsal premammillary nucleus differentially modulates defensive behaviors induced by different threat stimuli in rats.* Neuroscience Letters, 2003. **345**(3): p. 145-148.

44. Buccafusco, J.J. and H.E. Brezenoff, *Pharmacological study of a cholinergic mechanism within the rat posterior hypothalamic nucleus which mediates a hypertensive response.* Brain Research, 1979. **165**(2): p. 295-310.

45. Bayliss, D.A.; Wang, Y.M.; Zahnow, C.A.; Joseph, D.R.; and D.E. Millhorn, *Localization of histidine decarboxylase mRNA in rat brain.* Molecular and Cellular Neuroscience, 1990. **1**(1): p. 3-9.

46. Parmentier, R.; Ohtsu, H.; Djebbara-Hannas Z.; Valatx, J.L; Watanabe, T.; and J.S. Lin, *Anatomical, physiological, and pharmacological characteristics of histidine decarboxylase knock-out mice: evidence for the role of brain histamine in behavioral and sleep–wake control.* The Journal of Neuroscience, 2002. **22**(17): p. 7695-7711.

47. Fujita, A., et al., *Hypothalamic tuberomammillary nucleus neurons: electrophysiological diversity and essential role in arousal stability.* The Journal of Neuroscience, 2017.

48. Evans, M.C. and G.M. Anderson, *Neuroendocrine integration of nutritional signals on reproduction.* Journal of Molecular Endocrinology, 2017. **58**(2): p. R107-R128.

49. Zuure, W.A.; Roberts, A.L.; Quennell, J.H.; and G.M. Anderson, *Leptin signaling in GABA neurons, but not glutamate neurons, is required for reproductive function.* The Journal of Neuroscience, 2013. **33**(45): p. 17874-17883.

50. Evans, M.C.; Rizwan, M.Z.; and G.M. Anderson, *Insulin action on GABA neurons is a critical regulator of energy balance but not fertility in mice.* Endocrinology, 2014. **155**(11): p. 4368-4379.

51. Donato, J., Jr., et al., *Leptin's effect on puberty in mice is relayed by the ventral premammillary nucleus and does not require signaling in Kiss1 neurons.* The Journal of Clinical Investigation, 2011. **121**(1): p. 355-368.

52. Wu, Q.; Whiddon, B.B.; and R.D. Palmiter, *Ablation of neurons expressing agouti-related protein, but not melanin concentrating hormone, in leptin-deficient mice restores metabolic functions and fertility.* Proceedings of the National Academy of Sciences, 2012. **109**(8): p. 3155-3160.

53. Hill, J.W., et al., *Direct insulin and leptin action on pro-opiomelanocortin neurons is required for normal glucose homeostasis and fertility.* Cell Metabolism. **11**(4): p. 286-297.

54. Lerner, A.B. and J.S. McGuire, *Melanocyte-stimulating hormone and adrenocorticotrophic hormone: Their relation to pigmentation.* New England Journal of Medicine, 1964. **270**(11): p. 539-546.

55. Jacobowitz, D.M. and T.L. O'Donohue, *a-Melanocyte stimulating hormone: Immunohistochemical identification and mapping in neurons of the brain.* Proceedings of the National Academy of Sciences of the United States of America, 1978. **75**(12): p. 6300-6304.

56. Poggioli, R.; Vergoni, A.V.; and A. Bertolini, *ACTH-(1-24) and a-MSH antagonize feeding behavior stimulated by kappa opiate agonists.* Peptides, 1986. **7**: p. 843-848.

57. Gonzalez, M.I.; Vaziri, S.; and C.A. Wilson, *Behavioral effects of a-MSH and MCH after central administration in the female rat.* Peptides, 1996. **17**(1): p. 171-177.

58. Hughes, A.M.; Everitt, B.J.; and J. Herbert, *The effects of simultaneous or separate infusions of some pro-opiomelanocortin-derived peptides (B-endorphin, melanocyte stimulating hormone, and corticotrophin-like intermediate peptide) and their acetylated derivatives upon sexual and ingestive behavior.* Neuroscience, 1988. **27**(2): p. 689-698.

59. Rao, T.L.; Kokare, D.M.; Sarkar, S.; Khisti, R.T.; Chopde, C.T.; and N. Subhedar, *GABAergic agents prevent alpha-melanocyte stimulating hormone induced anxiety and anorexia in rats.* Pharmacology, Biochemistry, and Behavior, 2003. **76**(3-4): p. 417-423.

60. Sanchez, M.; Baker, B.I.; and M. Celis, *Melanin-concentrating hormone (MCH) antagonizes the effects of α-MSH and neuropeptide E-I on grooming and locomotor activities in the rat.* Peptides, 1997. **18**(3): p. 393-396.

61. Guy, J.; Vaudry, H.; and G. Pelletier, *Further studies on the identification of neurons containing immunoreactive alpha-melanocyte-stimulating hormone (a-MSH) in the rat brain.* Brain Research, 1982. **239**: p. 265-270.

62. Kiss, J.Z.; Cassell, M.D.; and M. Palkovits, *Analysis of the ACTH/B-END/a-MSH-immunoreactive afferent input to the hypothalamic paraventricular nucleus of the rat.* Brain Research, 1984. **324**: p. 91-99.

63. O'Donohue, T.L. and D.M. Jacobowitz, *Studies of -aMSH-containing nerves in the brain.* Progress in Biochemical Pharmacology, 1980. **16**: p. 69-83.

64. Umegaki, K., et al., *The distribution of aMSH in the CNS of the rat: An immunohistochemical study – I. Forebrain and upper brain stem.* Cellular and Molecular Biology, 1983. **29**(5): p. 377-386.

65. Jacobowitz, D.M. and M. Palkovits, *Topographic atlas of catecholamine and acetylcholinesterase-containing neurons in the rat brain. I. Forebrain (telencephalon, diencephalon).* The Journal of Comparative Neurology, 1974. **157**(1): p. 13-28.

66. König, J.F.R. and R.A. Klippel, *The rat brain : a stereotaxic atlas of the forebrain and lower parts of the brain stem*. 1963, New York: Robert E. Krieger.

67. Pritchard, L.E.; Turnbull, A.V.; and A. White, *Pro-opiomelanocortin processing in the hypothalamus: Impact on melanocortin signalling and obesity.* Journal of Endocrinology, 2002. **172**: p. 411-421.

68. Larsson, L., *Distribution of ACTH-like immunoreactivity in rat brain and gastrointestinal tract.* Histochemistry, 1978. **55**: p. 225-233.

69. Kawai, Y., et al., *The distribution and projection of y-melanocyte stimulating hormone in the rat brain: an immunohistochemical analysis.* Brain Research, 1984. **297**: p. 21-32.

70. Fodor, M., et al., *Distribution of Lys-y_2-melanocyte-stimulating hormone- (Lys-y_2-MSH)-like immunoreactivity in neuronal elements in the brain and peripheral tissues of the rat.* Brain Research, 1996. **731**: p. 182-189.

71. Leger, L., et al., *A monoclonal antibody directed against CLIP (ACTH 18-35). Anatomical distribution of immunoreactivity in the rat brain and hypophysis with quantification of the hypothalamic cell group.* Journal of Chemical Neuroanatomy, 1990. **3**(4): p. 297-308.

72. Watson, S.J.; Barchas, J.D.; and C.H. Li, *B-Lipotropin: Localization of cells and axons in rat brain by immunocytochemistry.* Proceedings of the National Academy of Sciences of the United States of America, 1977. **74**(11): p. 5155-5158.

73. Zakarian, S. and D.G. Smyth, *Distribution of B-endorphin-related peptides in rat pituitary and brain.* The Biochemical Journal, 1982. **202**: p. 561-571.

74. Kiss, J.Z., et al., *Topographical distribution of pro-opiomelanocortin-derived peptides (ACTH/B-END/a-MSH) in the rat median eminence.* Brain Research, 1985. **329**: p. 169-176.

75. Mezey, E.; Kiss, J.Z.; Mueller, G.P.; Eskay, R.; O'Donohue, T.L.; and M. Palkovits, *Distribution of the pro-opiomelanocortin derived peptides, adrenocorticotrope hormone, a-melanocyte-stimulating hormone and b-endorphin in the rat hypothalamus.* Brain Research, 1985. **328**: p. 341-347.

76. Zakarian, S. and D.G., Smyth, *B-endorphin is processed differently in specific regions of rat pituitary and brain.* Nature, 1982. **296**: p. 250-252.

77. Enami, M., *Melanophore-contracting hormone (MCH) of possible hypothalamic origin in the catfish, Parasilurus.* Science, 1955. **121**(3132): p. 36-37.

78. Kawauchi, H.; Kawazoe, I.; Tsubokawa, M.; Kishida, M.; and B.I. Baker, *Characterization of melanin-concentrating hormone in chum salmon pituitaries.* Nature, 1983. **305**(5932): p. 321-3.

79. Qu, D., et al., *A role for melanin-concentrating hormone in the central regulation of feeding behaviour.* Nature, 1996. **380**(6571): p. 243-7.

80. Shi, Y., *Beyond skin color: Emerging roles of melanin-concentrating hormone in energy homeostasis and other physiological functions.* Peptides, 2004. **25**(10): p. 1605-11.

81. Presse, F.; Sorokovksy, I.; Max, J.P.; Nicolaidis, S.; and J.L. Nahon, *Melanin-concentrating hormone is a potent anorectic peptide regulated by food-deprivation and glucopenia in the rat.* Neuroscience, 1996. **71**(3): p. 735-745.

82. Abbott, C.R., et al., *Identification of hypothalamic nuclei involved in the orexigenic effect of melanin-concentrating hormone.* Endocrinology, 2003. **144**(9): p. 3943-9.

83. Kennedy, A.R., et al., *Effect of direct injection of melanin-concentrating hormone into the paraventricular nucleus: Further evidence for a stimulatory role in the adrenal axis via SLC-1.* Journal of Neuroendocrinology, 2003. **15**(3): p. 268-72.

84. Kennedy, A.R., et al., *Melanin-concentrating hormone (MCH) suppresses thyroid stimulating hormone (TSH) release, in vivo and in vitro, via the hypothalamus and the pituitary.* Endocrinology, 2001. **142**(7): p. 3265-8.

85. Verret, L., et al., *A role of melanin-concentrating hormone producing neurons in the central regulation of paradoxical sleep.* BMC Neuroscience, 2003. **4**.

86. Ahnaou, A.; Drinkenburg, W.H.; Bouwknecht, J.A.; Acazar, J.; Steckler, T.; and F.M. Dautzenberg, *Blocking melanin-concentrating hormone MCH1 receptor affects rat sleep-wake architecture.* European Journal of Pharmacology, 2008. **579**(1-3): p. 177-88.

87. Lagos, P.; Torterolo, P.; Jantos, H.; Chase, M.H.; and J.M. Monti, *Effects on sleep of melanin-concentrating hormone (MCH) microinjections into the dorsal raphe nucleus.* Brain Research, 2009. **1265**: p. 103-10.

88. Borowsky, B., et al., *Antidepressant, anxiolytic and anorectic effects of a melanin-concentrating hormone-1 receptor antagonist.* Nature Medicine, 2002. **8**(8): p. 825-30.

89. Monzon, M.E.; Varas, M.M.; and S.R. De Barioglio, *Anxiogenesis induced by nitric oxide synthase inhibition and anxiolytic effect of melanin-concentrating hormone (MCH) in rat brain.* Peptides, 2001. **22**: p. 1043-1047.

90. Adamantidis, A. and L. de Lecea, *A role for melanin-concentrating hormone in learning and memory.* Peptides, 2009. **30**(11): p. 2066-70.

91. Bittencourt, J. and M.E. Celis, *Anatomy, function and regulation of neuropeptide EI (NEI).* Peptides, 2008. **29**(8): p. 1441-50.

92. Bittencourt, J.C. and C.F. Elias, *Melanin-concentrating hormone and neuropeptide EI projections from the lateral hypothalamic area and zona incerta to the medial septal nucleus and spinal cord.* Brain Research, 1998. **805**: p. 1-19.

93. Elias, C.F. and J.C. Bittencourt, *Study of the origins of melanin-concentrating hormone and neuropeptide EI immunoreactive projections to periaqueductal gray matter.* Brain Research, 1997. **755**(255-271).

94. Rossi, M.; Choi, S.J.; O'Shea, D.; Miyoshi, T.; Ghatei, M.A.; and S.R. Bloom, *Melanin-concentrating hormone acutely stimulates feeding, but chronic administration has no effect on body weight.* Endocrinology, 1997. **138**(1): p. 351-355.

95. Shimada, M.; Tritos, N.A.; Lowell, B.B.; Flier, J.S.; and E. Maratos-Flier, *Mice lacking melanin-concentrating hormone are hypophagic and lean.* Nature, 1998. **396**: p. 670-674.

96. Qu, D., et al., *A role for melanin-concentrating hormone in the central regulation of feeding behavior.* Nature, 1996. **380**: p. 243-247.

97. Risold, P.Y.; Fellmann, D.; Rivier, J.; Vale, W.; and C. Bugnon, *Immunoreactivities for antisera to three putative neuropeptides of the rat melanin-concentrating hormone*

precursor are coexpressed in neurons of the rat lateral dorsal hypothalamus. Neuroscience Letters, 1992. **136**: p. 145-149.

98. Bittencourt, J.C., *Anatomical organization of the melanin-concentrating hormone peptide family in the mammalian brain.* General and Comparative Endocrinology, 2011. **172**(2): p. 185-97.

99. Bittencourt, J.C., et al., *The melanin-concentrating hormone system of the rat brain: an immuno- and hybridization histochemical characterization.* The Journal of Comparative Neurology, 1992. **319**(2): p. 218-45.

100. Swanson, L.W.; Sanchez-Watts, G.; and A.G. Watts, *Comparison of melanin-concentrating hormone and hypocretin/orexin mRNA expression patterns in a new parceling scheme of the lateral hypothalamic zone.* Neuroscience Letters, 2005. **387**(2): p. 80-4.

101. Scherer-Singler, U.; Vincent, S.R.; Kimura, H.; and E.G. McGeer, *Demonstration of a unique population of neurons with NADPH-diaphorase histochemistry.* Journal of Neuroscience Methods, 1983. **9**(3): p. 229-34.

102. Vincent, S.R. and H. Kimura, *Histochemical mapping of nitric oxide synthase in the rat brain.* Neuroscience, 1992. **46**(4): p. 755-784.

103. Bredt, D.S.; Hwang, P.M.; and S.H. Snyder, *Localization of nitric oxide synthase indicating a neural role for nitric oxide.* Nature, 1990. **347**(6295): p. 768-770.

104. Paul, V. and P. Ekambaram, *Involvement of nitric oxide in learning & memory processes.* Indian Journal of Medical Research, 2011. **133**: p. 471-8.

105. Gaskin, F.S.; Farr, S.A.; Banks, W.A.; Kumar, V.B.; and J.E. Morley, *Ghrelin-induced feeding is dependent on nitric oxide.* Peptides, 2003. **24**(6): p. 913-918.

106. Calapai, G., et al., *Evidence that nitric oxide modulates drinking behaviour.* Neuropharmacology, 1992. **31**(8): p. 761-764.

107. Morley, J.E.; Farr, S.A.; Sell, R.L.; Hileman, S.M.; and W.A. Banks, *Nitric oxide is a central component in neuropeptide regulation of appetite.* Peptides, 2011. **32**(4): p. 776-780.

108. Farr, S.A.; Banks, W.A.; Kumar, V.B.; and J.E. Morley, *Orexin-A-induced feeding is dependent on nitric oxide*. Peptides, 2005. **26**(5): p. 759-765.

109. Fioramonti, X., et al., *Ventromedial hypothalamic nitric oxide production is necessary for hypoglycemia detection and counterregulation.* Diabetes, 2010. **59**(2): p. 519-528.

110. Nelson, R.J.; Kriegsfeld, L.J.; Dawson, V.L.; and T.M. Dawson, *Effects of nitric oxide on neuroendocrine function and behavior.* Frontiers in Neuroendocrinology, 1997. **18**(4): p. 463-491.

111. Schmidtko, A.; Tegeder, I.; and G. Geisslinger, *No NO, no pain? The role of nitric oxide and cGMP in spinal pain processing.* Trends in Neurosciences, 2009. **32**(6): p. 339-346.

112. Nelson, R.J., et al., *Behavioural abnormalities in male mice lacking neuronal nitric oxide synthase.* Nature, 1995. **378**(6555): p. 383-6.

113. Prast, H. and A. Philippu, *Nitric oxide as modulator of neuronal function.* Progress in Neurobiology, 2001. **64**(1): p. 51-68.

114. Volgushev, M.; Balaban, P.; Chistiakova, M.; and U.T. Eysel, *Retrograde signalling with nitric oxide at neocortical synapses.* European Journal of Neuroscience, 2000. **12**(12): p. 4255-67.

115. Taqatqeh, F.; Mergia, E.; Neitz, A.; Eysel, U.T.; Koesling, D.; and T. Mittmann, *More than a retrograde messenger: nitric oxide needs two cGMP pathways to induce*

hippocampal long-term potentiation. The Journal of Neuroscience, 2009. **29**(29): p. 9344-50.

116. Ng, Y.K.; Xue, Y.D., and P.T. Wong, *Different distributions of nitric oxide synthase-containing neurons in the mouse and rat hypothalamus.* Nitric Oxide, 1999. **3**(5): p. 383-392.

117. de Vente, J.; Hopkins, D.A.; Markerink-Van, I.M.; Emson, P.C.; Schmidt, H.H.; and H.W. Steinbusch, *Distribution of nitric oxide synthase and nitric oxide-receptive, cyclic GMP-producing structures in the rat brain.* Neuroscience, 1998. **87**(1): p. 207-241.

118. Bidmon, H.J.; Wu, J.; Godecke, A.; Schleicher, A.; Mayer, B.; and K. Zilles, *Nitric oxide synthase-expressing neurons are area-specifically distributed within the cerebral cortex of the rat.* Neuroscience, 1997. **81**(2): p. 321-330.

119. Yamada, K.; Emson, P.; and T. Hökfelt, *Immunohistochemical mapping of nitric oxide synthase in the rat hypothalamus and colocalization with neuropeptides.* Journal of Chemical Neuroanatomy, 1996. **10**(3–4): p. 295-316.

120. Iwase, K., et al., *Precise distribution of neuronal nitric oxide synthase mRNA in the rat brain revealed by non-radioisotopic in situ hybridization.* Molecular Brain Research, 1998. **53**(1–2): p. 1-12.

121. Khan, A.M., *Controlling feeding behavior by chemical or gene-directed targeting in the brain: What's so spatial about our methods?* Frontiers in Neuroscience, 2013. **7**: p. 182.

122. Paxinos, G. and C. Watson, *The Rat Brain in Stereotaxic Coordinates*. 4th ed. 1998: Academic Press.

123. Paxinos, G. and C. Watson, *The Rat Brain in Stereotaxic Coordinates*. 5th ed. 2005: Elsevier Academic Press.

124. Khan, A.M.; Ponzio, T.A.; Sanchez-Watts, G.; Stanley, B.G.; Hatton, G.I.; and A.G. Watts, *Catecholaminergic control of mitogen-activated protein kinase signaling in paraventricular neuroendocrine neurons in vivo and in vitro: A proposed role during glycemic challenges.* The Journal of Neuroscience, 2007. **27**(27): p. 7344-60.

125. Khan, A.M.; Walker, E.M.; Dominguez, N.; and A.G. Watts, *Neural input is critical for arcuate hypothalamic neurons to mount intracellular signaling responses to systemic insulin and deoxyglucose challenges in male rats: Implications for communication within feeding and metabolic control networks.* Endocrinology, 2014. **155**(2): p. 405-16.

126. Boyer, P.A.; Trembleau, A.; Leviel, V.; and M. Arluison, *Effects of intranigral injections of colchicine on the expression of some neuropeptides in the rat forebrain: An immunohistochemical and in situ hybridization study.* Brain Research Bulletin, 1994. **33**(5): p. 541-560.

127. Ribak, C.E.; Vaughn, J.E.; and K. Saito, *Immunocytochemical localization of glutamic acid de-carboxylase in neuronal somata following colchicine inhibition of axonal transport.* Brain Research, 1978. **140**: p. 315-332.

128. McGregor, R., et al., *Direct hypothalamic innervation of the trigeminal motor nucleus: A retrograde tracer study.* Neuroscience, 2005. **136**(4): p. 1073-1081.

129. Blasio, A.; Steardo, L.; Sabino, V.; and P. Cottone, *Opioid system in the medial prefrontal cortex mediates binge-like eating.* Addiction Biology, 2014. **19**(4): p. 652-662.

130. Fuxe, K., et al., *Dynamics of volume transmission in the brain. Focus on catecholamine and opioid peptide communication and the role of uncoupling protein 2.* Journal of Neural Transmission, 2005. **112**(1): p. 65-76.

131. Khan, A.M., et al., *Lateral hypothalamic signaling mechanisms underlying feeding stimulation: differential contributions of Src family tyrosine kinases to feeding triggered either by NMDA injection or by food deprivation.* The Journal of Neuroscience, 2004. **24**(47): p. 10603-10615.

132. Khan, A.M., et al., *Lateral hypothalamic NMDA receptor subunits NR2A and/or NR2B mediate eating: Immunochemical/behavioral evidence.* American Journal of Physiology - Regulatory, Integrative and Comparative Physiology, 1999. **276**(3): p. R880-R891.

133. Khan, A.M.; Perez, J.M.; Wells, C.E.; and O. Fuentes, *Computer vision evidence supporting craniometric alignment of rat brain atlases to streamline user-guided, first-order migration of hypothalamic spatial datasets*. Frontiers in Systems Neuroscience, 2017. *submitted*.

134. Rohlf, J. F. and L.F. Marcus, *A revolution in morphometrics.* Trends in Ecology & Evolution, 1993. **8**(4): p. 129-132.

135. Mitteroecker, P. and P. Gunz, *Advances in geometric morphometrics.* Evolutionary Biology, 2009. **36**(2): p. 235-247.

136. Bookstein, F.L.; Sampson, P.D.; Streissguth, A.P.; and Connor, P.D., *Geometric morphometrics of corpus callosum and subcortical structures in the fetal-alcohol-affected brain.* Teratology, 2001. **64**(1): p. 4-32.

137. Slice, D.E., *Geometric morphometrics.* Annual Review of Anthropology, 2007. **36**: p. 261-281.

138. Bookstein, F.L., *Morphometric Tools for Landmark Data: Geometry and Biology*. 1997: Cambridge University Press.

139. Bookstein, F.L., *Landmark methods for forms without landmarks: Morphometrics of group differences in outline shape*. Medical Image Analysis, 1997. **1**(3): p. 225-243.

Appendix

Abbreviations

Structures

3V, third ventricle; aco, anterior commissure, olfactory limb; act, anterior commissure, temporal limb; ADP, anterodorsal preoptic nucleus; AHA, anterior hypothalamic area; AHN; anterior hypothalamic nucleus; AHNa, anterior hypothalamic nucleus, anterior part; AHNc, anterior hypothalamic nucleus, central part; AHNd, anterior hypothalamic nucleus, dorsal part; AHNp, anterior hypothalamic nucleus, posterior part; ARC, arcuate hypothalamic nucleus, Paxinos & Watson nomenclature; ARH, arcuate hypothalamic nucleus; AVP, anteroventral preoptic nucleus; AVPV, anteroventral periventricular nucleus of the hypothalamus; BAC, bed nucleus of the anterior commissure; BST, bed nuclei of the stria terminalis; BSTal, bed nuclei of the stria terminalis, anterior division, anterolateral area; BSTam, bed nuclei of the stria terminalis, anterior division, anteromedial area; BSTdm, bed nuclei of the stria terminalis, anterior division, dorsomedial nucleus; BSTfu, bed nuclei of the stria terminalis, anterior division, fusiform nucleus; BSTif, bed nuclei of the stria terminalis, posterior division, interfascicular nucleus; BSTju, bed nuclei of the stria terminalis, anterior division, juxtacapsular nucleus; BSTmg, bed nuclei of the stria terminalis, anterior division, magnocellular nucleus; BSTov, bed nucleus of the stria terminalis, anterior division, oval nucleus; BSTpr, bed nuclei of the stria terminalis, posterior division, principal nucleus; BSTrh, bed nuclei of the stria terminalis, anterior division, rhomboid nucleus; BSTtr, bed nuclei of the stria terminalis, posterior division, transverse nucleus; BSTv, bed nuclei of the stria terminalis, anterior division, ventral nucleus; CP, caudoputamen; cpd, cerebral peduncle; DMH, dorsomedial hypothalamic nucleus; DMHa, dorsomedial hypothalamic nucleus, anterior part; DMHp, dorsomedial hypothalamic nucleus, posterior part; DMHv, dorsomedial hypothalamic nucleus, ventral part; em, external medullary lamina of the thalamus; fx, columns of the fornix; I, internuclear area, hypothalamic periventricular region; int, internal capsule; LH, lateral habenula, LHA, lateral

hypothalamic area; LHAad, lateral hypothalamic area anterior region, dorsal zone; LHAai, lateral hypothalamic area, anterior region, intermediate zone; LHAav, lateral hypothalamic area, anterior region, ventral zone; LHAd, lateral hypothalamic area, dorsal region; LHAjd, lateral hypothalamic area, juxtadorsomedial region; LHAjp, lateral hypothalamic area, juxtaparaventricular region; LHAjvd, lateral hypothalamic area, juxtaventromedial region, dorsal zone; LHAjvv, lateral hypothalamic area, juxtaventromedial region, ventral zone; LHAm, lateral hypothalamic area, magnocellular nucleus; LHAp, lateral hypothalamic area, posterior region; LHAs, lateral hypothalamic area, suprafornical region; LHAsfa, lateral hypothalamic area, subfornical region, rostral zone; LHAsfpm, lateral hypothalamic area, subfornical region, premammillary zone; LHAvl, lateral hypothalamic area, ventral region, lateral zone; LHAvm, lateral hypothalamic area, ventral region, medial zone; LM, lateral mammillary nucleus; LPO, lateral preoptic area; LV, lateral ventricle; MA, magnocellular nucleus; mct, medial corticohypothalamic tract; ME, median eminence; Mein, median eminence, internal lamina; MEAad, medial amygdalar nucleus, anterodorsal part; MEPO, median preoptic nucleus; mfb, medial forebrain bundle; MM, medial mammillary nucleus, body; MMme, medial mammillary nucleus, median part; mp, mammillary peduncle; MPN, medial preoptic nucleus; MPNc, medial preoptic nucleus, central part; MPNl, median preoptic nucleus, lateral part; MPNm, medial preoptic nucleus, medial part; MPO, medial preoptic area; MS, medial septal nucleus; mtg, mammillotegmental tract; mtt, mammillothalamic tract; NC, nucleus circularis; NDB, diagonal band nucleus; och, optic chiasm; opt, optic tract; OV, vascular organ of the lamina terminalis; PD, posterodorsal preoptic nucleus; PH, posterior hypothalamic nucleus; PMd, dorsal premammillary nucleus; PMv, ventral premammillary nucleus; PS, parastrial nucleus; PSCH, suprachiasmatic preoptic nucleus; PST, preparasubthalamic nucleus; PSTN, parasubthalamic nucleus; PV, periventricular hypothalamic nucleus; PVa, periventricular hypothalamic nucleus, anterior part; PVi, periventricular hypothalamic nucleus, intermediate part; PVp, periventricular hypothalamic nucleus, posterior part; PVpo, preoptic periventricular nucleus; PVH, paraventricular hypothalamic nucleus; PVHam, paraventricular hypothalamic nucleus, anterior

magnocellular part; PVHap, paraventricular hypothalamic nucleus, anterior parvicellular part; PVHdp, paraventricular hypothalamic nucleus, dorsal parvicellular part; PVHf, paraventricular hypothalamic nucleus, forniceal part; PVHlp, paraventricular hypothalamic nucleus, lateral parvicellular part; PVHmpd, paraventricular hypothalamic nucleus, medial parvicellular part, dorsal zone; PVHmpv, paraventricular hypothalamic nucleus, medial parvicellular part, ventral zone; PVHpml, paraventricular hypothalamic nucleus, posterior magnocellular part, lateral zone; PVHpmm, paraventricular hypothalamic nucleus, posterior magnocellular part, medial zone; PVHpv, paraventricular hypothalamic nucleus, periventricular part; RCH, retrochiasmatic area, lateral hypothalamic area; SBPV, subparaventricular zone of the hypothalamus; SCH, suprachiasmatic nucleus; SI, substantia innominata; sm, stria medullaris; smd, supramammillary decussation; SO, supraoptic nucleus, proper; sod, supraoptic decussation, Paxinos & Watson nomenclature; SOr, supraoptic nucleus, retrochiasmatic part; SPFm, subparafascicular nucleus of the thalamus, magnocellular part; st, stria terminalis; STN, subthalamic nucleus; SUM, supramammillary nucleus; SUMl, supramammillary nucleus, lateral part; SUMm, supramammillary nucleus, medial part; sup, supraoptic commissures; TMd, tuberomammillary nucleus, dorsal part; TMv, tuberomammillary nucleus, ventral part; TU, tuberal nuclei; TUi, tuberal nuclei, intermediate part; TUl, tuberal nuclei, lateral part; tuberal nuclei, subventricular part; TUte, tuberal nuclei, terete subnucleus; vlt, ventrolateral hypothalamic tract; VLP, ventrolateral preoptic nucleus; VMH, ventromedial hypothalamic nucleus; VMHc, ventromedial hypothalamic nucleus, central part; VMHdm, ventromedial hypothalamic nucleus, dorsomedial part; VMHvl, ventromedial hypothalamic nucleus, ventrolateral part; ZI, zona incerta; ZIda, zona incerta, dopaminergic group.

Molecular Species

AChE, acetylcholinesterase; ACTH, adrenocorticotropic hormone; AgRP, Agouti gene-related peptide; AROM, antisense RNA overlapping MCH gene; CART, cocaine- and amphetamine-related transcript; CCK, cholecystokinin; cGMP, cyclic guanosine

monophosphate; CLIP, corticotropin-like intermediate peptide; CRH, corticotropin-releasing hormone; β-END, β-endorphin; FSH, follicle-stimulating hormone; GABA, gamma-aminobutyric acid; GH, growth hormone; GHRH growth hormone-releasing hormone; GLP-1, glucagon-like peptide 1; GnRH, gonadotropin-releasing hormone; H/O, hypocretin/orexin; JP, joining peptide; LepR, leptin receptor; LPH, lipotropin; β-LPH, β-lipotropin; γ-LPH, γ-lipotropin; MCH, melanin-concentrating hormone; ppMCH, prepro-melanin-concentrating hormone; MGOP, MCH gene-overprinted polypeptide; MSH, melanocyte-stimulating hormone; α-MSH, α-melanocyte-stimulating hormone; γ-MSH, γ-melanocyte-stimulating hormone; NEI, neuropeptide EI; NGE, neuropeptide GE; NO, nitric oxide; eNOS, endothelial nitric oxide synthase; iNOS, inducible nitric oxide synthase; nNOS, neuronal nitric oxide synthase; NPY, neuropeptide Y; POMC, proopiomelanocortin; PYY, peptide YY; SF-1, steroidogenic factor 1; TRH, thyrotropin-releasing hormone; TSH, thyroid-stimulating hormone.

Miscellaneous

HPA, hypothalamic-pituitary-adrenal axis; HPG, hypothalamic-pituitary-gonadal axis; HPT, hypothalamic-pituitary-thyroid axis; LDP, long-term depression; LTP, long-term potentiation.

Brain Areas Included in Maps

For brain 13-082 (**Figures 2.12–233**), I mapped the hypothalamus, the ZI, the STN, and the PSTN. Steven Michelmann mapped fibers in the hypothalamus and the BST. White matter tracts were not in general mapped but contained little to no staining. For brain K10-053 (**Figures 4.1–4.13**), I mapped the hypothalamus, the BST, the ZI, the STN, the PSTN, and the ME, when it was not damaged during tissue processing. Otherwise white matter tracts were not in general mapped.

Hypothalamic Maps Based on a Different Brain

The maps presented in the Results section of Specific Aim 1 are based on brain 13–082. The following maps are based on brain K10–053 (**Figures 4.1-4.13**), for which a more limited range of tissue was collected. Therefore, only levels that include the LHA (levels 22–34) are represented. The legend is found in the Results section of Specific Aim 1 (**Table 2.2**).

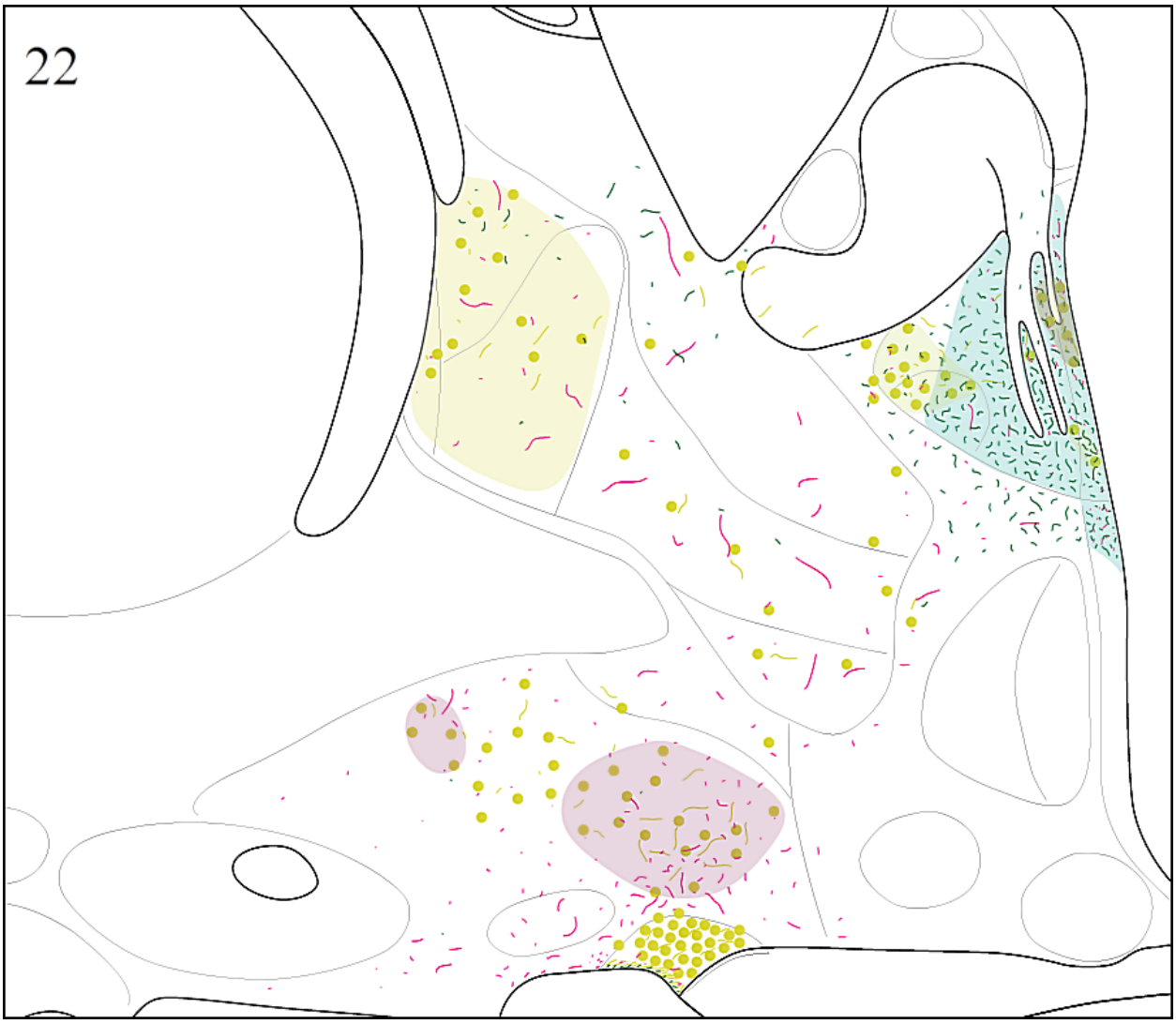

Figure 4.1: Level 22 Maps.

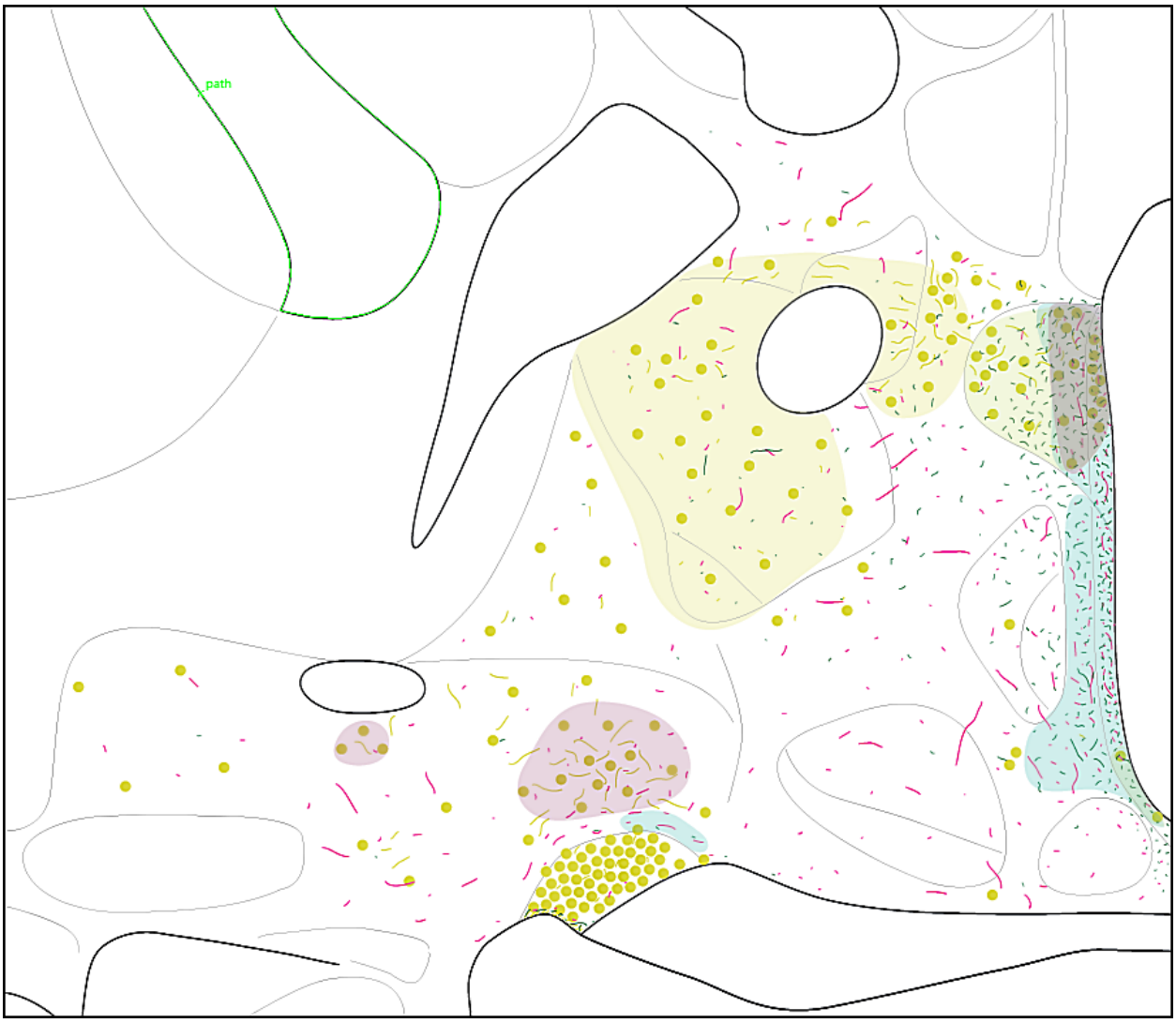

Figure 4.2: Level 23 Maps.

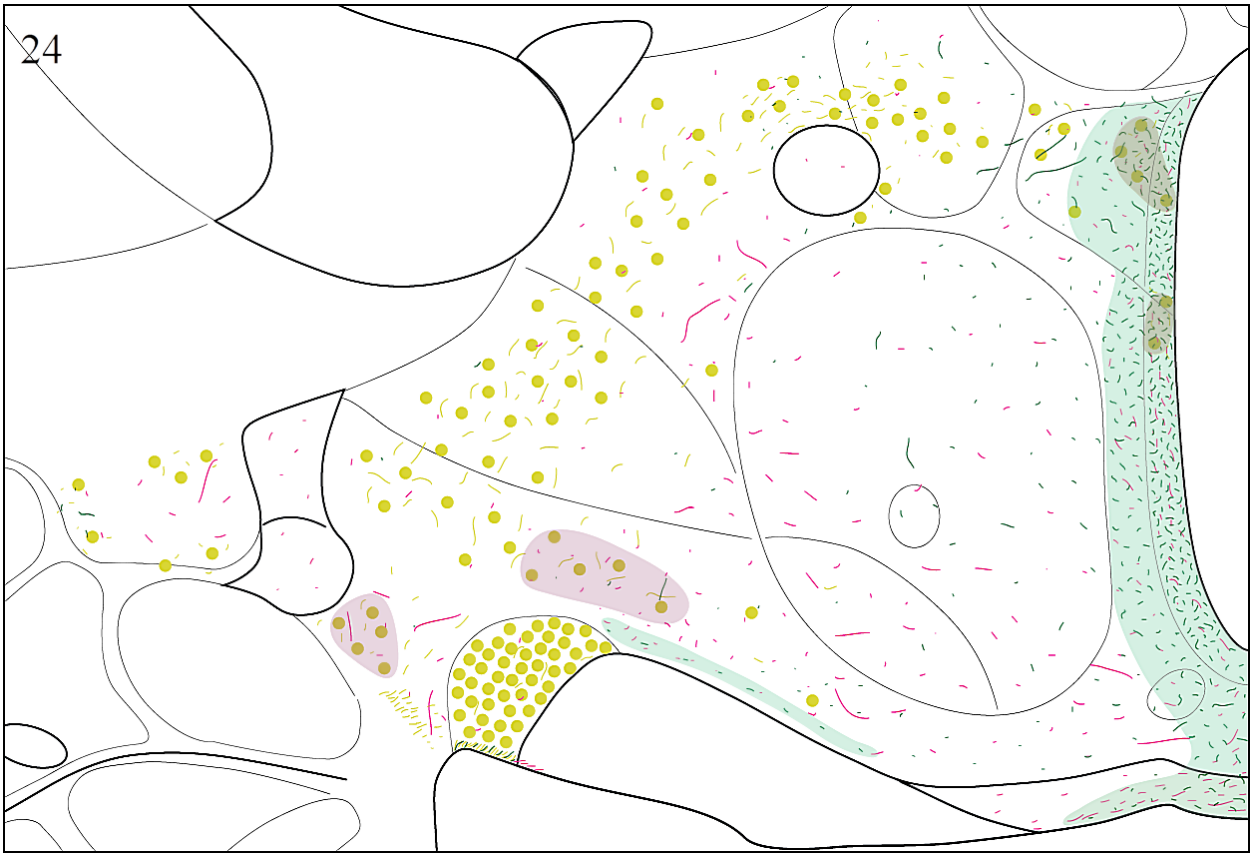

Figure 4.3: Level 24 Maps.

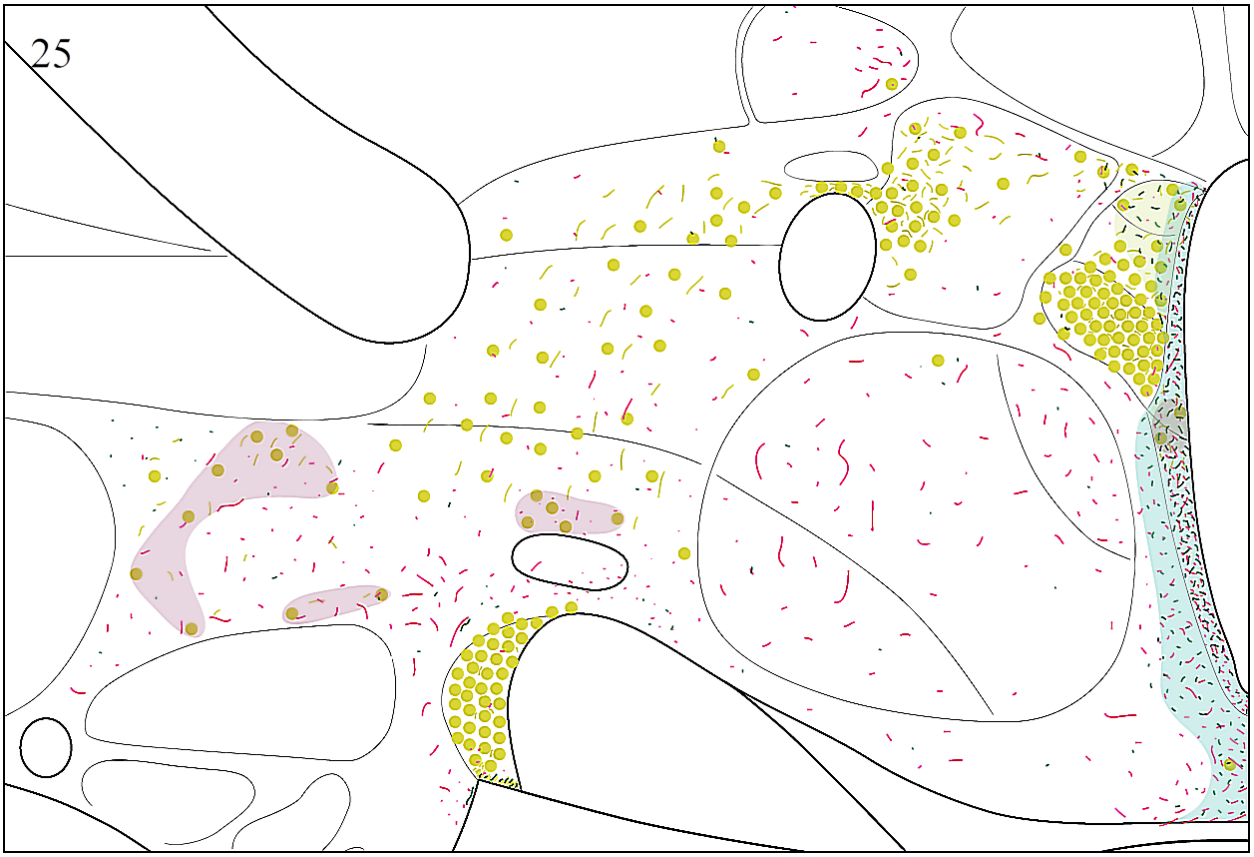

Figure 4.4: Level 25 Maps.

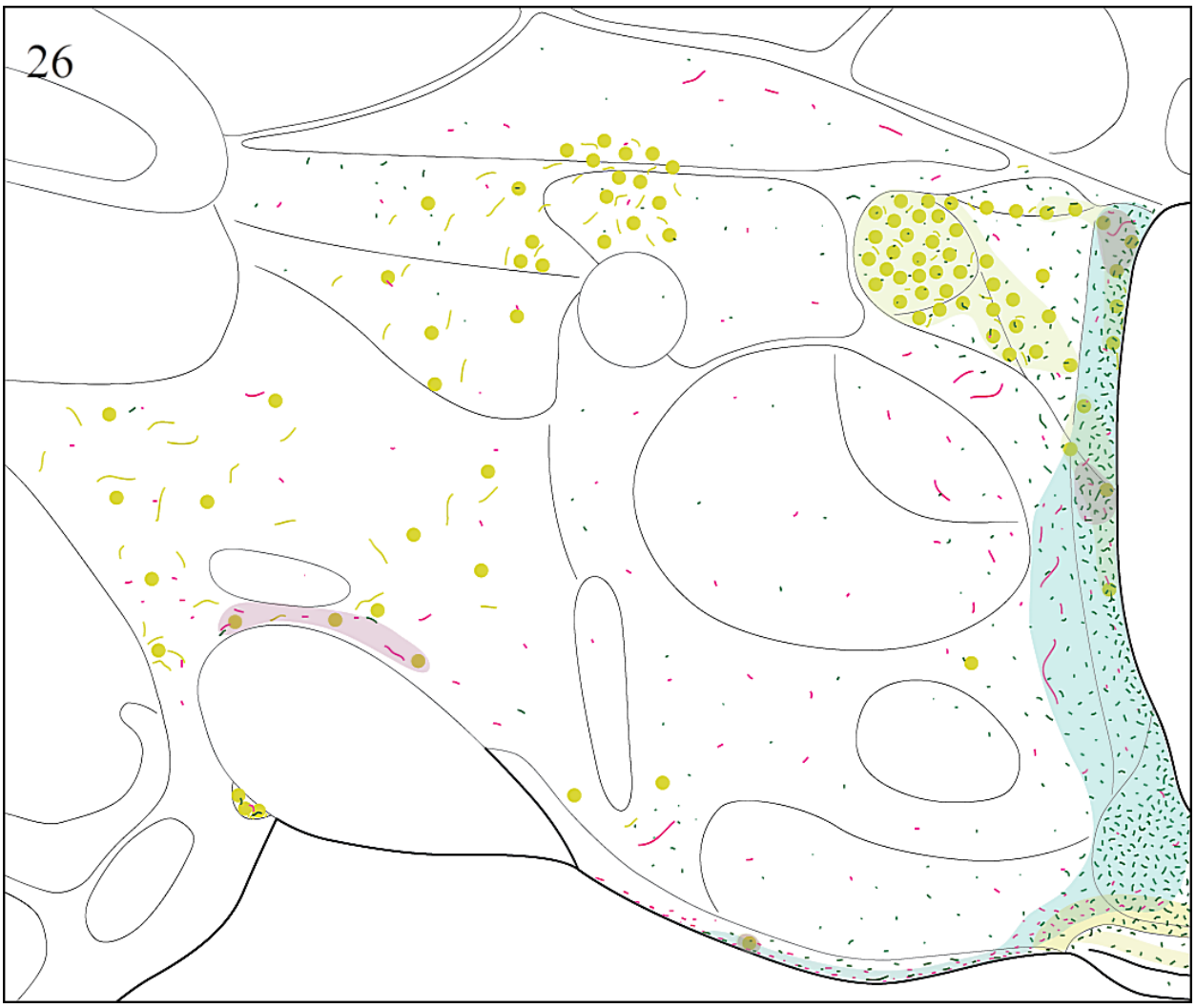

Figure 4.5: Level 26 Maps.

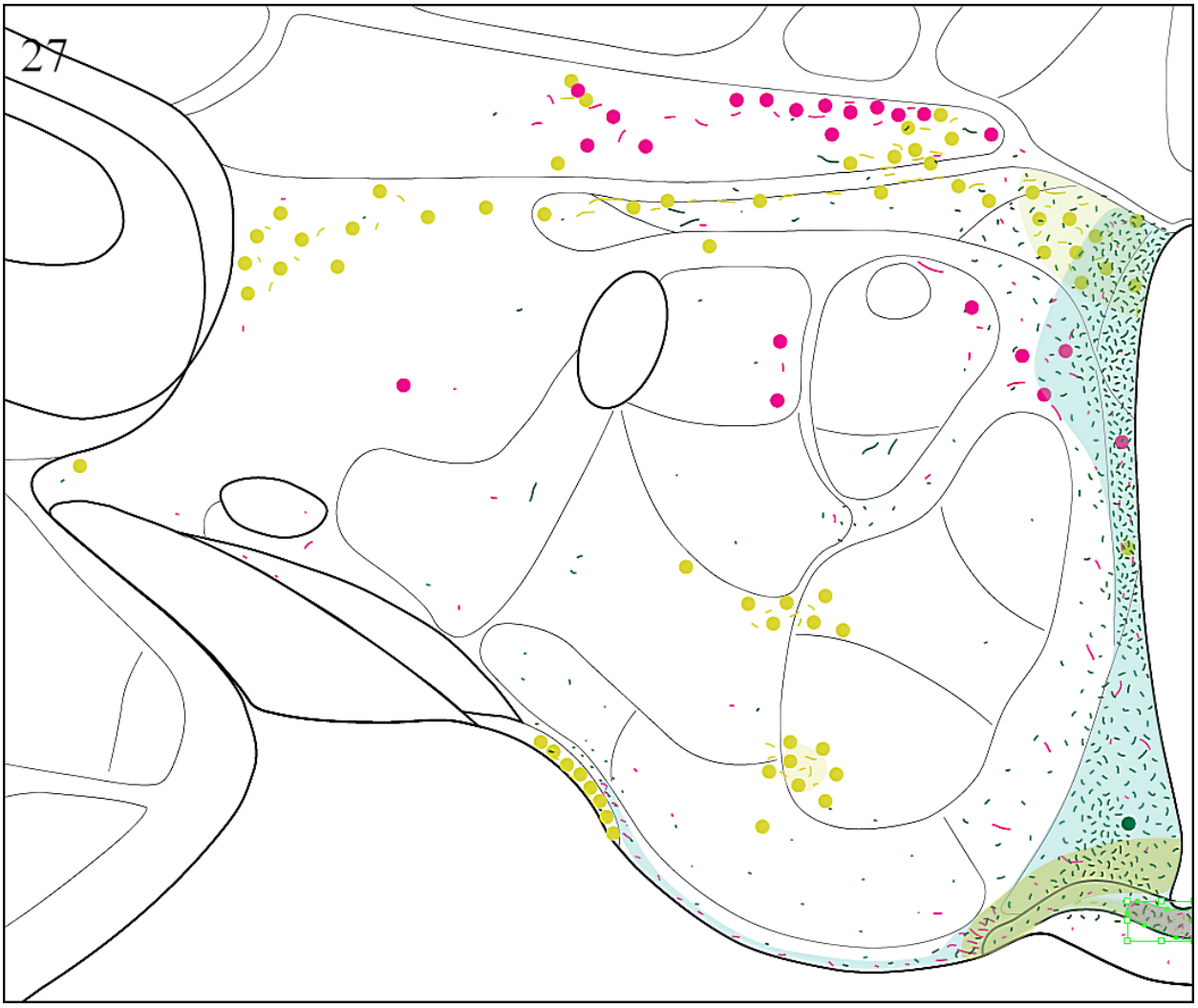

Figure 4.6: Level 27 Maps.

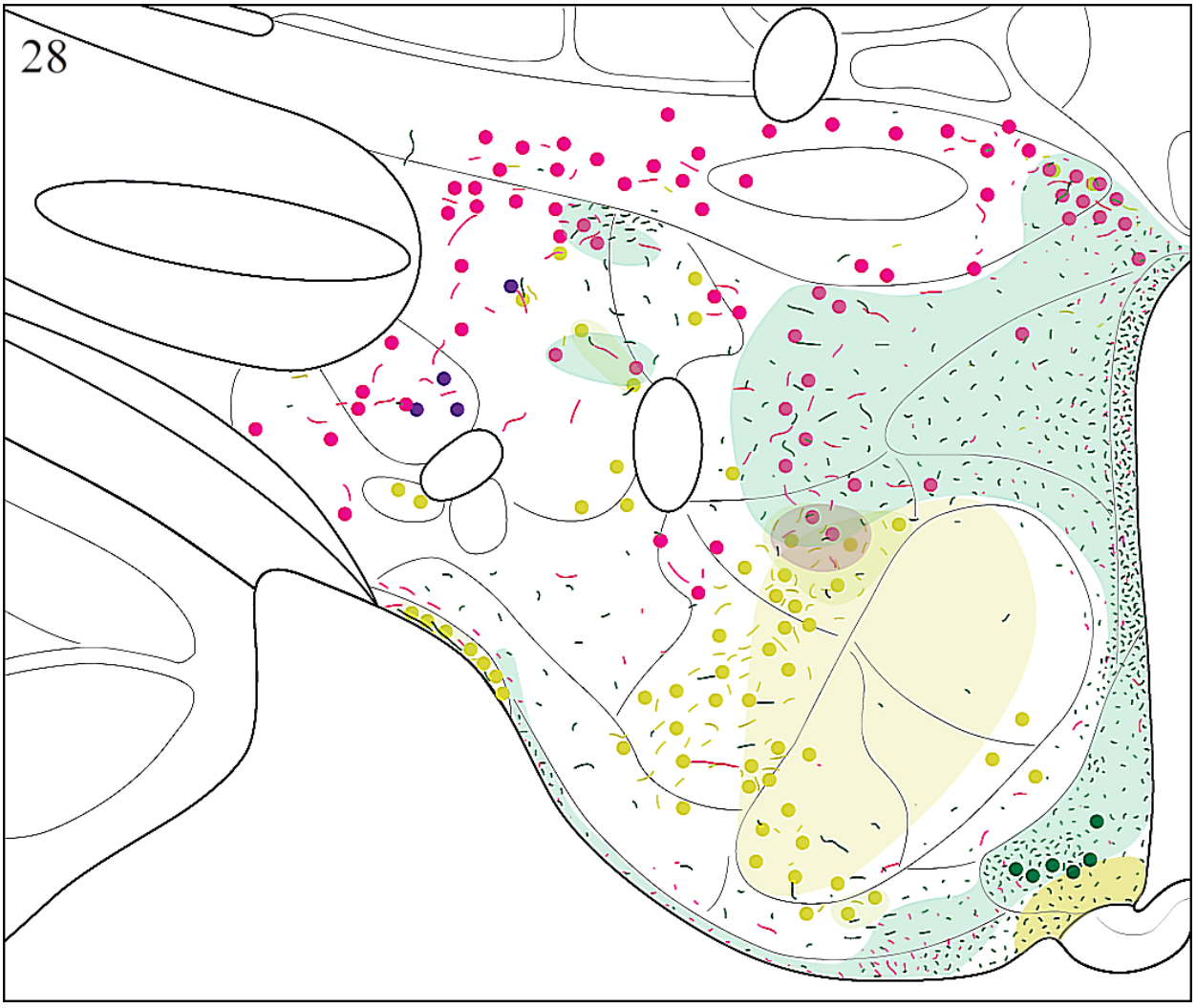

Figure 4.7: Level 28 Maps.

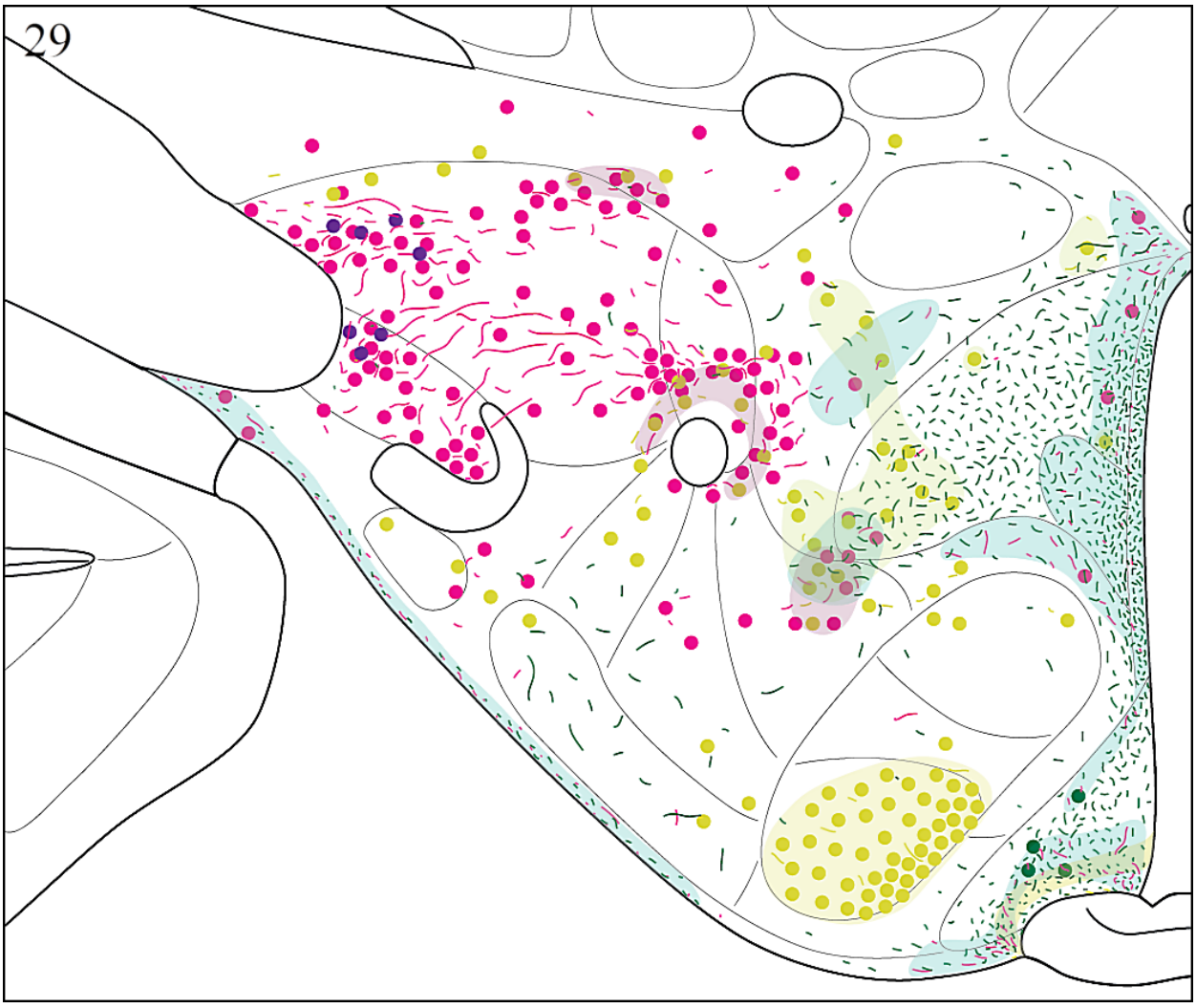

Figure 4.8: Level 29 Maps.

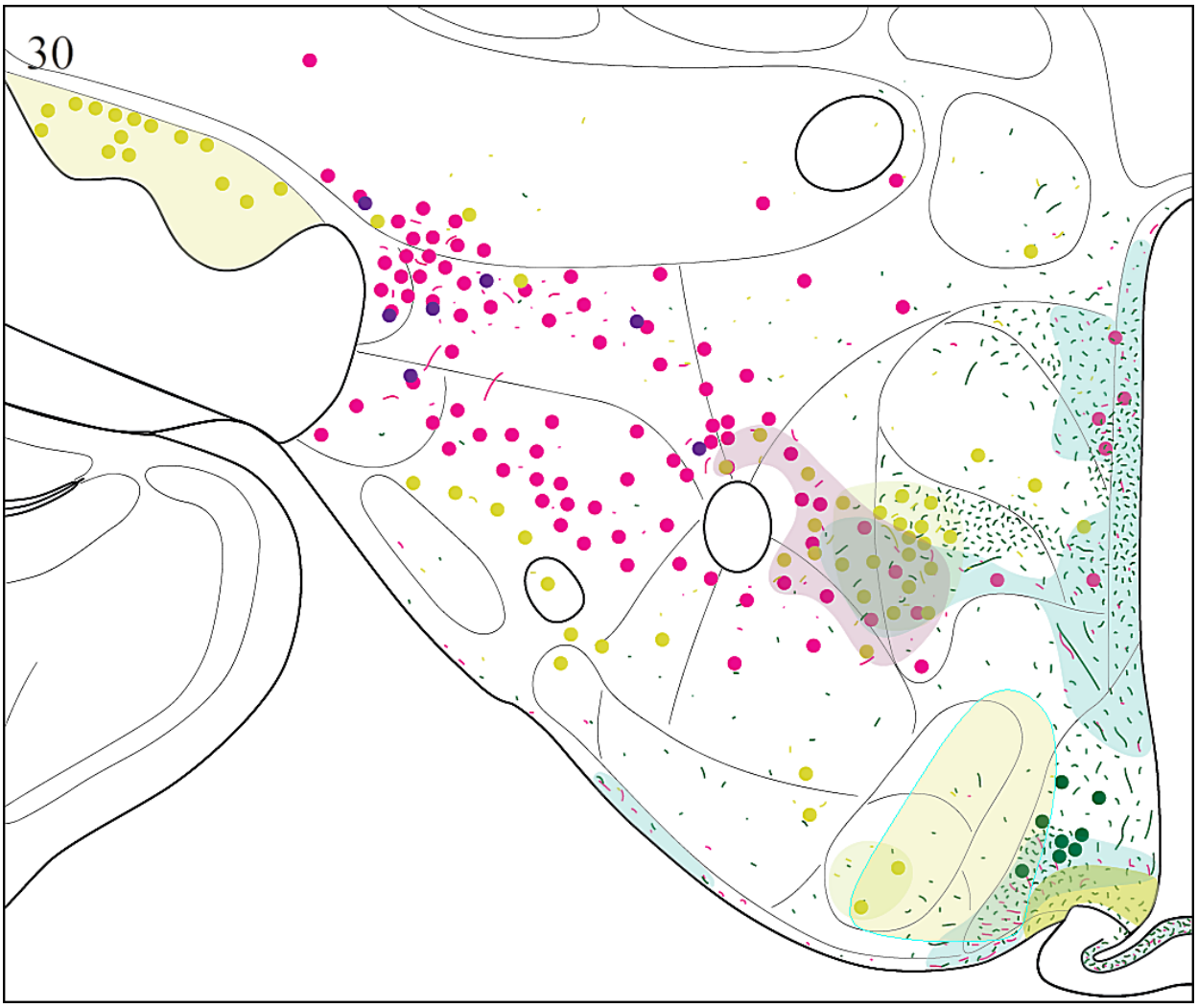

Figure 4.9: Level 30 Maps.

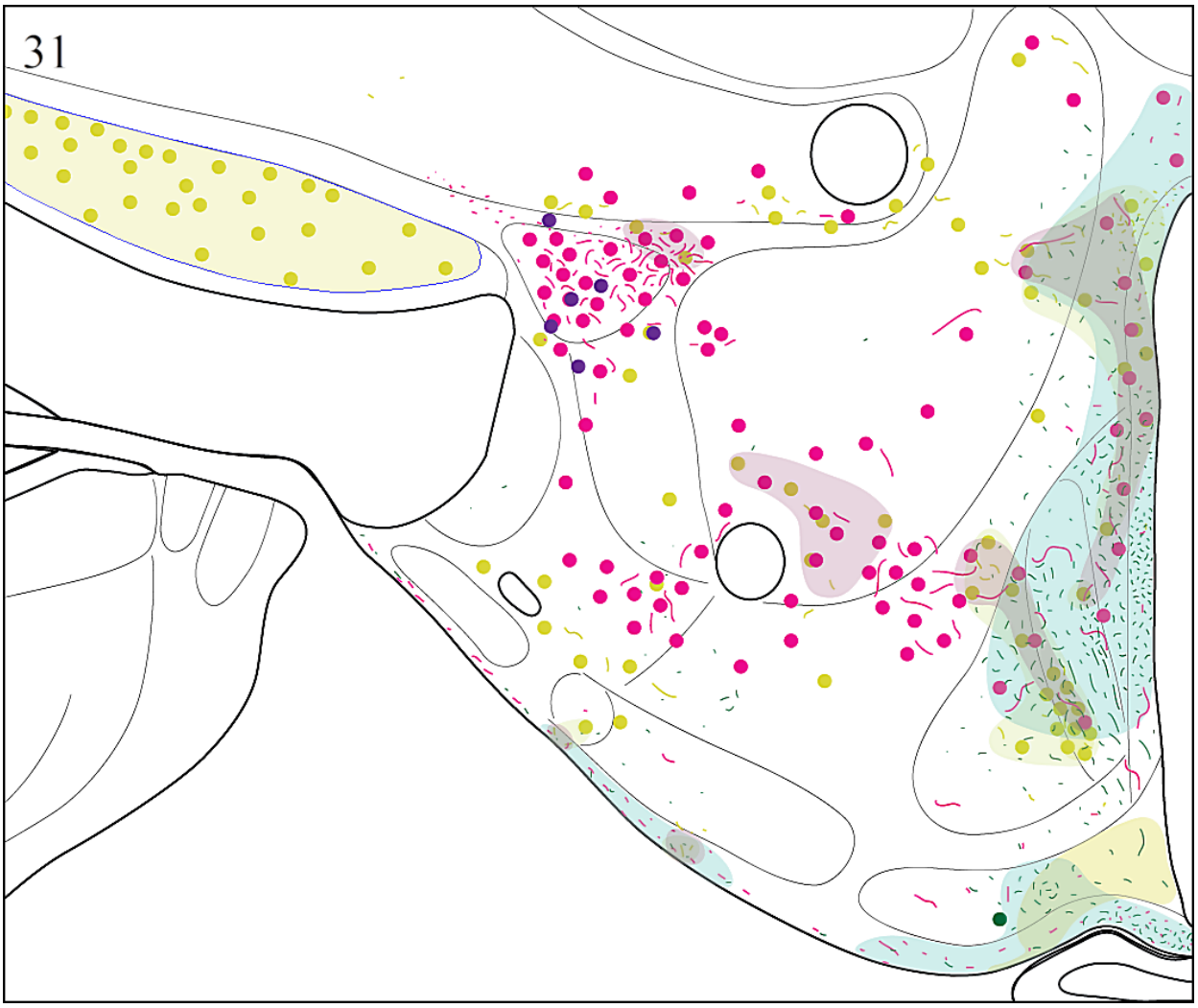

Figure 4.10: Level 31 Maps.

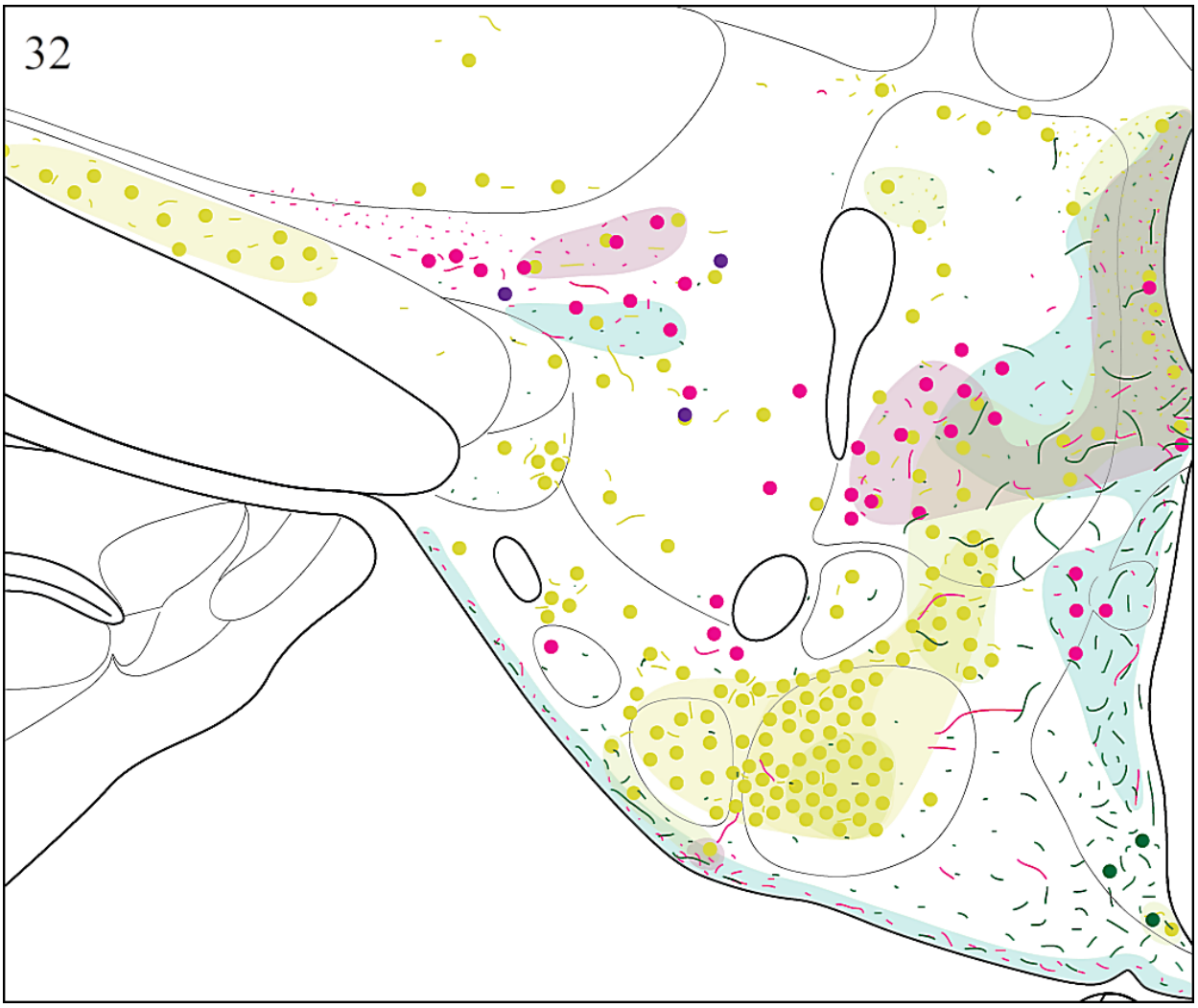

Figure 4.11: Level 32 Maps.

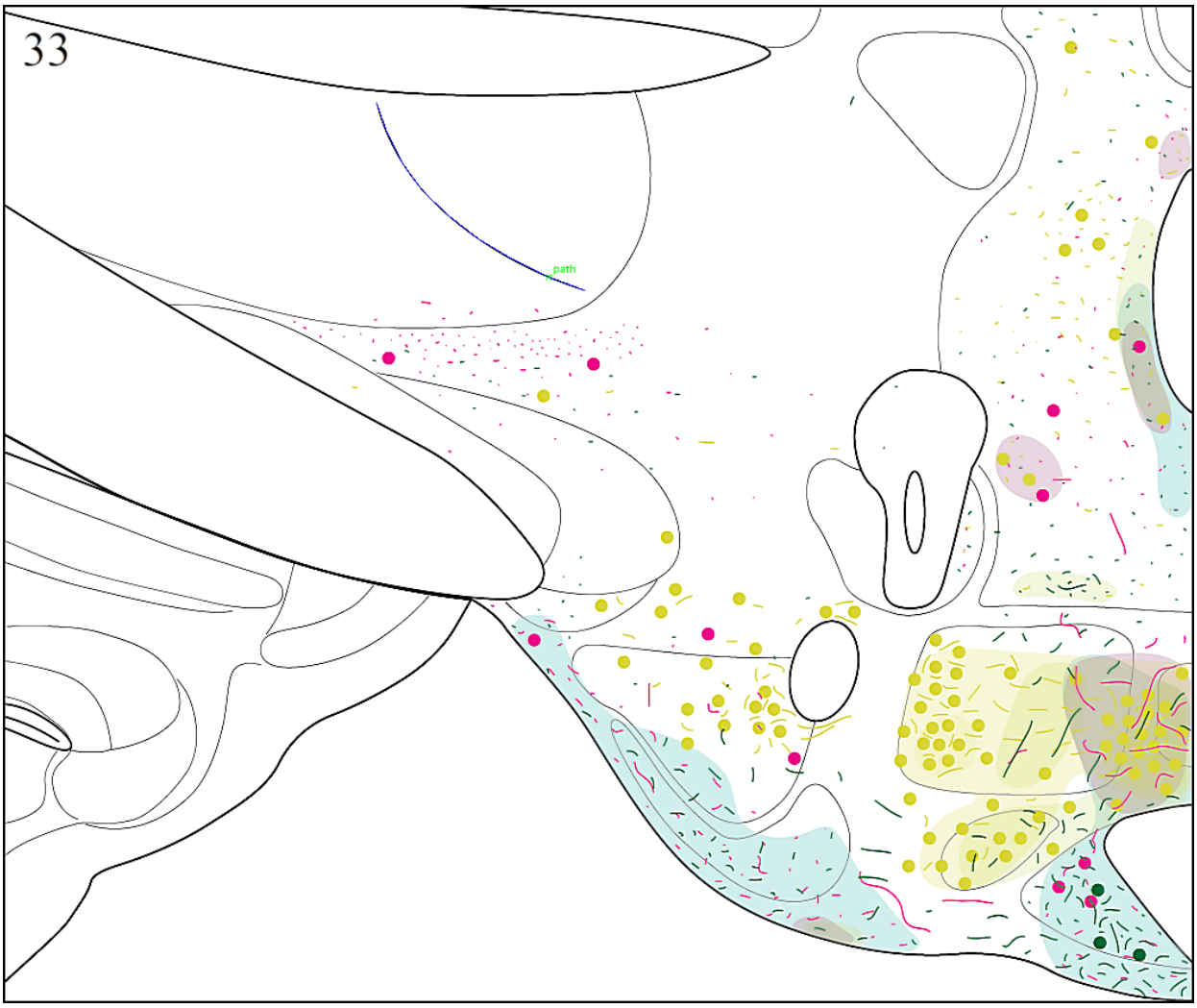

Figure 4.12: Level 33 Maps.

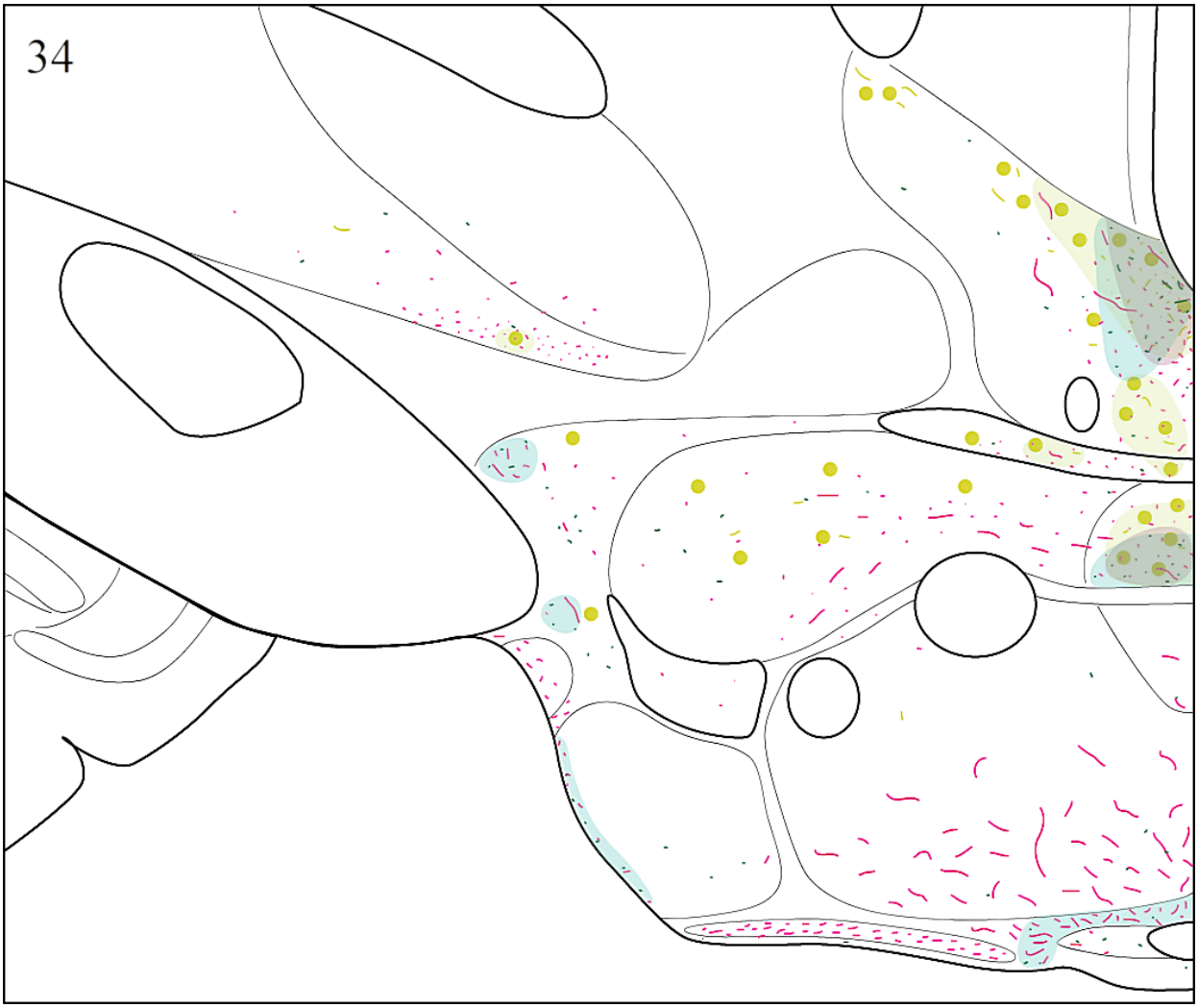

Figure 4.13: Level 34 Maps.

Systematic Comparison of Three Reference Spaces

Table 4.1: Stereotaxic Coordinates of Bounding Points of Corresponding Structures at Corresponding Levels in the Swanson 2004 atlas (S), Paxinos & Watson 1998 atlas (PW1), and Paxinos & Watson 2005 atlas (PW2).

Bounding point abbreviations are: D, most dorsal point; V, most ventral point; L, most lateral point; M, most medial point. Structure abbreviations are not shown. For the dorsal and ventral bounding points, the y-coordinate is shown; for the lateral and medial bounding points, the x-coordinate is shown. The coordinates not shown are available upon request. Some extraneous points were recorded early on (e.g. the aco on S level 1). Points were measured to three decimal places but the third was not significant, due to measurement error. Merged cells are used to indicate correspondence; e.g., the SEZ/RC in S and the E/OV in PW1 are separated into the E and OV in PW2 – the OV is internal to the E. Thus the appropriate cells in the rows for the E and OV are merged for S and PW1, and the bounding points for PW2 appear in the row for the E.

Level			Structure			S Coordinate (mm)				PW1 Coordinate (mm)				PW2 Coordinate (mm)			
S	**PW1**	**PW2**	**S**	**PW1**	**PW2**	**D**	**V**	**L**	**M**	**D**	**V**	**L**	**M**	**D**	**V**	**L**	**M**
1	1	1	MOBgl	G1	G1	1.96	5.73	2.12	0.21	2.06	6.66	2.96	0.24	1.97	6.43	2.10	0.02
			MOBopl	EP1	EP1	2.00	5.70	2.06	0.19	2.21	6.43	2.72	0.41	2.20	6.26	1.90	0.18
			MOBmi	Mi	Mi	2.29	5.40	1.66	0.38	2.38	6.11	2.33	0.71	2.41	6.09	1.60	0.34
			MOBipl	IP1	IP1	2.33	5.37	1.63	0.41	2.49	6.00	2.25	0.80	2.47	6.02	1.55	0.40
			MOBgr	GrO	GrO	2.35	5.35	1.61	0.43	2.87	5.55	1.87	1.14	2.55	5.94	1.50	0.47
			aco	aci		2.77	4.44	1.26	0.86								
			SEZ/RC	E/OV	E	2.80	4.40	1.24	0.88	3.95	5.19	1.68	1.38	3.12	5.26	1.15	0.79
					OV												
				ON													
3	2	3	von	vn		3.17	3.48	0.29	0.03	2.62	3.11	0.48	0.13				
			AOBgl	AOB	EP1A	2.70	3.40	0.87	0.37	2.92	3.70	1.93	1.10	3.38	4.17	1.26	0.65
			AOBmi		MiA	2.82	3.70	1.14	0.58					3.38	4.50	1.44	0.65
			AOBgr	GrA	GrA	3.27	4.15	1.30	0.80	2.36		2.97		3.51	4.85	1.67	0.77
			MOBgr	GrO	GrO	2.89	6.14	1.70	0.47				0.75	3.01	6.25	2.01	0.51
			MOBipl	IP1	IP1	2.82	6.18	1.65	0.45				0.60	2.91	6.29	2.01	0.44
			MOBmi	Mi	Mi	2.79	6.21	1.68	0.41	3.03	6.28	1.76	0.60	2.85	6.33	2.01	0.39
			MOBopl	EP1	EP1	2.61	6.46	1.86	0.14		6.69		0.30	2.57	6.46	2.09	0.19
			MOBgl	G1	G1	3.43	6.52	1.78	0.20	2.37	6.76	2.44	0.12	2.35	6.57	2.13	0.02
			lotd	dlo	dlo	3.08			0.63		5.93	2.76		3.42	4.76	2.01	0.76
			lot	lo	lo		5.84	1.95		3.09			1.33	4.67	5.86	2.06	1.28
			aco	aci	aci		5.75	1.60		3.75	5.48	2.14	1.25	3.73		1.85	
			SEZ/RC	E/OV	E	4.44	5.28	1.26	1.04	4.64	4.88	1.64	1.57	4.69	5.59	1.43	0.83
					OV												
			AONe1	AOE	AOE	3.84	5.62	1.89	1.49	4.02	5.47	2.33	2.11	4.56	5.82	1.96	1.12
			AONe2			3.76	5.61	1.72	1.40								
			AONl1	AOL	AOL	3.83	5.59	1.68	1.35	4.16	5.39	2.10	1.80	4.60	5.57	1.78	1.07
			AONl2			3.83	5.55	1.60	1.27								
				ON													

Level			Structure			S Coordinate (mm)				PW1 Coordinate (mm)				PW2 Coordinate (mm)			
S	**PW1**	**PW2**	**S**	**PW1**	**PW2**	**D**	**V**	**L**	**M**	**D**	**V**	**L**	**M**	**D**	**V**	**L**	**M**
4	4	5	FRP	FrA	FrA	2.15	5.36	3.20	0.11	2.09	4.58	3.49	0.06	1.90	4.81	3.21	0.10
			MOs														
			PL														
			ORBm	MO	MO		5.31		0.13	3.39	4.66	1.07	0.06	3.47	5.34	1.23	0.05
			ORBvl	VO	VO				0.43	3.74	4.76	1.15	0.37	3.83	5.38	1.31	0.35
			ORBl	LO	LO					3.49	4.53	2.53	1.01	3.59	4.81	2.38	1.09
					G1A												
				AOB													
					GrA												
			MOBgl	G1	G1	5.33	6.95	0.78	0.44	4.71	6.48	0.40	0.11	5.33	6.75	0.25	0.05
			MOBopl	EP1	EP1	4.68	7.62	2.77	0.48	4.35	7.11	3.00	0.03	5.51	7.03	2.37	0.03
			MOBmi	Mi	Mi	5.42	7.60	1.43	0.71	5.07	6.81	0.56	0.30	5.56	6.79	0.39	0.16
			MOBipl	IP1	IP1	5.41	7.60	1.52	0.73				0.30	5.59	6.82	0.44	0.19
			MOBgr	GrO	GrO	5.41	7.43	1.34	0.79	4.87	6.81	0.77	0.39	5.27	6.84	0.60	0.20
			AONm	AOM	AOM				1.09				0.78				0.51
			AONd	AOD	AOD	4.97				4.88				5.13			
			AONl	AOL	AOL			2.55				2.72				2.17	
			AONpv	AOV	AOV		7.15				6.83				6.68		
			AONe	AOE	AOE	7.14	7.30	1.64	1.34	4.51	5.26	2.16	0.86	4.90	6.96	1.81	0.60
			lot	lo	lo	4.57	7.54	2.88	1.05	4.43	7.06	3.13	0.92	4.69	7.04	2.46	0.57
			aco	aci	aci	5.62		2.06		5.29	6.42	1.93	0.88	5.55	6.52	1.69	0.53
			SEZ/RC	E/OV	E	6.19	6.65	1.25	1.57	5.91	6.21	1.21	0.91	5.90	6.19	1.17	0.46
					OV												
5	5	6		FrA													
			MOs		M2	1.76		4.39	0.08					1.36	4.18	4.06	0.11
			MOp														
			PL	PrL	PrL	3.61			0.05	2.78	4.01	1.12	0.00	2.60	3.62	1.30	0.00
			ORBm	MO	MO				0.08	3.85	5.53	0.76	0.00	3.58	5.77	1.19	0.00
			ORBvl	VO	VO		6.05		0.26	3.36	5.55	0.36	1.43	3.61	5.77	1.39	0.43
			ORBl	LO	LO					3.13	4.96	2.34	1.12	3.34	5.28	2.79	1.19
				DLO	DLO												
			AId														
			TTd														
			TTv														
			PIR														
				1a													
				1b													
					GrO												
			AONm	AOM	AOM	6.52			0.38		6.81		0.48		6.36		0.33
			AONd	AOD	AOD	5.88	6.30	2.33	1.22	5.10				5.19			
			AONl	AOL	AOL	6.51		2.44				2.85			6.92	2.61	
			AONpv	AOV	AOV P		7.57				7.02		0.67	6.42	6.88	0.95	0.44
			EPd														
			lot	lo	lo	5.48	7.88	2.81	0.88	4.72	7.44	3.27	1.33	4.95	7.22	2.93	1.22
			aco	aci	aci	6.39	7.05	1.75	0.61	5.56	6.70	2.16	0.71	5.82	6.55	1.86	0.42
			SEZ/RC	E/OV	E/OV	6.57	6.84	1.28	0.86	6.05	6.43	1.46	0.96	6.11	6.39	1.34	0.61
6	6	7	MOs	M2	M2	1.20		4.13	0.18	1.03	4.09	4.46	0.00	0.96	3.34	4.42	0.00
			MOp		M1	2.44	5.82	4.71						2.44	3.98	2.01	4.65
			ACAd														
			PL	PrL	PrL					2.31	3.50	1.83	0.00	2.67	4.17	1.51	0.00
			ORBm	MO	MO					3.47	5.34	1.29	0.00	4.13	5.95	0.86	0.00
			ORBvl	VO	VO					3.32	5.64	1.80	0.02	3.13	5.95	1.62	0.30
			ORBl	LO	LO					3.10	5.46	3.56	1.55	3.13	5.60	3.36	1.51
				DLO	DLO					3.28	5.47	4.41	4.41	3.42	5.61	4.40	2.10
					Fr3												

Level			Structure			S Coordinate (mm)				PW1 Coordinate (mm)				PW2 Coordinate (mm)			
S	PW 1	PW 2	S	PW1	PW2	D	V	L	M	D	V	L	M	D	V	L	M
6	6	7	ALd					4.04									
			TTd														
			TTv	VTT	VTT	6.78	7.35	0.82	0.58		7.18	1.16		6.75	7.21	0.93	0.52
			PIR1		Pir1												
			PIR2		Pir2	5.83	7.29	2.84	0.96					5.55	6.94	2.87	1.90
			PIR3														
			AONm	AOM	AOM	6.40	6.99	1.04	0.40				0.40				0.23
				AOD	AOD					5.10				5.46			
				AOL	AOL							3.16			7.08	2.60	1.04
			AONpv	AOV	AOVP	6.73	7.56	1.86	0.79		6.96			6.47	6.88	1.24	0.29
			EPd			6.14	6.92	2.05	1.11								
			lot	lo	lo	6.38	7.88	3.09	1.07	4.77	7.18	3.54	2.13	5.16	7.11	3.23	1.69
			aco	aci	aci	6.35	6.99	1.90	0.75	5.75	6.68	2.17	1.08	6.00	6.62	2.16	0.71
			SEZ/RC	E/OV	E/OV	6.45	6.69	1.32	1.07	6.10	6.30	1.60	1.23	6.22	6.44	1.46	0.80
7	7	8	MOs	M2	M2	0.88		2.97	0.09	0.85	3.23	2.46	0.05	0.73	3.00	2.72	0.19
			MOp	M1	M1	1.17	4.68	5.06		0.94	4.42	4.97	2.04	0.91	3.41	4.80	2.04
			ACAd	Cg1	Cg1	2.00				1.61	3.44	1.70	0.03	1.31	3.17	1.79	0.00
			PL	PrL	PrL					2.60	5.13	1.39	0.03	2.43	4.57	1.60	0.00
			ORBm	MO	MO		5.71			4.60	5.86	0.94	0.03	5.15	6.06	0.88	0.00
			ORBv	VO	VO		5.82	1.34		3.95		2.05		3.89	6.06	1.72	0.36
			ORBvl														
			ORBl	LO	LO			3.55		3.64	5.98	3.83	1.77	3.62	6.18	3.44	1.62
			ILA														
				DTr	DTr												
			AId	AI	Aid		6.50	4.24		3.64	6.00	4.91	2.25	3.37	5.80	4.50	2.21
					Aiv									3.53	6.18	3.88	2.17
					Fr3												
			GU														
			CLA	Cl	Cl	3.33	5.00	0.85	2.64	3.61	4.73	2.25	0.94	3.36	4.98	2.28	0.74
				fmi	fmi					3.18	4.73	2.38	0.93	2.96	4.53	2.26	0.87
			TTd1	DTT1	DTT1			0.79	0.05				0.03	6.20	6.99	0.34	0.00
			TTd2	DTT2	DTT2	5.72	6.21	0.98	0.29	5.98	6.61	0.83	0.23	6.27	6.80	0.46	0.17
			TTd3	DTT3	DTT3	5.82	6.14	1.16	0.41	5.98	6.51	1.31	0.40	6.30	6.75		0.27
			TTd4		DTT4	6.08	6.32	1.32	0.83							0.90	
			TTv1	VTT1	VTT1									7.14			0.26
			TTv2	VTT2	VTT2	6.62	7.41	0.93	0.50	6.82	7.66	1.39	0.45	7.07	7.76	1.19	0.43
			TTv3	VTT3	VTT3	6.63	7.12	0.98	0.60		7.50	1.39		7.09	7.50	1.04	0.60
			PIR1	Pir1	Pir1a			4.74		5.12			3.80				
					Pir1b									5.50		3.34	
			PIR2	Pir2	Pir2	5.51	7.41	2.99	0.99	5.55	7.30	3.51	1.27	5.86	7.27	3.01	1.13
			PIR3	Pir3	Pir3						7.10	3.22		5.95	6.65	2.82	1.10
			AONm	AOM		6.20	6.75	0.99	0.40	6.41	6.91		0.45				
					AOL												
			AONpv	AOV	AOVP	6.47	7.51	1.47	0.96	6.55	7.31	2.14	0.99	6.50	7.23	1.26	0.29
			EPd	DEn	DEn	6.06	6.98	2.16	1.16	5.99	6.71	2.48	1.05	6.07			0.72
					IEn										6.82	2.13	
			lot	lo	lo	6.54	7.79	3.29	0.70	5.73	7.79	3.89	1.87	6.24	7.50	3.36	2.12
			aco	aci	aca	6.15	6.86	1.87	0.42	6.17	6.66	2.08	1.25	6.31	6.70	1.79	1.05
			SEZ/RC	E/OV	E/OV	6.23	6.39	1.38	1.08	6.25	6.41	1.66	1.22	6.36	6.52	1.37	0.89
			MOs	M2	M2	0.65		3.00		0.63	3.34	2.05	0.00	0.68	2.81	2.22	0.24
8	8	9	MOp	M1	M1	1.00	3.46	5.39		0.64	4.77	5.31	1.85	0.72	3.82	5.21	1.85
			ACAd	Cg1	Cg1					1.31	3.51	1.81	0.00	1.34	3.00	0.00	1.66
			PL	PrL	Prl					2.62	4.54	1.56	0.00	2.59	4.73	1.53	0.00

Level			Structure			S Coordinate (mm)				PW1 Coordinate (mm)				PW2 Coordinate (mm)			
S	**PW 1**	**PW2**	**S**	**PW1**	**PW2**	**D**	**V**	**L**	**M**	**D**	**V**	**L**	**M**	**D**	**V**	**L**	**M**
8	8	9	ILA	IL	IL					4.54	5.69	1.21	0.00	4.72	5.43	0.99	0.01
				DP	DP					5.69	6.27	1.21	0.00	5.42	6.10	0.86	0.02
					DTr												
			ORBv	VO	VO		6.33	1.99	1.11	4.34			1.21	4.29		0.81	
			ORBvl	IL	IL	4.43				4.54	5.69	1.21	0.00	4.72	5.43	0.99	0.01
			ORBl	LO	LO					4.19	6.40	4.32	2.50	4.12	6.42	4.02	1.91
			AId	AID	AID		6.77	4.62		3.87	5.58	5.17	2.66	3.78	5.96	4.97	2.56
				AIV	AIV					4.06	6.38	4.90	2.69	4.03	6.39	4.42	2.51
					Fr3												
			GU														
			SSP														
			CLA	Cl	Cl	3.77	5.50	3.57	1.11	3.83	5.07	2.73	1.34	3.75	5.33	2.63	0.87
			fa	fmi	fmi	3.27	4.32	2.58	1.32	3.27	5.67	2.43	1.21	2.77	4.76	2.50	0.99
			TTd1	DTT1	DTT1					6.23			0.00	6.08	7.00	0.63	0.01
			TTd2	DTT2	DTT2	5.82	6.30	0.70	0.18	6.27	6.84	0.45	0.21	6.10	6.89	0.68	0.22
			TTd3	DTT3	DTT3	5.51	6.18	1.09	0.40	6.27			0.29	6.10	6.80		0.35
			TTd4		DTT4	5.51	6.14	1.23	0.89							1.18	
			TTv1	VTT1	VTT1									6.80			0.05
			TTv2	VTT2	VTT2	6.48	7.57	1.02	0.25	6.91	7.49	0.44	0.28	6.77	7.60	1.11	0.41
			TTv3	VTT3	VTT3				0.33					6.93	7.39	0.97	0.59
			PIR1	Pir1	Pir1			3.75				4.25				3.78	
			PIR2	Pir2	Pir2	6.41	7.65	3.48	1.25	6.16	7.61	4.00	2.19	6.04	7.49	3.54	1.86
			PIR3	Pir3	Pir3			3.28				3.87		6.07	7.40	3.37	1.91
				Tu													
			AONm														
			AONpv	AOP	AOP	6.19	7.34	1.63	0.91	6.51	7.74	2.20	0.44		7.61	1.99	
			PIR3	Pir3	AOVP			3.28				3.87		6.47			0.55
			EPd	DEn	DEn	6.19	7.18	2.41	1.48	6.17	7.01	2.72	1.20	6.20			1.12
			AONm		IEn										7.00	2.44	
			lot	lo	lo	7.34	8.08	3.51	1.13	6.98	8.01	3.98	2.50	6.93	7.72	3.66	2.46
			aco	aca	aca	6.12	6.95	1.95	0.90	6.35	6.91	2.24	1.44	6.44	6.90	2.08	1.42
			SEZ/RC	E/OV	E/OV	6.09	6.31	1.46	1.21	6.33	6.52	1.61	1.21	6.38	6.50	1.55	1.16
			MOs	M2	M2	0.57		1.65	0.06	0.53	3.27	1.87	0.00	0.57	2.82	1.89	0.53
			MOp	M1	M1	0.59		5.51	1.65	0.53	3.71	5.21	1.53	579.00	3.17	4.07	1.78
			ACAd	Cg1	Cg1	1.64			0.04	1.35	3.53	1.66	–0.01	0.93	2.93	1.77	0.00
			PL	PrL	PrL	3.31			0.03	3.01	4.59	1.49	–0.01	2.50	4.62	1.56	0.00
9	9	11	ILA	IL	IL		5.87		0.04	4.59	5.45	1.23	0.00	4.46	5.49	1.11	0.00
				DP	DP					5.44	6.08	1.07	0.00	5.30	6.16	1.01	0.00
			ORBv	VO	VO	5.22			1.04	4.86			2.06	5.04	6.52	3.20	0.84
			ORBvl	PrL	PrL					3.01	4.59	1.49	–0.01	2.50	4.62	1.56	0.00
				LO	LO					4.68	6.72	4.46	2.25	4.75	6.44	3.48	1.77
			AId	AID	AID		7.10	5.01		4.27	6.40	5.39	2.81	4.58	6.48	4.99	2.84
			AIv	AIV	AIV		7.12	4.23		4.46	6.72	4.97	2.57	4.68	6.71	4.49	2.73
				GI													
					DI												
			GU														
			SSp	S1J	S1J	2.95	5.84	5.73		2.51	5.44	5.72	2.77	1.65	5.18	5.45	2.65
					Fr3												
			CLA	Cl	Cl	4.21	6.65	3.79	1.58	4.20	6.03	2.84	1.51	4.34	5.74	2.92	1.23
					cg												
			fa	fmi	fmi	2.91	5.47	3.42	1.12	3.14	6.73	2.87	0.50	2.82	6.48	2.89	0.84
			TTd1		DTT1			0.55	0.03	6.06			0.00	6.13	6.88	0.34	0.00
			TTd2	DTT	DTT2	5.81	6.47	0.64	0.29	6.09	6.84	0.41	0.17	6.10	6.79	0.43	0.30
			TTd3		DTT3	5.89	6.41		0.52	6.07		0.82		5.90	6.90	0.93	0.43

Level			Structure			S Coordinate (mm)				PW1 Coordinate (mm)				PW2 Coordinate (mm)			
S	PW1	PW2	S	PW1	PW2	D	V	L	M	D	V	L	M	D	V	L	M
9	9	11	TTd4					1.03									
					Nv												
			TTv1														
			TTv2														
			TTv3														
					VP												
			OT1	TuPl	Tu1		8.55	1.99	0.48		8.59			7.73	8.20	2.91	
			OT2	TuDC	Tu2	7.77	8.44	1.77	0.77	7.78	8.57	2.75	0.58	7.68	8.12	2.63	0.86
			OT3	TuPo	Tu3	7.34	8.37	1.93	0.76		8.48	2.62	0.76	7.53	8.01	2.54	
			PIR1	Pir1	Pir1	7.29	7.47		1.82			4.54	2.42	6.37	7.97	4.21	2.63
			PIR2	Pir2	Pir2	6.73	8.01	3.67	1.81	6.60	7.92	4.27	2.34	6.65	7.73	3.99	2.54
			PIR3		Pir3		7.79	3.38	1.73			4.11		6.40	7.68	3.87	2.22
				mfba													
				ICj													
			AONpv	AOP	AOP	6.34	7.32	1.60	0.55	6.89	7.73	2.18	0.51	6.48	7.46	1.91	0.57
				SL													
			EPd	DEn	DEn	5.66	7.43	2.59	1.49	6.78	7.49	2.76	1.73	5.87		2.70	1.25
					IEn										7.45	2.70	
			ACB	AcbSh	AcbSh	5.81	6.76	1.86	1.09	5.77	7.50	1.96	0.68	6.07	7.14	1.73	0.92
				AcbC	AcbC					6.29	7.49	2.26	1.52	6.34	7.12	2.00	1.52
			lot	lo	lo	7.76	8.53	3.64	1.66	7.38	8.22	4.07	3.03	7.32	8.11	3.90	2.76
			aco	aca	aca	5.50	7.37	2.47	0.88	6.75	7.49	2.44	1.71	6.64	7.18	2.17	1.63
			SEZ/RC	E/OV	E/OV	5.67	6.26	1.45	1.04	5.61	6.18	1.43	0.96	5.86	6.20	1.41	1.05
10	10	13	MOs	M2	M2	0.36		2.04	0.05	0.35	3.03	1.89	0.01	0.37	2.70	1.81	0.21
			MOp	M1	M1	0.40				0.35	3.41	4.86	1.55	0.38	3.13	4.19	1.81
			ACAd	Cg1	Cg1				0.05	1.41	3.20	1.72	0.01	0.88	2.94	1.61	0.00
			PL	PL	PL				0.05	2.71	4.33	1.60	0.01	2.47	4.36	1.50	0.00
			ILA	IL	IL				0.06	4.30	5.11	1.11	0.01	4.12	5.30	0.88	0.00
				DP	DP					5.10	5.68	1.08	0.03	5.12	5.75	0.85	0.00
				VO	LO					5.48	6.80	4.93	3.06	5.81	6.98	3.44	2.16
			AId	AID	AID		7.00	5.16		5.07	6.40	5.69	3.55	5.31	6.88	5.02	3.16
			AIv	AIV	AIV		7.31			5.23	6.84	5.42	3.34	5.51	7.05	4.58	2.62
					DI												
				GI	GI					4.73	5.89	5.86	3.66	5.00	5.78	5.72	3.44
			GU														
			SSp	S1J	S1J	1.12	5.51	6.00		1.67	5.20	6.07	3.04		5.11	5.86	
					S1DZ												
					S1FL									1.23			2.75
			CLA	Cl	Cl	4.68	6.37	4.28	2.72	4.73	6.19	3.75	2.76	4.99	6.28	3.46	2.03
			fa	fmi	fmi				0.91	2.94	6.05	3.71	1.07	2.60	6.10	3.33	0.77
			cg		cg		4.05		0.91					2.59	4.66	1.85	0.76
			SEZ	E	E	3.10	5.30	2.60	0.94	4.73	5.97	1.41	0.92	3.94	5.85	1.76	0.83
			CP	CPu	CPu	3.10	6.11	3.66	1.17	3.87	7.20	2.96	1.01	3.71	6.21	2.72	1.00
			TTd1	DTT1	DTT1			0.43		5.66	6.39	0.42	0.01	5.69	6.44	0.15	0.00
			TTd2	DTT2	DTT2	5.29	6.02	0.56	0.27	5.66	6.38	0.47	0.24	5.71	6.44	0.27	0.11
			TTd3	DTT3	DTT3		6.08		0.30	5.66	6.42	0.91	0.42	5.59	6.42	0.81	0.22
			TTd4			5.15		0.89									
			SH	SHi		6.01	6.24	0.44	0.23	6.33	6.80	0.37	0.14				
				SL													
					Nv												
			LSr														
			OT1	Tu1	Tu1	6.47	8.57		0.21	7.54	8.88	3.31	0.19	7.33	8.56	2.90	0.20
			OT2	Tu2	Tu2	6.43	8.49	2.34	0.32	7.64	8.73	3.10	0.31	7.73	8.36	2.85	0.59

Level			Structure			S Coordinate (mm)				PW1 Coordinate (mm)				PW2 Coordinate (mm)			
S	PW1	PW2	S	PW1	PW2	D	V	L	M	D	V	L	M	D	V	L	M
10	10	13	OT3	Tu3	Tu3	6.46	8.31		0.41		8.61	3.00		7.22	8.19	2.75	0.33
			isl	ICj	ICj	7.47	8.08	1.67	0.81	7.87	8.45	1.11	0.58	7.19	7.77	0.62	0.18
				VP	VP					7.97	8.27	2.40	1.14	7.84	8.03	2.43	1.61
			SI														
			PIR1	Pir1	Pir1			4.33		6.71	8.45	5.02	3.10	6.91	8.21	4.39	2.84
			PIR2	Pir2	Pir2	6.99	8.01	3.97	2.28	6.86	8.17	4.77	3.00	6.98	8.02	4.13	2.75
			PIR3	Pir3	Pir3	6.75		3.80	1.79	6.23	8.12	4.66	2.61	6.36	7.94	4.00	2.10
			lot	lo	lo	7.84	8.50	3.68	2.18	7.63	8.26	4.42	3.60	7.74	8.26	4.04	2.96
			ccr	rcc			7.42	1.03	0.57		6.71		0.53				
			ACB	AcbSh	AcbSh	4.73	7.62	2.64	0.63				0.56	5.94	7.79	2.31	0.50
				AcbC	AcbC					5.89		2.75		5.74	7.35	2.27	0.83
			aco	aca	aca	6.62	7.07	2.22	1.68	6.87	7.56	2.63	2.00	6.79	7.26	2.20	1.61
				LSS													
			ec														
			EPd	DEn	DEn	6.27	7.75	3.09	1.64	6.15	7.98	3.50	2.38	6.59		2.88	
					IEn										7.74		1.93
14	13	20	IG	IG	IG	3.17	3.25	0.44	0.19	2.37	5.66	0.39	0.01	3.86	3.92	0.21	0.07
			ACAv	Cg2	Cg2		3.26		0.00	2.49	3.94	1.22	0.01	2.07		1.44	0.00
			ACAd	Cg1	Cg1	1.58			0.03	1.30	3.04	1.47	0.01	0.76	2.73	1.57	0.00
			MOs	M2	M2	0.16		1.52	0.03	0.23	2.71	1.67	0.01	0.59	2.71	2.05	0.63
			MOp	M1	M1			3.41	1.52	0.24	2.93	3.66	1.54	0.61	3.01	3.36	1.87
			SSp	S1FL	S1FL	0.51	5.61	6.52		0.70	3.21	4.31	2.81	0.89	3.52	5.14	2.76
				S1J	S1J					0.99			3.30	2.19	4.08	6.04	3.77
				S1JO													
				S1DZ	S1DZ					3.47		6.36		1.95	3.67	5.38	3.64
					S1DZO												
				S1ULp	S1ULp					3.69	5.07	6.49		3.51	6.13	6.38	4.14
				GI	GI					4.98	5.84	6.48	4.38	5.46	6.53	6.04	4.28
				DI	DI					5.80	6.59	6.30	4.24	5.88	6.90	5.85	4.31
			VISC														
			GU														
			AId	AID	AID		7.50	5.56		6.33		5.80		6.23	7.26	5.61	4.19
			AIv	AIV	AIV		7.69	5.09			7.26		4.14	6.67	7.56	5.36	3.90
			PIR1	Pir1	Pir1		8.74	4.95	2.91	7.07	8.76	5.40	3.57	7.48	8.81	5.23	3.53
			PIR2	Pir2	Pir2	7.28	8.36	4.60	2.87	7.09	8.57	5.02	3.47	7.45	8.58	4.95	3.44
			PIR3	Pir3	Pir3	6.76				6.65	8.48	4.98	3.23	6.91	8.48	4.87	3.25
			lot	lo	lo	8.12	8.71	4.36	3.13	8.08	8.61	4.76	3.87	8.36	8.80	4.51	3.72
			OT1	Tu1	Tu1		8.94		0.22		9.39	3.69	0.01	7.69	9.18	3.69	0.10
			OT2	Tu2	Tu2	6.86	8.90	3.04	0.43	7.91	9.27	3.57	0.08	7.75	9.02	3.53	0.24
			OT3	Tu3	Tu3	7.07	8.70	2.91	0.54		9.11	3.47	0.14	7.58	8.89	3.44	0.27
			isl	ICj	ICj	7.95	8.48	2.20	1.09	7.71	8.96	2.72	0.07	7.64	9.00	3.49	0.16
				VP	VP					7.46	8.80	3.11	0.33	8.14	8.58	3.21	1.28
				mfba	mfb					7.84	8.69	3.10	0.51				
			NDB	VDB	VDB		6.89	0.66		6.94	7.74	0.29	0.01		7.73	0.34	0.00
			MS	MS	MS	6.02			0.07	6.07	6.98	0.25	0.01	6.27			0.00
			LSr	LSI	LSI	4.13		1.03		4.99		0.88	0.01	4.97	7.65	0.79	0.00
			LSr.m						0.00								
			LSr.vl.d.m														
			LSr.vl.d.l														
			LSr.dl.l.d														
				LSV	LSV					5.18	6.17	1.03	0.45	5.25	6.14	1.01	0.65
			LSc.d.r	LSD	LSD	3.67		1.02	0.00	4.50	5.45	0.94	0.33	4.54	5.32	0.89	0.00

Level			Structure			S Coordinate (mm)				PW1 Coordinate (mm)				PW2 Coordinate (mm)			
S	**PW1**	**PW2**	**S**	**PW1**	**PW2**	**D**	**V**	**L**	**M**	**D**	**V**	**L**	**M**	**D**	**V**	**L**	**M**
14	13	20	SH	SH	SHi	4.22	5.37	0.29	0.10	5.53	6.03	0.16	0.01	4.77	5.74	0.34	0.00
			ccg	gcc	gcc		4.04		0.00		5.12		0.00		4.82		0.00
			cing	cg	cg	2.08	3.11		0.75	2.60				2.66	3.71	2.25	0.80
			SEZ	E	E	2.70	3.85	2.23	1.04					3.98	6.52	1.37	0.70
			ec	ec	ec		8.02	4.80	2.68		5.82	4.38			6.61	4.29	
			CLA	Cl	DCl	4.82	6.77	4.91	3.82	5.07	6.65	4.57	3.88	5.35		4.31	
					VCl										6.92		3.71
			EPd	DEn	DEn	6.49	8.02	4.00	2.72	6.45	8.36	4.36	3.12	6.57		4.15	
					IEn										8.30		3.08
			FS														
			SI														
				LSS	LSS					6.93	8.29	3.77	3.00	7.58	8.11	3.13	2.93
			ACB	LAcbSh	LAcbSh	5.07	7.34	2.43	0.60								
				AcbSh	AcbSh					6.08			0.49	5.92			0.48
				AcbC	AcbC					6.13	7.99	2.81	0.98	6.22	7.81	2.53	1.03
			aco	aca	aca	6.41	6.88	2.06	1.75	7.01	7.65	2.16	1.60	6.96	7.66	2.81	1.54
			islm	ICjM	ICjM	5.75	6.43	0.55	0.76	6.58	7.58	0.56	0.42	6.77	7.49	0.54	0.41
			CP	CPu	CPu	2.67	6.79	4.64	1.23	3.20		4.23	0.94	3.37		4.06	5.91
16	17	28	IG	IG	IG	2.76	2.85	0.40	0.14	3.25	3.33	0.29	0.11	4.77	4.82	0.28	0.00
			ACAv	Cg2	Cg2	1.91			0.04	1.92	3.34	1.23	–0.01	2.84	4.82	1.35	0.00
			ACAd	Cg1	Cg1	1.21			0.04	0.90	2.62	1.33	–0.01	1.80	3.74	1.51	0.00
			MOs	M2	M2	0.14			0.04	0.09	2.46	1.49	–0.01	1.50	3.68	1.89	0.60
			MOp	M1	M1	0.08		2.28	0.88	0.04	2.64	2.80	0.79	1.50	3.82	2.79	1.75
			SSp	S1FL	S1FL	0.15	4.61	6.73		0.27	3.15	4.64	2.21	1.60	4.43	2.47	5.38
				S1DZ	S1DZ					1.09	3.26	4.96	3.45	2.84	4.61	5.65	3.86
				S1ULp	S1ULp					1.34	4.69	6.71	3.64	3.13	5.69	6.69	4.07
			SSs	S2	S2		5.30	6.73		4.31	5.59	6.76	4.75	5.42	6.96	6.72	4.75
				GI	GI					5.50		6.67	4.84	6.56	7.44	6.59	4.91
				DI	DI						6.55			7.08	7.83	6.45	5.05
			VISC														
			GU														
					AID												
					AIV												
			AIp	AIP			7.50	5.82		6.27	7.52	6.39	4.73				
			PIR1	Pir1	Pir1		8.50	5.45		7.37	9.16	5.89	3.62	8.48	10.27	5.88	3.83
			PIR2	Pir2	Pir2	7.30	8.23	5.12	2.87	7.37	8.92	5.60	3.56	8.45	10.04	5.59	3.75
			PIR3	Pir3	Pir3					6.95	8.81	5.54	3.44	8.09	9.83	5.51	3.64
			lot	lo	lo	8.15	8.68	4.86	3.05	8.63	9.11	5.02	3.90	9.63	10.18	4.81	4.04
			OT1	Tu1	Tu1	7.45	8.81		0.87		9.59	3.66		9.95	10.55	3.86	1.52
			OT2	Tu2	Tu2	7.47	8.65	2.84	0.99	8.90	9.44	3.51	1.00	9.92	10.41	3.80	1.48
			OT3	Tu3	Tu3		8.53				9.37		1.07	9.63	10.29	3.75	1.70
			isl	ICj	ICj	7.74	8.33	2.42	1.16	8.99	9.18	2.57	1.36	9.89	10.18	3.00	1.81
				LSS	LSS					7.51	8.71	4.15	3.27	8.68	9.18	3.84	3.36
				VP	VP					7.32	9.09	3.27	0.93	7.74	9.91	3.47	0.72
				mfba	mfb												
			FS														
			SI	SI		6.00	7.96	3.02	0.54	7.42			0.93				
				SIB	SIB						9.03	1.86	1.12	8.53	9.48	1.57	0.75
			MA														
				mfbb													
			NDB	HDB	HDB		7.41	1.27			8.95	1.45			9.86	1.62	
				VDB	VDB												0.00

Level			Structure			S Coordinate (mm)				PW1 Coordinate (mm)				PW2 Coordinate (mm)			
S	**PW1**	**PW2**	**S**	**PW1**	**PW2**	**D**	**V**	**L**	**M**	**D**	**V**	**L**	**M**	**D**	**V**	**L**	**M**
16	17	28	MS	MS	MS	3.88		0.82	0.01	5.36				6.20			0.00
			LPO		LPO	5.54	6.32	1.10	0.51					7.75	8.88	0.81	0.51
			zl	ZL		5.00	5.61	1.55	1.02	5.91	6.91	1.36	0.85				
				Ld	Ld					4.67		0.55		5.77	7.46	0.48	0.00
				PLd	PLd					5.38	5.87	0.87	0.53	6.61	7.22	0.84	0.52
			LSr.vl.v	LSV	LSV	4.66	5.64	1.57	0.82	5.17	6.92	1.40	0.54	6.43	7.53	1.46	0.90
			LSr.m.d	LSI	LSI				0.01	3.76		1.39	0.00	5.22	7.41	1.46	0.00
			LSRr.m.v.r				5.64										
			LSr.dl.m.d			3.48											
			LSr.dl.m.v														
			LSr.dl.l.d														
			LSr.dl.l.v					1.60									
			LSc.d.d	LSD	LSD	2.99				3.60	4.41	1.25	0.31	5.01	5.57	1.15	0.27
			LSc.d.r						0.01								
			LSc.v.l.d				4.26	1.45									
			SH	SHi	SHi	3.25	3.78	0.30	0.06	3.80	4.40	0.18	–0.04	5.19	5.77	0.27	0.00
					SHy												
			cc	cc	cc				0.01	2.69			0.00			0.00	
			cing	cg	cg	1.88	2.78		0.62	2.38	2.98		0.96	3.63	4.57	2.51	0.83
			SEZ		E	2.34	2.86	2.32	1.49					4.23	5.91	2.17	1.43
			ec	ec	ec			5.05			6.61	4.84	4.63		7.94	4.88	4.49
			CLA	Cl	DCl	5.10	6.81	5.06	4.20	5.50	6.95	4.99	4.57	6.52			
					VCl										8.13	5.03	4.56
			ee														
			EPd	DEn	DEn	6.62	7.82	4.44	2.86	6.77	8.74	4.88	3.32	7.99		4.84	
					IEn										9.63		3.57
				CB	CB												
				IPAC	IPAC					6.83	8.61	2.82	1.46	8.37	8.83	2.81	1.99
			aco	aca	aca	5.71	6.27	1.72	1.12	6.84	7.40	1.76	1.06	7.78	8.61	2.37	1.27
					AcbC												
					AcbSh												
			BSTam	BSTMA	STMA	5.04	6.27	1.49	1.04	5.99	7.55	1.57	0.84	7.51	8.49	1.45	1.06
			BSTal	BSTL		5.03	6.03	1.68	1.45	6.13	7.07	1.65	1.21				
			CP	CPu	CPu	2.34	7.03	4.95	1.46	3.05		4.79	1.19	4.25		4.76	1.37
			och														
			ov		VOLT	6.88	7.22	0.09	0.01					8.62	9.59	0.44	0.00
			MPO														
19	19	35	IG	IG	IG	2.71	2.81	0.29	0.07	3.04	3.11	0.29	0.12	3.62	3.67	0.24	0.10
			ACAd	Cg2	Cg2	0.90			0.02	1.88	2.37	1.01	0.04	2.26	3.67	1.17	0.00
			ACAv	Cg1	Cg1	1.51	2.81		0.00	0.95	2.40	1.15	–0.01	0.96	2.79	1.30	0.00
			MOs	M2	M2	0.09			0.02	0.26	2.20	1.23	–0.01	0.54	2.65	1.62	0.36
			MOp	M1	M1	0.07		2.22	1.05	0.16	2.35	1.99	0.63	0.53	2.64	2.40	1.48
			SSp	S1HL	S1HL	0.18		6.83		0.18			1.74	0.56			2.12
				S1FL	S1FL												
				S1DZ	S1DZ												
				S1BF							4.59	7.02					
					S1ULp										4.91	6.99	
			SSs	S2	S2	0.18	6.09	6.88		4.12	5.79	7.16	5.08	4.39	6.17	7.09	5.00
			VISC														
			GU														
				GI	GI												
				DI	DI												

Level			Structure			S Coordinate (mm)				PW1 Coordinate (mm)				PW2 Coordinate (mm)			
S	PW1	PW2	S	PW1	PW2	D	V	L	M	D	V	L	M	D	V	L	M
19	19	35	AIp	AIP	AIP		7.84	5.93		6.38	7.50	6.94	5.24	6.85	7.82	6.74	5.44
			PIR1	Pir1	Pir1		9.11	5.68	2.69	7.43		6.46		7.73	9.52	6.52	4.35
			PIR2	Pir2	Pir2	7.70	8.82	5.39	2.77	7.41	8.60	6.14	4.49	7.71	9.15	6.21	4.36
			PIR3	Pir3	Pir3			5.33		7.19		6.08		7.42	8.96	6.15	4.07
			lot	lo	lo	8.82	9.25	4.64	2.69	8.25	9.17	5.93	4.49	9.31	9.70	5.23	3.87
				CxA1	CxA1												
				CxA2	CxA2												
				CxA3	CxA3												
			OT1	Tu1	Tu1		8.94		1.11		9.72			9.26	9.67	3.63	1.85
			OT2	Tu2		8.08	8.76	2.66	1.22								
			OT3	Tu3		8.01	8.66	3.23									
				ICj													
			CLA	Cl	DCl	5.56	7.37	5.27	4.35	5.79	7.19	5.46	5.07	6.03			
					VCl										7.59	5.52	4.88
			ee														
			EPd	DEn	DEn	7.12	8.00	4.70	3.62	7.03		5.50		7.35		5.35	
				VEn	IEn						8.65		3.59		8.74		3.80
				LSS	LSS												
				IPACL	IPACL												
				IPACM	IPACM												
			IA														
			FS														
					AA												
			MA	MCPO	MCPO	7.36	8.26	3.21	1.45	8.26	9.05	3.60	2.65	8.59	9.33	3.19	2.00
			NDB	HDB	HDB	7.28	7.82	1.93	1.05	8.55	9.14	2.74	1.38	8.55	9.36	2.12	1.25
				mfba	mfba												
				mfbb	mfbb												
				VP	VP												
			SI	SIB	SIB	6.23	7.70	2.92	1.32	8.15	8.63	2.65	1.87	8.17	8.68	2.35	1.64
			och	ox	och	7.64	7.84	0.45	0.73	9.10	9.69	0.72	0.07	9.01	9.59	0.90	0.00
			PSCH														
				VMPO	VMPO												
			AVPV	AVPe													
				Pe	Pe												
			MEPO	MnPO	MnPO	5.33	6.76	0.18	0.00	5.91	7.72	0.29	0.08	6.08	7.53		0.00
			MPO	MPA	MPA	5.84				7.19			0.12	7.68	9.45	1.98	0.37
			I														
			ADP	ADP													
				StA	StA												
			MPNl	MPOL	MPOL	6.60	7.09	0.59	0.27	7.84	8.50	0.86	0.38	7.72	8.98	0.75	0.34
					MPOM												
			AVP	VLPO	VLPO	7.25	7.70	0.89	0.54	9.00	9.30	1.20	0.91	8.91	9.33	1.30	0.65
					SO												
			LPO	LPO	LPO	5.19	7.53	1.74	0.00	7.50	8.94	2.21	0.80	7.50	8.76	1.97	1.07
					SHy												
			PS	PS	PS	6.26	6.64	1.34	0.89	7.40	7.76	1.43	0.93	7.31	7.73	1.23	0.71
			BSTam	BSTMV	STMV	4.82	6.63	2.09	0.83		7.45				7.37		0.59
				BSTMA	STMAM					5.51		1.90					
					STMAL									6.06		1.49	
			BSTd		STD												
			BSTal	BSTLP	STLP	5.65	6.63	2.25	1.48	6.21			0.95	5.63		1.85	
				BSTLV	STLV						7.66	2.13			7.60		
					STI												0.96

Level			Structure			S Coordinate (mm)				PW1 Coordinate (mm)				PW2 Coordinate (mm)			
S	**PW1**	**PW2**	**S**	**PW1**	**PW2**	**D**	**V**	**L**	**M**	**D**	**V**	**L**	**M**	**D**	**V**	**L**	**M**
19	19	35	BSTfu	Fu	Fu	6.39	6.63	1.90	1.52	7.37	7.63	1.99	1.72	7.36	7.56	1.40	1.13
			BSTov	BSTLD	STLD	4.83	6.22	2.21	1.78	5.86	6.95	1.99	1.56	5.90	6.51	1.84	1.59
			BSTju	BSTLJ	STLJ	5.40	6.14	2.19	2.07	6.16	6.92	2.07	1.93	6.51	7.16	1.85	1.77
			int	ic	ic	4.72	6.32	2.41	2.16	5.13	7.19	2.23	1.82	5.29	7.22	2.16	1.83
				st													
			GPe	LGP	EGP	4.81	6.40	2.59	2.23	5.75	7.20	2.87	2.15	5.88	7.43	2.66	
			aco	ac	ac	5.51	6.14	1.41	–0.01	6.49	7.24	1.08	0.09	6.59	7.26	1.28	0.00
			act	acp	acp	5.76	7.61	3.67	1.27	6.67	7.86	4.34	0.94	7.19	8.08	3.79	2.03
					CST												
					LTer												
			MS														
			fx	f	f		4.67		0.01		6.28	0.62	0.07		6.52	0.43	0.00
			fxpr	pcf	fi		4.86	0.84				0.80	0.04	4.29	6.25	0.90	0.00
				df													
			SF	SFi	SFi	3.62	5.22	0.71	0.13	4.54	5.61	0.65	0.33	5.59	6.13	0.25	0.05
					TS												
			SH		SHi												
			LSc.d.d	LSD	LSD	2.96			0.00	3.37	4.26	1.39	0.13	3.89	4.64	1.33	0.11
			LSc.d.v														
			LSc.d.l				3.82	1.51									
			LSc.v.l.d	LSI	LSI					3.63	6.13	1.55	0.02	4.06	5.87	1.45	0.06
			LSc.v.m.d						0.25								
			LSc.v.i			3.25											
			LSc.v.m.v														
			LSc.v.l.v					1.65									
			LSr.m.v.c				5.49										
			LSv	LSV	LSV	4.93	5.53	1.43	0.47	4.92	6.44	1.57	0.58	5.54	6.08	1.39	0.57
			cc	cc	cc				0.00	2.52			0.00	2.65			0.00
			cing	cg	cg	1.90	2.71		0.71	2.18	2.99		0.61	2.65	3.51	2.18	0.73
			SEZ		E												
			ec	ec	ec		8.11	5.27				5.32			6.91	5.27	
			CP	CPu	CPu	2.51	7.90	5.18	1.72	2.99	7.81	5.27	1.36	3.22	8.10	5.19	1.71
23	22	42	IG	IG	IG	2.78	2.86	0.37	0.11	2.89	2.95	0.21	0.04	3.44	3.49	0.24	0.09
			ACAv	Cg2	Cg2	1.49	2.87		0.01	1.48	2.95	0.90	–0.02	1.98	3.49	1.10	0.00
			ACAd	Cg1	Cg1	0.72			0.03	0.55	2.22	0.99	–0.01	0.88	2.55	1.20	0.00
			MOs	M2	M2	0.32			0.23	0.20	2.13	1.02	–0.01	0.57	2.49	1.50	0.49
			MOp	M1	M1	0.16		1.78		0.16	2.26	1.88	0.70	0.52	2.53	2.18	1.37
			SSp	S1HL	S1HL	0.16		6.82		0.20			1.47	0.52			1.97
				S1FL	S1FL												
				S1DZ	S1DZ												
				S1BF	S1BF						4.32	6.62					
					S1ULp										5.27	7.05	
			SSs		S2												
			VISC														
				GI	GI												
				DI	DI												
			AIp	AIP	AIP			6.65		6.52	7.41	6.87	5.34	7.28	8.27	6.59	5.21
			PIR1	Pir1	Pir1		9.99	6.30		7.34		6.59		8.16		6.52	
			PIR2	Pir2	Pir2	7.93	9.69	6.00	3.51	7.37	9.16	6.25	4.56	8.15	9.78	6.11	4.33
			PIR3	Pir3	Pir3		9.48	5.96		7.21		6.18		7.81	9.52		6.01
				CxA1	CxA1												
				CxA2	CxA2												
				CxA3	CxA3												
			COAa	ACo	ACo	9.09	9.42	3.52	3.10	8.71	9.19	3.76	3.36	9.07	9.51	3.93	3.53

Level			Structure			S Coordinate (mm)				PW1 Coordinate (mm)				PW2 Coordinate (mm)			
S	**PW1**	**PW2**	**S**	**PW1**	**PW2**	**D**	**V**	**L**	**M**	**D**	**V**	**L**	**M**	**D**	**V**	**L**	**M**
23	22	42	IG	IG	IG	2.78	2.86	0.37	0.11	2.89	2.95	0.21	0.04	3.44	3.49	0.24	0.09
			ACAv	Cg2	Cg2	1.49	2.87		0.01	1.48	2.95	0.90	–0.02	1.98	3.49	1.10	0.00
			ACAd	Cg1	Cg1	0.72			0.03	0.55	2.22	0.99	–0.01	0.88	2.55	1.20	0.00
			MOs	M2	M2	0.32			0.23	0.20	2.13	1.02	–0.01	0.57	2.49	1.50	0.49
			MOp	M1	M1	0.16		1.78		0.16	2.26	1.88	0.70	0.52	2.53	2.18	1.37
			SSp	S1HL	S1HL	0.16		6.82		0.20			1.47	0.52			1.97
				S1FL	S1FL												
				S1DZ	S1DZ												
				S1BF	S1BF						4.32	6.62					
					S1ULp										5.27	7.05	
			SSs		S2												
			VISC														
				GI	GI												
				DI	DI												
			AIp	AIP	AIP			6.65		6.52	7.41	6.87	5.34	7.28	8.27	6.59	5.21
			PIR1	Pir1	Pir1		9.99	6.30		7.34		6.59		8.16		6.52	
			PIR2	Pir2	Pir2	7.93	9.69	6.00	3.51	7.37	9.16	6.25	4.56	8.15	9.78	6.11	4.33
			PIR3	Pir3	Pir3		9.48	5.96		7.21		6.18		7.81	9.52		6.01
				CxA1	CxA1												
				CxA2	CxA2												
				CxA3	CxA3												
			COAa	ACo	ACo	9.09	9.42	3.52	3.10	8.71	9.19	3.76	3.36	9.07	9.51	3.93	3.53
			NLOT1	LOT	LOT1		9.57		1.99	8.94	9.24	3.43	3.07		9.88	3.59	2.44
			NLOT2		LOT2			3.11									
			NLOT3		LOT3	8.52								8.69			
			lot	lo	lo	9.52	9.99	3.98	2.89	8.02	9.57	6.26	3.71	9.66	9.96	5.40	3.59
			CLA	Cl	DCl	5.65	7.76	5.57	4.76	5.91	7.21	5.47	5.09	6.39		5.37	
					VCl										7.83		4.91
			EPd	DEn	DEn	7.68	8.73	5.26	4.35	6.92	7.99	5.51	4.83	7.52	8.54	5.26	4.54
			EPv	VEn	VEn	8.77	9.01	4.36	3.79	7.23	8.63	4.84	3.86	8.43	8.93	4.84	3.76
			IA		I												
				LSS													
				IPACL	IPACL												
				IPACM	IPACM												
			CEAm														
			CEAc														
			AAA	AAD	AA	8.35	8.84	3.81	3.11	7.79		4.33		8.44	9.17	3.92	2.45
				AAV									2.62				
			BMAa														
				VP	VP												
				B	B												
					EAC												
			MA	MCPO	MCPO	8.13	8.45	3.27	2.47	8.21	8.92	3.39	2.56	8.10	8.95	3.14	2.26
			MEAd		MeAD												
				HDB	HDB												
				VLH	VLH												
					ESO												
			vlt														
			SI	SIV													
				SID													
				SIB													
				LPO	LPO												
			LHAav														
			LHAai														

Level			Structure			S Coordinate (mm)				PW1 Coordinate (mm)				PW2 Coordinate (mm)			
S	PW1	PW2	S	PW1	PW2	D	V	L	M	D	V	L	M	D	V	L	M
23	22	42	LHAjp														
			SO	SO	SO	8.18	8.52	1.86	1.33	9.30	9.52	1.49	1.04	9.14	9.47	2.13	1.41
			opt	ox	och	8.29	8.77	1.68	0.00	9.22	9.72	1.16	–0.02	9.23	9.72	1.85	0.44
					sod												
			SBPV		SPa												
			SCH	SCh	RCh	8.07	8.39	0.38	0.06	8.95	9.33	0.47	0.09	8.93	9.35	0.29	0.00
				mfb	mfb												
			AHNc		AHA												
			AHNa		LA												
			I														
			AHA														
			MPNm	MPOM	MPOM	7.33	7.78	0.43	0.30	7.98	8.89	0.56	0.05	7.86	8.71	0.42	0.03
			MPNc	MPOC													
			MPNl	MPOL													
			PVpa	Pe	Pe		8.24		0.00	6.67	9.26	0.18	–0.02	7.32	9.29	0.03	0.00
			PVpo														
			PVHpv			6.47		0.25									
			MPO	MPA	MPA												
			PVHap	PaAP	PaAP	6.44	7.09	0.59	0.22	6.92	7.63	0.56	0.08	6.87	7.65	0.47	0.02
				PaAM													
				StHy	StHy												
			fx	f	f	6.39	6.80	1.18	0.82	6.60	7.19	1.01	0.54	6.90	7.30	1.10	0.60
				mch													
			PVT	PVA	PVA	4.89	6.43	0.72	0.00	5.19	6.71	0.57	0.04	5.59	6.89	0.39	0.04
			PT	PT	PT	5.01	5.60	0.90	0.36	5.25	6.14	0.76	0.20	5.54	6.42	0.79	0.27
					AM												
			REa		Re												
			sm	sm	sm	4.77	7.25	2.16	0.68	5.05	6.51	1.29	0.55	5.32	6.81	1.63	0.48
			BSTv	BSTMPM, MPL, MPI	BSTMPM, MPI, MPL, MP		7.49			5.75	7.78	1.98	0.66	6.71	7.88	1.66	0.62
			BSTif			6.36		1.69	0.79								
					SM												
					RtSt												
				AV	AV												
					cst												
			st	st	st	4.18	5.04	3.01	2.15	4.85	6.28	2.20	1.31		5.77		1.75
			int	ic	ic	3.77	6.49	3.32	2.08	4.08	6.90	2.64	1.89	4.23	7.21	3.10	1.93
			GPi	LGP					2.51	5.09	7.34	3.72	2.19				
			GPe		EGP	4.68	7.09	4.22						4.95	7.79	3.85	2.37
			SFO	SFO	SFO	3.95	4.45	0.58	0.00	4.82	5.21	0.83	0.00	4.93	5.14	0.16	0.00
			vhc	vhc	vhc				0.00		4.87		–0.10				0.00
			fi		fi												
			df	df	df	3.10	3.38	1.03	0.00	3.35			–0.05	3.72	3.99	0.77	0.00
			SF	SFi	SFi	3.23	4.14	1.81	0.13		4.87	1.86		4.10	4.46	1.30	0.45
				TS	TS												
				LSD													
			cc	cc	cc	2.36			0.00	2.49			–0.04	2.67			0.00
			cing	cg	cg	2.07	2.79		0.62	2.11	2.92		0.33	2.45	3.40		0.61
			SEZ														
			ec	ec	ec		7.93	5.51			6.65	5.34				5.28	
			amc														
				acp	acp												
			CP	CPu	CPu	2.88	7.87	5.44	2.61	3.12	7.68	5.28	1.75	3.32	8.11	5.17	2.47
24	24	45	IG	IG	IG	2.84	2.90	0.33	0.12								
			ACAv	Cg2	Cg2	1.61	2.90		0.00	1.36	3.00	0.93	0.01	2.04	3.52	1.07	0.00

Level			Structure			S Coordinate (mm)				PW1 Coordinate (mm)				PW2 Coordinate (mm)			
S	PW1	PW2	S	PW1	PW2	D	V	L	M	D	V	L	M	D	V	L	M
24	24	45	ACAd	Cg1	Cg1	0.58			0.03	0.56	2.41	0.98	0.01	0.73	2.55	1.17	0.00
			MOs	M2	M2	0.40			0.46	0.37	2.36	1.02	0.01	0.53	2.51	1.46	0.47
			MOp	M1	M1	0.25		1.98	0.95	0.33	2.40	1.59	0.71	0.50	2.53	2.05	1.27
			SSp	S1HL	S1HL	0.28		6.94		0.33			1.41	0.51			1.96
				S1FL	S1FL												
				S1DZ	S1DZ												
				S1BF	S1BF												
					S1ULp						4.66	7.11			5.38	7.10	
			SSs	S2	S2	3.26	6.11	7.30		3.85	6.13	7.38	5.03	5.06	6.62	7.15	5.15
				GI	GI												
				DI	DI												
			VISC														
			AIp	AIp	AIp			6.58		6.76	7.71	7.01	5.34	7.26	8.44	6.78	5.21
			PIR1	Pir1	Pir1	7.99	10.18	6.49		7.69		6.79		8.35		6.68	
			PIR2	Pir2	Pir2	7.95	9.92	6.18	3.45	7.71	9.66	6.45	4.60	8.34		6.43	
			PIR3	Pir3	Pir3		9.75			7.62		6.40		7.95		6.37	
				CxA1	CxA1												
				CxA2	CxA2												
				CxA3	CxA3												
			COAa1	ACo	ACo		9.85		2.38	8.98	9.72	4.14	3.49	9.49	10.00	4.14	3.26
			COAa2			9.13		3.43									
			NLOT1	LOT1	LOT1		9.38		2.06	9.44	9.86	3.58	2.67	9.57	10.16	3.29	2.59
			NLOT2	LOT2	LOT2	8.81	9.18	2.71	2.26	8.98	9.56	3.59	2.69	9.45	9.81	3.48	2.91
			NLOT3	LOT3	LOT3	8.71	9.14	3.00	2.32	8.65	9.23	3.77	2.74	8.89	9.55	3.60	2.91
			lot	lo													
			CLA	Cl	DCl	5.92	7.99	5.66	4.93	6.76	7.62	5.50	5.13	7.15		5.36	
					VCl										7.97		4.92
			BLAa														
			IA		I												
			EPd	DEn	DEn	7.90	8.90	5.36	4.34	7.30	8.22	5.52	4.79	7.82	8.81	5.33	4.67
			EPv	VEn	VEn	8.94	9.38	4.41	3.71	7.86	8.95	5.16	4.28	8.21	9.14	4.82	4.16
			BMAa	BMA	BMA	8.88	9.39	3.57	3.00	8.63	9.14	4.29	3.57	8.88	9.59	4.17	3.47
				AStr													
				LSS													
				IPACL	IPAC												
				IPACM													
					EAC												
					EAM												
			CEAc														
			CEAm		CeM												
			AAA	AAD	AA	8.12	8.99	3.86	2.80	8.27		4.49		8.57	9.25	4.12	2.76
				AAV							9.43		2.16				
			MEAad	MeAD	MeAD	8.17	8.70	2.88	2.26	8.89	9.65	2.96	2.33	9.15	9.78	3.04	2.43
			sm	sm													
					HDB												
				MCPO	MCPO												
				mfb	mfb												
				VLH	VLH												
			vlt														
			LHAav	LH	PLH		8.71	3.06				2.55				2.43	
			LHAai														
			LHAad														
			LHAjp		JPLH	6.35			0.57								
					ESO												
			SO	SO	SO	8.28	8.72	2.04	1.61	9.23	9.57	2.07	1.55	9.31	9.72	2.39	1.82

Level			Structure			S Coordinate (mm)				PW1 Coordinate (mm)				PW2 Coordinate (mm)			
S	**PW1**	**PW2**	**S**	**PW1**	**PW2**	**D**	**V**	**L**	**M**	**D**	**V**	**L**	**M**	**D**	**V**	**L**	**M**
24	24	45	opt	ox	opt	8.39	8.96	1.86	0.54	9.29	9.99	1.74	0.00	9.41	10.06	2.24	0.99
			sup		sod												
			RCH		RChL												
			SCH	SCH	RCh	8.43	8.58	0.26	0.11	9.20	9.67	0.41	0.06	9.62	10.04	0.28	0.00
			AHNc	AHA	AHA	7.13	8.57	1.31	0.35	8.25	8.98	1.25	0.42	8.13	9.27	1.29	0.45
			AHNa	LA	LA	8.04	8.57	1.24	0.64	8.70	9.38	1.25	0.43	8.88	9.54	1.21	0.51
			NC	Cir	Cir	7.89	8.08	0.92	0.79	8.66	8.76	0.75	0.63	8.72	8.87	0.72	0.57
				MPO													
			SBPV		SPa												
			PVa	Pe	Pe	6.74	8.48	0.27	0.00	7.72	9.56	0.09	–0.01		9.69		0.00
					PaV									8.15		0.13	
					ANS												
			fx	f	f	6.83	7.10	1.21	0.94	7.55	8.01	1.25	0.82	7.65	8.11	1.21	0.76
				BSTMPL	STMPM												
			I														
			PVHap	PaAP	PaMP, PaMM	6.75	7.32	0.59	0.18	7.52	8.18	0.55	–0.02	7.57	8.38	0.38	0.03
			PVHpv														
			RE	Re, VRe	Re, VRe	5.77	6.74	0.73	0.00	6.69	7.40	0.75	0.01	6.48	7.54	0.78	0.00
			REv														
			REd														
			REm	PVA	Xi	5.81	6.54	0.08	0.00	6.73	7.19	0.12	0.04	6.89	7.41	0.08	0.00
			PVT	PVA	PVA	4.87	5.77	0.66	0.00	4.81	5.82	0.40	0.07	5.35	6.02	0.33	0.00
			PT	PT	PT	5.01	5.63	0.85	0.29	5.05	5.74	0.76	0.23	5.35	6.21	0.82	0.14
				PC	PC												
				CM	CM												
			IAD	IAD	IAD	5.09	5.68	1.03	0.50	5.19	6.22	1.09	0.12	5.59	6.36	1.03	0.35
			AMd	AM	AM	5.26	6.00	1.39	0.50	5.43	6.68	1.45	0.17	5.59	6.62	1.58	0.34
			AMv	AMV	AMV	5.79	6.24	1.29	0.48	6.45	6.71	0.87	0.22	6.53	6.83	1.36	0.38
			AD	AD	AD	4.17	5.05	1.70	1.20	4.50	5.32	1.55	0.92	4.83	5.68	1.56	0.86
			AV	AVDM	AVDM	4.27	6.10	2.05	1.12				1.02	4.85			1.03
				AVVL	AVVL					4.52	6.14	2.00			6.33	2.11	
					RtSt												
					STSM												
					STSL												
			RT	Rt	Rt	4.48	6.64	2.81	0.92	4.73	7.14	2.34	0.93	5.02	7.29	2.73	0.87
			int	ic	ic	3.44	7.31	3.67	1.72	4.58	7.28	3.32	1.88	4.48	7.92	3.47	2.16
			st														
			st	st	cst	4.35	4.98	3.30	2.47	4.60	5.23	2.64	2.11				
					st									4.56	5.28	2.92	2.23
			fi	fi	fi		4.52	2.80			4.75	2.46			4.98	2.77	
			vhc	vhc	vhc		3.86		0.00				–0.04				0.00
			SF	SFO	SFO	3.28	3.55	1.17	0.19	4.24	4.55	0.43	–0.07	4.66	4.77	0.30	0.00
			df	df	df	3.11	3.32	0.99	0.00	3.24	3.59	1.04	0.01	3.73	3.97	0.84	0.00
				TS	TS												
			cc	cc	cc	2.48			0.00	2.74			0.01	2.81			0.00
			cing	cg	cg	2.03	2.84		0.61	2.34	2.92		0.62	2.48	3.44		0.58
			SEZ														
			ec	ec	ec		8.44	5.63			6.60	5.44			8.36	5.34	
			amc														
			CP	CPu	CPu	3.04	8.00	5.53	2.98	3.39	7.95	5.39	2.31	3.56	8.31	5.28	2.87
			GPi	LGP					2.48	5.19	7.64	3.97	2.44				
			GPe		EGP	4.73	7.27	4.38						5.09	7.95	3.96	2.59

Level			Structure			S Coordinate (mm)				PW1 Coordinate (mm)				PW2 Coordinate (mm)			
S	**PW1**	**PW2**	**S**	**PW1**	**PW2**	**D**	**V**	**L**	**M**	**D**	**V**	**L**	**M**	**D**	**V**	**L**	**M**
24	24	45	SI	SI													
				B	B												
				SM	SM												
25	25	46	IG	IG	IG	2.88	2.94	0.32	0.13	2.68	2.75	0.21	0.01	3.51	3.58	0.16	0.01
			RSPv	RSGb			2.94		0.00								
			RSPd	RSA		0.67											
					Cg2	0.43			0.54								
					Cg1	0.29		2.03	1.09								
			MOs	M2	M2	0.30		6.87		0.04	1.99	1.01	0.12	0.67	2.55	1.52	0.66
			MOp	M1	M1					0.04	2.09	1.07	0.95	0.64	2.60	2.06	1.41
			SSp	S1HL	S1HL					0.10			1.38	0.64			1.97
				S1FL	S1FL												
				S1DZ	S1DZ												
				S1BF	S1BF												
					S1ULp										5.47	7.31	
				S1							4.51	6.98					
			SSs	S2	S2	3.83	6.09	7.12		3.71	6.05	7.41	4.87	5.16	6.70	7.32	5.29
				GI	GI												
				DI	DI												
			VISC														
			AIp	AIp	AIp		8.29	6.49		6.76	7.78	6.94	5.19	7.29	8.43	6.81	5.38
			PIR1	Pir1	Pir1	8.18	10.27	6.25	3.13	7.74		6.67		8.36	10.27	6.69	5.01
			PIR2	Pir2	Pir2	8.14	9.97	5.98	3.46	7.73	9.67	6.37	4.68	8.33	9.98	6.38	4.99
			PIR3	Pir3	Pir3	7.95	9.89	5.95		7.62		6.30		7.89	9.81	6.28	4.27
				CxA1	CxA1												
				CxA2	CxA2												
				CxA3	CxA3												
			COAa1	ACo	ACo		9.94		2.31					9.58	9.99	4.21	3.36
			COAa2			9.02		3.44									
				LOT1													
			NLOT2	LOT2													
				LOT3													
			lot														
			CLA	Cl	DCl	5.78	8.18	5.48	4.86	7.00	7.66	5.32	5.06	6.69		5.42	
					VCl										7.96		5.01
			LA														
			BLAa	BLA	BLA	7.74	9.03	4.58	4.00	7.40	8.39	5.06	4.33	8.16	8.92	4.80	4.23
			IA	I	I	8.54	9.11	4.13	3.46	8.04	8.28	4.39	4.12	8.76	9.01	4.30	4.04
			EPd	DEn	DEn	7.81	9.02	5.19	4.44	7.40	8.38	5.39	4.68	7.84	8.21	5.01	4.80
			EPv	VEn	VEn	9.10	9.43	4.23	3.71	8.32	9.01	5.10	4.24	8.74	9.24	4.97	4.23
			BMAa	BMA	BMA	8.73	9.50	3.64	2.83	8.61	9.30	3.99	3.29	9.05	9.72	4.30	3.37
				AStr	ASt												
				LSS													
				IPAC													
					EAC												
					EAM												
			CEAc	CeC	CeC	7.72	8.62	4.44	3.21	7.57	8.46	4.18	3.35	8.00	8.83	4.21	3.70
			CEAm	CeM	CeM	7.57	8.57	4.03	2.88	7.45	8.38	3.90	3.16	7.97	8.81	3.87	3.21
			AAA	AA	AA	8.66	8.91	2.97	2.53	8.24	9.58	4.71	2.26	8.69	9.72	4.46	2.86
			MEAad	MeAD	MeAD	8.27	8.67	2.96	2.17	8.91	9.70	2.91	2.38	8.96	9.71	3.17	2.63
					aot												
			BA2		BAOT												
					HDB												
				MCPO	MCPO												
				mfb	mfb												

Level			Structure			S Coordinate (mm)				PW1 Coordinate (mm)				PW2 Coordinate (mm)			
S	**PW1**	**PW2**	**S**	**PW1**	**PW2**	**D**	**V**	**L**	**M**	**D**	**V**	**L**	**M**	**D**	**V**	**L**	**M**
25	25	46			VLH												
			vlt														
			LHAav	LH	PLH, TuLH		8.97	3.06							9.89	2.97	
			LHAai														
			LHAad														
			LHAjp		JPLH	6.72			0.34					7.40			0.01
			SO	SO	SO	8.24	8.76	2.05	1.75	9.18	9.53	2.19	1.75	9.26	9.64	2.56	2.11
			opt	ox	opt	8.23	8.99	1.89	0.83	9.29	10.06	2.08	0.04	9.32	9.96	2.49	1.55
			sup	sox	sod	8.44	9.01	1.33	0.00	9.63	9.87	1.16	0.04	9.32	10.00	1.97	1.07
			RCH	RCH	RChL	8.10	8.85		0.00		9.80		0.04			1.14	
					RCh									9.65	10.14		0.01
			AHNp	AHA, AHC	AHC				0.29	8.12	9.34	1.34	0.34	8.18	9.50	1.32	0.17
			AHNc			7.41	8.55										
			AHNa					1.41									
					SPa												
			PVa	Pe	Pe		8.54	0.26	0.00	7.90	9.53	0.13	0.04		8.26		0.01
			PVHpv		PaV	7.02								9.71		0.18	
					ANS												
			fx	f	f	7.00	7.37	1.20	0.95	7.80	8.26	1.36	0.96	7.79	8.29	1.34	0.99
			I														
			PVHdp	PaAP		6.96			0.12	7.58	8.55	0.59	0.04				
			PVHmpd		PaMP									7.73		0.52	0.01
			PVHpmm		PaMM		7.63	0.53							8.46		
			PVHpml														
			RE	Re, VRe	Re, VRe	5.91	6.97		0.00	6.45	7.41	0.72	0.04	6.53	7.48	0.85	0.01
			REl					0.76									
			REd														
			REm		Xi	6.28	6.83	0.07	0.00								
					PaXi												
			PVT	PVA	PVA	4.74	5.59	0.44	0.00	4.50	5.57	0.44	0.01	5.27	5.93	0.44	0.01
			sm	sm	sm	4.42	5.03	1.20	0.48	4.39	4.89	1.06	0.34	4.94	5.50	1.06	0.01
			MDm	MD													
			MDl														
			PT	PT	PT	4.94	5.49	0.85	0.30	4.92	5.59	0.87	0.18	5.27	5.97	0.87	0.20
				PC	PC												
			CM		CM												
			IAD		IAD												
			IAM	IAM													
			AMd	AM	AM	5.19	6.09	1.53	0.43	5.43	6.54	1.44		5.59	6.76	1.67	0.15
			AMv	AMV	AMV	5.66	6.43	1.60	0.45	6.35	6.55	0.84	0.15	6.40	6.95	1.38	0.10
				RH													
			AD	AD	AD	4.20	5.15	1.79	1.02	4.19	5.06	1.77	0.99	4.71		1.72	
			AV	AVDM	AVDM	4.23	5.64	2.52	1.24	4.24			0.90	4.74			
				AVVL	AVVL						6.06	2.18			6.08	2.10	1.08
				mt													
			VAL	VA	VA	5.41	6.10	2.40	1.61	5.30	6.54	2.02	1.36	5.37	6.74	2.21	1.41
					RtSt												
					STSM												
					STSL												
			RT	Rt	Rt	4.76	7.05	3.20	1.22	4.45	7.23	2.79	0.93	4.85	7.64	2.89	0.67
			ZI	ZI													
			int	ic	ic	3.81	7.44	3.94	1.98	3.94	7.18	3.32	2.15	4.44	8.09	3.65	2.07
			st		cst												

Level			Structure			S Coordinate (mm)				PW1 Coordinate (mm)				PW2 Coordinate (mm)			
S	**PW1**	**PW2**	**S**	**PW1**	**PW2**	**D**	**V**	**L**	**M**	**D**	**V**	**L**	**M**	**D**	**V**	**L**	**M**
25	25	46	st	st	cst	4.31	4.87	3.31	2.64	4.32	4.90	2.85	2.31		5.13		
					st									4.54		3.23	2.47
			fi	fi	fi		4.50	3.19			4.52	2.72			4.91	3.04	
			vhc	vhc	vhc				0.00				0.00				0.01
			SF	SFO	SFO	3.36	3.48	0.36	0.04	3.78	3.90	0.27	–0.02	4.58	4.65	0.20	0.01
			df	df	df	3.20	3.39	0.62	0.00	2.99	3.31	0.79	0.03	3.80	4.01	0.70	0.01
				TS													
				CA3													
				DG	MoDG												
			cc	cc	cc				0.00	2.95							0.01
			cing	cg	cg	2.15	2.88		0.59	1.98	2.72		0.53	2.55	3.47		0.56
			ec	ec	ec		8.48	5.45							8.89	5.40	
			amc														
			CP	CPu	CPu	2.94	7.76	5.33	2.85	3.34		5.28	2.57	3.49		5.31	3.07
			GPi	LGP						4.68	7.43	4.02	2.28				
			GPe		EGP	4.67	7.18	4.38	2.58					4.91	8.13	4.17	2.65
			SI	SI													
				B	B												
26	27	48	IG	IG	IG	3.03	3.03	0.26	0.26	2.95	3.01	0.18	–0.02	3.30	3.38	0.22	0.09
			RSPv	RSGb	RSGc		3.13		0.00	1.47	3.01	0.84	–0.03	1.81	3.38	1.16	0.00
			RSPd	RSA	RSD	3.13				0.56	2.37	0.90	0.00	0.56	2.39	1.33	0.00
			MOs	M2	M2	0.58			0.00	0.46	2.31	1.23	0.29	0.45	2.34	1.59	0.55
			MOp	M1	M1	0.35			0.93	0.47	2.52	2.08	0.95	0.45	2.39	2.03	1.39
				S1HL	S1HL					0.56			1.38	0.45			2.03
					S1Sh												
				S1FL													
			SSp	S1DZ	S1DZ	0.33		6.86									
				S1BF	S1BF												
					S1ULp						4.66	6.67			5.04	7.21	
				S1													
			SSs	S2	S2	3.61	5.99	7.14		3.69	5.88	7.38	4.74	4.61	6.36	7.23	5.19
				GI	GI												
				DI	DI												
			VISC														
			AIp	AIp	AIp		8.48	6.62		6.69	7.80	7.11	5.23	6.98	8.06	6.96	5.33
			PIR1	Pir1	Pir1		10.48	6.39		7.69		6.68		7.99	10.26	6.80	
			PIR2	Pir2	Pir2	8.40	10.25	6.14	3.68	7.71	9.84	6.37	4.73	7.96	10.02	6.41	4.30
			PIR3	Pir3	Pir3		10.05	6.09		7.29		6.37		7.62	9.88	6.27	3.98
				CxA1													
				CxA2													
				CxA3													
			COAa1	ACo	ACo		10.16		2.49	9.25	9.85	4.19	3.09	9.27	10.01	4.39	2.97
			COAa2			9.10		3.68									
			CLA	Cl	DCl	5.84	8.30	5.62	5.06	6.83	7.49	5.38	5.13	6.53		5.52	
					VCl										7.62		5.10
			LA	LaDL													
			BLAa	BLA	BLA	7.90	9.16	4.85	4.03	7.73	8.68	5.01	4.20	7.81	8.84	4.95	4.30
			IA	IM	I	8.68	8.91	4.01	3.12	8.44	9.40	4.68	3.89	8.63	9.00	4.56	3.78
			EPd	DEn	DEn	8.09	9.33	5.51	4.52	7.22	8.50	5.63	5.05	7.54	8.71	5.53	5.01
			EPv	VEn	VEn	9.26	9.65	4.47	3.90	7.89	9.26	5.40	4.23	8.45	9.06	5.12	4.55
			BMAa	BMA	BMA	8.79	9.69	4.11	2.94	8.83	9.49	4.23	3.18	8.91	9.54	4.18	3.07
					ASt												
				IPAC													
					EA												
			CEAc	CeC	CeC	7.97	8.70	4.52	2.99	7.64	8.40	4.16	3.67	7.73	8.75	4.30	3.79

Level			Structure			S Coordinate (mm)				PW1 Coordinate (mm)				PW2 Coordinate (mm)			
S	PW1	PW2	S	PW1	PW2	D	V	L	M	D	V	L	M	D	V	L	M
26	27	48	CEAl	CeL													
			CEAm	CeM	CeM	7.49	8.54	4.08	2.99	7.40	8.56	4.16	3.12	7.72	8.75	3.89	3.23
					AA												
			MEAad	MeAD	MeAD	7.89	9.07	3.08	2.40	8.27	9.48	3.25	2.39	8.18	9.24	3.05	2.55
			MEAav		MeAV												
			st	cst	cst	8.37	8.47	3.37	3.30	8.58	8.89	3.58	3.34	8.73	8.88	3.65	3.49
			BA2	BAOT	BAOT	8.94	9.27	2.58	2.32	9.19	9.59	3.09	2.68	9.39	9.77	3.08	2.74
				al													
				ns	ns												
				mfb	mvb												
			SI	SI													
			vlt		vlh												
			LHAav	LH	PLH		9.03	2.91		7.53	8.98	2.64	1.27			2.84	
			LHAai														
			LHAad			7.12											
			LHAsfa		TuLH										9.94		
			LHAjvv														
			LHAjp		JPLH												
			SO	SO	SO	8.84	8.94	2.23	2.14	9.06	9.43	2.33	2.21	9.16	9.39	2.44	2.36
			opt	opt	opt	8.42	9.08	2.31	1.43	8.96	10.05	2.26	0.78	9.08	9.72	2.38	1.79
			sup	sox	sod	8.75	9.39	1.65	0.32	9.06	10.11	1.79	0.03	9.11	9.90	2.13	1.39
			MEin		ME												
			MEex														
			ARH		Arc												
					VMHSh												
			VMHa		VMH												
			TUsv														
				RCH	RChL												
			AHNp	AHP	AHP	7.67	8.14	0.83	0.39	8.17	8.83	1.03	0.31	8.13	8.66	0.92	0.27
			AHNc	AHC	AHC	7.66	8.49	1.30	0.38	8.35	9.51	1.35	0.34	8.13	9.23	1.36	0.26
			SBPV		SPa												
			PVl	Pe	Pe		8.87	0.28			9.61		0.03	8.82	9.38	0.11	0.00
			PVHpv			7.28			0.09								
					ANS												
			fx	f	f	7.41	7.72	1.43	1.18	8.08	8.62	1.48	1.12	7.95	8.61	1.37	1.14
			I														
			PVHdp	PaDC	PaDC	7.21	7.32	0.60	0.23	7.84	7.95	0.67	0.25	7.71	7.82	0.39	0.07
			PVHmpd	PaMP	PaMP	7.29	7.93	0.68	0.23	7.88		0.50		7.71	8.31	0.48	0.00
			PVHmpv	PaV	PaV	7.45	7.75	0.69	0.39	8.07		0.54		7.98	8.88	0.69	0.00
			PVHpml	PaLM	PaLM	7.25	7.58	0.79	0.50	7.92	7.92	0.77	0.49	7.74	8.01	0.72	0.36
			RE	Re, VRe	Re, VRe	6.40	7.30		0.00	6.83	7.75	0.76	0.02	6.65	7.58	0.96	0.01
			REl					0.79									
			REd														
			REm	Xi	Xi	6.95	7.20	0.06	0.00	7.14	7.66	0.07	0.03	7.39	7.65	0.05	0.00
					PaXi												
			PVT	PVA	PVA	4.67	5.61	0.48	0.00	4.74	5.52	0.31	–0.02	5.06	5.86	0.32	0.00
			MH	MHb	MHb	4.48			0.46	4.53	4.85	0.44	0.17	4.74	4.95	0.55	0.37
			sm	sm	sm	4.43	4.75	1.32		4.51	4.93	0.97	0.28	4.72	5.14	1.09	0.32
			MDm	MD	MD	4.70	5.20		0.48	4.53	5.33	1.13	0.24	5.02	5.62	1.00	0.26
			MDl					1.18									
			PT	PT	PT	4.92	5.52	1.11	0.42	5.28	5.72	0.82	0.10	5.34	5.80	0.96	0.26
				PC	PC												
			CM	CM	CM	5.59	5.89	0.52	0.22	5.47	5.98		–0.01	5.65	6.06		0.00
			IAD	IAD	IAD	5.10	5.68	1.24	0.53	5.51	5.97	1.11	0.26	5.52	5.98	1.10	0.55

Level			Structure			S Coordinate (mm)				PW1 Coordinate (mm)				PW2 Coordinate (mm)			
S	**PW1**	**PW2**	**S**	**PW1**	**PW2**	**D**	**V**	**L**	**M**	**D**	**V**	**L**	**M**	**D**	**V**	**L**	**M**
26	27	48	IAM	IAM	IAM	5.68	6.30	0.52	0.00				–0.02				0.00
			AMd	AM	AM	5.34	6.45	1.54	0.44	5.62	6.96	1.18		5.36	6.69	1.38	
			AMv	AMV	AMV	6.23	6.87	1.51	0.39	6.55	6.92	0.51	0.00	6.55	6.85	0.93	0.01
			RH	RH	RH	6.23	6.40	0.39	0.09	6.66	7.03	0.52	0.01	6.61	6.96	0.18	0.01
				Sub													
			AD	AD	AD	4.15	5.04	2.02	1.17	4.36	5.04	1.53	0.94	4.43	5.30	1.91	0.95
			AV	AVDM	AVDM	4.32	5.74	2.36	1.26								1.13
				AVVL	AVVL					4.71	5.99	2.12	1.06	4.55	6.06	2.37	
			LD	LDVL	LDVL	4.22	4.57	2.54	2.16	4.31	4.96	2.47	1.43	4.47	4.72	2.38	1.87
				mt	mt												
			VAL	VA	VA	4.99	6.67	3.41	1.49	5.11	7.00	2.74	1.01		6.87		1.19
					VL									5.07		2.85	
				VM	VM												
					RtSt												
			RT	Rt	Rt	4.55	7.11	3.56	1.56	4.78	7.50	3.03	1.05	4.55	7.53	3.23	0.88
			ZI	ZI													
			int	ic	ic	3.96	7.31	4.12	2.25	4.10	7.74	3.63	1.98	4.21	7.94	3.95	2.06
			st	st	st	4.32	4.72	3.52	2.84	4.47	5.07	3.07	2.44	4.29	4.88	3.43	2.72
			fi	fi	fi		4.53	3.41			4.74	2.96			4.69	3.28	
			vhc		vhc												
			SF		SFO												
			df	df	df	3.18	3.44	0.84	0.00	3.29	3.48	0.70	0.00	3.63	3.81	0.56	0.13
				DHC													
				dhc													
					alv												
			CA3sp	CA3	CA3Py					3.37	3.96	1.62	0.40				
			CA3so		CA3Or	2.89	3.77	2.23	0.58					3.20	4.18	2.01	0.34
			DGmb-sg	DG	GrDG	3.87					4.56		–0.01				
			DGmb-mo		MoDG		4.03	1.00	0.58					4.03	4.78	1.32	0.00
			cc	cc	cc	3.22				3.66			–0.01	2.61			0.00
			cing	cg	cg	2.10	3.00		0.62	2.28	2.90		0.56	2.33	3.32		0.39
			ec	ec	ec		8.82	5.53			7.69	5.26			8.85	5.40	
			amc														
			CP	CPu	CPu	3.24	8.05	5.42	3.40	3.57	7.67	5.21	2.65	3.43		5.30	3.34
			GPi	LGP	B		7.22		2.41								
			GPe		EGP	4.96		4.47		5.48	7.78	4.11	2.39	5.14	8.09	4.27	2.29
27	28	50	IG	IG	IG	3.00	3.08	0.32	0.12	2.84	2.92	0.29	0.11	3.25	3.35	0.25	0.05
			RSPv	RSGb	RSGc		3.08		0.00	1.40	2.93		–0.01	1.75	3.35		0.00
			RSPd	RSA	RSD	0.69				0.55			–0.01	0.66			0.00
			MOs	M2	M2	0.44			0.53	0.41			0.23	0.56			0.67
			MOp	M1	M1	0.28			1.14	0.38		1.48	0.82	0.55		2.00	0.67
				S1HL	S1HL					0.38				0.55			
				S1FL													
					S1Sh												
			SSp	S1DZ	S1DZ	0.28		7.14	1.82								
				S1BF	S1BF												
					S1ULp											7.11	
				S1								7.29					
			SSs	S2	S2	4.20	5.95	7.31		4.26		7.38		5.12	6.45	7.11	
				GI	GI												
				DI	DI												
			VISC														
			AIp	AIP	AIP		8.45	6.77			7.71	7.24			8.30	6.63	

Level			Structure			S Coordinate (mm)				PW1 Coordinate (mm)				PW2 Coordinate (mm)			
S	**PW1**	**PW2**	**S**	**PW1**	**PW2**	**D**	**V**	**L**	**M**	**D**	**V**	**L**	**M**	**D**	**V**	**L**	**M**
27	28	50	PIR1	Pir1	Pir1		10.68	6.64			10.17	7.00		8.21	10.46	6.53	
			PIR2	Pir2	Pir2	8.36	10.40	6.41	3.88	7.82	9.87	6.66	4.81	8.19	10.19	3.98	3.98
			PIR3	Pir3	Pir3	8.09	10.23			7.41				7.94	10.06	6.17	3.98
				CxA1													
				CxA2													
				CxA3													
			COApl														
			COAa1	ACo	ACo		9.95		2.33	9.16	9.76	4.50	3.22		10.06		
			COAa2			9.20		3.34									
			CLA														
			EPd	DEn	DEn	7.92	9.41	5.76	4.75	7.46	8.47	5.96	5.39	7.63	8.82	5.68	5.08
			EPv	VEn	VEn	9.16	9.75	4.59	3.93	7.46	9.14	5.57	4.74	8.40	9.28	5.20	4.68
			LA	LaDL	LaDL	7.62	8.62	5.31	5.07	7.25	8.24	5.42	4.83	7.51	8.66	5.07	4.54
			BLAa	BLA	BLA	7.87	9.37	5.11	4.12	7.74	8.72	5.35	4.59	7.97	9.15	4.97	4.03
					BLV												
			BMAa	BMA	BMA	8.84	9.59	4.06	3.03	8.58	9.41	4.73	3.24	8.94	9.71	4.26	3.21
			BMAp														
				AStr	ASt												
				IPAC													
				IMG													
			CEAl	CeL	CeL	7.60	8.43	4.67	4.05	7.42	8.18	4.31	3.83	7.83	8.34	4.00	3.70
			CEAm	CeM	CeM	7.60	8.68	4.34	3.33	7.51	8.48	4.20	3.43	7.55	8.84	3.97	3.29
			CEAc	CeC	CeC	8.03	8.73	4.66	3.16	7.39	8.43	4.59	4.01	7.55	8.76	4.34	3.82
			IA	IM	IM	8.77	8.96	3.61	3.24	8.28	8.78	4.64	3.76	8.71	9.07	4.13	3.56
			MEAad	MeAD	MeAD	8.28	9.16	3.26	2.53	8.16	9.33	3.34	2.78	8.13	9.41	3.77	2.75
			MEAav	MeAV	MeAV	8.79	9.18	2.63	2.44	9.03	9.24	3.03	2.81	9.12	9.70	3.22	2.75
			st	cst	cst	8.22	8.38	3.61	3.43	8.21	8.45	3.82	3.69	8.39	8.53	3.60	3.47
				aot													
				vaf													
				BAOT	BAOT												
			opt	opt	opt	8.38	9.01	2.76	1.74	8.75	9.84	2.69	1.68	8.80	9.73	2.65	1.96
			sup	sox	sod	8.47	9.00	2.45	1.63	8.90	10.18	2.44	0.50	9.00	9.79	2.34	1.74
			vlt		vlh												
				Acc													
				ns	ns												
				al													
				mfb	mfb												
			LHAd	LH	PLH	7.43		2.81		7.92	9.13	2.64	1.42	7.30	9.58	3.42	
			LHAjd														
			LHAjvd						0.83								
			LHAjvv				9.12										
			LHAsfa														
			LHApc														
			SOr	SOR	SOR	8.97	9.35	1.77	1.39	9.10	9.95	2.63	1.37	9.76	9.98	1.85	1.39
					TuLH												
				TC													
			TUi														
			TUsv														
			MEex	ME	MEE		9.74		0.00		10.19		0.01		10.23	0.37	0.00
			MEin		MEI	9.44		0.51									
			ARH	ArcL	ArcL	8.61	9.54	0.47	0.03			0.45			10.20	0.65	
				ArcM	ArcM						10.13		–0.01				
				ArcD	ArcD					9.20				9.26			0.00
			PVi	Pe	Pe	7.98	8.82	0.24	0.13	7.92	9.38	0.12	–0.01	8.30	9.35	0.05	0.00
			I														

Level			Structure			S Coordinate (mm)				PW1 Coordinate (mm)				PW2 Coordinate (mm)			
S	**PW1**	**PW2**	**S**	**PW1**	**PW2**	**D**	**V**	**L**	**M**	**D**	**V**	**L**	**M**	**D**	**V**	**L**	**M**
27	28	50	PVHpv														
			PVHmpd	PaMP	PaMP	7.50	7.98	0.57	0.09	7.89	8.47	0.49	0.11	7.92	8.31	0.13	0.00
			PVHlp	PaPo	PaPo	7.45			0.28	7.88	8.19	0.31	1.32	7.90	8.28	1.53	0.08
			PVHf				7.68	1.60									
			SBPV	SPa	SPa												
			AHNd	Stg	Stg	7.71	7.87	0.79	0.64	8.21	8.31	0.95	0.64	8.18	8.39	0.77	0.56
			AHNp	AHP	AHP	7.69	8.20	0.93	0.47	8.22	8.88	1.25	0.48	8.18	8.83	1.11	0.23
			AHNc	AHC	AHC	8.17	8.38	0.92	0.61	8.71	9.02	1.21	0.62	8.60	8.98	1.12	0.43
			VMHdm		VMHDM												
			VMHc		VMHC												
			VMHvl		VMHVL												
				VMHA													
					VMHSh												
			fx	f	f	7.74	8.12	1.49	1.27	8.19	8.76	1.59	1.33	8.35	8.86	1.48	1.24
			ZI	ZI	ZIR	7.02	7.49	2.44	0.46	7.24	7.88	2.00	0.53	7.30	7.92	2.28	0.69
			REcd	VRe, Re	VRe, Re			0.62		6.91	7.84	0.77	–0.06	6.92	7.72	0.91	0.00
			REcp			6.60	7.60		0.00								
			REcm	Xi													
					PaXi												
					A13												
			PR														
			SMT	Sub	Sub	6.44	6.90	0.89	0.50	6.67	7.34	0.84	0.31	6.74	7.43	0.95	0.36
			RH	Rh	Rh	6.23	6.61	0.47	0.00	6.61	6.99	0.51	–0.07	6.67	7.09	0.42	0.00
			VM	VM	VM	6.22	7.13	1.94	1.02	6.77	7.72	2.17	0.59	6.95	7.63	1.69	0.71
			mtt	mt	mt	6.17	6.97	1.21	0.94	6.61	7.27	1.17	0.75	6.61	7.25	1.18	0.76
			AMd	AM	AM	5.32	6.37	1.54	0.54	6.02		0.71		5.71		1.23	
			AMv														
			IAM	IAM	IAM	5.89	6.37	0.63	0.00				–0.07				0.00
			RT	Rt	Rt	4.31	7.27	3.94	2.23	4.66	7.46	3.50	1.86	4.70	7.31	3.48	1.69
				eml													
			VPL	VPL													
			VAL	VL	VL	4.63	6.93	3.41	1.36	5.05		2.80		5.03		3.19	
				VA	VA						6.94		0.53		7.26		1.13
			LD	LDVL	LDVL	3.93	4.59	3.00	1.76	4.13	5.01	2.64			5.09	2.67	
				LDDM	LDDM								1.35	4.37			1.51
			AV	AV	AVDM	4.71	5.42	2.13	1.57	4.84	5.72	1.87	1.21				1.10
					AVVL									4.87	5.82	2.00	
			AD	AD	AD	4.21	4.77	1.82	1.21	4.36	4.84	1.50	1.09	4.48	5.22	1.56	0.94
			MDl	MDL	MDL	4.59	5.56	1.58	0.78	4.67	5.61	1.09	0.75	5.21	5.54	1.06	0.68
			MDm	MDM	MD	4.72	5.60	1.06	0.33	4.66	5.77	0.93	–0.04	4.98	5.75	1.06	0.17
					PT												
			IAD														
				iml													
				CL													
				PC	PC												
			CM	CM	CM	5.59	5.85	0.58	0.00	5.34	6.12	0.82	0.04	5.70	6.19		0.00
			PVT	PVA	PVA	4.65	5.64	0.57	0.00	4.77	5.42	0.27	–0.01	5.01	5.73	0.27	0.00
			sm	sm	sm	4.37	4.68	1.20	0.54	4.44	4.82	1.08	0.26	4.78	5.06	0.95	0.30
			LH	LHb													
			MH	MHb	MHb	4.33	4.66	0.71	0.38	4.44	4.73	0.39	0.16	4.72	5.02	0.35	0.18
			CA3sr	CA3	CA3Rad					2.90	4.24	2.43	–0.04				
			CA3slu		CA3SLu												
			CA3sp		CA3Py												
			CA3so		CA3Or	2.61	4.05	3.09	0.06					2.91	4.51	2.45	0.05

Level			Structure			S Coordinate (mm)				PW1 Coordinate (mm)				PW2 Coordinate (mm)			
S	**PW1**	**PW2**	**S**	**PW1**	**PW2**	**D**	**V**	**L**	**M**	**D**	**V**	**L**	**M**	**D**	**V**	**L**	**M**
27	28	50	DGmb-po	DG						3.74	4.51	1.68	–0.04				
			DGmb-sg		GrDG									3.88			
			DGmb-mo		MoDG	3.68	4.35	1.68	0.09						4.83	1.51	0.00
			alv	alv	alv	2.52	4.08		0.29	2.84				2.76			
			fi	fi	fi		4.65	3.95			4.68	3.34			4.70	3.47	
			df	df	df	3.06	3.45	0.91	0.00	3.22	3.35	0.53	–0.01	3.55	3.71	0.42	0.00
				dhc	dhc												
				DHC													
			SF														
			cc	cc	cc				0.00	2.59			–0.01				0.00
			cing	cg	cg	2.17	3.04		0.49	2.28	2.93		0.27	2.29	3.25		0.42
			ec	ec	ec		8.67	5.68			7.54	5.53			9.14	5.19	
			amc														
			st	st	st	4.28	4.82	3.99	3.46	4.34	4.90	3.46	2.73				
					cst									4.40	4.93	3.60	2.83
					RtSt												
			tp														
			int	ic	ic	4.56	8.15	4.16	2.32	4.16	7.99	4.26	2.02	4.40	8.20	4.01	2.05
				MGP	IGP												
			CP	CPu	CPu	3.67	8.24	5.60	3.90	3.60	7.41	5.46	3.23	3.63	8.37	5.11	3.57
			GPe	LGP	EGP	5.02		4.74		5.74	7.80	4.43	2.97	5.36	7.97	4.38	2.99
			GPi				7.72		2.59								
			SI	SI													
				B	B												
28	31	55	IG	IG	IG	3.76	3.81	0.21	0.06	2.78	2.81	0.18	0.07	3.11	3.18	0.25	0.08
			RSPv	RSGb	RSGc		3.81		0.00	1.08	2.85		0.01	1.14	3.19		–0.01
			RSPd	RSA	RSD	1.53			0.02	0.50			0.00	0.41			0.06
			MOs	M2	M2	1.46			0.65	0.37			0.45	0.26			0.84
			MOp	M1	M1	1.32			1.03	0.34		1.80	1.11	0.23		2.02	1.53
			SSp	S1Tr	S1Tr	1.30		7.01	1.60	0.34				0.23			
				S1DZ	S1DZ												
				S1BF	S1BF							7.28					
					S1ULp											7.24	
			SSs	S2	S2	4.44	6.70	7.31		4.09		7.60		3.92		7.52	
				GI	GI												
				DI	DI												
			VISC														
			AIp		AIP		7.96	6.89									
				Ect													
			PERI	PRh													
			ENTI	LEnt													
			PIR1	Pir1	Pir1	8.74	10.81	6.66	4.15	7.89	10.39	7.27		7.80	10.31	7.10	4.75
			PIR2	Pir2	Pir2	8.69	10.58	6.45	4.25	7.90	10.18	7.03	4.66	7.80	10.16	6.94	4.69
			PIR3	Pir3	Pir3		10.47	6.39	4.26	7.61	10.05	7.00		7.39	10.00	6.87	4.62
			PAA1														
			PAA2														
			PAA3														
			COApl1		PLCo1		10.45		3.05								
			COApl2	PLCo	PLCo2	9.76	10.27	4.01	3.24	9.59	10.24	4.79	3.89	9.80	10.17	4.75	3.93
					PLCo3												
			COAa1	ACo	ACo		10.09		2.83	9.32	9.93	3.97	3.29	9.39	10.08	4.02	3.46
			COAa2			9.57		3.34									
			CLA														
			EPd	DEn	DEn	8.68	9.58	5.86	5.09	7.61	8.56	5.97	5.67	7.38	8.71	5.95	5.54
			EPv	VEn	VEn	9.64	9.91	4.93	4.39	8.52	9.34	5.72	5.28	8.65	9.22	5.80	5.25

Level			Structure			S Coordinate (mm)				PW1 Coordinate (mm)				PW2 Coordinate (mm)			
S	**PW1**	**PW2**	**S**	**PW1**	**PW2**	**D**	**V**	**L**	**M**	**D**	**V**	**L**	**M**	**D**	**V**	**L**	**M**
28	31	55	LA	LaDL	LaDL	8.00	8.97	5.41	4.49	6.97		5.74		7.08		5.52	
				LaVM	LaVM								4.88				4.88
				LaVL	LaVL						8.19				8.48		
			BLAa	BLA	BLA	8.77	9.38	4.64	3.87	7.88	8.97	5.37	4.41	7.95	9.12	5.25	4.28
			BLAp	BLP	BLP	8.81	9.60	5.30	4.06	8.06	8.97	5.68	5.23	8.27	9.12	5.59	5.20
				BLV	BLV												
			BMAa	BMA	BMA	9.28	9.72	3.65	3.26	8.86	9.50	4.64	3.60	8.87	9.52	4.06	3.55
			BMAp	BMP	BMP	9.36	9.98	4.36	3.54	9.05	9.51	4.64	4.13	8.80	9.53	4.62	4.00
				AStr	ASt												
					IMG												
				IPAC													
			CEAl	CeL	CeL	8.12	8.69	4.60	4.18	7.45	8.07	4.65	4.31	7.44	8.10	4.60	4.18
			CEAm	CeM	CeM	7.88	8.86	4.40	3.90	7.43	8.37	4.53	3.82	7.44	8.45	4.37	3.82
			CEAc	CeC	CeC	8.04	9.12	4.59	3.71	7.50	8.27	4.94	4.37	7.51	8.49	4.88	4.12
			IA	I	I	7.80	9.30	5.54	3.61	8.43	8.78	4.13	3.93	8.73	9.01	4.04	3.77
			MEApd-c	MePD	MePD	8.22		3.91		7.90	8.46	3.78	3.37	7.91	8.60	3.79	3.47
			MEApd-b				9.31										
			MEApd-a						2.46								
			MEApv	MePV	MePV	9.25	9.71	3.24	2.46	9.18	9.69	3.53	2.81	9.39	9.95	3.55	2.87
				MeAD	MeAD												
				BSTIA	STIA												
				lab													
			st	cst	cst	8.36	8.70	4.02	3.89	7.57	7.76	4.06	3.96	7.55	7.74	4.06	3.94
			opt	opt	opt	8.06	9.10	3.89	2.01	7.94	9.46	3.57	2.34	7.93	9.43	3.53	2.41
			sup	sox	sod	8.17	9.10	3.44	2.01	8.45	9.58	2.95	2.11	7.94	9.41	3.44	2.28
			vlt		vlh												
				ns	ns												
				mfb	mfb												
			LHAd	LH, MCLH, PeF	PLH, MCLH, PeFLH, PeF					7.88	9.26	2.65	1.19	7.58		0.76	
			LHAs														
			LHAjd			8.01			0.01								
			LHAjvd														
			LHAjvv				9.63										
			LHAsfp														
			LHAsfa														
			LHApc					2.36									
			LHAm														
			SOr	SOR													
					TuLH												
					PTe												
					MTu												
				TC													
			TUl														
			TUi														
			TUsv														
			MEex	MEE	MEE	9.86	10.05	0.33	0.00	10.34	10.45		0.00		10.28		–0.01
			MEin	MEI	MEI	9.81	9.96	0.24	0.00		10.34		0.02	10.12	10.20		–0.01
			ARH	ArcL	ArcL	9.15	9.90	0.52	0.09			0.67			10.22	0.50	
				ArcM	ArcM												
				ArcD	ArcD									9.41			–0.01
			PVi	Pe	Pe	8.19	9.28	0.20	0.01	8.17			0.02	8.18	9.56	0.10	–0.01
			I														
			DMHa	DMD	DMD	8.23	8.90	0.75	0.10	8.40	9.09	1.10	0.10	8.31	9.09	0.55	0.03
			VMHdm	VMHDM	VMHDM	8.84	9.47	0.83	0.24	9.22	9.75	0.81	0.19	8.95	9.54	0.54	0.09
			VMHc	VMHC	VMHC	9.18	9.80	0.85	0.37	9.38	9.99	0.94	0.28	9.05	9.86	0.87	0.17

Level			Structure			S Coordinate (mm)				PW1 Coordinate (mm)				PW2 Coordinate (mm)			
S	**PW1**	**PW2**	**S**	**PW1**	**PW2**	**D**	**V**	**L**	**M**	**D**	**V**	**L**	**M**	**D**	**V**	**L**	**M**
28	31	55	VMHvl	VMHVL	VMHVL	9.21	9.88	1.12	0.70	9.51	10.16	1.15	0.50	9.36	10.01	1.12	0.42
					VMHSh												
			fx	f	f	8.51	8.86	1.37	1.20	8.81	9.20	1.57	1.35	8.69	9.03	1.49	1.28
			ZI	ZI	ZIR	7.31	8.28	3.14	0.20	7.25	7.96	2.73	0.76	7.26	8.08	2.89	0.55
			ZIda														
				Subl													
				DA													
			REcd	VRe, Re	VRe, Re			0.45		7.08	7.71	0.84	0.01	6.96	7.84	0.90	–0.01
			REcp			7.28	8.15		0.00								
			REcm														
					PaXi												
				A13	A13												
			PR														
				scp													
			SMT	SubD	SubD	6.81	7.62	1.14	0.34	6.62				6.58			0.22
				SubV	SubV						7.44	0.89	0.18		7.53	1.11	
			RH	Rh	Rh	6.73	7.27	0.58	0.00	6.58	7.11	0.42	0.01		7.09		0.00
			VM	VM	VM	6.79	7.75	1.69	1.06	6.71	7.73	2.28	0.71	6.72	7.61	2.81	0.95
			mtt	mt	mt	7.56	7.85	1.08	0.87	7.46	7.78	1.15	0.83	7.37	7.73	1.17	0.80
			RT	Rt	Rt	4.85	7.42	4.24	3.14	4.49	7.30	4.01	2.52	4.43	7.27	4.12	2.48
			em	eml	ml	7.29	7.63	3.09	2.19					6.87	7.12	3.19	2.58
			VPL	VPL	VPL	5.72	7.40	3.88	2.70	5.09	7.31	3.67	1.96	4.91	7.11	3.79	2.34
			VPM	VPM	VPM	5.66	7.47	3.51	2.24	5.24	6.93	3.33	1.92	5.54	6.96	3.29	2.26
			VAL	VL	VL	5.29	7.69	3.34	1.54	5.91	7.36	2.40	0.39	5.89	7.09	2.43	
				Po	Po												
				Ang	AngT												
			LD	LDVL	LDVL	4.60	5.47	3.27	1.75	4.06	5.29	3.11		4.05	5.20	3.34	
				LDDM	LDDM								1.35				1.37
			MDl	MDL	MDL	5.03	6.32	1.84	0.81	4.79	5.86	1.18	0.86	4.65	6.22	1.45	0.40
			MDc	MDC	MDC	5.57	6.20	1.01	0.67		5.83	0.43		4.75	5.66	1.18	0.67
			MDm	MDM	MDM	5.40	6.32	0.95	0.14	4.85	6.08	0.13	1.02	4.93	5.95	0.89	0.13
			IMD	IMD	IMD	5.91	6.30	0.24	0.00	5.22	5.77	0.16	0.00	5.36	5.91	0.31	–0.01
			CL	CL	CL	4.96	6.19	2.47	1.54	4.41	5.88	1.57		4.59		1.74	1.25
			PCN	PC	PC	6.09	6.74	2.02	1.35	5.81	6.45	1.43	0.66				
			CM	CM	CM	6.30	6.87	1.34	0.00	5.72	6.59	0.89	–0.01	5.90	6.70		0.00
			PVT	PV	PV	5.28	5.97	0.36	0.00	4.68	5.29	0.36	–0.02	4.90	5.46	0.29	0.00
			sm	sm	sm	5.03	5.34	1.34	0.38	4.33	4.90	1.05	0.17	4.60	4.79	1.26	0.32
			LH	LHb	LHb	5.15	5.38	1.27	0.54	4.54	4.86	0.96	0.35	4.68	4.97	1.17	0.42
			MH	MHb	MHb	5.03	5.35	0.52	0.22	4.43	4.85	0.38	0.10	4.55	4.96	0.46	0.14
			CA1slm	CA1	CA1LMol		4.41			2.61	3.99		0.02				
			CA1sr		CA1Rad												
			CA1sp		CA1Py												
			CA1so		CA1Or	3.21			0.00					2.36			–0.01
			CA2sr	CA2	CA2Rad												
			CA2sp		CA2Py												
			CA2so		CA2Or												
			CA3sr	CA3	CA3Rad												1.26
			CA3slu		CA3SLu						3.98	3.38					
			CA3sp		CA3Py				1.08								
			CA3so		CA3Or		4.77	3.84							4.15	3.45	

Level			Structure			S Coordinate (mm)				PW1 Coordinate (mm)				PW2 Coordinate (mm)			
S	**PW1**	**PW2**	**S**	**PW1**	**PW2**	**D**	**V**	**L**	**M**	**D**	**V**	**L**	**M**	**D**	**V**	**L**	**M**
28	31	55	DGlb-mo, DGmb-mo	PoDG, DG	MoDG	3.88	5.04	2.03	0.00	3.50	4.52	1.98	0.02		4.66		–0.01
			DGlb-sg, DGmg-sg		GrDG												
			DGlb-po, DGmb-po		PoDG												
			alv	alv	alv	3.17	4.74		0.23	2.55				2.32			
			fi	fi	fi		5.24	4.45			4.66	4.00			4.54	4.15	
			df	df	df	3.97	4.13	0.61	0.00	3.06	3.19	0.53	0.03	3.34	3.51	0.48	0.06
				dhc	dhc												
				DHC													
			FC														
			cc	cc	cc	3.01			0.00	2.42			0.04	2.20			–0.01
			cing	cg	cg	2.88	3.79		0.39	2.13	2.78		0.59	1.88	3.05		0.53
			ec	ec	ec		9.24	5.78			7.64	5.75			9.10	5.67	
			amc														
			st	st	st	5.01	5.46	4.53	3.62	4.41	4.87	4.10	3.37	4.31		4.23	
					cst										4.76		3.50
			int	ic	ic	5.01	8.49	4.96	1.90	4.19	8.39	4.65	2.23	3.92	8.45	4.95	2.35
			cpd														
			GPi	MGP	IGP	8.00	8.26	2.85	1.92	7.30	8.24	3.53	2.28	7.31	8.05	3.61	2.69
			CP	CPu	CPu	4.33	8.64	5.68	4.45	3.89	7.50	5.65	3.93	3.55		5.60	4.23
			GPe	LGP	EGP	6.28	7.79	5.04	3.73	5.54		4.73		5.60	7.88	4.79	3.37
			SI														
				B	B												
29	32	58	IG	IG	IG	2.99	3.06	0.18	0.06	2.64	2.70	0.25	0.11	3.20	3.21	0.13	0.08
			RSPv	RSGb	RSGc		3.06			0.80	2.71		0.01	1.44	3.27		0.00
			RSPd	RSA	RSD	0.63				0.37			0.01	0.50			0.00
			MOs	M2	M2	0.51			0.59	0.28			0.66	0.46			1.00
			MOp	M1	M1	0.42			1.06	0.26		1.92	1.23	0.46		2.48	1.72
			SSp	S1Tr	S1Tr	0.39		6.94		0.27				0.49			
				S1DZ	S1DZ												
				S1BF	S1BF							6.54					
					S1ULp											7.10	
			SSs	S2	S2	3.57		7.30		3.05		6.91		4.22		7.27	
					GI												
					DI												
				AuD	AuD												
			AUDv	AuV													
			TEa														
			ECT	Ect	Ect			6.99		6.34		7.19			7.16	7.29	
			PERI	PRh	PRh					7.11		6.97			8.18	6.99	
			ENTI	LEnt													
			PIR1	Pir1	Pir1		10.72	6.67	4.52	7.82	10.44	6.98		8.14	10.36	6.88	5.28
			PIR2	Pir2	Pir2	8.46	10.53	6.39	4.56	7.83	10.21	6.84	4.67	8.10	10.18	6.67	5.24
			PIR3	Pir3	Pir3		10.40	6.37		7.83	10.07	6.79		7.72	9.99	6.54	5.13
			PAA1		RAPir1												
			PAA2		RAPir2												
			PAA3		RAPir3												
			COApl1	PLCo1	PLCo1	9.58	10.46		2.95						10.44	4.88	
			COApl2	PLCo2	PLCo2	9.53	10.21	4.05	3.01	9.42	10.08	4.40	3.67	9.95	10.21	4.84	3.95
			COApl3	PLCo3	PLCo3	8.75			2.76					9.36	10.03	4.82	3.57
			COAa1														
			COAa2														

Level			Structure			S Coordinate (mm)				PW1 Coordinate (mm)				PW2 Coordinate (mm)			
S	PW1	PW2	S	PW1	PW2	D	V	L	M	D	V	L	M	D	V	L	M
29	32	58	EPd	DEn	DEn	8.35	9.58	5.82	4.93	7.84	8.82	5.94	5.57	7.82	8.90	5.79	5.42
			EPv	VEn	VEn	9.45	9.75	4.90	4.54	8.41	9.21	5.61	5.18	8.90	9.34	5.56	5.20
			LA	LaDL	LaDL	7.57	8.47	5.44	4.45	6.93		5.58		7.14		5.52	
				LaVM	LaVM								4.63				4.51
				LaVL	LaVL						8.39				8.65		
			BLAa	BLA	BLA	8.47	9.15	4.55	3.84	8.05	8.78	5.13	4.29	8.42	9.15	4.98	4.12
			BLAp	BLP	BLP	8.38	9.40	5.35	4.38	8.24	8.90	5.56	4.85	8.50	9.25	5.47	4.78
				BLV	BLV												
				BMA													
			BMAp	BMP	BMP	9.05	9.65	4.51	3.75	8.62	9.41	4.85	4.19	9.08	9.67	4.67	3.66
				AStr	ASt												
			CEAl	CeL	CeL	7.64	8.31	4.53	4.13	7.14	8.06	4.52	4.12	7.64	8.06	4.56	4.16
					CeM												
			CEAc	CeC	CeC	7.94	8.41	4.70	4.10	7.45	8.09	4.82	4.34	7.66	8.46	4.76	4.08
			IA	I	I	7.82	8.90	4.14	3.55	8.57	9.18	4.12	3.73	8.69	9.47	4.07	3.52
			MEApd-c	MePDc	MePD							3.85		7.75	9.25	4.09	2.87
			MEApd-b	MePDb						7.72							
			MEApd-a	MePDa		7.85	8.75	3.90	2.54		8.79		2.97				
			MEApv	MePV	MePV	8.61	9.80	3.02	2.26	8.51	9.49	3.82	2.77	9.00	9.94	3.66	2.82
				BSTIA	STIA												
			st	st	cst	7.36	8.96	4.47	2.74	7.02	7.77	4.26	3.93				
					st									7.04	7.87	4.52	3.77
			st														
			opt	opt	opt	7.51	8.56	4.05	2.38	7.45	9.15	3.83	2.42	7.54	9.11	3.92	2.58
			sup	sox	sod	7.29	7.62	4.33	3.73	8.11	9.29	3.02	2.26	7.87	9.09	3.40	2.55
			vlt														
				ns	ns												
				mfb	mfb												
			LHAd	LH, MCLH, PeF	PLH, MCLH, PeFLH, PeF					8.07		2.65	1.08	7.51	9.65	2.94	0.52
			LHAs														
			LHAjd			7.49			0.00								
			LHAjvd														
			LHAjvv				9.51										
			LHAsfp														
			LHAvm					2.63									
			LHAm														
					TuLH												
					PTe												
				MTu	MTu												
					Te												
				TC													
			TUl														
			TUi														
			TUsv														
			MEex	MEE	MEE	9.72	9.98	0.42	0.00	10.15	10.36		0.00	10.11	10.27		0.01
			MEin	MEI	MEI	9.71	9.83	0.27	0.00	10.10	10.19	0.30	0.00	10.08	10.21	0.21	0.01
			ARH	ArcL	ArcL	9.11	9.88	0.63	0.09		10.20	0.71			10.26	0.47	
				ArcM	ArcM								–0.01				
				ArcD	ArcD					9.31				9.43			0.00
			PVi	Pe	Pe	7.86	9.16	0.16	0.00	7.99	9.52	0.12	0.01	8.19	9.50	0.08	0.00
			I														
			DMHa	DMD	DMD	7.87	8.75	0.89	0.02	8.21	9.08	1.00	0.10	8.31	9.10	0.84	0.07
			DMHp	DMC	DMC	8.39	8.90	0.38	0.15	8.70	9.15	0.41	0.09	8.76	9.27	0.39	0.06

Level			Structure			S Coordinate (mm)				PW1 Coordinate (mm)				PW2 Coordinate (mm)			
S	PW1	PW2	S	PW1	PW2	D	V	L	M	D	V	L	M	D	V	L	M
29	32	58	VMHdm	VMHDM	VMHDM	8.78	9.26	0.78	0.23	9.19	9.60	0.98	0.15	9.15	9.62	0.73	0.15
			VMHc	VMHC	VMHC	9.03	9.49	1.01	0.32	9.48	9.86	1.09	0.19	9.34	10.02	0.94	0.21
			VMHvl	VMHVL	VMHVL	9.32	9.79	1.07	0.52	9.62	10.14	1.18	0.49	9.59	10.11	1.12	0.63
					VMHSh												
			fx	f	f	8.34	8.53	1.30	1.16	8.71	9.06	1.51	1.28	8.87	9.17	1.42	1.14
			ZI	ZI	ZID	6.88	7.89	3.26	0.80	7.00		2.94		7.23	8.06		0.95
					ZIV						7.95		0.70				
			PH														
				Subl	Subl												
				DA	DA												
				Do													
					PHD												
			REcd	VRe, Re	VRe, Re	6.78		0.45		6.94	7.53	1.02	0.03	7.11	7.83	0.78	0.00
			REcp				7.85		0.00								
				A11													
			PR														
				scp													
			SMT	Sub	Sub	6.50	7.27	1.09	0.35	6.74	7.16	0.73	0.32	6.81	7.51	0.94	0.18
			RH	Rh	Rh	6.08	6.97	0.80	0.00	6.62	6.84	0.49	0.01	6.82	7.13	0.48	0.00
			VM	VM	VM	6.35	7.38	1.50	0.77	6.62	7.49	2.65	0.88	6.88	7.66	2.45	0.90
			mtt	mt	mt	7.34	7.55	1.12	0.87	7.48	7.80	1.15	0.83	7.61	7.95	1.08	0.72
			RT	Rt	Rt	4.33	7.04	4.26	3.22	4.47		4.04		4.51		4.12	
			em	ml	ml	6.62	7.33	3.19	1.79	6.85	7.05	2.98	1.86	6.75	7.32	3.50	2.09
				eml													
			VPL	VPL	VPL	5.19	7.09	4.00	2.13		7.00	3.71	1.97	5.28	7.24	3.77	2.45
			VPM	VPM	VPM	4.95	7.07	3.66	1.90	5.00	6.88	3.38	1.84	5.14	7.23	3.53	2.02
			VAL	VL	VL	4.86	7.29	3.35	1.44	5.81		2.05		6.00	7.16	2.30	0.56
				Po	Po												
			LD	LDVL	LDVL	3.95	5.11	3.58	1.52	3.97		3.47	1.60	4.12	5.37	3.46	
				LDDM	LDDM						5.18						1.26
				LPMR													
			MDl	MDL	MDL	4.80	5.89	1.59	0.81	4.71	5.83	1.20	0.89	4.93	6.50	1.52	0.37
			MDc	MDC	MDC	4.90	5.75	1.20	0.48	4.69	5.88	1.08	0.42	4.82	6.29	1.18	0.65
			MDm	MDM	MDM	4.81	5.86	0.95	0.13	4.75	6.07	1.07	1.07	5.10	6.36	0.81	0.14
			IMD	IMD	IMD	5.09	5.78	0.53	0.00	5.25	5.82	0.17	0.02	5.75	6.36	0.37	0.00
			CL	CL	CL	4.37	5.68	1.90	1.12	4.39	5.81	1.60	1.05	4.65			1.17
			PCN	PC	PC	5.66	6.30	1.75	1.14	5.80	6.59	1.43	0.68				
			CM	CM	CM	5.75	6.33	1.10	0.00	5.80	6.64	0.91	0.04	6.32	6.84		0.00
			PVT	PVP	PVP	4.73	5.10	0.15	0.00	4.63	5.39	0.31	0.00	5.02	5.84	0.40	0.00
			sm	sm	sm	4.30	4.59	1.32	0.37	4.16	4.56	1.10	0.26	4.53	4.88	1.26	0.17
			LH	LHbL	LHbL	4.48	4.87	1.24	0.47			1.09				1.06	
				LHbM	LHbM					4.42	4.89		0.29	4.74	5.18		0.35
			MH	MHb	MHb	4.30	4.80	0.55	0.14	4.26	4.75	0.45	0.16	4.56	5.03	0.40	0.10
			CA1slm	CA1	CA1LMol		3.72			2.42			0.03		4.06		
			CA1sr		CA1Rad												
			CA1sps		CA1Py												
			CA1spd														
			CA1so		CA1Or	2.32			0.00					2.42			0.00
			CA2sr	CA2	CA2Rad												
			CA2sps		CA2Py												
			CA2so		CA2Or												

Level			Structure			S Coordinate (mm)				PW1 Coordinate (mm)				PW2 Coordinate (mm)			
S	PW1	PW2	S	PW1	PW2	D	V	L	M	D	V	L	M	D	V	L	M
29	32	58	CA3sr	CA3	CA3Rad				1.29		3.86	3.77					
			CA3slu		CA3SLu												
			CA3sps		CA3Py												1.51
			CA3so		CA3Or		4.04	4.19							4.08	3.85	
			DGlb-mo, DGmb-mo	PoDG	MoDG	3.05	4.42		0.03	3.06	4.41		0.02	3.15	4.69	2.93	0.01
			DGlb-sg, DGmg-sg		GrDG												
			DGlb-po, DGmb-po		PoDG												
			alv	alv	alv	2.27		4.33	0.19	2.35			0.42	2.33			0.00
			fi	fi	fi		4.72	4.66			4.69	4.21			4.81	4.38	
			df	df	df	3.07	3.35	0.80	0.00	2.93	3.02	0.50	0.12	3.35	3.57	0.59	0.11
				dhc	dhc												
			FC		FC												
			cc	cc	cc	2.06			0.00	2.17			0.05	2.25			0.00
			cing	cg	cg	1.93	3.02		0.43	1.92	2.69		0.41	2.06	3.19		0.26
					dcw												
			ec	ec	ec		8.27	5.78			8.17	5.67			9.25	5.59	
			amc														
			st	st	st	4.59	5.22	4.67	3.79	4.44	5.02	4.39	3.57	4.62		4.50	3.77
					cst										5.04		
			int	ic	ic	4.60		5.09		4.42	8.51		1.94	3.82	8.69	5.03	2.22
			cpd				8.26		2.12								
				MGP													
			CP	CPu	CPu	4.85	8.09	5.67	4.28	3.94	7.30	5.55	4.26	4.09		5.51	4.67
			GPe	LGP	EGP	6.55	7.55	4.94	4.51	5.77	7.49	4.71	3.66	6.03	7.73	4.83	3.55
			SI														
				B	B												
30	33	60	IG	IG	IG	2.97	3.04	0.20	0.08	2.71	2.78	0.17	0.01	3.11	3.09	0.11	0.04
			RSPv	RSGb	RSGc		3.04		0.00	0.61	2.78		–0.01	1.17	3.14		0.00
			RSPd	RSA	RSD	0.61				0.40			0.11	0.38			0.05
			MOs	M2	M2	0.41			0.57	0.35			0.82	0.27			1.06
			MOp	M1													
					MPtA												
					LPtA												
			SSp	S1Tr	S1Tr	0.38		6.87		0.36				0.52			
				S1DZ	S1DZ												
				S1BF	S1BF							6.48				7.00	
				S2	S2									2.95		7.31	
			AUDd	AuD	AuD	3.33		7.03		3.47		7.29		3.62		7.56	
			AUDp	Au1	Au1	3.91		7.36		4.27		7.52		4.44		7.69	
			AUDv	AuV	AuV	5.18		7.40		5.35		7.53		5.34	6.14	7.69	
			TEa														
			ECT	Ect	Ect		7.83	7.13		6.33	7.14	7.45			6.89	7.65	
			PERI	PRh	PRh		8.29	6.73			7.68	7.01			7.67	7.48	
			ENTI	LEnt	LEnt			6.77			7.97	7.01			8.03	7.48	
			PIR1	Pir1	Pir1	8.56	10.86	6.77	4.87	7.92		6.95		8.00	10.34	7.44	5.89
			PIR2	Pir2	Pir2	8.55	10.68	6.55	4.91	7.94	10.32	6.73	4.91	7.99	10.13	7.20	5.85
			PIR3	Pir3	Pir3		10.57	6.51		7.72	10.13	6.66		7.83	10.01	7.13	5.64
			PAA1		RAPir1												
			PAA2		RAPir2												
			PAA3		RAPir3												
			COApl1	PLCo1	PLCo1		10.60										

Level			Structure			S Coordinate (mm)				PW1 Coordinate (mm)				PW2 Coordinate (mm)			
S	PW1	PW2	S	PW1	PW2	D	V	L	M	D	V	L	M	D	V	L	M
30	33	60	COApl2	PLCo2	PLCo2	9.56	10.32	4.08	3.06	9.49	10.20	4.27	3.47	10.02	10.32	5.38	4.17
			COApl3	PLCo3	PLCo3		10.09										
			COApm1														
			COApm2	PMCo2	PMCo	8.58	9.63	3.06	2.37	9.36	9.85	3.63	3.15	9.56	10.19	4.30	3.29
			COApm3														
			EPd	DEn	DEn	8.54	9.65	5.87	5.24	7.72	8.87	5.93	5.51	7.83	8.97	6.32	5.88
			EPv	VEn													
			LA	LaDL	LaDL	7.61	9.06	5.58	4.58	6.84		5.58		6.91			
				LaVM	LaVM								4.48				4.85
				LaVL	LaVL						8.55				8.72	5.88	
				BLA	BLA												
			BLAp	BLP	BLP	8.57	9.78	5.23	4.40	8.35	9.08	5.44	4.69	8.62	9.23	5.89	5.27
				BLV	BLV												
			BMAp	BMP	BMP	8.66	9.57	4.73	3.72	8.94	9.60	4.97	3.77	9.00	9.68	4.13	5.38
			PA														
					AHiAL												
				AStr	ASt												
			CEAl	CeL	CeL	7.76	8.13	4.78	4.48	7.48	7.84	4.41	4.12	7.75	8.12	4.64	4.41
					CeM												
				CeC	CeC												
			IA	I	I	8.35	8.58	4.66	4.46	8.68	9.35	4.12	3.63	8.70	9.10	4.37	3.96
			MEApd-c	MePD	MePD	8.06	8.69	3.90	2.80	7.84	9.14	3.89	2.63	7.80	9.01	4.27	3.25
				MePV	MePV												
				BSTIA	STIA												
			st	st	st	6.39	9.09	4.88	2.83	6.84		4.43		6.81	8.19	4.85	4.24
			st														
			opt	opt	opt	7.24	8.49	4.36	2.44	7.28	9.08	3.95	2.33	7.11	8.80	4.42	3.00
			sup	sox	sod	6.23	7.47	4.79	4.03	7.77	9.05	3.44	2.32	7.25	8.79	4.23	2.94
			vlt														
				ns	ns												
				mfb	mfb												
			LHAd	LH, MCLH, PeF	PLH, PeFLH, PeF					8.10		2.50	0.67	8.06		2.81	0.69
			LHAs						0.00								
			LHAjd														
			LHAjvv				9.55										
			LHAsfp														
			LHAvm														
			LHAvl														
			LHAm														
					TuLH												
				MTu	MTu												
			TUl														
			TUte	Te	Te	9.11	9.46	1.68	1.50	9.27	9.61	1.87	1.56	9.18	9.47	2.25	1.90
			TUi														
			TUsv														
			MEex	MEE	MEE	9.88	10.14	0.40	0.00	10.41	10.54		–0.06		10.31	0.34	0.00
			MEin	MEI	MEI		10.07	0.28	0.00		10.47	0.32	–0.06		10.23		0.00
			ARH	ArcL	ArcL	9.12	10.01	0.59	0.09			0.71			10.15	0.80	
				ArcM	ArcM						10.41						0.02
				ArcD	ArcD					9.59			–0.01	9.36			
			PVi	Pe	Pe	7.76	9.24	0.22	0.00	8.18	9.68	0.12	–0.02	8.16	9.37	0.09	0.00
			I														
			DMHa	DMD	DMD	8.10	8.68	0.63	0.20	8.45	9.20		0.07	8.27	8.72	0.84	0.08

Level			Structure			S Coordinate (mm)				PW1 Coordinate (mm)				PW2 Coordinate (mm)			
S	**PW1**	**PW2**	**S**	**PW1**	**PW2**	**D**	**V**	**L**	**M**	**D**	**V**	**L**	**M**	**D**	**V**	**L**	**M**
30	33	60	DMHp	DMC	DMC	8.16	9.01	0.80	0.21	8.61	9.59	0.84	0.07	8.51	9.04	0.86	0.08
			DMHv	DMV	DMV	8.45	9.22	0.81	0.32		9.42	1.00	0.16	8.61	9.35	0.86	0.08
				VMHDM													
			VMHc	VMHC													
			VMHvl	VMHVL													
					VMH												
					VMHSh												
			fx	f	f	8.63	8.89	1.24	1.07	8.96	9.22	1.42	1.13	8.83	9.09	1.56	1.27
			ZI	ZID	ZID	6.82	8.00	3.47	0.68								
				ZIV	ZIV					7.18	8.10	2.85	0.66	6.66	8.13	3.97	1.34
			PH	PH													
				Subl	Subl												
			STN		STh												
					DA												
					PHD												
			REcp	Re	Re	6.83	7.77	0.31	0.00	6.99	7.52	0.20	–0.11	7.01	7.66	0.44	0.00
				VRe	VRe												
				A11													
			PR														
				scp													
			SMT		Sub	6.77	7.07	0.93	0.43								
			RH		Rh												
			VM	VM	VM	6.48	7.36	1.64	0.83	6.70	7.64	1.76	0.60	6.80	7.55	2.14	0.74
			mtt	mt	mt	7.49	7.77	1.01	0.74	7.72	8.00	1.05	0.77	7.69	8.02	1.19	0.84
			RT	Rt	Rt	4.49	7.36	4.28	3.07	4.58	7.40	3.99	2.61	4.54	6.78	4.43	3.61
			em	ml	ml	4.57	7.18	3.98	1.82	5.02		3.78			7.29		1.87
				eml	eml						7.71		0.83	4.90		4.10	
			VPL	VPL	VPL	5.29	6.91	3.92	1.99	5.17	7.20	3.64	2.04	5.27	7.07	4.02	2.85
			VPM	VPM	VPM	4.86	6.82	3.74	1.85	5.02	7.22	3.34	1.33	4.95	7.19	3.77	1.70
			VAL														
			PO	Po	Po	5.02	5.83	2.98	1.85				0.97	4.76	6.94	3.63	1.11
			LP	LPMR	LPMR	4.57	5.18	2.34	1.62	4.09	5.23	1.98	1.15	4.10	5.33	2.38	1.45
			LD	LDVL	LDVL	3.92	4.99	3.69	1.58	4.05		3.39		3.98	5.03	3.79	2.09
				LDDM							5.09		1.55				
			MDl	MDL	MDL	4.69	6.24	1.57	0.53	4.99	5.90	1.11	0.87	4.69	6.21	1.56	1.07
			MDc	MDC	MDC	4.90	6.05	1.24	0.35	5.09	6.00	0.93	0.41	4.98	5.91	1.17	0.71
			MDm	MDM	MDM	4.93	6.24	0.73	0.14	5.00	6.23		0.09	5.12	6.23	1.11	0.24
			IMD	IMD	IMD	5.56	6.25	0.49	0.00	5.18	6.06	0.23	0.02	5.49	6.17	0.38	0.00
			CL	CL	CL	4.39	6.02	1.81	1.37	4.46	5.93	1.39	0.99	4.52	5.93	1.81	1.25
			PCN	PC	PC	6.03	6.45	1.71	1.10	5.86	6.80	1.28	0.37	5.91		1.74	
			CM	CM	CM	6.25	6.71	1.16	0.00	6.07	6.80	0.55	0.02	6.16			0.00
				iml													
				imvc	imvc												
					OPC												
			PVT	PVP	PVP	4.84	5.61	0.19	0.00	4.78	5.38	0.35	–0.02	4.99	5.56	0.53	0.00
			sm	sm	sm	4.24	4.78	1.33	0.42	4.24	4.57	1.03	0.23	4.27	4.77	1.31	0.29
			LH	LHbL	LHbL	4.39	4.96	1.28	0.45	4.55	5.13	1.01	0.64			1.25	
				LHbM	LHbM					4.49	5.13	0.67	0.26	4.54	5.09		0.30
			MH	MHb	MHb	4.23	4.90	0.61	0.13	4.32	4.86	0.33	0.08	4.34	4.99	0.47	0.09

Level			Structure			S Coordinate (mm)				PW1 Coordinate (mm)				PW2 Coordinate (mm)			
S	PW1	PW2	S	PW1	PW2	D	V	L	M	D	V	L	M	D	V	L	M
30	33	60	CA1slm	CA1	CA1LMol		3.82			2.36	3.78		–0.01		4.20		0.00
			CA1sr		CA1Rad												
			CA1sps		CA1Py												
			CA1spd														
			CA1so		CA1Or	2.23			0.08					2.22			
			CA2sr	CA2	CA2Rad												
			CA2sps		CA2Py												
			CA2so		CA2Or												
			CA3sr	CA3	CA3Rad				1.44								
			CA3slu		CA3SLu							3.85	1.22				
			CA3sps		CA3Py												1.83
			CA3so		CA3Or		4.01	4.48							4.01	4.37	
			DGlb-mo, DGmb-mo	PoDG	MoDG	2.95	4.43				4.51		–0.01	2.94	4.63	3.59	0.35
			DGlb-sg, DGmg-sg		GrDG												
			DGlb-po, DGmb-po		PoDG												
			DGcr														
			alv	alv	alv	2.20			0.20	2.30		4.06	0.19	2.17			
			fi	fi	fi		5.03	4.86			4.85	4.30			4.86	4.73	
			df	df	df	3.12	3.36	0.72	0.00	2.89	3.03	0.53	0.09	3.19	3.41	0.73	0.26
				dhc	dhc												
			FC	FC	FC	3.33	3.60	0.31	0.00								
			cc	cc	cc				0.00				0.01				0.00
			cing	cg	cg	2.00	2.99		0.44	2.02	2.63		0.55	1.92	2.97		0.52
			ec	ec	ec		8.48	5.88			7.94	5.61			9.23	5.93	
			amc														
			st	st	st	4.82	5.47	4.93	4.01	4.71	5.08	4.33	3.66	4.74		4.74	4.10
					cst										5.16		
			int	ic	ic	4.71		5.51			8.72		1.89		8.84		2.40
			cpd				8.51		2.10								
				MGP													
			CP	CPu	CPu	5.46	8.10	5.79	4.50	4.33		5.51		4.96		5.80	
				LGP													
31	34	62	IG	IG	IG	2.97	3.03	0.20	0.05	2.70	2.75	0.30	0.14	3.04	3.05	0.16	0.10
			RSPv	RSGb	RSGc		3.03		0.00	0.80	2.79		0.06	1.01	3.10		0.00
			RSPd	RSA	RSD	0.80				0.48			0.07	0.33			0.00
			MOs	M2													
			MOp	M1													
					MPtA												
					LPtA												
			SSp	S1Tr		0.43		6.83		0.35							
				S1BF	S1BF							6.47		0.98		7.03	
				S2	S2												
			AUDd	AuD	AuD	3.09		7.02		3.18		7.22		3.92		7.47	
			AUDp	Au1	Au1	3.53		7.35		4.04		7.53		4.56	5.69	7.55	
			AUDv	AuV	AuV	4.80		7.41		5.75		7.53			6.33	7.55	
			TEa														
			ECT	Ect	Ect		7.90	7.18		6.32		7.51			7.12	7.48	
			PERI	PRh	PRh			6.77		7.01		7.24			7.72	7.22	
			ENTI	LEnt	LEnt	8.31	8.89	6.81		7.56	7.83	7.26			8.16	7.22	
			PIR1	Pir1	Pir1	8.79		6.77		7.81		7.25		8.12	10.27	7.15	5.92
			PIR2	Pir2	Pir2	8.80		6.51		7.84	10.20	7.09	5.55	8.11	10.11	6.99	5.89

Level			Structure			S Coordinate (mm)				PW1 Coordinate (mm)				PW2 Coordinate (mm)			
S	PW1	PW2	S	PW1	PW2	D	V	L	M	D	V	L	M	D	V	L	M
31	34	62	PIR3	Pir3	Pir3	8.63		6.47		7.72	10.07	7.06		7.88	9.96	6.94	5.65
			PAA1		RAPir1												
			PAA2		RAPir2												
			PAA3		RAPir3												
			COApl1	PLCo1	PLCo1					9.71			3.39	9.93	10.35	5.49	
			COApl2	PLCo2	PLCo2					9.60	10.21	5.15	3.49	9.81	10.16	5.47	4.06
			COApl3	PLCo3	PLCo3					9.26			3.76	9.39	10.04	5.45	4.11
			COApm1	PMCo	PMCo					8.99	9.73	3.89	2.67	9.32	10.07	4.11	2.98
			COApm2														
			COApm3														
			EPd	DEn	DEn	8.56	9.52	5.82	5.38	7.74	8.75	6.12	5.72	7.73	9.03	6.15	5.72
			EPv	VEn													
			LA	LaDL	LaDL	7.35	9.02	5.63	4.59	6.65		5.88		7.06		5.79	
				LaVM	LaVM								4.77		8.80		4.61
				LaVL							8.39						
			BLAp	BLP	BLP	8.86	9.97	5.26	4.41	8.21	9.21	5.75	4.42	8.35	9.32	5.71	4.45
				BLV													
			BMAp	BMP	BMP	8.88	9.70	4.82	3.84	8.62	9.57	5.33	4.02	8.76	9.48	5.34	3.66
			PA														
			DGb														
			TEP														
			CA3														
				AHiAL	AHiAL												
				AStr	ASt												
				MePD	MePD												
					MePV												
				BSTIA	STIA												
			st	st	st	5.13	9.16	4.99	2.59	4.93	8.36	4.91	3.99		8.92	4.96	3.43
					cst									5.00			
			st	st													
			st														
			opt	opt	opt	7.56	8.41	4.23	2.83	6.88	8.70	4.28	2.86	6.93	8.47	4.39	3.29
				sox	sod												
			vlt														
				ns	ns												
				mfb	mfb												
			LHAd	LH, PeF	PLH, PeFLH, PeF					8.14	9.44	2.48	1.00				0.55
			LHAjvv						0.00								
			LHAvm					2.11									
			LHAvl														
					TuLH												
					MTu												
			TUl														
			TUte	Te	Te	9.15	9.36	1.60	1.44	9.35	9.70	1.92	1.58	9.30	9.61	1.94	1.58
			TUi														
			INFex	InfS	InfS	9.90	10.18	0.45	0.00	10.42	10.60	0.37	–0.01	10.14	10.32	0.28	0.00
			INFin														
				ArcL	ArcMP, ArcLP												
				ArcM													
				ArcD													
			PVi	Pe	Pe	7.72	9.54	0.18	0.00	7.83			–0.02	7.94	9.45	0.09	0.00
			PVp														
			I														

Level			Structure			S Coordinate (mm)				PW1 Coordinate (mm)				PW2 Coordinate (mm)			
S	PW1	PW2	S	PW1	PW2	D	V	L	M	D	V	L	M	D	V	L	M
31	34	62	DMHa	DMD	DMD	8.37	9.31	0.35	0.16	8.84	9.49	0.23	0.09	8.78			0.07
			DMHp		DMC												
			DMHv	DMV	DMV	8.72	9.62	0.70	0.24	8.84	9.49	0.62	0.17		9.71		0.08
				VMHC													
				VMHVL													
			fx	f	f	8.72	8.94	1.19	1.02	9.01	9.30	1.41	1.09	8.95	9.24	1.49	1.22
			ZI	ZID	ZID	6.81	7.86	3.90	0.66	6.89			1.43	6.64		3.92	1.66
				ZIV	ZIV						7.91	3.46			7.94		
			PH	PH	PH	7.22	8.96	1.29	0.23	7.42	8.86	0.86	0.06	7.70	8.83	0.84	0.06
				Subl													
			PST														
			STN	STh	STh	7.25	8.11	3.60	1.71	7.30	8.67	3.19	2.11	7.15	8.79	3.51	2.22
					PHD												
					Re												
				A11	A11												
				scp													
			SMT	Sub													
			VM	VM	VM	6.72	7.47	1.77	0.55	7.17	7.50	1.72	0.97	6.95	7.49	1.61	0.54
			mtt	mt	mt	7.51	7.80	0.95	0.72	7.76	8.21	1.08	0.80	7.72	8.13	1.11	0.83
			RT	Rt	Rt	4.53	6.97	4.55	3.66	4.78	6.91	4.18	3.04	4.77	6.81	4.37	3.55
			em	ml	ml	4.43	7.23	4.14	1.39		7.23		1.38		7.27		1.73
				eml	eml					5.04		3.82		5.03		4.03	
			VPL	VPL	VPL	5.32	6.96	4.03	2.02	5.34	7.14	3.71	2.20	5.23	7.04	3.88	2.81
			VPM	VPM	VPM	4.92	6.90	3.87	1.42	5.03	7.17	3.56	1.37	5.10	7.19	3.63	1.41
				VPPC	VPPC												
			PO	Po	Po	5.15	6.43	3.13	1.60	4.76	6.75	3.35	1.21	4.93	6.80	3.82	0.99
			LP	LPMR	LPMR	4.04	5.17	2.58	1.61	4.02	5.29	2.61	1.25	4.00	5.56	2.77	1.45
			LD	LDVL	LPVL	4.02	5.10	3.57	2.56	4.03	5.06	3.64	2.06	4.00	4.96	3.85	2.41
			LGd	DLG	DLG	4.13	4.59	4.06	3.54	4.12	4.78	3.76	2.95	4.10	4.58	3.85	3.29
				VLG	VLG												
			MDl	MDL	MDL	5.23	6.53	1.52	0.33	4.81	6.45	1.36	0.51	5.04	6.50	1.34	0.40
			MDc														
			MDm	MDM	MDM	5.31	6.49	0.59	0.19	5.41	6.45	0.88	0.11	5.28	6.48	0.91	0.08
			lMD	lMD	lMD	5.54	6.48	0.24	0.00	5.41	6.10	0.17	–0.04	5.42	6.22	0.14	0.00
			CL	CL	CL	4.40	6.25	1.80	1.26	4.48		1.65	1.12	4.50		1.58	
			PCN	PC	PC	6.21	6.67	1.54	0.86		6.75						
			CM	CM	CM	6.53	7.43	0.83	0.00	6.00	6.90		–0.04	6.18	7.01		0.00
				iml													
				OPC	OPC												
			PVT	PVP	PVP	4.87	5.58	0.53	0.00	4.85	5.67	0.60	0.03	5.08	5.52	0.59	0.00
				fr	fr												
			sm	sm	sm	4.22	4.73	1.35	0.58	4.29	4.71	1.13	0.33	4.22	4.78	1.28	0.32
			LH	LHbL	LHbL	4.36	5.16	1.35	0.53		5.18	1.14				1.25	
				LHbM	LHbM					4.51			0.27	4.57	5.19		0.35
			MH	MHb	MHb	4.17	4.98	0.65	0.18	4.29	4.99	0.44	0.13	4.30	5.03	0.46	0.06
			CA1slm	CA1	CA1LMol		3.98		0.00	2.31	4.09		0.05		4.37		
			CA1sr		CA1Rad												
			CA1sps		CA1Py												
			CA1spd														
			CA1so		CA1Or	2.21								2.24			0.00
			CA2sr	CA2	CA2Rad												
			CA2sps		CA2Py												
			CA2so		CA2Or												

Level			Structure			S Coordinate (mm)				PW1 Coordinate (mm)				PW2 Coordinate (mm)			
S	PW1	PW2	S	PW1	PW2	D	V	L	M	D	V	L	M	D	V	L	M
31	34	62	CA3sr	CA3	CA3Rad				1.75		4.16	4.29	1.77				
			CA3slu		CA3SLu												
			CA3sps		CA3Py												2.07
			CA3so		CA3Or			4.73							4.20	4.66	
			DGlb-mo, DGmb-mo	PoDG, DG	MoDG	2.93	4.47		0.00	2.98	4.56		0.38	2.91	4.60	3.86	0.65
			DGlb-sg, DGmg-sg		GrDG												
			DGlb-po, DGmb-po		PoDG												
			alv	alv	alv	2.18		4.89	0.35	2.24			0.71	2.13		4.82	
			fi	fi	fi		5.40	4.96			5.15	4.58			5.18		
					fi												
			df	df	df	3.12	3.41	0.78	0.00		3.15	0.62	0.04	3.14	3.37	0.79	0.19
				dhc	dhc												
			FC		FC												
			cc	cc	cc		3.30		0.00				0.04				0.00
			cing	cg	cg	1.92	3.02		0.30	1.98	2.68		0.66	1.89	2.95		0.49
					dcw												
			ec	ec	ec		8.02	5.88			7.69	5.91			9.00	5.87	
			amc														
			cpd	ic	ic	4.74	8.73	4.82	1.69		8.80		2.23	5.59		4.48	
					cp										8.95		2.32
			CP	CPu	CPu	5.26	8.01	5.71	4.75	4.50	7.23	5.76	4.83	4.58	7.71	5.77	4.83
32	35	65	IG	IG	IG	2.92	2.97	0.18	0.05	2.60	2.65	0.21	0.07	2.89	2.90	0.22	0.11
			RSPv	RSGb	RSGc		2.98		0.00	0.57	2.73		0.01	0.94	2.95		0.00
			RSPd	RSA	RSD	0.44				0.32			0.12	0.27		1.56	0.14
			PTLp	PTA	MPtA	0.39		4.73	1.18	0.31		4.05	1.08	0.27			
					LPtA												
					PtPD											5.42	
			SSp	S1BF	S1BF	0.95		6.77		0.92		6.77		1.46			
					S1											6.95	
					S2												
			AUDd	AuD	AuD	3.01		7.07		3.07		6.98		3.70		7.44	
			AUDp	Au1	Au1	3.66		7.40		3.49		7.53		4.29		7.65	
			AUDv	AuV	AuV	4.99	5.57	7.41		5.50		7.57		5.72	6.27	7.64	
			TEa	TeA													
			ECT	Ect	Ect		7.91	7.28			7.08	7.55			7.18	7.59	
			PERI	PRh	PRh			6.78				7.48			7.81	7.22	
			ENTI	LEnt	LEnt	8.30		6.81		7.59	7.99	7.50			8.07	7.22	
			PIR1	Pir1	Pir1		10.73	6.77	4.67	7.99		7.50		8.07	10.48	7.17	5.48
			PIR2	Pir2	Pir2	8.84	10.54	6.53	4.80	8.00	10.16	7.15	5.36	8.07	10.29	7.01	5.48
			PIR3	Pir3	Pir3		10.37	6.49	4.84	7.97		7.12		7.98	10.14	6.95	5.52
			TR, PAA		APir1												
					APir2												
					APir3												
			COApl1	PLCo1	PLCo1		10.48							10.19	10.55	5.08	
			COApl2	PLCo2	PLCo2	9.91	10.18	4.65	3.85	9.55	10.22	5.20	3.76	10.08	10.40	5.08	3.52
			COApl3	PLCo3	PLCo3	8.93	10.09	4.60		9.17			3.93	9.60	10.29	5.08	3.68
			COApm1	PMCo	PMCo		10.32	3.87		9.03	9.80	3.95	2.55	9.22	10.21	3.81	2.70
			COApm2														
			COApm3			8.99											
			SUBv														
			DGlb-sg														

Level			Structure			S Coordinate (mm)				PW1 Coordinate (mm)				PW2 Coordinate (mm)			
S	PW1	PW2	S	PW1	PW2	D	V	L	M	D	V	L	M	D	V	L	M
32	35	65	CA3sr														
			CA3sp														
			CA3so														
				CPu	CPu												
			LA	LaDL	LaDL	7.25	8.96	5.69	4.91	6.43		5.92		7.10		5.85	
				LaVM	LaVM						8.51		4.80		8.87		4.81
			EPd	DEn	DEn	8.81	9.41	5.77	5.32	7.97	8.76	6.09	5.74	7.79	9.14	6.03	5.46
			EPv														
			BLAp	BLP	BLP	8.91	9.72	5.30	4.51	8.33	9.59	5.77	4.57	8.66	9.39	5.57	4.38
			BMAp	BMP	BMP	8.91	9.54	4.97	3.96	8.66	9.41	5.27	4.43	8.95	9.78	5.04	3.94
				AHiAL	AHiAL												
				BSTIA													
				MePD													
			PA														
			NL														
			IL														
			AL														
				InfS	InfS												
			I														
			PVp														
				ArcMP	ArcMP												
				ArcLP	ArcLP												
			TMd	DTM	DTM	8.69	8.89	0.26	0.10	9.13	9.48	0.32	0.06	9.24	9.52	0.44	0.12
			PMv	PMV	PMV	8.99	9.60	1.12	0.54	9.25	9.70	1.38	0.60	9.24	9.87	1.31	0.51
			PMd														
			fx	f	f	8.68	8.92	1.14	0.96	8.98	9.30	1.33	1.06	9.10	9.38	1.21	0.94
			TUte	Te	Te	9.09	9.46	1.40	1.14	9.37	9.69	1.73	1.38	9.38	9.63	1.69	1.38
				VTM	VTM												
			PH	PH	PH	7.34	8.77	0.95	0.17	7.35	9.10	0.98	0.02	7.44	8.92	0.87	0.11
			mtt	mt	mt	7.68	8.40	0.92	0.74	7.85	8.84	1.05	0.72	8.05	9.03	0.97	0.64
				ns	ns												
				Imfb	Imfb												
			LHAp	LH, Gem	PLH, PeFLH	7.14			0.67	7.67	9.42	2.55	1.03		9.51		0.63
			LHAvm														
			LHAsfpm														
			LHAvl														
			PSTN	PSTh	PSTh	7.93	8.33	1.87	1.55	8.21	8.92	2.20	1.79	8.63	9.08	1.95	1.51
			STN	STh	STh	7.34	8.37	3.21	1.70	7.37	8.90	3.20	1.94	7.59	9.15	3.10	1.89
			ZI	ZID	ZID	6.32	7.69	3.80	1.16	6.73			1.67	6.40			1.76
				ZIV	ZIV						7.85	3.56			8.00	3.63	
					PR												
			RT	RT	RT	5.28	6.56	4.32	3.71	5.08	6.82	4.13	3.18	5.15	7.16	4.06	3.61
					IGL												
					IMA												
			LGvl	VLG	VLG	4.81	5.67	4.46	3.91	4.82	5.48	4.12	3.61	5.08	5.86	4.08	3.66
			LGd	DLG	DLG	4.12	5.13	4.30	3.24	4.04	4.91	4.04	2.68	4.09	5.13	3.98	3.02
			bsc														
			em	eml	eml	4.76	6.93	3.98	0.89	5.11		3.82		5.20		3.71	
				ml	ml						7.19		1.45		7.36		1.32
			VPL	VPL	VPL	5.33	6.50	3.78	2.69	5.12	6.74	3.62	2.77	5.25	7.04	3.56	2.44
			VPM	VPM	VPM	5.06	6.53	3.71	2.14	5.05	7.07	3.31	1.40	5.11	7.04	3.37	1.40
			VPLpc	VPPC	VPPC			2.96		6.63	7.10	1.49	0.46	6.79	7.24	2.44	0.59
			VPMpc			6.31	6.88		0.69								

Level			Structure			S Coordinate (mm)				PW1 Coordinate (mm)				PW2 Coordinate (mm)			
S	**PW1**	**PW2**	**S**	**PW1**	**PW2**	**D**	**V**	**L**	**M**	**D**	**V**	**L**	**M**	**D**	**V**	**L**	**M**
32	35	65	PO	Po	Po	4.57	6.43	3.54	1.72	4.68	6.66	2.93	1.41	4.86	6.81	3.63	1.34
			LP	LPLR	LPLR	4.06	5.29	3.25	1.65	4.05		3.07		4.03		3.51	
				LPMR	LPMR						3.89		1.27		5.53		1.17
			CL	CL	CL	4.42	5.76	1.66	1.30	4.40		1.71		4.64			1.17
			PF	PF	PF	5.90	6.49	1.72	1.15		6.64	1.63		5.41	6.13	1.08	0.50
					PC												
				OPC	OPC												
			im	iml	iml	5.92	6.61	1.43	0.76								
				scp	scp												
					A11												
			VM	VM													
			SPFm	SPF	SPF	6.99	7.37	0.55	0.20	6.89	7.39	0.71	0.18	7.05	7.55	0.96	0.20
					RRe												
			CM	CM	CM	6.67	7.29	0.78	0.00	6.33	6.74		–0.02	6.00	6.81		0.00
				PoMn	PoMn												
			IMD														
			MDm	MD	MDM	5.64	6.63	0.92	0.12	4.60	6.44	1.37					0.13
			MDl		MDL	5.34	6.48	1.45	0.34					4.95	6.46	1.45	
			PVT	PVP	PVP	4.95	5.78	0.49	0.00	5.03	5.80	0.49	0.03	5.21	5.92	0.52	0.00
			fr	fr	fr	5.25	5.38	1.15	0.64	5.12	5.66	1.20	0.42	5.00	5.75	1.21	0.00
			LH	LHbL	LHbL	4.35	5.30	1.31	0.30		5.33	1.10				1.22	
				LHbM	LHbM					4.41			0.30	4.59	5.38		0.35
			MH	MHb	MHb	4.11	4.99	0.70	0.10	4.21	5.01	0.40	0.13	4.53	5.19	0.57	0.10
			sm	sm	sm	4.16	4.66	1.24	0.58	4.15	5.26	1.16	0.33	4.31	4.68	0.00	0.30
			CA1slm	CA1LMol	CA1LMol		4.15		0.03						4.53		0.00
			CA1sr	CA1Rad	CA1Rad						4.13		0.01				
			CA1sps	CA1Py	CA1Py												
			CA1spd														
			CA1so	CA1Or	CA1Or	2.15				2.23				2.11			
			CA2sr	CA2Rad	CA2Rad												
			CA2sps	CA2Py	CA2Py												
			CA2so	CA2Or	CA2Or												
			CA3sr	CA3Rad	CA3Rad				2.01								
			CA3slu	CA3SLu	CA3SLu												
			CA3sps	CA3Py	CA3Py								1.92				2.29
			CA3so	CA3Or	CA3Or		4.39	4.94			4.41	4.63			4.64	4.75	
			DGlb-mo, DGmb-mo	PoDG, Hil, DG	MoDG	2.89			0.81	2.85	4.47		0.62	2.84	4.49		1.10
			DGlb-sg, DGmg-sg		GrDG												
			DGlb-po, DGmb-po		PoDG												
			FC		FC												
				dhc	dhc												
			df	df	df	3.10	3.39	0.79	0.00	2.90	3.00	0.54	0.05	3.21	3.36	0.62	0.19
			cc	cc	cc				0.00				0.01	1.88			0.00
			cing	cg	cg		2.94		0.34	1.87	2.64		0.59	1.64	2.77		0.60
			ec	ec	ec		8.86	5.94			7.97	5.82			7.13	5.90	
			amc														

Level			Structure			S Coordinate (mm)				PW1 Coordinate (mm)				PW2 Coordinate (mm)			
S	PW1	PW2	S	PW1	PW2	D	V	L	M	D	V	L	M	D	V	L	M
32	35	65	st	st	st	8.70	9.49	5.33	2.66	5.42	6.70	4.51	4.00	8.52	9.10	4.90	2.82
			alv	alv	alv	2.10	8.87	5.09	0.29	2.15		4.77	0.26	2.06		4.81	
			fi	fi	fi						8.18	5.08			6.13		
			opt	opt	opt		8.15	4.57	3.08		8.43	4.41	3.15	4.01	8.36	4.45	2.53
			cpd	ic	ic	5.81	8.50	4.41	1.82	6.39	8.92	4.11	2.06	3.62		5.50	
					cp										9.28		1.98
				sox	sod												
33	36	66	IG	IG	IG	2.84	2.91	0.16	0.06	2.73	2.78	0.22	0.07	2.87	2.88	0.13	0.07
			RSPv	RSGb	RSGb		2.92		0.00	0.85	2.78		0.00	1.00	2.90		0.00
					RSGc												
			RSPd	RSA	RSD	0.43				0.48			0.14	0.40		1.49	0.17
					V2MM												
					V2ML												
			PTLp	PTA	PtPD	0.40		5.39	1.43	0.46		4.77	1.21	0.77			
					PtPR											5.95	
			SSp	S1BF	S1BF	1.36		6.81		1.16		7.24		1.88			
					S1											7.19	
			AUDd	AuD	AuD	2.92		7.12		3.33		7.44		3.44		7.51	
			AUDp	Au1	Au1	3.57		7.50		3.83		7.62		4.12		7.78	
			AUDv	AuV	AuV	5.13		7.53		5.45		7.62		5.50	6.38	7.78	
			TEa	TeA													
			ECT	Ect	Ect		8.02	7.32		6.52		7.50			7.20	7.66	
			PERI	PRh	PRh			6.85		7.03	7.61	7.30			7.95	7.33	
			ENTI	LEnt	LEnt	8.25	8.94	6.92			8.03	7.35			8.32	7.32	
			PIR1	Pir1	Pir1		10.64	6.89			10.45	7.34		8.27	10.20	7.27	5.92
			PIR2	Pir2	Pir2	8.85	10.43	6.65	5.12	8.07	10.19	7.14	5.49	8.23	10.03	7.09	5.84
			PIR3	Pir3	Pir3		10.34	6.61		7.87	10.01		5.72	7.94	9.91	6.95	5.24
			TR2, TR3	APir	APir1	9.34		5.51		9.32	9.89	5.88	5.53		10.35	6.04	
					APir2												
					APir3									9.13			4.84
			COApl1	PLCo1	PLCo		10.50							9.19	10.46	5.29	3.45
			COApl2	PLCo2				4.93				5.41					
			COApl3	PLCo3		9.22							4.17				
			COApm1	PMCo	PMCo		10.39	4.37		9.08			3.13	9.52	10.27	4.06	2.86
			COApm2														
			COApm3														
			SUBv														
			SUBv-sp														
			DGlb-mo	DG	GrDG				1.97		9.24		2.53	8.70	9.35	2.75	2.23
			DGlb-sg					2.54									
			DGlb-po			8.50											
			CA3sr	CA3						6.33	8.70	5.59	3.39				
			CA3slu														
			CA3sp														
			CA3so		CA3Or	7.49		4.81	2.45					7.39	8.59	4.74	3.40
			CA1sr														
			CA1sps														
			CA1spd														
			CA1so														
				LaDL	La												
				LaVM													
			EPd	DEn	DEn	8.54	9.54	5.89	5.41	7.84	8.88	6.25	5.97	7.96	9.07	5.89	5.42
			EPv														

Level			Structure			S Coordinate (mm)				PW1 Coordinate (mm)				PW2 Coordinate (mm)			
S	PW1	PW2	S	PW1	PW2	D	V	L	M	D	V	L	M	D	V	L	M
33	36	66	BLAp	BLP	BLP	8.96	9.53	5.28	4.35	8.55	9.45	5.90	4.89	8.91	9.30	5.36	4.50
			BMAp	BMP													
				AHiAL													
					AHiPL												
				AHiPM	AHiPM												
			PA														
			NL														
			IL														
			AL														
				InfS													
			PVp	ArcMP	ArcMP	9.33	9.78	0.47	0.00		10.32		–0.02	9.73	10.15		0.00
				ArcLP	ArcLP					9.67		0.84				0.98	
				DTM													
			PMv	PMV													
			PMd	PMD													
			MMme		MnM												
					MM												
					ML												
					LM												
					SuMM												
			fx	f	f	8.68	9.00	1.10	0.91	9.00	9.36	1.23	0.99	8.99	9.41	1.20	0.98
			TMv	VTM	VTM	8.99	9.57	1.58	0.93	9.40	9.98	2.08	1.38	9.29	9.92	1.81	0.97
			PH	PH	PH	6.47	8.65	0.69	0.00	6.82	8.81	0.64	–0.02	7.51	8.37	0.67	0.13
			pm	mt'	mt	7.89	8.64	0.92	0.56	7.97	9.04	1.07	0.59	8.37	9.14	0.91	0.53
			SUMI	SuM, SMT	SuML, SMT	8.17	8.66	1.05	0.57	8.49	8.91	0.96	0.32	8.22	8.98	1.06	0.26
				ns	ns												
				mfb	mfb												
			LHAp	LH, Gem	PLH, Gem	6.88			0.54	6.94			0.51	7.02	9.48		
			LHAsfpm														
			LHAvl														
			PSTN	PSTh													
			STN	STh	STh	7.68	8.51	2.80	1.72	7.65	8.90	2.96	1.99	7.66	8.20	2.94	2.33
			ZI	ZID	ZID	6.47	7.75	4.18	1.62	6.31		4.11	1.66	6.53		3.73	
				ZIV	ZIV						7.90				7.97		1.89
			FF	F	F	7.00	7.65	2.23	1.48	7.11	7.75	2.27	1.04	7.23	7.85	1.97	1.35
				PR	PR												
			RT	RT													
				SubG	SubG												
				IGL	IGL												
				IMA	IMA												
			LGvl	VLGMC	VLG1, 2, 3	4.79		4.62		5.13		4.45		5.21	6.65	4.35	3.71
			LGvm	VLGPC			6.70		3.84		6.27		3.74				
			LGd	DLG	DLG	4.07	5.20	4.40	3.09	4.13	5.25	4.22	2.70	4.10	5.45	4.19	2.79
			bsc	bsc													
			em	str	str	4.70		4.14		4.76		4.02		4.84		3.81	
			ml	ml	ml		7.02		1.15		7.18		1.61		7.30		1.45
			VPL	VPL	VPL	5.08	6.64	3.94	2.86	5.31	6.57	3.58	3.01	5.38	6.79	3.56	2.95
			VPM	VPM	VPM	5.06	6.48	3.68	2.31	4.88	6.89	3.46	1.57	4.99	6.90	3.42	1.88
			VPLpc	VPPC	VPPC			3.15		6.60	7.00	2.20	0.61	6.58	6.93	2.56	1.20
			VPMpc			6.28	6.86		1.01								
			PO	Po	Po	4.72	6.39	3.45	1.74	4.84	6.63	2.85	1.32	4.91	6.57	3.13	1.61

Level			Structure			S Coordinate (mm)				PW1 Coordinate (mm)				PW2 Coordinate (mm)			
S	**PW1**	**PW2**	**S**	**PW1**	**PW2**	**D**	**V**	**L**	**M**	**D**	**V**	**L**	**M**	**D**	**V**	**L**	**M**
33	36	66	LP	LPLR	LPLR	4.12	5.36	3.32	1.64	4.17		3.06		4.10		3.26	
				LPMR	LPMR						5.30		1.46		5.52		1.28
			CL		CL												
				APTD													
			PF	PF	PF	5.15	6.67	1.88	0.27	5.25	6.65	1.70	0.50	5.30	6.89	1.73	0.52
					PVG												
					PrC												
			im														
				scp	scp												
					A11												
			SPFm	SPF	SPF	6.81	7.31	0.91	0.45	6.53	7.38	1.04	0.35	6.92	7.31	1.07	0.39
					SPFPC												
				pv													
			CM														
			IMD														
			MDm														
			PVT	PVP													
			fr	fr	fr	5.20	6.05	0.99	0.55	5.40	6.42	1.05	0.67	5.55	6.63	1.03	0.64
			LH	LHbL	LHbL	4.54	5.21	1.28	0.33	4.58	5.34	0.99		4.64	5.27	1.02	
				LHbM	LHbM								0.38				0.42
			MH	MHb	MHb	4.18	5.12	1.08	0.19	4.46	5.16	0.52	0.11	4.62	5.16	0.60	0.10
			sm	sm	sm	4.14	4.67	1.03	0.53	4.19	4.62	0.90	0.25	4.23	4.67	0.87	0.28
					hbc												
			CA1slm	CA1	CA1LMol		4.22		0.00	2.28	4.43		0.01		4.59		0.01
			CA1sr		CA1Rad												
			CA1sps		CA1Py												
			CA1spd														
			CA1so		CA1Or	2.13								2.14			
			CA2sr	CA2	CA2Rad												
			CA2sps		CA2Py												
			CA2so		CA2Or												
			CA3sr	CA3	CA3Rad						4.78	4.93	2.22				
			CA3slu		CA3SLu												
			CA3sps		CA3Py				2.39								2.66
			CA3so		CA3Or		4.76	5.22							5.14	5.11	
			DGlb-mo, DGmb-mo	PoDG, IBI, DG, OBI	MoDG	2.91	4.33		1.19	2.95	4.50		0.99	2.86	4.17		1.76
			DGlb-sg, DGmg-sg		GrDG												
			DGlb-po, DGmb-po		PoDG												
			FC		FC												
			dhc	dhc	dhc	2.93	3.47	1.00	0.00	2.93	3.30	0.86	0.03	2.58	3.58	1.42	0.00
			df	df	df	3.16	3.28	0.65	0.02	3.06	3.16	0.55	0.09	3.20	3.41	0.74	0.08
			cc	cc	cc				0.00				0.00				0.00
			cing	cg	cg	1.79	2.85		0.38	2.00				1.82			
			ec	ec	dcw		9.22	6.06			8.02	6.12				6.07	
			st														
			alv	alv	alv	2.06	9.08	5.34	0.14	2.28	8.56	5.66	0.73	2.09		5.22	0.26
			fi	fi	fi												
			opt	opt	opt		7.99	4.74	3.43		7.88	4.57	3.69		7.90	4.44	3.52
				sox	sod												

Level			Structure			S Coordinate (mm)				PW1 Coordinate (mm)				PW2 Coordinate (mm)			
S	PW1	PW2	S	PW1	PW2	D	V	L	M	D	V	L	M	D	V	L	M
33	36	66	cpd	cp	cp	6.62	8.61	4.40	1.77		9.09		2.03		9.23		1.78
				ic	ic					6.66		4.08		6.94		3.88	
34	38	69	IG	IG	IG	2.73	2.80	0.20	0.05	2.52	2.54	0.21	0.08	2.85	2.85	0.18	0.12
			RSPv	RSGb	RSGb		2.81		0.00	0.63	2.59		0.01		2.91		0.00
					RSGc									0.00			
			RSPd	RSA	RSD	0.42				0.36		1.65	0.22	0.38			0.20
				V2MM	V2MM												
					V2ML												
			PTLp	PTA	PtPD	0.37		6.91	1.33	0.44		4.56		0.59			
					PtPR											5.35	
				S1	S1BF												
					S1												
			AUDd	AuD	AuD	3.00		7.21		2.64		6.98		2.78		7.19	
			AUDp	Au1	Au1	3.68		7.58		3.08		7.73		3.58		7.47	
			AUDv	AuV	AuV	5.68	6.34	7.58		5.49		7.74		5.05		7.50	
			TEa	TeA													
			ECT	Ect	Ect		7.88	7.17		6.47		7.71		5.87	6.66	7.50	
			PERI	PRh	PRh			6.89		7.16		7.39			7.39	7.42	
			ENTI	LEnt	LEnt		10.22	6.94		7.51		7.42			7.73	7.42	
				Pir1	Pir1												
				Pir2	Pir2												
				Pir3	Pir3												
			TR1	APir	APir		10.34	6.22		9.08	9.90	5.86	5.52	8.58	9.60	6.49	4.83
			TR2														
			TR3			8.96											
			COApl1	PLCo1	PLCo		10.14	4.89			10.36			9.01	10.08	5.53	3.90
			COApl2	PLCo2													
			COApl3	PLCo3		9.12				8.92			4.47				
			COApm1	PMCo	PMCo		10.15	4.38	3.21	9.13	10.11	4.65	3.29	9.37	10.07	4.53	3.42
			COApm2														
			COApm3														
			SUBv														
			SUBv-sp														
			DGlb-mo	DG	GrDG		8.93	2.89	2.20				2.10	8.81		2.80	2.52
			DGlb-sg														
			DGlb-po			8.37											
			CA3slm	CA3						5.62		5.81					
			CA3sr														
			CA3slu														
			CA3sp		CA3Py												
			CA3so		CA3Or	5.84		5.64	2.56					6.17		5.47	2.73
			CA2sr														
			CA2sp														
			CA2so														
			CA1slm														
			CA1sr														
			CA1sps														
			CA1spd														
			CA1so														
				DEn	DEn												
			EPv														
			BLAp	BLP	BLP	8.86	9.29	5.09	4.13	8.58	9.15	5.66	4.57	8.52	9.01	5.51	4.64
			BMAp														

Level			Structure			S Coordinate (mm)				PW1 Coordinate (mm)				PW2 Coordinate (mm)			
S	**PW1**	**PW2**	**S**	**PW1**	**PW2**	**D**	**V**	**L**	**M**	**D**	**V**	**L**	**M**	**D**	**V**	**L**	**M**
34	38	69		AHiAL													
					AHiPL												
				AHiPM	AHiPM												
			PA														
			NL														
			IL														
			AL														
			PVp	ArcMP	ArcMP	9.37	9.46	0.33	0.08	9.72	10.16	0.51	–0.03	9.90	10.08	0.47	0.00
			MMme	MMn	MnM	8.48	8.79	0.23	0.00	8.86	9.55	0.25	–0.03	8.98	9.47	0.22	0.00
			MM	MM	MM	8.47	9.36	1.03	0.00	9.00	9.62	0.45	0.03	8.95	10.01	0.73	0.00
				ML	ML												
			LM		LM												
			pm	pm	pm	8.34	8.63	0.67	0.38	8.37	9.15	0.82	0.50	8.67	9.09	0.74	0.41
			mp														
			smd	sumx	sumd	7.95	8.15	0.76	0.00	8.16		0.60	0.03		8.52		0.01
			mtg	mtg	mtg	7.86	8.01	0.31	0.23	7.79	8.05	0.72	0.50	7.90	8.17	0.65	0.53
			fx	f	f	8.64	8.85	0.97	0.80	8.99	9.34	1.06	0.84	9.06	9.48	1.16	0.88
			TMv	VTM	VTM	8.58	9.48	1.66	0.43	9.38	9.72	1.51	1.13	9.29	9.90	1.75	0.91
			PH	PH	PH	6.94	8.08	0.84	0.00	6.94	8.23	0.54	0.00	7.58	8.22	0.53	0.06
			SUMI, SUMm	SuM, SMT	SuML, SuMM	8.01	8.65	1.40	0.00	8.31	8.82	1.05	–0.02	8.45	9.27	1.80	0.00
				ns	ns												
				mfb	mfb												
				Gem													
			LHAp	LH	PLH, Gem	7.96	8.85	1.73	0.74	8.11				7.15	9.38	3.45	
			VTA														
			SNr		SNR												
				STh													
			ZI	ZID	ZID	6.00	7.87	3.92	1.19	6.14			1.75				1.96
				ZIV	ZIV						7.99	4.01		6.35	7.97	3.75	
			FF	F	F	6.78	7.79	2.24	1.16	7.04	7.69	2.07	1.19	7.24	7.79	1.98	1.46
				PR	PR												
				SubG	SubG												
			IGL	IGL	IGL	5.43	5.78	4.53	3.91	5.14	5.40	4.32	3.59	4.99	5.41	4.29	3.61
				IMA	IMA												
			LGvl	VLGMC	VLG1, 2, 3	5.65		4.54		5.18	6.45	4.43		5.08	6.48	4.40	3.65
			LGvm	VLGPC			6.99		3.70				3.74				
			LGd	DLG	DLG	4.16	5.62	4.49	3.38	4.07	5.24	4.29	2.76	4.00	5.31	4.24	2.96
			bsc	bsc	bsc	4.04	4.29	3.97	1.52	4.00	4.45		1.43	3.93			2.09
			em	str, ar, ml	str, ml	4.90		3.94		4.78	7.09	3.86	1.46	4.88	7.35	3.77	1.52
			ml				7.14		1.41								
			VPL	VPL	VPL	5.71	6.42	3.73	3.30	5.39	6.57	3.42	2.78	5.32	6.69	3.52	2.95
			VPM	VPM	VPM	5.29	6.46	3.73	2.63	5.40	6.67	3.21	1.46	5.11	6.75	3.32	2.12
				VPPC	VPPC												
			PO	Po	Po	5.27	6.32	2.78	1.76	5.00	6.76	3.37	0.80	4.91	6.64	3.02	1.60
			LP	LPLR	LPLR	4.12	5.64	3.42	2.12	4.10	5.24	3.09		3.98	5.00	3.27	
				LPMR	LPMR								1.50				1.83
			MRNm														
			SPFpm	SPFPC	SPFPC	6.36	6.77	2.32	1.12	6.65	6.92	1.83	1.05	6.68	6.98	2.06	1.03
					VLi												
			APN	APTD	APTD	4.22	5.25	2.22	1.63	4.45	4.93	1.73	1.30	4.22	4.92	1.96	1.54
				RI	RI												
			NPC														
			MPT														
			OP														

Level			Structure			S Coordinate (mm)				PW1 Coordinate (mm)				PW2 Coordinate (mm)			
S	PW1	PW2	S	PW1	PW2	D	V	L	M	D	V	L	M	D	V	L	M
34	38	69	PAGm		PVG												
			PAGrm														
			PAGrl														
			PF	PF	PF	5.97	6.29	0.93	0.74	5.36	6.66	1.76	0.53	5.47	6.80	1.77	0.51
			PRC	PrC	PrC	4.79	5.35	1.09	0.29	4.91	5.82	1.12	0.24	5.00	5.71	0.91	0.21
					CL												
				scp	scp												
					A11												
				pv													
				PVP													
			fr	fr	fr	6.27	6.97	0.92	0.64	5.67	6.83	1.01	0.58	6.02	6.93	0.95	0.57
					LHb												
			MH	MHb	MHb	4.24	5.01	0.64	0.00	4.41	5.06	0.65	0.18	4.66	5.18	0.51	0.19
			pc														
			sm, hbc	sm, hbc	sm, hbc	4.07	4.74	0.64	0.24	4.13	4.69	0.73	0.34	4.34	4.81	0.77	0.31
			CA1slm	CA1	CA1LMol		4.22		0.00	2.20	4.41		0.02		4.58		0.08
			CA1sr		CA1Rad												
			CA1sps		CA1Py												
			CA1spd														
			CA1so		CA1Or	2.15											
			CA2sr	CA2	CA2Rad												
			CA2sps		CA2Py												
			CA2so		CA2Or												
			CA3sr	CA3	CA3Rad				2.83		5.62	5.17	2.39				
			CA3slu		CA3SLu												
			CA3sps		CA3Py												2.79
			CA3so		CA3Or		5.84	5.50									
			DGlb-mo, DGmb-mo	PoDG, IBI, DG, OBI	MoDG	2.96	4.12		1.83	2.89	4.31		1.17	2.85	4.12		1.85
			DGlb-sg, DGmg-sg		GrDG												
			DGlb-po, DGmb-po		PoDG												
			FC		FC	3.44	3.58	0.20	0.09								
			dhc	dhc	dhc	2.52	3.52	1.51	0.00	2.76	3.24	1.06	0.02				0.00
				df	df												
			ccs	cc	cc				0.00				0.01				0.00
			cing	cg	cg		2.74		0.45		2.59		0.50		2.80		0.44
			ec	ec	dcw			6.19				6.11				6.14	
			st														
			alv	alv	alv	2.08	9.12	5.72	0.30	2.12	8.75	5.89	0.33	2.02	8.88	5.59	
				fi													
			opt	opt	opt	4.85	7.34	4.73	3.92		7.67	4.57	3.66		7.63	4.48	3.77
				sox	sod												
			cpd	cp	cp	6.91	8.60	4.08	1.57		9.05		1.82	6.83	9.27	3.95	1.88
				ic						6.71		3.99					
36	39	72	IG		IG	2.78	2.84	0.16	0.07								
			RSPv	RSGb	RSGb		2.84		0.00	0.70	2.54		0.00		2.86		0.00
					RSGc									0.97			
			RSPd	RSA	RSD					0.43			0.25	0.37			0.22
			RSPagl			0.39											

Level			Structure			S Coordinate (mm)				PW1 Coordinate (mm)				PW2 Coordinate (mm)			
S	PW1	PW2	S	PW1	PW2	D	V	L	M	D	V	L	M	D	V	L	M
36	39	72	VISam	V2MM, V2ML, V2L	V2MM, V2ML	0.36			1.19	0.40		5.90	1.34	0.37		3.83	1.56
			VISrl														
			VISal					6.29									
			VISp		V1												
			PTLp	PtA	PtPD	2.24		6.91		1.76		6.57		1.11		6.40	
					PtPR												
			AUDd	AuD	AuD	3.01		7.11		2.44		6.86		2.35		7.03	
			AUDp	Au1	Au1	3.47		7.59		2.85		7.71		3.25		7.59	
			AUDv	AuV	AuV	5.48	6.21	7.61		4.75		7.83		5.15	6.11	7.60	
			TEa	TeA	TeA		7.39	7.60		5.42		7.85			6.75	7.55	
			ECT	Ect	Ect			7.21		6.36		7.84			7.24	7.36	
			PERI	PRh	PRh			7.04		6.83	7.34	7.73			7.76	7.22	
			ENTI	LEnt	LEnt	7.99	9.50	7.10				7.79			8.33	7.22	
					Pir1												
					Pir2												
					Pir3												
			TR1	APir	APir	8.88	10.03	6.84		8.76	9.90	6.82	5.04	9.00	10.06	6.37	4.37
			TR2														
			TR3														
					PLCo												
			COApm1	PMCo	PMCo		9.95	4.54	3.68	9.32	10.15	5.42	3.85	9.54	10.30	4.58	3.30
			COApm2														
			ENTmv														
				DEn													
			EPv														
				BLP	BLP												
				AHiPM	AHiPM												
			PA														
			NL														
			IL														
			AL														
			MM	MM	MM	8.68	9.34	0.80	0.00	8.76	9.84	0.60	0.02	8.88	9.55	0.36	0.00
				ML	ML												
				LM	LM												
			pm			8.86	9.13	0.48	0.38								
			mp	mp	mp	8.29	8.52	1.16	0.76	8.75	9.23	1.24	0.77	8.91	9.17	1.40	0.92
				sumx	sumd												
			mtg	mtg	mtg	7.32	7.90	0.51	0.28	7.59	7.94	0.53	0.30	7.68	8.02	0.45	0.35
			fr	fr	fr	7.21	7.88	0.68	0.36	7.13	7.90	0.76	0.44	6.85	7.68	0.86	0.48
				f	f												
				mt													
			TMv		VTM												
			MT														
			PH														
			SUMm	SuMM	SuMM	8.44	8.75	0.60	0.00	8.34			0.01	8.41	8.92	0.53	0.01
			SUMI	SuML	SuML	8.50	8.94	0.89	0.52		9.03	1.05		8.44	9.33	1.53	0.34
				ns	ns												
				mfb													
				LH													
			VTA		VTAR												
			SNc	SNCD	SNCD	7.13	8.51	3.34	1.28	7.47	8.68	3.14	1.44	7.74	8.86	2.59	1.67
			SNr	SNR	SNR	7.23	8.74	3.31	1.37	7.47	8.94	3.46	1.53	7.70	9.06	3.16	1.69
					SNL												

Level			Structure			S Coordinate (mm)				PW1 Coordinate (mm)				PW2 Coordinate (mm)			
S	**PW1**	**PW2**	**S**	**PW1**	**PW2**	**D**	**V**	**L**	**M**	**D**	**V**	**L**	**M**	**D**	**V**	**L**	**M**
36	39	72		PBP	PBP												
			ZI	ZID	ZIC	6.56	7.57	3.63	1.57	6.38		3.59	1.79	6.00	7.57	3.67	2.08
				ZIV							7.79						
				PR	PR												
					SubG												
					LT												
			IGL	IGL	IGL	5.91	6.39	4.45	3.84	5.43	6.29	4.37	3.72	5.28	6.12	4.25	3.66
				IMA	IMA												
			LGvl	VLGMC	VLG1, 2, 3	6.33	7.33	4.36		5.52	6.69	4.48		5.45	6.86	4.32	3.66
			LGvm	VLGPC					3.59				3.85				
			LGd	DLG	DLG	4.42	5.98	4.46	3.59	4.21	5.63	4.32	2.94	4.18	5.64	4.22	3.25
			bsc	bsc	bsc	3.99			0.88	4.12			1.28	4.02			1.44
			ml	ml	ml	6.99	7.73	2.65	1.05	6.87	7.66	2.72	1.34	7.06	7.71	2.68	1.52
					VPM												
			LP	LPLC	LPLC		5.20	3.64		4.21	5.28	3.33			5.16	3.33	
				LPMC	LPMC	4.20			2.55				2.14	4.09			2.10
			MRNm														
					LPMR												
			SPFpm	SPFPC	SPFPC	6.62		3.34		6.63	6.83	3.05	2.20	6.70	6.99	3.08	1.56
			SPFpl				7.07		1.81								
			MGm	MGM													
			MGv	MGV													
			MGd	MGD													
			bic	str	str	5.08	6.65	3.99	2.72	5.26	6.10	3.80	3.31	5.18	6.59	3.66	2.56
			PO	PoT	Po	5.52	5.82	2.95	2.79	4.68		3.02		5.23	6.85	3.30	
			SGN	SG													
					VLi												
			APN	APTD	APTD	4.46	6.22	2.78	1.70	4.33				4.30			1.45
				APTV	APTV						6.23	2.26	1.38		5.95	2.48	
				RI	RI												
				PLi	PLi												
			NPC	PCom													
			MPT	MPT	MPT	4.24	5.06	1.68	0.08	4.25	4.88	1.33	0.26	4.42	4.93	1.31	0.45
			OP	OPT	OPT	4.07	4.53	1.69	0.95	4.31	4.66	1.73	0.93	4.25	4.65	1.52	1.05
			NOT	OT	OT	4.07	4.50	2.54	1.54	4.22	4.34	2.40	1.31	4.24	4.48	1.77	1.50
			SCig.b														
			PAGm	PAG	PVG	5.34			0.00	5.43	7.28	0.92	–0.01	5.27	7.02	1.13	0.02
			PAGrm				7.72	0.92									
			COM														
			ND	Dk	Dk	6.75	7.00	0.63	0.43	6.43	6.82	0.63	0.23	6.76	7.11	0.72	0.42
				SCom													
			SCO	SCO	SCO	5.36	5.44	0.07	0.00	5.40	5.47	0.07	–0.02	5.26	5.40	0.14	0.00
			pc	pc	pc	5.03	5.74	0.90	0.00	5.09	5.88	1.01	–0.02	4.83	5.52	1.03	0.00
					MCPC												
					RPF												
					Lth												
				IMLF													
					REth												
					Sc												
				Eth	Eth												
				PIL													
					PrC												
				scp	scp												

Level			Structure			S Coordinate (mm)				PW1 Coordinate (mm)				PW2 Coordinate (mm)			
S	**PW1**	**PW2**	**S**	**PW1**	**PW2**	**D**	**V**	**L**	**M**	**D**	**V**	**L**	**M**	**D**	**V**	**L**	**M**
36	39	72		dlf													
				ctg													
				hbc	hbc												
			PIS														
			CA1slm	CA1	CA1LMol				0.23	2.29		6.45	–0.01				0.00
			CA1sr		CA1Rad												
			CA1sps		CA1Py												
			CA1spd				9.14										
			CA1so		CA1Or	2.08								2.17		5.72	
			CA2sr	CA2	CA2Rad												
			CA2sps		CA2Py												
			CA2so		CA2Or												
			CA3sr	CA3	CA3Rad	3.68								3.59			
			CA3slu		CA3SLu												
			CA3sps		CA3Py												
			CA3so		CA3Or				3.11								
			DGlb-mo, DGmb-mo	PoDG, IBI, DG, OBI	MoDG	3.18	8.84		2.24	3.04	9.27		1.73	3.05	9.33		2.15
			DGlb-sg, DGmg-sg		GrDG												
			DGlb-po, DGmb-po		PoDG												
			SUBv		VS												
			SUBv-sp														
			SUBd														
			FC		FC												
			dhc	dhc	dhc	2.00	3.50	2.49	0.00	2.32	3.35	1.78	–0.01	2.42	3.61	1.66	0.00
				df													
			ccs	scc	cc		3.30		0.00				0.00				0.00
			cing	cg	cg		2.80		0.35	1.85	2.50		0.60	1.77	2.73		0.44
			ec	ec													
			alv	alv	alv	1.98	9.22	6.16	0.48	2.23	9.05	6.49	0.61	2.07		5.80	0.60
			opt	opt	opt		7.09	4.52			7.06	4.52			7.23	4.41	
			cpd	cp	cp	6.90	8.82	3.71	1.24	6.85	9.20	3.88	1.45	6.94	9.29	3.81	1.71
37	40	76	IG		IG												
			RSPv	RSGb	RSGb		2.99		0.00	0.64	2.51		0.06		3.19		0.00
					RSGc									0.70			
			RSPd	RSA	RSD					0.27			0.21	0.35			0.25
			RSPagl			0.41											
			VISp		V1												
			VISam	V2MM, V2ML, V2L	V2MM, V2ML	0.37			1.25	0.27		6.49	1.50	0.35		3.42	1.52
			VISrl														
			VISal					6.37									
			PTLp	PtA	PtPD	2.38		6.90		1.94		6.95		1.11			
					PtPR											6.83	
			AUDd	AuD	AuD	3.04		7.09		2.51		7.25		2.70		7.15	
			AUDp	Au1	Au1	3.45		7.59		2.98		7.90		3.29		7.66	
			AUDv	AuV	AuV	5.50	6.28	7.64		4.89		7.94		5.34	5.98	7.67	
			TEa	TeA	TeA		7.34	7.64		5.34	6.37	7.94			6.52	7.67	
			ECT	Ect	Ect		7.72	7.38		6.37	6.84	7.87			7.00	7.62	
			PERI	PRh	PRh			7.04			7.17	7.73			7.54	7.46	
			ENTI	LEnt	LEnt	8.03	10.01	7.17	5.53			7.93			9.31	7.49	5.68
			TR	APIR	APIR	8.98	10.06	6.44	4.29	8.72	9.59	7.00	4.69	8.91	9.79	6.91	4.99

Level			Structure			S Coordinate (mm)				PW1 Coordinate (mm)				PW2 Coordinate (mm)			
S	**PW1**	**PW2**	**S**	**PW1**	**PW2**	**D**	**V**	**L**	**M**	**D**	**V**	**L**	**M**	**D**	**V**	**L**	**M**
37	40	76	EPv														
				DEn													
				PMCo	PMCo												
				AHiPM	AHiPM												
			ENTmv														
			SUBv-slm		VS												
			SUBv-sr														
			SUBv-sp														
			CA1slm	CA1	CA1LMol				0.24	2.32		6.47	0.06				0.15
			CA1sr		CA1Rad												
			CA1sps		CA1Py												
			CA1spd				9.10										
			CA1so		CA1Or	2.13		6.22						2.39			
			CA2sr	CA2	CA2Rad												
			CA2sp		CA2Py												
			CA2so		CA2Or												
			CA3slm	CA3	CA3LMol												
			CA3sr		CA3Rad									3.96	8.97		
			CA3slu		CA3SLu	3.87											
			CA3sp		CA3Py												
			CA3so		CA3Or		8.20		3.15								
			DGlb-mo, DGmb-mo	DG	MoDG	3.33	8.88		2.56	3.13	9.10		1.94	3.33	9.32	5.48	2.44
			DGlb-sg, DGmg-sg		GrDG												
			DGlb-po, DGmb-po		PoDG												
			SUBd		DS												
			FC	FC													
			alv	alv	alv	2.04	9.31	6.27	0.40		8.94	6.57		2.27	9.54	6.31	
			dhc	dhc	dhc	2.06	3.46	2.39	0.00		3.33		0.72		3.57		
			ccs	scc	scc				0.00	1.98			0.06				0.00
			cing	cg	cg		2.89		0.43	1.74	2.42		0.65	2.03	3.09		0.36
			ec														
					dcw												
			AL														
			IL														
			NL														
			MM	MM													
					ML												
			mp	mp	mp	8.46	8.77	1.09	0.45	8.47	8.81	1.03	0.37	8.83	9.19	1.10	0.46
			aot														
			cpd	cp	cp	6.98	8.95	3.76	1.32	6.59	9.11	3.79	1.26	7.17	9.44	3.80	1.27
			SNr	SNRVL	SNR	7.20	8.83	3.23	1.47	7.18	8.87	3.33		7.65	9.19	3.34	1.30
				SNRDM									1.40				
			SNc	SNCD	SNCD	6.99	8.41	3.32	1.44	7.14	8.27	3.10	1.48	7.55	8.59	2.78	1.53
			ZI	ZI	ZIC	6.95	7.56	2.46	1.57	7.18	7.63	2.35	1.69	7.08	7.40	3.21	2.59
			ml	ml	ml	6.80	7.64	2.33	1.26	6.87	7.86	2.52	0.99	7.35	8.28	2.61	1.18
			MT	MT	MT	8.37	8.81	1.43	1.07	7.92	8.91	1.60	0.98	8.48	9.36	1.58	1.10
			VTA	VTA													
			fr	fr	fr	7.85	8.22	0.51	0.33	7.93	8.32	0.57	0.31	8.17	8.71	0.52	0.27
			mtg	mtg	mtg	7.76	8.10	0.32	0.25	7.45	7.80	0.34	0.24	7.56	8.11	0.28	0.13
			IF	IF	IF	8.16	8.49	0.21	0.00	7.89	8.25	0.16	–0.01	8.26	8.70	0.20	0.00

Level			Structure			S Coordinate (mm)				PW1 Coordinate (mm)				PW2 Coordinate (mm)			
S	**PW1**	**PW2**	**S**	**PW1**	**PW2**	**D**	**V**	**L**	**M**	**D**	**V**	**L**	**M**	**D**	**V**	**L**	**M**
37	40	76	RL	RLi	RLi	7.63	8.17	0.30	0.00	7.06	7.94	0.14	–0.01		8.33	0.20	0.00
				PBP	PBP												
				PN	PN												
				SNM													
				vtgx													
				VTRZ													
			MRNm	DpMe													
			PAGrm	PAG	PAG		7.59	0.78	0.00	4.90	6.72	0.61	–0.06	5.45		0.67	0.00
			PAGm			5.39											
			ND	Dk	Dk	6.47	6.84	0.49	0.17	6.08	6.57	0.50	0.12	6.36	6.98	0.55	0.14
			COM														
			INC	IMLF	InC	6.82	7.27	0.68	0.35				0.33				
				IMLFG	InCSh					6.22	7.00	1.08		6.36	7.13	0.84	0.26
					Lth												
				EW	EW												
				MA3	MA3												
				PR	RPC												
				scp	scp												
				MCPC	MCPC												
				PCom	PCom												
				dlf													
				dtg													
				ctg													
					PaC												
			SCO														
			pc	pc	pc		5.92	0.91	0.00	4.99	5.57	0.71	–0.05	5.20	5.74	0.74	0.00
				PCom	PCom												
			csc	csc	csc	5.08	5.29	0.51	0.00	4.76	5.11	0.54	–0.08	4.89		0.61	0.00
			SCdg														
			SCig-c														
			SCig-b														
					InWh												
			PIS														
			MPT	MPT	MPT	4.27	4.83	0.80	0.14	4.27	4.77	0.95	0.10	4.21	4.79	1.46	0.27
			PPT	PPT	PPT	4.30	4.70	1.50	0.82	4.21	4.67	1.26	0.43	4.21	4.82	1.95	1.11
			OP	OPT	OPT	4.57	5.04	2.09	1.46	4.43	4.81	1.87	1.21	4.41	4.84	2.49	1.80
			NOT	OT	OT	4.06	4.68	2.70	1.20	4.15	4.59	2.37	0.90	4.15	4.52	2.58	1.52
			bsc	bsc	bsc	4.00			0.70	3.99			0.20	4.06			0.72
			APN	APTD	APTD	4.73	6.49	2.83	1.76	4.67		2.47	1.66	4.72		2.68	
				APTV	APTV						6.33				6.95		1.61
			LP	LPMC	LPMC	4.39	5.38	3.77	2.75	4.24			2.37	4.28			2.43
				LPLC	LPLC						5.06	3.42			5.42	3.38	
			LGd	DLG	DLG	4.65	5.78	4.18	3.61	4.49	5.52	4.09	3.46	4.49	6.05	4.21	3.34
					VLG												
			opt	opt	opt		6.75	4.42			6.97	4.23			6.99	4.32	
			bic														
				MZMG	MZMG												
			MGv	MGV	MGV	5.56	6.68	4.13	3.17	5.32	6.34	3.90	2.94	5.93	6.88	3.90	3.04
			MGd	MGD	MGD	5.30	6.03	3.82	3.07	5.02	5.73	3.54	2.74	5.48	6.04	3.85	3.03
			SGN	SG	SG	5.23	5.84	3.13	2.86	4.99	5.73	2.94	2.62	5.56	5.96	3.10	2.88
			POL	PLi	PLi	5.18	6.45	2.88	2.53	4.82	6.38	2.56	2.05	4.75	6.95	2.76	2.01
			MGm	MGm	MGM	5.88	6.55	3.14	2.75	5.68	6.22	3.13	2.66	5.92	6.73	3.06	2.85
			SPFpl	SPFPC	SPFPC	6.51	6.90	3.64	2.08	6.58	6.87	3.36	2.47	6.95	7.18	3.25	2.68

Level			Structure			S Coordinate (mm)				PW1 Coordinate (mm)				PW2 Coordinate (mm)			
S	PW1	PW2	S	PW1	PW2	D	V	L	M	D	V	L	M	D	V	L	M
37	40	76		IMA	IMA												
				PoT	PoT												
					Po												
				PP	PP												
				PIL	PIL												
				REth	REth												
				SNL	SNL												
			LT	LT	LT	6.39	7.53	4.10	3.59	6.72	7.24	3.84	3.69	6.92	7.50	4.09	3.68
38	42	79	RSPv	RSGa	RSGa		3.62				3.48				3.58		
				RSGb	RSGb					0.86			–0.01				
					RSGc									0.89			0.00
			RSPd	RSA	RSD					0.29			0.30	0.36			0.25
			RSPagl			0.36											
			VISam	V2MM, V2ML	V2MM, V2ML	0.34		2.36	1.32	0.29		3.48	1.63	0.34		3.08	0.25
			VISp	V1M	V1	0.37		4.37		0.61				0.40		5.57	
				V1B								4.80					
			VISal	V2L	V2L	0.72		6.28		1.03		6.65		1.25		6.01	
			PTLp	PtA	PtPD	2.24		6.79		2.47		6.96		1.53			
					PtPR											7.05	
			AUDd	AuD	AuD	2.88		7.06		2.96		7.18		2.53		7.40	
			AUDp	Au1	Au1	3.36		7.62		3.43		7.54		3.07		7.90	
			AUDv	AuV	AuV		6.42	7.64		4.92	5.63	7.61		4.94	5.61	7.92	
			TEa	TeA	TeA		7.44	7.64			6.41	7.61			6.16	7.92	
			ECT	Ect	Ect		7.78	7.42			7.22	7.56			6.65	7.86	
			PERI	PRh	PRh			7.11			7.68	7.20			7.29	7.67	
			ENTI	LEnt	LEnt	8.05	9.92	7.24				7.27			8.73	7.68	
			TR	APIR	APIR		9.65	5.72		8.47	9.63	6.26	4.67	8.57	9.30	7.07	4.77
				DEn													
				PMCo	PMCo												
				AHiPM	AHiPM												
			ENTmv														
			SUBv-m		VS												
			SUBv-sr														
			SUBv-sp														
			CA1slm	CA1	CA1LMol					2.54		6.04	2.76				2.77
			CA1sr		CA1Rad				1.55						7.87		
			CA1sps		CA1Py												
			CA1spd				8.65										
			CA1so		CA1Or	2.50		6.34						2.35		6.43	
				CA2													
			CA3slm	CA3	CA3LMol												
			CA3sr		CA3Rad	4.25	7.70									5.12	
			CA3slu		CA3SLu												
			CA3sp		CA3Py									4.01	7.89		3.63
			CA3so		CA3Or				3.91								
			DGlb-mo, DGmb-mo	DG, PoDG	MoDG	3.61	8.82	5.57	2.92	3.39			2.63	3.38	8.96	5.54	2.78
			DGlb-sg, DGmg-sg		GrDG												
			DGlb-po, DGmb-po		PoDG												
			SUBd	S	DS	2.68	3.54	3.42	1.54		3.64		1.63	2.41	3.48	2.94	1.14
				Post													

Level			Structure			S Coordinate (mm)				PW1 Coordinate (mm)				PW2 Coordinate (mm)			
S	PW1	PW2	S	PW1	PW2	D	V	L	M	D	V	L	M	D	V	L	M
38	42	79	alv	alv	alv	2.39		6.40	1.70		8.31	6.11		2.20	9.30	6.49	1.11
			ab				9.12										
			dhc		dhc												
			cing	cg	cg		3.08	1.64	0.96	1.79				1.71	3.02		1.07
			ec		dcw												
			fp	fmj	fmj	1.67	3.00		1.19		3.05		1.09	1.87			
			AL														
			IL														
			NL														
				MM													
			mp	mp	mp	8.51	8.87	1.26	0.56	8.87	9.17	0.87	0.53	8.72	9.03	0.98	0.56
			IIIn	3n	3n												
			cpd	cp	cp	7.16	9.18	3.60	0.78	6.76	9.26	3.50	0.97	6.93	9.18	3.73	0.93
			SNr	SNR	SNR	7.41	9.02	3.14	1.08	7.14	9.02	3.02	1.10	7.22	8.91	3.24	0.80
			SNc	SNCD	SNCD	7.23	8.91	3.21	0.91	7.13	8.54	2.60	1.03	7.21	8.85	2.74	0.79
				SNM													
			ml	ml	ml	7.36	8.12	2.05	0.99	7.32	8.29	1.73	0.82	7.11	8.02	2.07	0.98
			rust														
					MT												
			VTA	VTA													
			fr	fr	fr	8.21	8.78	0.64	0.27	8.98	9.17	0.48	0.30	8.70	8.92	0.45	0.18
			mtg	mtg	mtg	7.33	7.83	0.29	0.18	7.05			0.01	7.19	7.75	0.24	0.09
			IF	IF	IF	8.05	8.62	0.25	0.00	8.19	8.52	0.05	–0.10	8.20	8.60	0.15	0.00
				IPDM													
				IPR													
				IPRL													
				IPC													
					IP												
					PN												
					PIF												
				PN													
			RL	RLi	RLi	7.41	8.01	0.22	0.00	7.03	8.34	0.07	–0.10	7.15	7.81	0.21	0.00
			RN	RPC	RPC	7.16	7.95	1.51	0.73	6.97		1.58		6.99		1.60	0.61
				RMC	RMC						7.89		0.30		7.91		
				PaR	PaR												
				PBP	PBP												
				vtgx	vtdg												
				Min													
				ELm													
				VTRZ													
				3n													
			MRNm	DpMe													
			PAGrm	DMPAG, DLPAG, LPAG	PIPAG, DMPAG, LPAG		7.38			4.70	6.49	0.77	–0.04	4.90	6.84	0.94	0.00
			PAGm						0.00								
			PAGvl														
			PAGd			5.09		0.81									
			ND	Dk	Dk	6.30	6.96	0.59	0.15	5.92	6.53	0.51	0.10	6.16	6.63	0.55	0.11
			COM														
			INC	IMLF	InC	6.50	7.20	0.72	0.30	5.87	6.84	1.20	0.33	6.18	7.20	0.83	0.22
				IMLFG	InCSh												
			EW	EW	EW	6.67	7.32	0.06	0.00	6.14	6.77	0.03	–0.05	6.41	7.14	0.10	0.01
				MA3	MA3												
				scp	scp												

Level			Structure			S Coordinate (mm)				PW1 Coordinate (mm)				PW2 Coordinate (mm)			
S	PW1	PW2	S	PW1	PW2	D	V	L	M	D	V	L	M	D	V	L	M
38	42	79		mlf	mlf												
				dlf													
				dtg													
				ctg													
					PaC												
					pc												
			csc	csc	csc	4.76	5.52	1.01	0.00	4.55	5.14	1.07	0.04				
			SCdw	DpWh	DpWh	5.70	6.21	0.83	0.66		5.14	1.07			5.52	1.86	
			SCdg	DpG	DpG	5.44	6.23	1.76	0.79		5.80	2.05	0.01	4.83	5.38	2.22	1.19
				InWh	InWh												
			SCig-c	InG	InG					3.98			0.33	4.09	5.23	2.82	0.00
			SCig-b				5.90	2.17									
			SCig-a			4.20			0.00								
			SCop	Op	Op	4.01			0.00	3.83			0.32	3.86	4.28		0.22
			SCsg	SuG	SuG	3.70	4.29	2.21	0.33	3.49		2.05		3.63	4.10	2.07	0.17
			SCzo	Zo	Zo	3.62	4.25	2.28	0.26	3.38	4.01	2.18	0.12	3.57	4.16	2.16	0.06
			PIS														
			PPT	PPT	PPT	4.68	5.60	2.65	2.17	4.21	5.03	2.59	1.97	4.20	4.75	2.87	2.26
			NOT	OT	OT	4.33	4.98	2.93	2.08	4.10	4.69	2.79	1.85	3.94	4.47	2.82	2.04
			bsc	bsc	bsc		5.77	4.29									
			APN	APT	APTD	5.03	6.72	2.89	1.88	5.31	6.35	2.53	1.86	5.06		2.82	
					APTV										6.58		1.82
			LP	LPMC	LPMC	4.85	5.33	3.90	2.98	4.53	5.03	3.49	2.76	4.22	5.13	3.80	2.79
			opt	opt	opt	6.59	7.27	4.23	3.51		6.22	4.07			5.64	4.30	
			bic														
				MZMG	MZMG												
			MGv	MGV	MGV	5.74	6.83	4.36	3.32	5.38	6.52	3.90	2.88	5.55	6.55	4.23	3.26
			MGd	MGD	MGD	5.22	6.02	4.32	3.25	4.97	5.74	3.67	2.81	5.00	5.71	4.23	3.24
			SGN	SG	SG	5.07	5.94	3.38	2.97	5.01	5.86	2.65	2.95	5.00	5.71	3.34	3.10
			POL	PLi	PLi	5.68	6.72	2.96	2.68	5.26	6.34	2.26	2.65	5.03	6.64	2.89	2.01
			MGm	MGm	MGM	5.94	6.66	3.38	2.96	5.73			2.65	5.69	6.54	3.40	3.05
			SPFpl														
					EpP												
				PoT	PoT												
					Po												
			PP	PP	PP	6.97	7.19	3.68	3.28	6.37	6.81	3.93	3.06	6.28	7.08	4.25	3.21
				PIL	PIL												
				SNL	SNL												
				LT													
39	44	83	RSPv-a	RSGa	RSGa				0.90		3.42		0.31		3.29		0.92
			RSPv-b/c	RSGb	RSGb	1.41	3.19		0.12	1.36	2.87		–0.01		3.19		
					RSGc									0.91			0.00
			RSPd	RSA	RSD				0.23	0.48			–0.01	0.36			0.34
			RSPagl			0.28											
			VISam	V2MM, V2ML	V2MM, V2ML	0.24		2.93	1.52	0.48		3.07	1.58	0.33		3.12	1.49
			VISp	V1M	V1M	0.24		4.57		0.64				0.47			
				V1B	V1B							5.36				5.57	
			VISal	V2L	V2L	0.78		6.18		1.38		7.17		1.27		7.04	
			PTLp		PtPC	2.14		6.97									
			AUDd	AuD	AuD	3.20		7.16		3.18		7.42		2.83		7.64	
			AUDpo	Au1	Au1	3.65	6.20	7.54		3.72		7.84		3.27		8.04	
				AuV	AuV												
			TEa	TeA	TeA		7.21	7.53		6.06	6.76	7.91			6.17	8.02	

Level			Structure			S Coordinate (mm)				PW1 Coordinate (mm)				PW2 Coordinate (mm)			
S	PW1	PW2	S	PW1	PW2	D	V	L	M	D	V	L	M	D	V	L	M
39	44	83	ECT	Ect	Ect		7.40	7.36			7.40	7.81			6.76	7.95	
			PERI	PRh	PRh		7.66	7.09			7.84	7.41			7.29	7.81	
			ENTI	LEnt	LEnt		9.41	7.26	4.55			7.44			9.11	7.75	
				APIR	APIR												
				DEn													
				PMCo													
				AHiPM													
			ENTmv		MEnt												
			SUBv-m		VS												
			SUBv-sr														
			SUBv-sp														
			CA1slm	CA1	CA1LMol												3.31
			CA1sr		CA1Rad		8.19										
			CA1sps		CA1Py												
			CA1spd														
			CA1so		CA1Or	2.76		6.31						2.69	7.49	6.53	
				CA2													
			CA3sr		CA3Rad			5.13						4.62		5.25	
			CA3sp		CA3Py												4.45
			CA3so		CA3Or	4.53	6.81		4.06						6.66		
			DGlb-mo, DGmb-mo	DG, PoDG	MoDG	3.66	8.09	5.55	3.15					3.63	8.67	5.74	3.03
			DGlb-sg, DGmg-sg		GrDG					3.64	8.52		2.74				
			DGlb-po, DGmb-po		PoDG												
			SUBd	S	DS	2.76	3.51	4.10	2.36		3.78		2.10	2.57	3.41	4.25	2.05
			POST	Post	Post			2.45		2.88	3.56	2.29	1.67	2.66	3.40	2.72	1.81
			alv	alv	alv	2.64		6.36	2.42		8.82	6.43		2.41	9.01	6.58	2.26
			ab				8.68										
			dhc		dhc												
			cing		cg												
			ec		dcw												
			fp	fmj	fmj	1.76			1.65	1.93			1.66	1.85			1.86
			AL														
			IL														
			NL														
			mp		mp												
			cpd	cp	cp	6.99	9.09	3.35	0.81	6.65	9.26	3.93	0.96	7.04	9.26	3.56	0.86
			SNr	SNR	SNR	6.90	8.91	3.25	0.99	7.04	8.95	3.14	1.11	7.33	9.06	3.04	0.95
			SNc	SNCD	SNCD	6.85	8.72	3.14	0.96	7.31	8.60	2.55	1.21	7.31	8.64	2.72	1.09
				SNCV	SNCV												
				SNM	SNCM												
			ml	ml	tth	7.34	8.43	2.23	0.83	7.53	8.93	1.68	0.72	7.68			0.70
					ml										8.69	1.81	
			rust														
			VTA	VTA													
			fr														
			mtg	mtg	mtg	7.19	7.76	0.20	0.14					7.05	7.52	0.17	0.05
			IF		IF												
			IPNr	IPR	IPR	8.29	8.55	0.24	0.00	8.49	9.03	0.34	–0.01	8.63	9.14	0.48	0.00
			IPNc	IPDL, IPL, IPI, IPC	IPC		8.93		0.00	8.81	9.41	0.91	–0.01		9.39		0.00
			IPNlr		IPL	8.34		0.45						8.86		0.67	

Level			Structure			S Coordinate (mm)				PW1 Coordinate (mm)				PW2 Coordinate (mm)			
S	PW1	PW2	S	PW1	PW2	D	V	L	M	D	V	L	M	D	V	L	M
39	44	83		IPDM													
			CLi	CLi													
					PN												
					PIF												
			RL	RLi	RLi	7.18	7.65	0.14	0.00					7.08	7.53	0.11	0.00
			RN	RPC	RPC	6.77	7.86	1.87	0.45	6.89			0.38	6.95		1.28	0.36
				RMC	RMC						7.80	1.01			7.97		
				PaR	PaR												
				PBP	PBP												
				dtgx	vtgd												
				vtgx													
				3n													
			MRNm	DpMe	DpMe	5.10		3.25		4.80		3.28		4.91		3.40	
			PAGm	DMPAG, DLPAG, LPAG	DMPAG, DLPAG, LPAG				0.00	4.63	6.23	1.06	–0.01	4.71	6.52	1.12	0.00
			PAGvl				7.15										
			PAGd			4.65		0.90									
			ND														
			COM														
			INC	IMLF	InC	6.53	6.99	0.51	0.20		6.63		0.49				
				IMLFG	InCSh					5.88		1.12		5.96	6.87	0.99	0.35
			EW	EW	EW	6.33	7.03	0.05	0.00	6.18	6.62	0.07	–0.02	6.28	6.65	0.12	0.01
			MAN		MA3												
				3													
				3PC													
				Su3	Su3												
				Su3C													
				scp													
			mlf	mlf	mlf	6.49	7.15	0.26	0.05	6.21	6.94	0.56	0.04	6.28	7.07	0.51	0.08
				dlf													
				dtg													
				ctg													
			csc	csc	csc	4.45	4.67	1.13	0.00				0.10	4.52			0.00
			SCdw	DpWh	DpWh	5.08	5.95	1.14	0.72		5.90	2.16	0.10	4.52	5.92	1.73	0.00
			SCdg	DpG	DpG	4.67	6.02	1.63	0.77		5.90	2.16	0.10	4.14	5.93	2.60	0.00
				InWh	InWh												
			SCig-c	InG	InG					3.89	5.85	2.73	0.25	3.70	5.28	2.89	0.00
			SCig-b				6.01										
			SCig-a			3.94		2.79	0.00								
			SCop	Op	Op	3.63			0.00	3.61	4.59	2.69		3.47	5.13	3.00	0.11
			SCsg	SuG	SuG	3.31	4.31	2.68	0.00	3.28	4.28	2.69	0.10	3.22	4.15	2.76	0.06
			SCzo	Zo	Zo	3.21	4.45	2.76	0.02	3.18	4.28	2.80	0.01	3.13	4.24	2.85	0.00
			PIS														
				OT													
			DT	DT	DT	5.05	5.26	3.21	2.94	4.71	4.90	3.21	2.86	4.84	5.11	3.21	2.96
			bsc	bsc	bsc		5.41	3.83		4.85	5.34	4.12	3.12	4.82	5.17	3.62	2.94
			opt		opt	6.55	7.08	4.01	3.30								
			bic	bic	bic	5.95	6.32	3.28	3.02	5.71	5.96	3.16	2.97	5.68	5.98	3.24	2.92
				MZMG	MZMG												
			MGv	MGV	MGV	5.19	6.62	4.25	3.36	5.37	6.49	4.21	3.16	5.33	6.59	4.33	3.24
			MGd	MGD	MGD	5.04	5.43	3.84	3.28	5.11	5.80	3.95	3.13	4.91	5.53	4.12	3.26
			SGN	SG	SG	5.33	6.07	3.53	3.10	5.20	5.80	3.17	2.95	5.06	5.82	3.28	2.93
			MGm	MGm	MGM	6.07	6.62	3.50	3.11	5.88	6.41	3.19	2.99	5.82	6.58	3.35	2.92
			SPFpl														

Level			Structure			S Coordinate (mm)				PW1 Coordinate (mm)				PW2 Coordinate (mm)			
S	PW1	PW2	S	PW1	PW2	D	V	L	M	D	V	L	M	D	V	L	M
39	44	83			SubB												
					PoT												
			PP	PP		6.73	7.02	3.83	3.11	6.55	7.04	4.02	2.87				
				PIL	PIL												
				SNL	SNL												
41	45	88	RSPv-a	RSGa	RSGa		3.06		1.26		3.08		0.33		3.23		1.34
			RSPv-b/c	RSGb	RSGb		2.84		0.30	1.05	2.67		–0.03		2.94		
					RSGc									1.09			0.11
			RSPd	RSA	RSD		2.04		0.24	0.38			–0.01	0.45			0.18
			RSPagl			0.47											
			VISpm	V2MM, V2ML	V2MM, V2ML	0.35		2.35	1.60	0.32		2.60	1.44	0.43		2.58	1.20
			VISp	V1M	V1M	0.34		4.62		0.32				0.51			
				V1B	V1B							5.18				5.34	
			VISlm	V2L	V2L	0.99				1.01		7.24		1.47		6.93	
			VISli														
			VISlla					6.03									
			PTLp														
				AuD	AuD												
				Au1	Au1												
				AuV	AuV												
			TEa	TeA	TeA	2.95	6.40	7.46		5.30	6.19	7.57		4.91	5.76	7.92	
			ECT	Ect	Ect		7.19	7.45			6.81	7.49			6.49	7.88	
			PERI	PRh	PRh		7.25	7.12			7.29	7.11			7.03	7.69	
			ENTI	LEnt	DLEnt		9.17	7.19	4.20		8.88	7.08	3.08			7.44	
					DIEnt												
					VIEnt										9.33		
					APIR												
			ENTmv	MEntV	MEnt	7.30	8.80		3.71		8.08		3.07	8.03	9.34		3.25
			PAR	PaS	PaS	6.73			3.76	7.18	7.54	4.04	3.72	7.52	7.96	3.90	3.63
			PRE	PrS	PrS	6.40			4.12	7.06	7.55	4.55	3.91	7.01	7.72	4.35	3.52
			SUBv-m	S	VS						7.62		3.21	6.45	8.24	6.17	4.62
			SUBv-sr														
			SUBv-sp			3.25	7.88	6.21	3.65								
				CA1	CA1LMol												
					CA1Rad												
					CA1Py												
					CA1Or												
			DGcr-mo	DG, PoDG	MoDG	4.40	6.81	5.44	4.14	3.70	6.87	5.25	2.94	4.34	7.20	5.37	3.62
					GrDG												
				S	DS												
			PRE														
			POST	Post	Post		3.88		2.26	2.59	3.43	2.63	1.86	2.43	4.40	3.50	2.10
			alv		alv												
			ab														
			dhc		dhc												
			ec		dcw												
			fp	fmj	fmj	1.75			1.88	1.66			1.49	1.83			1.74
				bas	bas												
				s5	s5												
					m5												
			mcp	tfp	tfp	9.28	10.18	1.81	0.39	9.09	10.12	1.69	–0.04	9.20	9.76	1.15	0.01
			cpd	cp	cp	7.85	9.42	2.58	0.63	7.16	9.12	3.11	0.74	7.27	9.21	2.98	0.70

Level			Structure			S Coordinate (mm)				PW1 Coordinate (mm)				PW2 Coordinate (mm)			
S	PW1	PW2	S	PW1	PW2	D	V	L	M	D	V	L	M	D	V	L	M
41	45	88	SNr	SNR	SNR	7.54	8.82	2.68	1.84	7.55		2.67		7.25	8.93	2.82	0.92
			RR	RRF	RRF	6.98	8.82	2.82	0.81	7.21	7.95	2.54	0.81	7.28	7.77	2.05	0.64
				SNCD	SNCD												
					SNCV												
					SNCM												
			ml	ml	tth	8.64	9.13	1.84	0.56	7.86	8.74	1.74	0.66	8.19			0.39
					ml										9.00	1.40	
			dtd	dtgx	dtgd				0.00				0.02				0.08
			vtd	vtgx		8.45					7.75						
				dtg													
			tsp		ts												
			scp	scp	scpd	7.69	8.31	1.63	0.53	6.80	7.55	1.02	0.34		8.41		0.00
			rust	rs	rs		8.47	1.61		6.77	7.81	1.16	0.32	7.91	8.21	0.90	0.41
			VTA	VTA													
				mtg													
			IPNd	IPDM													
			IPNr	IPR	IPR	8.54	8.83	0.52	0.00	8.22	8.76	0.38	0.01	8.40	8.74	0.27	0.00
			IPNi	IPI	IPI	8.82	9.46	0.39	0.00	8.66	9.26	0.51	0.16	8.67	9.43	0.39	0.04
			IPNc	IPC	IPC	9.12	9.49	0.16	0.00	8.72	9.29	0.29	–0.04	8.63	9.44	0.13	0.00
			IPNld	IPDL	IPDL	8.73	8.94	0.56		8.49	8.76	0.60	0.27	8.60	8.88	0.56	0.22
			IPNli	IPL	IPL	8.86			0.30	8.69	9.16	0.75	0.32	8.71	9.35	0.75	0.16
			IPNlv				9.33	0.63									
			CLi	CLi	CLi	7.44	8.25	0.32	0.00	7.68	8.20	0.27	0.03		8.10	0.28	0.00
					PIF												
			mlf	mlf	mlf	6.51	7.05	0.59	0.05	6.23	6.84	0.62	0.07	6.29	7.10	0.63	0.04
			III	3	3N	6.42	6.88	0.52	0.05	6.39	6.74	0.42	0.05	6.38	6.90	0.44	0.03
				3PC	3PC												
				Su3	Su3												
				Su3C	Su3C												
					me5												
					Me5												
			RL														
			RN	RPC		7.07	7.78	0.92	0.40	6.80			0.34				
				RMC	RMC						7.55	1.02		7.18	7.48	0.75	0.45
			EW	EW	EW	6.09	6.42	0.14	0.00	6.19	6.47	0.04	–0.02	6.05	6.53	0.11	0.02
			ND														
				PaR	PaR												
			MRNm	DpMe	DpMe	4.79	7.72	2.95	0.05					4.94		3.42	
			PAGm														
			PAGvl	LPAG	LPAG	4.83	7.00	1.23	0.00	5.18	6.20	1.09	–0.02	5.29		1.25	
					VLPAG												0.00
			PAGd	DMPAG	DMPAG	4.48	5.23	0.58	0.00	4.47	5.32	0.50	0.00	4.56	5.29	0.71	0.00
			PAGdl	DLPAG	DLPAG	4.49	5.41	1.00	0.22	4.52	5.39	1.08	0.03	4.63	5.36	1.24	0.07
				IMLF	InC												
				IMLFG													
				dlf													
				ctg													
				ltg													
				csc													
			SCdw	DpWh	DpWh	4.71	5.99	1.31	0.95	4.05	5.73	2.27	–0.03	4.44	5.42	1.76	0.00
			SCdg	DpG	DpG	4.42	6.01	2.23	0.76	4.05	5.73	2.27	–0.03		5.46	2.31	0.00
			SCiw	InWh	InWh	4.36	5.54	2.50	1.06	3.87	5.63	2.32	–0.03	3.70	5.45	2.80	0.52

Level			Structure			S Coordinate (mm)				PW1 Coordinate (mm)				PW2 Coordinate (mm)			
S	PW1	PW2	S	PW1	PW2	D	V	L	M	D	V	L	M	D	V	L	M
41	45	88	SCig-c	InG	InG					3.55	5.62	2.71	0.14	3.45	5.34	3.06	
			SCig-b				5.25		0.00								
			SCig-a			3.32		2.77									
			SCop	Op	Op	3.27			0.00	3.30	5.30	3.14	–0.01	3.21	4.97	3.10	0.14
			SCsg	SuG	SuG	2.94	4.35	2.72	0.05	2.98	4.26	2.69	0.10	2.95	4.38	2.94	0.07
			SCzo	Zo	Zo	2.88	4.36	2.78	0.03	2.84	4.26	2.77	–0.01	2.83	4.35	2.96	0.00
			PIS														
			bsc	bsc													
			bic	bic	bic	4.85	6.65	3.39	2.86	5.88	6.10	3.30	3.03	5.44	6.40	3.54	3.04
			NB		BIC												
					MZMG												
				MGV	MGV												
				MGD													
				SG													
				MGm													
				SubB	SubB												
42	47	90	RSPv-a	RSGa	RSGa		2.92		1.54		3.04		0.42		3.17		0.68
			RSPv-b/c	RSGb	RSGb		2.77		0.45	1.51	2.46		0.03		2.63		
					RSGc									1.44			0.24
			RSPd	RSA	RSD		2.18		0.23	0.77			0.05	0.62			0.24
			RSPagl			0.51											
			VISpm	V2MM, V2ML	V2MM, V2ML	0.35		2.53	1.72	0.57		2.04	0.80	0.45		2.44	0.86
			VISp	V1M	V1M	0.35		4.76		0.57				0.50			
				V1B	V1B							5.19				5.37	
			VISlm	V2L	V2L	1.11				1.40		7.05		1.48		6.63	
			VISli														
			VISlla					6.16									
			PTLp														
					AuD												
					Au1												
					AuV												
			TEa	TeA	TeA	2.72		7.37		4.12	5.92	7.21		4.83	5.76	7.78	
			ECT	Ect	Ect	5.76	7.06	7.38			6.75	7.20			6.52	7.75	
				PRh	PRh												
			ENTl	LEnt	DLEnt		9.05	7.14	4.26		8.82	6.55	3.36			7.36	
					DIEnt												
					VIEnt										9.29		4.84
					APIR												
			ENTm	MEnt	MEnt		8.45		3.80		8.24		3.18	8.15	9.33	5.10	3.86
				Dsc													
					CEnt												
			PAR	PaS	PaS	6.61			3.74	6.46			3.33	6.19	7.82	3.78	3.57
			PRE	PrS	PrS	6.03	6.82	5.08	4.18	6.14	7.36	4.34	3.73	4.23	7.35	4.56	3.36
			SUBv-m	S	VS, MoS, DS					2.35	7.35	5.66		3.30	7.81	6.06	3.61
			SUBv-sr														
			SUBv-sp			3.54	7.50	6.09									
					CA1												
			DGcr-mo	DG	MoDG	5.21	5.98	4.75	4.58	4.34	5.97	4.70	3.34	4.93	6.72	5.08	4.20
			PRE		PrS												
			POST	Post	Post		4.04		2.30	2.78	4.05	3.53	2.00		4.60	3.78	2.04
			alv		alv												
			ab														
			dhc		dhc												

Level			Structure			S Coordinate (mm)				PW1 Coordinate (mm)				PW2 Coordinate (mm)			
S	**PW1**	**PW2**	**S**	**PW1**	**PW2**	**D**	**V**	**L**	**M**	**D**	**V**	**L**	**M**	**D**	**V**	**L**	**M**
42	47	90	ec		dcw												
			fp	fmj	fmj	1.81			2.03	2.01			1.96	1.85			1.82
				bas	bas												
				s5	s5												
				m5	m5												
			mcp	tfp	tfp	9.30	10.51	2.12	0.00		10.52		0.00	9.30	10.32	1.79	0.00
				bp						8.94		2.21					
			PG	Pn	Pn	9.03	10.27	1.64	0.26	9.13	10.42	1.84	0.02	9.37	10.03	1.32	0.00
			cpd	cp	cp	8.26	9.64	2.40	0.65	7.15	9.47	3.01	0.53	7.53	9.52	2.86	0.75
			cst														
			RR	RRF	RRF	7.13	9.03	2.75		7.17	7.61	2.28	0.68	7.08	7.63	2.46	0.54
			ml	tth	tth	8.73	9.18	1.65	0.44	8.53		1.80	0.46	8.70		1.71	0.40
				ml	ml						9.17				9.38		
			dtd	dtgx													
			vtd														
				dtg													
			tsp	ts	ts	7.07	7.55	0.61		5.79			1.07	5.97	8.04	1.40	0.15
			scp	xscp	scpd	7.60	8.40	1.65	0.13	7.52		1.23	0.00	8.02	8.48	0.35	0.00
					ID												
			rust	rs	rs	8.43	8.84	1.83	1.44		8.40	1.63		7.98	8.27	1.65	1.11
			VTA	VTA	VTA	8.33	8.85	1.05	0.49	8.19	8.73	0.63	0.10	8.50	8.89	1.09	0.15
			PPN	PPTg	PPTg					7.69	8.03	2.18	1.67	7.76	8.11	2.21	1.74
				mtg													
				Rbd													
				A8													
				B9	B9												
			IPNi	IPI	IPI	8.77	9.41	0.34	0.00		9.31	0.29	0.07	8.82	9.61	0.38	0.00
			IPNc	IPC	IPC	8.98	9.43	0.18	0.00		9.33	0.13	–0.01	9.02	9.61	0.15	0.00
			IPNd	IPDM, IPA, IPL	IPA, IPDL, IPL	8.41					9.28	0.53	–0.01	8.48	9.48	0.53	0.00
			IPNr						0.00								
			IPNld														
			IPNli														
			IPNlv				9.36	0.55									
			CLi	CLi	CLi	7.34	8.24	0.41	0.00	7.24	8.10	0.23	0.00	8.53	8.05	0.25	0.00
			mlf	mlf	mlf	6.52	7.09	0.65	0.06	6.35	7.03	0.54	0.07	6.54	7.26	0.56	0.03
			III	3	3N	6.48	6.89	0.54	0.08	6.30	6.81	0.48	0.08	6.45	7.01	0.41	0.05
				3PC	3PC												
				Su3	Su3												
				Su3C	Su3C												
				me5	me5												
				Me5	Me5												
			RL														
			EW	EW	EW	6.33	6.63	0.17	0.00	5.94	6.31	0.08	0.01	5.91	6.10	0.07	0.00
					DR												
			MRNm	DpMe	DpMe	4.58	7.70	2.90		5.23		3.22	0.33	5.30		3.01	
			PAGm														
			PAGvl	LPAG	LPAG	4.78		1.43	0.00	5.02	6.03	1.12	0.00	5.34		1.18	
					VLPAG										6.08		0.00
			PAGdl	DLPAG	DLPAG	4.45	5.33	1.10	0.24	4.38	5.34	1.08	0.03	4.57	5.41	1.18	0.12
			PAGd	DMPAG	DMPAG	4.35	5.13	0.55	0.00	4.36	5.19	0.53	0.00	4.52	5.35	0.70	0.00
				dlf													
				ctg													
				ltg													

Level			Structure			S Coordinate (mm)				PW1 Coordinate (mm)				PW2 Coordinate (mm)			
S	**PW1**	**PW2**	**S**	**PW1**	**PW2**	**D**	**V**	**L**	**M**	**D**	**V**	**L**	**M**	**D**	**V**	**L**	**M**
42	47	90	SCdw	DpWh	DpWh	4.54	5.77	1.49	0.84	4.33	5.92		0.18		5.97		
			SCdg	DpG	DpG	4.14	5.92	2.18	0.63	3.78		2.15	0.00	3.84		2.87	
			SCiw	InWh	InWh	4.10	5.32	2.36	0.86	3.62	5.38	2.62	0.22	3.67	5.22	3.02	0.42
			SCig-c	InG	InG					3.42	5.30	2.79	0.27	3.44	5.05	3.09	
			SCig-b				4.99		0.00								
			SCig-a			3.22		2.62									
			SCop	Op	Op	3.19			0.00	3.11	4.99	2.89		3.15	4.47	2.96	0.17
			SCsg	SuG	SuG	2.88	4.20	2.59	0.05	2.83	4.13	2.67	0.06	2.86	4.31	2.87	0.10
			SCzo	Zo	Zo	2.80	4.27	2.68	0.02	2.73	4.19	2.76	0.00	2.75	4.36	2.94	0.02
			PIS														
			bsc	bsc													
			bic	bic	bic	4.66	6.46	3.35	2.74	4.91	6.59	3.43	2.81	4.80	6.59	3.49	3.04
			NB	BIC	BIC	4.87	6.47	3.21	2.72	4.99	6.08	3.22	2.70	5.06	6.57	3.23	2.74
			SAG														
			PBG														
					MiTg												
				SubB	SubB												

Table 4.2: Correspondence of Structures at Corresponding Levels in the Swanson 2004 (S), Paxinos & Watson 1998 (PW1), and Paxinos & Watson 2005 (PW2) Atlases.

The formatting of Table 4.2 matches that of the 'Structure' column of **Table 4.1** with regard to the indication of structural correspondence**,** but is condensed.

Level			Structure			Level			Structure			Level			Structure		
S	**PW1**	**PW2**	**S**	**PW1**	**PW2**	**S**	**PW1**	**PW2**	**S**	**PW1**	**PW2**	**S**	**PW1**	**PW2**	**S**	**PW1**	**PW2**
43	48	91	RSPv-a	RSGa	RSGa	44	51	97	RSPv-a	RSGa	RSGa	45	52	98	RSPv-a	RSGa	RSGa
			RSPv-b/c	RSGb	RSGb					RSGb					RSPd	RSA	RSD
			RSPd	RSA	RSD				RSPd	RSA	RSD				VISpm	V2MM	V2MM
			RSPagl						VISpm	V2MM	V2MM						V2ML
			VISpm	V2MM	V2MM						V2ML				VISp	V1M	V1M
					V2ML				VISp	V1M	V1M					V1B	V1B
			VISp	V1M	V1M					V1B	V1B				VISpl	V2L	V2L
				V1B	V1B				VISlm	V2L	V2L				TEa	TeA	TeA
			VISlm	V2L	V2L				VISli						ECT	Ect	Ect
			VISli						VISll							PRh	PRH
			VISll						TEa	TeA	TeA				ENTl	LEnt	DLEnt
			TEa	TeA	TeA				ECT	Ect	Ect						VIEnt
			ECT	Ect	Ect					PRh	PRH				ENTm	MEnt	MEnt
				PRh	PRH				ENTl	LEnt	DLEnt					Dsc	
			ENTl	LEnt	DLEnt						VIEnt						CEnt
					DIEnt				ENTm	MEnt	MEnt				PAR	PaS	PaS
					VIEnt					Dsc					PRE		
			ENTm	MEnt	MEnt						CEnt				POST	Post	Post
				Dsc					PAR	PaS	PaS					fmj	fmj
					CEnt				PRE	PrS					ec		dcw
			PAR	PaS	PaS				POST	Post	Post				dhc		
			PRE	PrS	PrS					fmj	fmj				Vn	s5	s5
			POST	Post	Post				ec		dcw				mcp	mcp	mcp
			SUBv-sp	S	MoS, STr				dhc							tfp	tfp
			SUBv-sr						Vn	s5	s5					bp	
				fmj	fmj					m5	m5				tb		
				hf						mcp	mcp				moV	m5	m5
			ec		dcw				mcp	tfp	tfp				ll	ll	ll
			dhc		dhc					bp					cst	lfp	lfp
			alv		alv				ll	ll	ll				ml	ml	ml
			ab						cst	lfp	lfp					tth	tth
				m5	m5				ml	ml	ml				rust	rs	rs
				s5	s5					tth	tth				PG	DLPn	Pn
			mcp	tfp	tfp				rust	rs	rs					LPn	
				bp					PG	DLPn	Pn					VMPn	
			cpd	cp	cp					LPn						MPn	
			cst							VMPn						DMPn	
			ml	ml	ml					MPn						DPPn	
				tth	tth					DMPn						VPPn	
			rust	rs	rs					DPPn						B9	
			PG	Pn	Pn					VPPn					TRN	RtTgP	
			IPNd	IPA	IPA					B9						RtTg	RtTg
			IPNa													Rbd	Rbd

Level			Structure			Level			Structure			Level			Structure		
S	PW1	PW2	S	PW1	PW2	S	PW1	PW2	S	PW1	PW2	S	PW1	PW2	S	PW1	PW2
43	48	91	IPNi	IPI	IPI	44	51	97	TRN	RtTgP		45	52	98	PRNr	PnO	PnO
			IPNc	IPC	IPC					RtTg					AT	ATg	ATg
			IPNld	IPL	IPL					Rbd	Rbd				CSl	PMnR	PMnR
			IPNli						PRNr	PnO	PnO				CSm	MnR	MnR
			IPNlv						AT	ATg	ATg					SPTg	SPTg
				B9	B9				CSl	PMnR	PMnR						ERS
			VTA						CSm	MnR	MnR				PPN	PPTg	PPTg
				Rbd	Rbd					SPTg	SPTg				scp	xscp	scp
			CSm								RR				dscp		dscp
			RR	RRF	RRF				PPN	PPTg	PPTg				tsp	ts	ts
				RR					scp	xscp	dscp				mlf	mlf	mlf
			PPN	PPTg	PPTg				dscp						sctv		
			II						tsp	ts	ts					PL	PL
				ipt					mlf	mlf	mlf						Tr
					ID					PL	PL					ILL	
			scp	xscp	scpd					ILL					NLLd		
			dscp						NLLd						NLLh		
			tsp	ts	ts				NLLh						NLLv	VLL	VLL
			mlf	mlf	mlf				NLLv	VLL	VLL					dtg	
			NLLV							dtg							PrCnF
				A8							PrCnF				CUN		CnFI
				mtg					CUN								CnFV
				dtg					MRNp	DpMe	DpMe				MRNp	DpMe	DpMe
				ctg					DR	DRV	DRV				DR	DRV	DRV
				ltg						DRVL	DRL					DRVL	DRL
			MRNp	DpMe	DpMe						PDR						PDR
			MRNm							DRD	DRD					DRD	DRD
			CLi	CLi	CLi						Pa4						Pa4
			III	3	3N				IV		4n				IVn		4n
				3PC	3PC				MEV	Me5	Me5				MEV	Me5	Me5
				Su3	Su3				PAGvl	LPAG	LPAG				PAGvl	LPAG	LPAG
				Su3C	Su3C					VLPAG	VLPAG					VLPAG	VLPAG
			DR	DR	DR				PAGm						PAGm		
			MEV	Me5	Me5				PAGdl	DLPAG	DLPAG				PAGdl	DLPAG	DLPAG
			PAGvl	LPAG	LPAG				PAGd	DMPAG	DMPAG				PAGd	DMPAG	DMPAG
					VLPAG				mtV	me5	me5				LDT		
			PAGm						bic	bic	bic				mtV	me5	me5
			PAGdl	DLPAG	DLPAG				PBG	PBG	PBG					bic	bic
			PAGd	DMPAG	DMPAG					MiTg	MiTg					PBG	PBG
				dlf					SAG							MiTg	MiTg
			mtV	me5	me5				NB	BIC	BIC				SAG		
			bic	bic	bic				ICe	ECIC1	ECIC					BIC	BIC
			ll							ECIC2					ICe	ECIC1	ECIC
			PBG		PBG					InCo						ECIC2	
				MiTg	MiTg				SCdw	DpWh	DpWh						CIC
			SAG						SCdg	DpG	DpG					InCo	
			NB	BIC	BIC				SCiw	InWh	InWh						cic
				SubB	SubD				SCig-a	InG	InG				SCdw	DpWh	DpWh
			ICe		ECIC				SCig-b						SCdg	DpG	DpG
			SCdw	DpWh	DpWh				SCig-c						SCiw	InWh	InWh
			SCdg	DpG	DpG				SCop	Op	Op				SCig	InG	InG
			SCiw	InWh	InWh				SCsg	SuG	SuG				SCop	Op	Op

Level			Structure			Level			Structure			Level			Structure		
S	PW1	PW2	S	PW1	PW2	S	PW1	PW2	S	PW1	PW2	S	PW1	PW2	S	PW1	PW2
43	48	91	SCig-a	InG	InG	44	51	97	SCzo	Zo	Zo	45	52	98	SCsg	SuG	SuG
			SCig-b						PIN		Pi				SCzo	Zo	Zo
			SCig-c			47	55	106		RSGa	RSGa				PIN		Pi
			SCop	Op	Op				RSPd	RSA	RSD						
			SCsg	SuG	SuG				VISpm	V2MM	V2MM						
			SCzo	Zo	Zo				VISp	V1M	V1M						
			PIS							V1B	V1B						
46	53	102		RSGa	RSGa				VISpl	V2L	V2L						
			RSPd	RSA	RSD				TEa	TeA	TeA						
			VISpm	V2MM	V2MM				ECT	Ect	Ect						
			VISp	V1M	V1M					PRh	PRH						
				V1B	V1B				ENTl	LEnt	DLEnt						
			VISpl	V2L	V2L				ENTm	MEnt	MEnt						
			TEa	TeA	TeA					Dsc							
			ECT	Ect	Ect						CEnt						
				PRh	PRH				PAR	PaS	PaS						
			ENTl	LEnt	DLEnt				POST	Post	Post						
			ENTm	MEnt	MEnt				Vn	s5	s5						
				Dsc					mcp	mcp	mcp						
					CEnt						tfp						
			PAR	PaS	PaS				tb	tz							
			POST	Post	Post				moV	m5	m5						
			Vn	s5	s5				ll	ll	ll						
			mcp	mcp	mcp					py							
					tfp				cst		lfp						
			tb	tz					ml	ml	ml						
			moV	m5	m5					tth	tth						
			ll	ll	ll				rust	rs	rs						
				py					POR	RPO							
			cst		lfp				PG		Pn						
			ml	ml	ml						DPPn						
				tth	tth					Tz							
			rust	rs	rs				TRN	RtTgP	RtTgP						
			POR	RPO						RtTg	RtTg						
			PG		Pn					VLTg							
					DPPn					Rbd	Rbd						
				Tz					PRNr	PnO	PnO						
			TRN	RtTgP	RtTgP				CSl	PMnR	PMnR						
				RtTg	RtTg				CSm	MnR	MnR						
				VLTg					VTN	VTg	VTg						
				Rbd	Rbd					SPTg	SPTg						
			PRNr	PnO	PnO						A7						
			CSl	PMnR	PMnR				PPN	PPTg	PPTg						
			CSm	MnR	MnR				scp	scp	scp						
			VTN	VTg	VTg				tsp	ts	ts						
				SPTg	SPTg				mlf	mlf	mlf						
					A7				sctv	vsc							
			PPN	PPTg	PPTg					PL	MPL						
			scp	scp	scp						Tr						
			tsp	ts	ts					ILL	ILL						
			mlf	mlf	mlf				NLLd	DLL	DLL						

Level			Structure			Level			Structure		
S	PW1	PW2	S	PW1	PW2	S	PW1	PW2	S	PW1	PW2
46	53	102	sctv	vsc		47	55	106	NLLh		
				PL	MPL				NLLv	VLL	VLL
					Tr					cII	cII
				ILL	ILL					dtg	
			NLLd	DLL	DLL				CUN	CnF	CnFI
			NLLh								CnFV
			NLLv	VLL	VLL						CnFD
				cII	cII				MRNp		
				dtg					DR	DRV	DRV
			CUN	CnF	CnFI					DRI	
					CnFV					DRVL	
					CnFD					DRD	DRD
			MRNp						IVn	4n	4n
			DR	DRV	DRV				MEV	Me5	Me5
				DRI					PAGvl	LPAG	LPAG
				DRVL						VLPAG	VLPAG
				DRD	DRD				PAGm		
			IVn	4n	4n				PAGdl	DLPAG	
			MEV	Me5	Me5				PAGd	DMPAG	DMPAG
			PAGvl	LPAG	LPAG				LDT		LDTg
				VLPAG	VLPAG				mtV	me5	me5
			PAGm						ICe	ECIC1, ECIC2, ECIC3	ECIC1
			PAGdl	DLPAG							ECIC2
			PAGd	DMPAG	DMPAG						ECIC3
			LDT		LDTg						CIC
			mtV	me5	me5						DCIC
			ICe	ECIC1, ECIC2, ECIC3	ECIC1						Com
					ECIC2						Sag
					ECIC3						bic
					CIC				cic	cic	cic
					DCIC				SCdg		
					Com				PIN	Pi	Pi
					Sag						
					bic						
			cic	cic	cic						
			SCdg								
			PIN	Pi	Pi						

Vita

Claire Eugenia Wells is a resident of the Southwest United States, and an aspiring city hermit. She has received a Bachelor of Arts in Biological Sciences with a Chemistry minor from Clemson University. She has taught sections of the Molecular Cell Biology Laboratory for three and a half years at The University of Texas at El Paso; and has also taught sections of the Anatomy & Physiology I Laboratory and a Brain Mapping Course funded through the PERSIST grant, for one year each. Outside the world of academics, she has worked as a clerk and as a happy, dirty field grunt. She hopes one day to become a teacher, and a provider for her family. She likes green things, critters, stories, and role-playing games.

Contact Information: claire.eugenia.wells@gmail.com